Cranfield University

Daniel Melling

The Impact of Structural Changes on the Actuation of Polypyrroles

School of Applied Sciences

PhD Thesis

Cranfield University

Daniel Melling

The Impact of Structural Changes on the Actuation of Polypyrroles

School of Applied Sciences

PhD Thesis

Academic Years 2009-2012

Supervisors:

Dr. Ir. Edwin W. H. Jager

Dr. Alexandros A. Skordos

Dr. Stephen A. Wilson

August 2012

This thesis is submitted in partial fulfilment of the requirements for the degree of PhD.

Abstract

A new non-contact method for characterizing the time-dependent mechanical performance of electro-active polymer films has been developed and is described in detail. We first illustrate our new measuring technique by investigating the impact of film thickness on the actuation performance of polypyrrole. Our method is simple to perform and serves as a valuable tool for studying the long term stability and operational failure of the films, the effects of synthesis conditions and for the optimization of actuator performance.

We have used our technique to investigate the impact that structural changes, such as crosslinking, have on the actuation of polypyrroles. An understanding of this relationship is necessary if forms of polypyrrole are to be produced that are capable of greater movement, operating speeds, in service lifetimes and force generation. In order to do this we have developed a logical synthetic strategy (blocking approach) which allows us to change the degree of crosslinking in electro-synthesised polypyrrole. Using our blocking approach we have been able to show the impact that structural changes make on the actuation performance of polypyrroles.

We have shown that it is possible to monitor crosslinking and branching changes in polypyrroles indirectly using the irreversible expansion of these films. Our measurements are a form of "dynamic swelling study" and are analogous with solvent swelling studies used in the polymer industry for monitoring cross-linking changes.

The irreversible expansion of polypyrrole films has been used to investigate the effects that polymerization potential has upon the levels of cross-linking and branching. We go on to identify the optimal conditions for producing the maximum expansion, strain and strain rate for PPy(DBS). In addition, we have used instrumented indentation as a secondary method for monitoring crosslinking changes. This has provided information that is consistent with those revealed by changes in the irreversible expansion of the polymer.

Finally we present an in-depth theoretical discussion of how elemental analysis could be used as a more direct way to quantitatively determine the levels of crosslinking within polypyrroles.

This work represents the first study of its kind aimed at understanding the impact that crosslinking and branching has upon the actuation performance of polypyrroles. As a result we are closer to being able to synthesize polypyrroles with improved actuator properties such as greater strains and strain rates.

Dedicated to my grandparents:

Charlie and Mary Keenan.

Acknowledgements

I would like to thank my PhD supervisors: Dr. Stephen Wilson, Associate Prof. Edwin Jager and Dr. Alex Skordos for their help and support throughout my PhD studies.

Thank you, Stephen, for giving me the opportunity to undertake a PhD and for arranging for me to study in Sweden. You have changed my life for the better.

Thanks Edwin for giving me the opportunity to develop your LSM setup and your idea of using copolymerization to alter the levels of crosslinking in polypyrrole. The support that you have given me both scientific and personal during my PhD has been excellent and is greatly appreciated. Thank you for being a friend to me.

Thank you, Alex, for your support and advice. It has been good to have someone with such a warm and friendly spirit to support and guide me, particularly during the final months of writing.

I would also like to take this opportunity to thank the many people who have given me their help during my PhD.

In particular I would like to thank Mr Hans Mennborg for the many scientific discussions and the great practical help that you have given me over the years.

In addition I would like to thank to my current employer, IMSaT, for generously giving me the time to write and submit my thesis, particularly Prof. Sir Alfred Cuschieri.

During my studies I have made good friends and colleagues and would like to acknowledge their help and support. At Cranfield: Susan Libor, Sam Owens and Ola Kosmala. In Norrköping: Zia Ullah Khan, Hui Wang, Olga Bubnova and Negar Sani. In Linköping: Valerio Beni, Abeni Wickham, Ted Chang, Roger Karlsson and Jeffrey Mason.

I would like to thank my family members who have given me their support and encouragement during my PhD and throughout my life. Particularly my aunts: Joyce Chadwick and Debra Keenan.

Thanks to my wife Dr. Tracey Melling for her love and support during my PhD, and for accompanying me to Sweden. Without your support and encouragement I would not have been able to undertake my PhD studies. I am fortunate to have such a capable, supportive and loving wife. I look forward to our future together.

Finally, I would like to thank my mother, Valerie Mennborg, for her love and undying support throughout my life, particularly during difficult times. Thank you for being an exceptional parent.

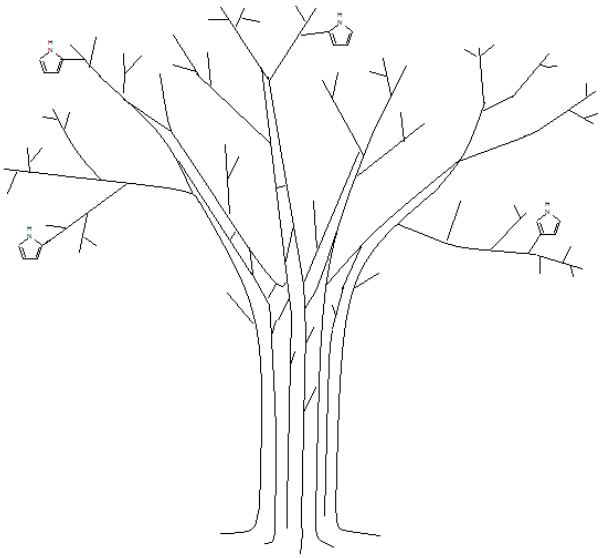

“Pauca sed matura.”

Table of contents

Page No.

Section C Research contribution:

List of figures

Section B

Section C

List of tables

Abbreviations

Symbol	Definition
Py	Pyrrole
PPy	Polypyrrole
NaDBS	Sodium dodecylbenzenesulphonate
DBS^-	Dodecylbenzenesulphonate anion
PPy(DBS)	Polypyrrole dodecylbenzenesulphonate polymerized using an aqueous electrolyte
EAP	Electroactive polymer
LSM	Laser scan micrometer
DPI	Data point interval
WE	Working electrode
RE	Reference electrode
CE	Counter (auxiliary) electrode
AuWE	Gold working electrode
pAuWE	Porous gold working electrode
Ag/AgCl RE	Silver / silver chloride reference electrode
AFM	Atomic force microscopy
FTIR	Fourier Transform Infrared Spectroscopy
NMR	Nuclear Magnetic Resonance Spectroscopy
ppm	Chemical Shift in parts per million
TMS	Tetramethylsilane
SSNMR	Solid-State Nuclear Magnetic Resonance Spectroscopy
CP/MAS	Cross polarization/magic angle spinning with dipolar decoupling
DEPT	Distortionless Enhancement by Polarization Transfer
GCMS	Gas Chromatography - Mass Spectrometry
$M^{+\cdot}$	Molecular ion
EDX	Energy-dispersive X-ray spectroscopy
TEM	Transmission electron microscopy
XPS	X-ray photoelectron spectroscopy
H	Micro-hardness
E	Elastic modulus
KBr	Potassium bromide
NIST	National Institute of Standards and Technology

Section A: Introduction

1.1 Context of research

Polypyrroles are conducting polymers that are capable of undergoing reversible volume change when they are switched between their oxidized and reduced state, whilst in contact with an electrolyte, which acts as a source of ions. They can be readily synthesized as thin films and further modified using on-chip fabrication techniques to form microstructures[1-4]. These properties make polypyrroles suitable for use in microactuating devices or MEMS. The ability of polypyrroles to operate within aqueous environments, their biocompatibility and various other properties, makes them highly suited for use in medical devices[5] and cell biology applications[6-7].

Although the use of polypyrroles as actuating polymers or "artificial muscles" is an established field and many actuating devices have been developed, there is still a need for their actuating properties to be further developed if their full potential as actuating materials is to be realized. For example, polypyrroles are relatively slow to actuate compared to other actuating materials[8], with films of one to five microns, typically being limited to frequency of a few Hertz.

To date no research into the affect that crosslinking has on the actuation of polypyrroles has been presented in the literature. Crosslinking is however an important factor in the swelling of gels and this should also be the case for polypyrroles.

Gels are polyelectrolytes that have been swollen by solvents such as water (hydrogels) and can be synthesized with different degrees of crosslinking. They can be switched from a swollen to a contracted state by changing the ionization of the polyelectrolyte by pH or electrical stimuli[9]. The amount of volume change is much larger than for conducting polymers and can be as much as a 1000-fold[10].

It has been shown that low levels of crosslinking in hydrogels result in increased levels of swelling[11]. The diffusion of water and ions in hydrogels has also been shown to increase with decreasing crosslinking[12-16].

This work on gels suggests that there exist optimal levels of crosslinking in polypyrroles capable of producing improved actuation performance. By understanding the relationship between the crosslinking and actuation of polypyrroles, forms of polypyrrole capable of greater: movement, operating speeds, in service lifetimes and force generation might be possible.

1.2 Research aims

The principle aim of the work presented in this thesis has been to understand how crosslinking impacts upon the actuation of polypyrrole films.

A secondary aim is to identify optimum or optimal levels of crosslinking resulting in maximum expansion and speed.

By increasing understanding of the relationship between polymer network structure and actuation, the synthesis of forms of polypyrroles that are capable of increased strains, speeds and strength, would be closer to being realized

1.3 Main Challenges

The first challenge that we have faced in undertaking this work has been to develop a means of characterizing the actuation of polypyrrole films to produce reliable actuation metrics. This has enabled us to compare the actuation performance of films containing different levels of crosslinking.

Two further challenges that needed to be overcome in order to undertake this work have been the development of synthetic strategies capable of changing the levels of crosslinking within electropolymerized films of polypyrrole and to develop a method(s) for monitoring crosslinking changes.

Although the properties of polypyrrole films are dependent upon many synthesis conditions, it is difficult to exercise control over a process that has as its first step the formation of highly reactive chemical species (free-radical cations) which tend to be non-selective in how they couple together to form the polymer network.

We have developed a strategy employing blocking groups and copolymerization, which allows the levels of crosslinking to be changed. For this strategy to be successful it was necessary to overcome further challenges. The first was to identify a suitable range of crosslinking in which actuation measurements could be successfully undertaken. If the level of crosslinking was too low, actuation measurements could not be completed due to brittle fracture or deformation of the polymer film. An additional challenge was that the large expansions observed for relatively low levels of crosslinking, typically lead to delamination of the films before actuation measurements could be completed. Delamination was prevented by using a porous gold electrode to distribute the stress at the polymer-substrate interface.

Two approaches capable of monitoring the degree of crosslinking have been implemented in our work. The first approach has been to monitor the relative changes in the irreversible expansion of the polymer, which is a highly analogous approach to the swelling studies which are used in the polymer industry for monitoring crosslinking

changes. The second approach has been to use instrumented indentation to monitor the change in the strength of the polymer films which is known to strongly correlate with crosslinking changes. We have found that the elastic modulus and materials parameter H/E^2 to be very useful in this respect.

Despite many hours of searching the literature and thinking it has proved very difficult to develop a direct and quantitative means of determining the levels of crosslinking in polypyrroles. In some polymers the crosslink is chemically distinct from the rest of the polymer, for example it contains a different functional group that can be readily quantified using techniques such as FTIR spectroscopy. Unfortunately the type of crosslinks present within polypyrroles is very difficult to detect and quantify since the linear, branched and crosslinked structures are very similar chemically. Despite this, we have been able to propose a method for quantifying the levels of crosslinking, based on an in-depth theoretical consideration of the changes that occur within the polymer network with crosslinking.

1.4 Thesis structure

Section B of this thesis reviews relevant literature necessary to support the research described in later sections.

Section C discusses the original research contributions undertaken during this work and comprises five subsections. The first of these describes in detail the development of a new method for measuring the actuation performance of electroactive films and illustrates with a study into the impact of film thickness variation on actuation performance. The second describes the synthesis of 3,4-dimethyl-1H-pyrrole by the author of this thesis, which was necessary to undertake the work in the third section. This next section describes the implementation of a blocking group approach as a strategy for changing the levels of crosslinking in polypyrroles and our findings. The fourth subsection makes use of the main findings in the previous section to study the change in crosslinking within polypyrroles with different polymerization potential, using two different methods to indirectly monitor crosslinking levels. In the final section we detail theoretically, the changes that occur in the network structure with increasing crosslinking i.e. the change in the ratio of nitrogen to hydrogen within the polymer network. The use of elemental analysis as a more direct and quantitative means of determining crosslinking is proposed.

Section D summarizes and evaluates the work that has been undertaken and includes a subsection briefly outlining future work that might be undertaken to further support and build upon this work.

Section B: The state of the art / literature review

1.0 Polymer actuators as artificial muscles

Although the term actuator may be unfamiliar to the reader, the concept of a material or structure that can cause something to move is very familiar to us. Our muscles are actuators and are essential to life. For the author of this thesis to type the words on this page and for the reader to read them, requires muscles of different sizes to control and produce movement.

A number of materials have been investigated for use as artificial muscles. Among these, polymer actuators appear to provide a combination of properties with the potential of providing true muscle-like action. Polymer actuators possess inherent compliance, are lightweight, and are in general low cost.

Electroactive polymers (EAPs) are a type of polymer actuator that responds to an electric field to generate mechanical motion. The number of EAPs has grown in recent years and range from rigid carbon nanotubes to soft dielectric elastomers. EAPs can be divided into two categories on the basis of their mode of actuation: ionic or field-activated.

One of the most commonly used ionic EAPs is polypyrrole. Polypyrroles are conducting polymers which undergo volume change when electrochemically switched between their oxidized and reduced states. This volume change is due to the movement of ions between the polymer and an electrolyte.

As with all the materials that have been investigated for use as artificial muscles, polypyrroles have a number of advantages, but also have a number of limitations. They are capable of being operated at low voltage (≈ 1V) in a liquid environment producing strains of up to 40 % with force densities of 100 MPa or higher. This makes them highly suitable for use in medical applications. However, they display low operating efficiencies (≈ 1%) and low electromechnical coupling (< 1%). In addition the actuation speeds are limited due to an actuation mechanism which depends upon the diffusion of ions. The need for them to be in contact with an electrolyte can also be a disadvantage when required to operate outside of a liquid.

Polypyrroles have been used to produce actuating devices with a range of applications both at the macro and microscale. Applications of macro-scale actuators include: refreshable Braille displays[17,18], steerable guide wires[8], microanastomosis connectors for reconnecting blood vessels[19]. Microscale devices and applications include: microrobotic arms[3] and devices for studying individual cells[7].

Electroactive polymers, particularly polypyrroles, display a range of properties that make them suitable for applications such as micro-robotics, medical applications and cell biology. These properties are listed below[5].

Electroactive polymers:

- can be electrically controlled.
- have large strain (3% in plane to >30% out-of-plane) that can be exploited in either: linear, volumetric, or bending actuators.
- have high strength (stresses are 1000 times as great as skeletal muscle)
- require low voltages for actuation, typically 1 V or less. Can be positioned continuously between minimum and maximum values.
- hold a fairly constant strain under d.c. voltage without expending power. (A degree of positional drift occurs, and the actuator system may consume small currents because of discharge through the electrolyte or parasitic electrochemical reactions.)
- work at body temperature.
- are light-weight.
- can be readily microfabricated.
- can operate in liquid environments including body fluids.

Polypyrroles:

- are biocompatible, both in vitro and in vivo.
- are tissue-compatible and implantable for long periods.
- improve regeneration of tissues.
- can serve as suitable substrates for the growth of cell cultures.
- can be produced in biodegradable/bio-erodible forms.
- can be doped with and can release biomolecules.
- are widely studied as biosensors.

However, as impressive as this list of properties is, there is still a need for improvement. Although polypyrroles can display strains of up to 40 %, natural muscle can give strains of up to 100 %. Therefore, increased strains would be advantageous. Of even greater importance is the need to increase the rate of actuation (strain rate) of polypyrrole if its full potential is to be realized. If both the strain and strain rate could be increased, then many exciting applications could be envisaged, such as swimming micro-robots[20].

Much work has been undertaken aimed at improving the properties of polypyrrole. Most of these approaches have focused on the chemicals (dopant and solvent), conditions (concentrations and temperature) and methods (polymerization potential, current

density) employed during electropolymerization. To date no research has been conducted into the impact that the polymer network structure has upon the actuation polypyrrole. Two major obstacles would need to be overcome in order to undertake such an investigation. The first would be to devise a method for altering the levels of crosslinking and branching and the second would be to develop a method for monitoring changes in the polymer network.

The impact that network structure, specifically crosslinking, has upon the actuation of polypyrrole is the subject of the work presented in this thesis. Prior to presenting our research findings, a discussion of the pertinent issues and relevant literature will be given.

2.0 The structure of polypyrroles

2.1 Neutral and oxidized forms

Polypyrroles are conjugated polymers containing a system of alternating double and single carbon-carbon bonds, allowing the delocalization of pi electron density along the polymer chain as shown in figure 2.1(a). However, this representation is just one of two forms that polypyrrole can take.

(a)

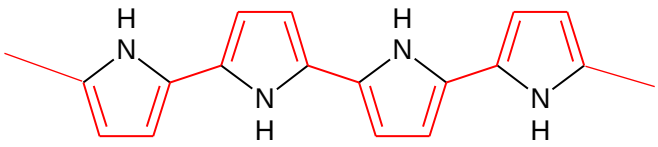

(b)

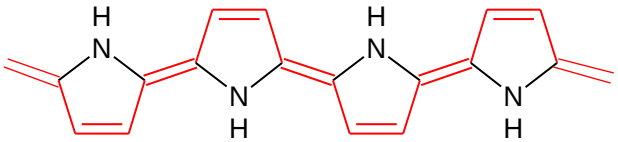

Fig 2.1 Forms of polypyrrole (a) neutral (aromatic) form (b) oxidized (quinoid) form.

The form shown in figure 2.1(a) is the "neutral" form of the polymer. This form contains pyrrole units that are more aromatic in nature than the alternative, oxidized forms of the polymer, shown in figure 2.1(b), which contains pyrrole units that are

"quinoid-like" in nature. The oxidized form can be converted to the neutral form by reduction and visa versa. However the neutral form is particularly unstable with respect to the oxidized form of the polymer, and special steps need to be taken in order to study this form of polypyrrole e.g. synthesis within a oxygen-free environment, such as a glove-box, followed by dedoping.

Since it is more stable, the oxidized form is the form typically obtained during synthesis. This is due to the fact that the polymerization potential of polypyrrole is greater than the oxidation potential of the polymer. As a consequence the polymer undergoes oxidation as it is formed. The removal of electrons upon oxidation leads to the formation of "hole" like structures known as polarons. Further oxidation of polarons typically occurs and results in the formation of related structures known as bipolarons[21]. These structures have a unit charge in the case of a polaron and two unit charges in the case of a bipolaron and are depicted in figure 2.2.

(a)

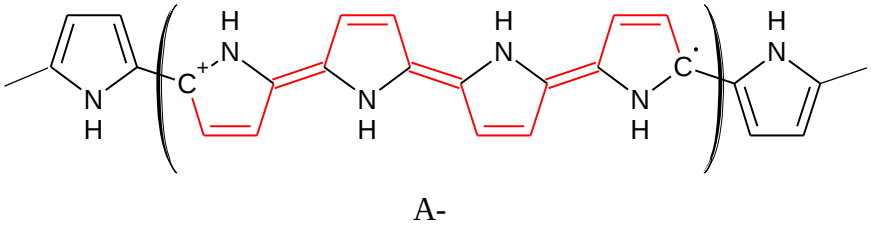

(b)

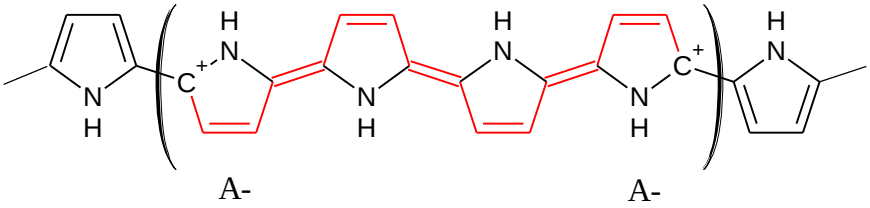

Fig 2.2 Structure of (a) polaron and (b) bipolaron. (A^- represents dopant / counter anions)

Both structures are able to accommodate positive charge by delocalization across adjacent monomer units, giving a positively charged section of the polymer chain which is "quinoid like" in nature. These structures can be thought of as positively charged "particles" or "holes" due to the fact that they can move throughout the polymer network and are responsible for the conducting properties of these polymers. Conduction within these polymers has been shown to be the result of both the direct

movement of polarons and bipolarons along the polymer chains by a process of localized "relaxation" of the polymer chain (quisi-1D conduction of the polymer) and also between chains by a process known as "hopping" (inter-chain coupling). The relative contribution of these modes towards conduction depends upon conditions such as the doping level and temperature. In addition, it also depends upon the structural properties such as the degree of ordering of the chains, the density of structural and/or chemical defects. Great advancement in the understanding of conduction within conjugated polymers has taken place in recent decades and excellent reviews exist on the topic[22,23].

For polarons and bipolarons to form the polymer chain has to be capable of undergoing rotation to be coplanar with adjacent pyrrole units. This is a necessary condition for pi electron density to be delocalized via conjugation and hence for polarons to form. Substituents within the pyrrole molecule at the pyrrollic nitrogen or beta positions can increase steric crowding and make it more difficult for the polymer chain to become coplanar, making polaron and bipolaron structures more difficult to form. This results in an increase in the torsional angle between adjacent rings of the polymer chain and typically leads to lower conductivity within the polymer[24].

2.2 Counter-ion / dopant

Electropolymerization of polypyrrole necessitates the use of a suitable electrolyte containing counter ions which are typically employed in high concentrations. Not only are these counter ions necessary for the electropolymerization process to take place, but they are also incorporated at high levels within the polymer matrix to become an integral part of the polymer. The properties of the counter ion have a major influence on both the polymerization process and subsequent structure and properties of the resultant polymer.

The counter ion should be capable of being readily incorporated into the growing polypyrrole film and also be chemically and electrochemically stable for efficient polymerization to take place.

As the polypyrrole network is formed and oxidized to form polaron and bipolaron structures the counter ion is incorporated into the growing polymer, where it becomes associated with the polaron and bipolarons in order to compensate the charge. In this context the counter ions are referred to dopant ions. Dopant levels can be as high as one dopant ion for every three pyrrole monomers[25].

The presence of dopant ions within the polymer matrix is essential for actuation to take place. In particular, the size of the dopant will determine whether or not it can be readily exchanged between the polymer film and the surrounding electrolyte during actuation. Relatively small dopants tend to be mobile and large dopants immobile. The mobility

will determine the nature of the actuation mechanism that takes place. Large immobile dopants such as dodecylbenzenesulphonate (DBS^-) tend to give better actuating films and have been used exclusively in the work presented in this thesis. The structure of DBS^- is shown below in figure 2.3.

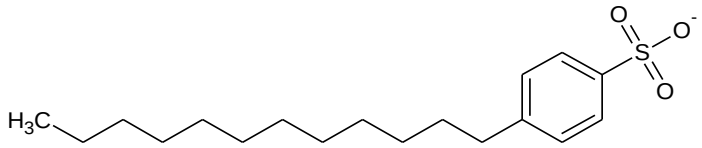

Fig 2.3 The structure of the DBS^- ion; a large immobile dopant.

The high concentrations of counter ions employed during electropolymerization will affect the conductivity of the solution and hence the rate of polymerization. In addition, the high levels of dopant incorporated within the polypyrrole matrix will exert a major influence on the physical and mechanical properties of the film. For example the type of counter ion employed can exert a marked effect on the polymer-solvent interactions. This type of interaction is well known for similar macromolecules (proteins) where it can lead to dehydration of the macromolecule. Dehydration of polypyrrole films can have a marked effect on the structure and stability of the resulting films.

Polypyrrole films are known to be biocompatible and this makes them suitable for cell biology and medical application. However, the type of dopant ion incorporated within the polypyrrole matrix can influence their biocompatibility. One recent study has shown that immobile dopants such as DBS^- are more biocompatible than smaller mobile dopants[6].

2.3 Solvent

The solvent used to prepare electropolymerization solutions is more than just a reactive medium as it participates in the auxiliary (counter) electrode and becomes an integral part of the polymer matrix. A number of solvents can be used: water, organic solvents and ionic liquids.

The solvent should be as pure as possible, capable of dissolving the monomer and counter ion in suitable concentrations and not undergo decomposition at the potential employed during electropolymerization.

The nature of the solvent can determine the conformational nature of the resulting polymer, with the chain folding and unfolding in different solvents to either protect or expose their hydrophobic groups, in a similar manner to proteins. The solvent will also influence conditions close to the surface of the working electrode (the electroreaction

zone), where polypyrrole is formed and deposited. Adsorption at the surface of the working electrode depends upon its solubility in the solvent. If the polymer is too soluble it can lead to poor deposits due polymer moving away from the electroreaction zone before it is deposited.

It is possible that in cases where the solvent is unlikely to solvate the anions, such as acetonitrile, pyrrole monomer can possibly solvate the anions instead. This would explain why polypyrrole films formed using acetonitrile and perchlorate are less porous and more dense, as might be expected due to the higher monomer concentrations that would be present in the electroreaction zone by anions solvated with pyrrole molecules[26].

The use of solvents which are capable of stabilizing pi segments along the polymer chain, such as propylene carbonate, can increase both the reactivity and stability of the polymer[27].

Recently ionic liquids have been employed as electrolytes in the synthesis of polypyrroles. These solvents are molten (liquid) salts at low temperatures (less than 100^{o}C). These electrolytes act as both the solvent for the pyrrole monomer and at the same time provide the electrolyte ions necessary for electropolymerization. The use of ionic liquids results in distinctly different morphologies compared to conventional electrolytes[28].

2.4 Network structure and defects.

The electropolymerization of polypyrrole results in a polymer network structure containing linear, branched and crosslinked sections. Substitution in both the alpha and beta positions is necessary for branching and crosslinking to take place. Branching and crosslinking are often referred to as defects since they adversely affect the geometry of the chain and disrupt its conjugation, impacting upon its conductivity[29].

The ratio of linear: branched: crosslinked structures likely depend upon a number of variables employed during synthesis such as the polymerization potential[30]. An excellent series of publications by Yurtsever et al. have employed quantum mechanical techniques to estimate the probability of branch formation in polypyrrole[31,32]. Their simulations give a branching of 20% for room temperature polymerization and show a slight dependence on temperature, with increasing temperature resulting in increased branching.

Linear sections of the polymer network are considered more likely to undergo a form of non-bonding interaction known as pi stacking. The presence of pi stacking and the increased ability of linear sections to pack more efficiently/closely compared to branched and crosslinked chains, is believed to result in a more dense polymer[33].

Whereas, an increase in the branching and crosslinking makes it more difficult for the polymer network to be packed as efficiently/closely and likely leads to a less dense and a more open/porous structure.

It is possible to efficiently extract non-crosslinked material (gel) from polymers that display low levels of crosslinking using continuous (soxhlet) extraction with a suitable solvent. This forms the basis of gel content determination and can be used to make an indirect assessment of the levels of crosslinking of some polymers.

Additional defects can occur as a result of the chemical decomposition of the polymer chain. This can occur if too high a polymerization potential is used during polymerization and is known as overoxidation. Figure 4.3 (SectionC) shows examples of this type of defect. In addition defects can be formed due to the twisting of the polymer chain, so that the delocalization of pi electron density in that section of the polymer is made more difficult or even prevented.

2.5 Crystallinity and molecular order

Electropolymerized films of polypyrrole are highly disordered and display only diffuse X-ray scattering[34]. However, evidence for small crystalline regions embedded within the amorphous matrix has been provided by electron diffraction patterns. A monoclinic structure for these small regions has been proposed for neutral polypyrrole by Geiss et al., from their analysis of the line spacing of diffraction patterns[35]. The orientation of the nitrogen atoms is such that adjacent nitrogen atoms are on opposite sides of the chain. These authors propose that the crystalline regions are made up of planar chains which arrange themselves into sheets with spacing similar to graphite. Support for such a packing arrangement comes from studies on single crystal X-ray analysis of pyrrole dimers and trimer[36].

One specific study of the X-ray diffraction patterns of polypyrrole alkyl-sulphonates[37] shows evidence of a higher degree of order compared to polypyrroles containing smaller dopant anions e.g. BF_4^- (See figure 2.4). In addition to the typical peak originating from polypyrrole phase, a second peak is displayed corresponding to a dopant phase. The long spacings, d, of these peaks are linearly correlated to the alkyl chain length, n, by the linear formula: $d(n) = (0.19n + 1.21)$ nm. These authors have proposed a lamella structure for these ordered regions which extend only about three “lattice planes” in each direction embedded in an amorphous matrix. The fact that the majority of the polymer is in a state of disorder is indicated by the absence of higher orders of the small angle peak and by its shape.

(a) (b)

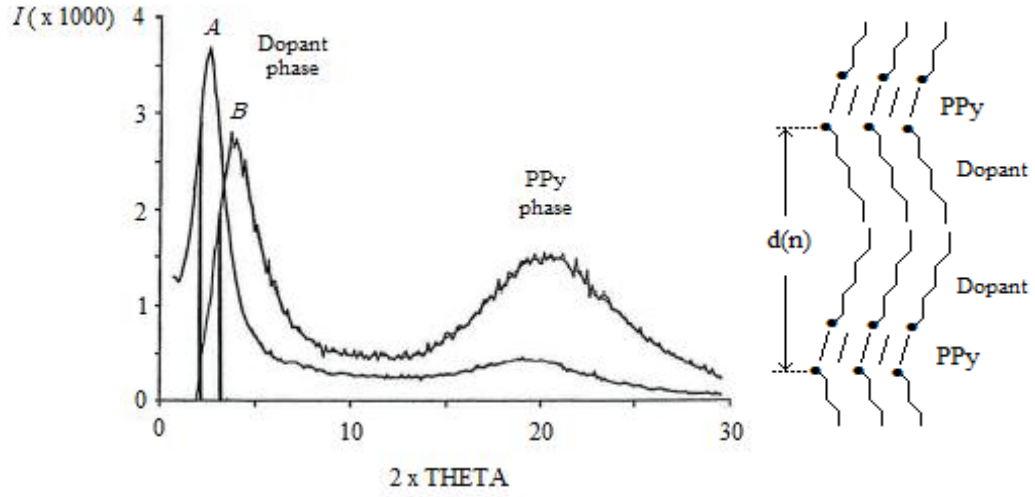

Fig 2.4 X-ray diffraction pattern for PPy doped with tetradecane-1-sulphonate (A) and octane-1-sulphonate (B). The peaks at $2\nu = 15^{o}$ to 30^{o} correspond to the oxidized PPy phase and the intense small angle peaks at $2\nu = 2^{o}$ to 5^{o} correspond to the dopant phase.

Planar dopants such as DBS^{-} tend to increase the degree of anisotropy compared to nonplanar dopants such as ClO_4^{-} which appear isotropic in X-ray diffraction studies[38,39]. In this sense the dopant is considered to act as a template for ordering the polymer chains.

The degree of anisotropy found in polypyrroles has also been found to be dependent on a number of other factors. The molecular order has been found to increase with low polymerization temperatures[40], high anodic polymerization potentials[40], high dopant: monomer ratios in the polymerization electrolyte[41] and by mechanical stretching[42].

Anisotropy has been shown to be greater for very thin films which have been prepared using very short polymerization times[43]. The increase in molecular order has been explained by the influence of the working electrode, with the polymer films being more ordered close to the electrode. However, this degree of order decreases at greater distances from the surface of the electrode.

Conditions which favour increased order in the polymer have also been found to increase the conductivity and visa versa. It is likely that the molecular ordering is driven by an increase in the conjugation length of the polymer.

Despite the preceding discussion which has centred on the level of order observed within some polypyrrole films, the degree of crystallinity is very low in these polymers, and the bulk film is typically amorphous.

2.6 **Surface morphology and film density**

Polypyrrole films are typified by a "cauliflower-like" surface morphology when observed under a microscope. However, it has been shown to be possible to eliminate this morphology through the careful polishing of the electrode[44].

One factor that has been identified as influencing the morphology is the type of dopant. However, in one study using a range of dopants, the differences in morphology only became noticeable as the film thickness increased. Below one micron thickness the films were indistinguishable and were typified by globules of diameter 100-300 nm and height 10-30 nm. For films having a thickness greater than five micron, differences in the size of the "cauliflower" structures were observed.

AFM has been used to observe the formation of these cauliflower-like structures, which form very early on as "micro-islands" on the surface of the gold working electrode, which merge as the film grows to form close-packed nodular grains[45]. Another study has shown a correlation between the nodular surface morphology and the surface potential and propose that the nodular regions are more dopant rich and highly conducting[46]. Transmission electron microscopy (TEM) has been used to examine the cross-sectional structure of polypyrrole films and reveals that the large cauliflower-like structures are the "caps" of cone-shaped structures that extend down to the surface of the electrode[47].

It has been shown that the densities of electropolymerized polypyrrole films depends upon the dopant and other synthesis conditions. Polypyrrole films electropolymerized at low temperature (- 40 ^{0}C) with PF_6^- have given films of density of 1.4 g/cm^3, whereas the density of the same films grown at room temperature decreased to (0.6-0.8 g/cm^3)[44].

2.7 Physical properties.

The physical properties of polypyrrole depend upon several factors, such as: the extent of crosslinking and branching present within the polymer network, the type and levels of dopant and solvent within the polymer matrix. These factors are determined by the synthesis condition employed during electropolymerization such as: the type and concentration of electrolyte, the current density, potential employed, the temperature, pH and other variable within the electrochemical cell.

Polypyrrole display good strength. Their high Young's modulus (0.05 to 100 GPa) and tensile strengths (1MPa to 1 GPa) enables them to exert considerable forces during actuation[5]. The range in these values serves to illustrate that the strength of the polypyrrole produced depends on the system (dopant/solvent) and synthesis conditions employed, and is under the control of the person undertaking the synthesis.

Like all polymers, polypyrroles undergo plastic deformation under sustained loads (creep). However, for applications which do not typically involve high loads for extended periods of time e.g. biomedical applications, this will not be a problem

The strength and resistance to plastic deformation will increase with increased levels of crosslinking within the polymer network. Increased levels of solvent such as water which enter the polymer during actuation (solvent swelling via the Osmotic effect) will also affect the strength of the polymer[48,49]. The presence of solvent within a polymer matrix is known to exert a plasticizing effect, the extent of which will be dependent upon the type and amount of solvent present[50].

Polypyrrole can demonstrate large actuation strains from a few percent (in plane) to over 30 percent (out of plane)[51]. They do however display relatively slow actuation speeds (> 1 Hz) for films several microns thick, due to the volume change being dependent upon mass transport (diffusion limited process). In addition polypyrroles display poor electrical to mechanical efficiency (typically 1 % or less)[5].

The actuation speed of polypyrrole films can be increase by employing thinner films, higher driving potentials and incomplete electrochemical cycling. For medical applications such as those within the body it is possible to use the temperature of the body to actuate the material but this is limited to applications requiring a single movement of the device upon insertion such as stents[5].

Despite these current limitations, other artificial muscle technologies face greater challenges[5].

3.0 Synthesis of polypyrrole

3.1 Electropolymerization

Polypyrroles can be synthesized by chemical or electrochemical polymerization. However, electropolymerization tends to be favoured because it provides good control of film thickness and morphology, and produces cleaner polymers compared to chemical polymerization. More recent techniques are plasma polymerization[52] and enzyme catalysis[53].

Different methods can be employed to deposit the polypyrrole films electrochemically including: potentiostatic (constant potential), galvanostatic (constant current) and potentiodynamic (scanning potential) techniques[26].

The intrinsic properties of polypyrrole are highly dependent upon the electropolymerization conditions employed. There are many parameters which have been shown to influence the properties of the polypyrrole formed such as: the nature of the electrolyte, solvent, pH, temperature, monomer and dopant concentrations.

The global polymerization reaction is summarized in figure 2.5 and reveals that hydrogen ions are formed which is observed by an increase in the pH of the solution and that there is a net release of electrons. It also serves to illustrate that the polymer is produced in its oxidized form (as indicated by the np^+ term).

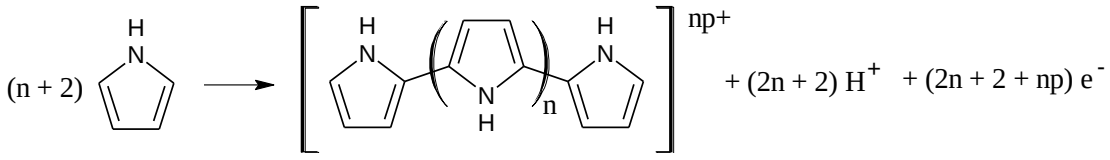

Fig 2.5 Global polymerization reaction for polypyrrole.

3.2 Mechanism of pyrrole electropolymerization

The mechanism of pyrrole electropolymerization is a controversial subject. Several alternative mechanisms have been proposed, with no one mechanism being universally accepted[54]. Although the mechanism proposed by Diaz[55,56] is the one most encountered in the literature, other mechanisms have been proposed and have evidence supporting them. The main difference between the different mechanisms that have been proposed to-date is the initiation step, with each mechanism proposing a different one, ranging from electron transfer, proton transfer and direct radical formation[54].

The main difficulties that have been encountered in determining the different stages in the reaction are the speed of polymerization, intractable and non-crystalline nature of polypyrrole. The last two factors make structural characterization and the analysis of physical properties exceedingly difficult.

It may very well be that electropolymerization can take place via more than one mechanism operating in parallel. The discussion that follows will outline the mechanism proposed by Diaz's, which is the most accepted mechanism in the literature.

3.3 Diaz's mechanism

The first step is the oxidation of the monomer at the surface of the electrode to form the radical cation (I):

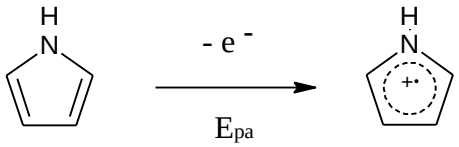

(I)

The second step is the dimerization of two radical cations via their alpha positions to give the dihydromer dication (II):

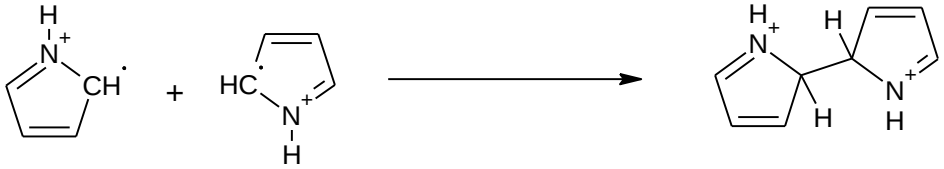

(II)

Step three is the loss of two protons to form the aromatic dimer (III):

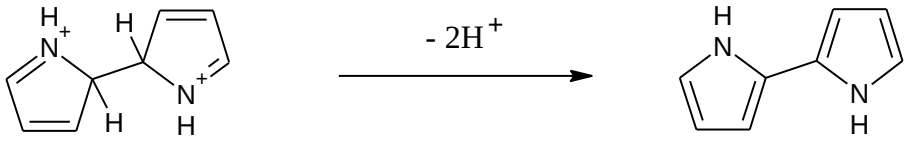

(III)

Step four involves the oxidation of the dimer formed in step three to give the dimer radical cation (IV):

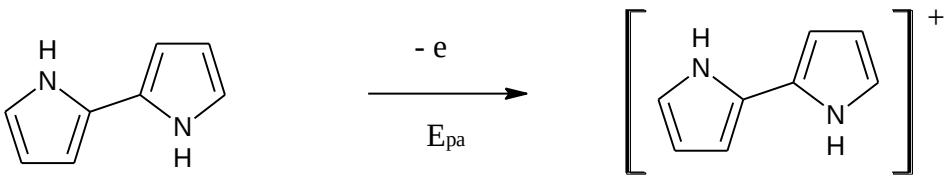

(IV)

Step five is the reaction between dimer radical cation (IV) and a monomer radical cation to give the trimer dication (V):

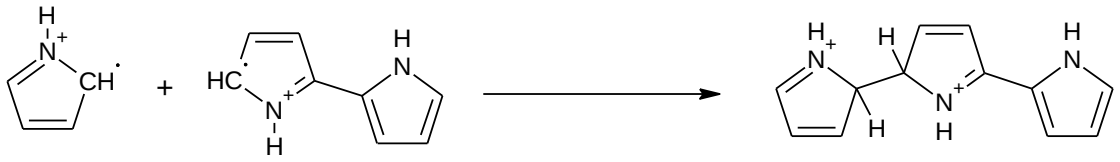

(V)

Step six is deprotonation of (VI) to give the neutral trimer:

(VI)

This process continues (propagates), giving longer length pyrrole oligomers and ultimately polypyrrole. The steps illustrated above depict coupling exclusively in the alpha position. Although exclusive coupling in the alpha positions is likely to occur for dimers – short chain oligomers, it is believed that a critical chain length is reached where coupling in the beta positions also becomes possible leading to alpha-beta and beta-beta bonds in addition to alpha-alpha bonds. Coupling in three positions of the pyrrole ring leads to branch formation and the possibility of crosslinking. Ultimately, coupling in all four positions in the pyrrole ring is a possibility that cannot be ruled out for some positions along the growing polymer chain for highly branched and crosslinked polymer. However this type of coupling will be more difficult compared to incomplete substitution of the pyrrole ring, due to steric factors.

Electropolymerization does not lead to the neutral polymer, but rather produces a highly oxidized structure which exists in equilibrium with the neutral (reduced) form:

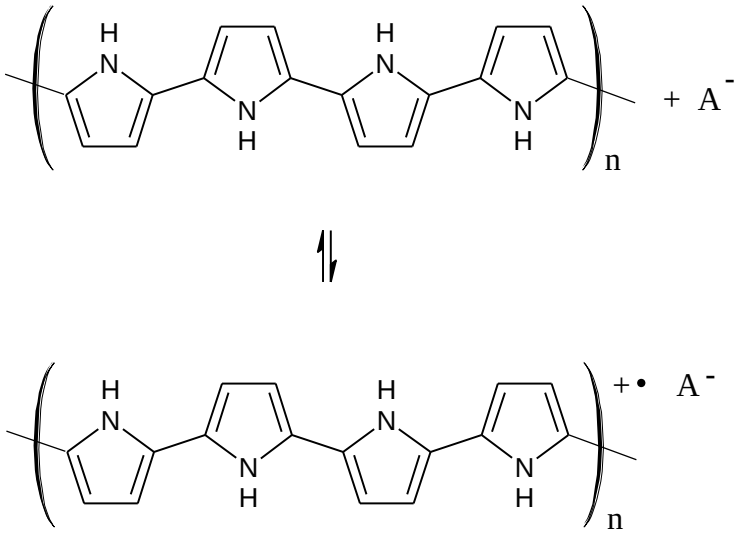

The extent of oxidation of the polymer network will impact upon the conductivity and ability to actuate. These oxidized structures (polarons and bipolarons) will be paired with dopant/counter ions, due to the requirement for charge neutrality. The equilibrium that exists allows the polymer to be "switched" between oxidized and reduced forms by application of a suitable electrical potential.

4.0 Crosslinking in polypyrroles

4.1 Evidence for crosslinking in polypyrrole

The intractable nature of polypyrrole is considered to be strong evidence of substantial crosslinking in the unsubstituted form of the polymer[57]. Only when specific steps are taken has it proved possible to obtain soluble forms of the polymer. Two approaches have been used. One approach has been to substitute the beta positions of the pyrrole ring and thereby block substitution leading to crosslinking[58]. The second approach has been the use of solubilizing dopants such as sodium bis(2-ethylhexyl) sulfosuccinate, which are believed to destabilize the polymer-polymer interactions relative to the polymer-solvent interactions[59]. The size of the dopant is another factor which might contribute towards dopant induced solubility, with large dopant ions reducing inter-chain interactions and increasing the separation between chains making crosslinking more difficult.

The ingenious use of dipyrrinone end groups in one study[60] has supplied one of the few reported pieces of evidence for the presence of α–β and β–β bonding. The dipyrrinone

molecule when incorporated within a growing polypyrrole chain leads to chain termination, hence the term dipyrrinone "end group". Dipyrrinone can be synthesized with different substituents within the β–positions. The authors of this study used both methyl and ethyl substituents as part of the study. They did so for two reasons. The first was to alter the C:H ratio of the polypyrrole formed once incorporated within the growing chain. The increase in C:H for these copolymers then allowed the mean chain lengths of the polymer to be determined via elemental analysis. The second reason was to be able to block some or all of the β–positions within the dipyrrinone end groups and be able to selectively allow or block substitution of the end group.

Their approach was to copolymerize pyrrole and dipyrrin-1(10*H*)-one end groups together and determine the average chain lengths, polymer yields and soluble residue (gel content). They noticed that the copolymers had relatively short average chain lengths of 20-50 units terminated by two dipyrrinone end groups. The polymer films gave relatively low soluble residues compared to similar length polymer chains that they produced using 3,4-dimethyl-1H-pyrrole and dipyrrinone end groups with all of their β–positions substituted with ethyl groups. This form of polypyrrole cannot produce α–β and β–β bonding since all the beta positions are substituted by either methyl or ethyl groups. The significantly lower soluble residues obtained for the copolymers of pyrrole with dipyrrinone compared to the similar length copolymer chains for 3,4-dimethyl-1H-pyrrole with dipyrrinone, the authors propose, can only be explained by the presence of crosslinking via α–β and β–β bonding.

This ingenious approach makes use of a β–blocking strategy and the formation of copolymers and is a similar approach to one that has been implemented in the work here (see Section 3).

4.2 **Indirect assessment of crosslinking**

For crosslinked polymers the molecular weight parameter is meaningless and it is the density of crosslinking which is of greater value in understanding their behaviour.

The crosslinking density of polymers is known to correlate strongly with physical properties such as solvent swellability[57]. It also correlates with the extractable content of the polymer, known as the gel content[61]. The determination of the degree of swelling of a polymer and its gel content are commonly used for assessing the extent of crosslinking by the polymer industry. For example, they have been used to monitor the affect that UV irradiation time has on the crosslinking reaction of epoxy-acrylate polymers[62].

Crosslinking density is also known to correlate with the physical properties of polymers such as their strength and toughness[57]. Techniques such as instrumented

nanoindentation are being increasingly used to study polymers and obtain metrics related to their physical strength, such as: the reduced Young's modulus of elasticity, hardness and creep[63-65].

These methods measure changes in the crosslinking density indirectly through a correlation with related changes e.g. solvent swellability. A direct assessment of crosslinking would be inherently more satisfying. However, despite an extensive search of the literature, there are few reports of a direct assessment of crosslinking (and branching) in polypyrroles. These are discussed in the next section.

4.3 Direct assessment of crosslinking

4.3.1 X-ray photoelectron spectroscopy (XPS)

The structure of electrochemically synthesized polypyrrole films has been investigated using XPS. In addition to revealing information on the nature of the polymeric cation (polaron/bipolaron) and its counter ion (dopant) it has been used to reveal the degree of "structural disorder"[66].

Standard line shape analysis of the "complex" C1s signal using Gaussian decomposition resulted in three peaks (see figure 2.6). The two peaks centered at 283.6 eV and 284.5 eV have been assigned by these authors to pyrrole β and α atoms in the idealized α–α'-linked linear chain monomer (see insert in figure 2.6). The third peak centered at 285.4 eV on the higher binding energy side of the C1s peak has been assigned by the authors to crosslinked, chain-terminating or non-α–α' bonded carbons as well as carbons in partially saturated rings. They refer to these types of carbon atoms as "disorder" type carbons, in that they represent a departure from the "idealized" structure for polypyrrole (infinitely long α–α'-bonded linear chain).

We considered using this approach in our work to correlate increases in crosslinking and branching with an increase in the area of the "disorder" peak. However, after seeking expert advice[68], a number of concerns were raised. The first concern was over the uniqueness of the curve fitting analysis, given the relatively featureless C1s peak. A second concern raised was that the broadening of the C1s peak might more likely be due to doping effects and hence it would be very hard to extract information about possible changes in crosslinking or branching. In light of these issues, this approach was not used in the work presented in this thesis. However, even if the approach were valid, this "disorder" represents a range of different non-idealized structures and is not specific to crosslinking or branching e.g. changes in the "disorder" might be the result changes in the number of non-α–α' bonded carbons as well as carbons in partially saturated rings.

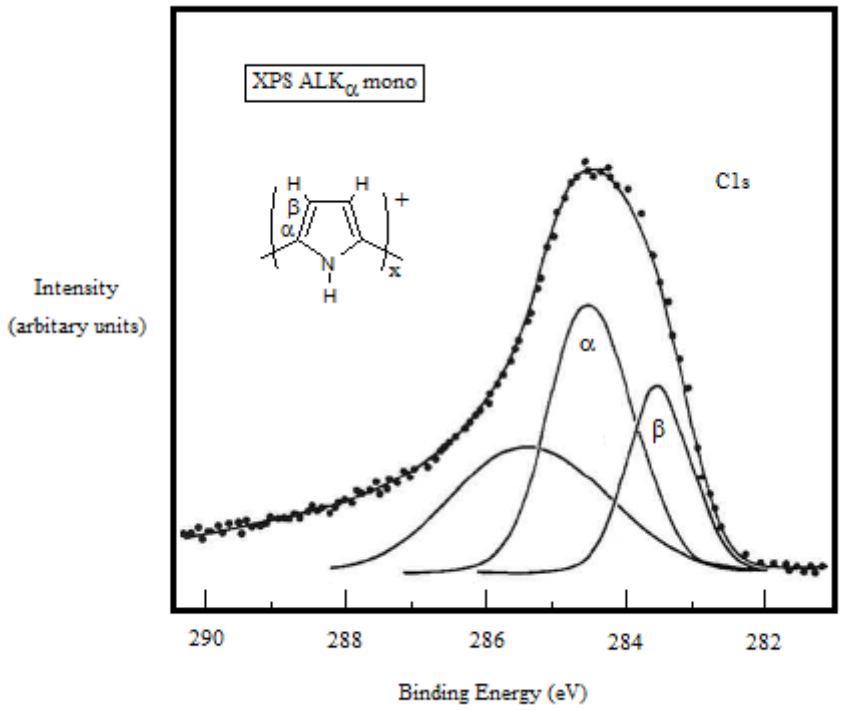

Fig 2.6 C1s XPS core level of polypyrrole perchlorate. The line through the data points represents the best fit obtained from superposition of Gaussian peaks. The lower lines show the contribution from β, α, and disorder-type carbon atoms.

4.3.2 Chronoamperometry

The general formula for electropolymerization (figure 2.5) reveals that two electrons are involved for each C-C bond formed. Therefore each time a monomer unit is added to the end of a growing linear chain two electrons are involved. For an infinite linear polypyrrole chain this would require 2n electrons. Higher values than this indicate crosslinking of the polymer chains. If it were possible to reliably calculate the number of electrons for each monomer unit that yields bonds with other monomers of the polymer, it would allow a quantitative assessment of the degree of crosslinking to be made.

This is an approach that has been adopted by one group[69] in studying crosslinking in polythiophene, which is an analogous polymer to polypyrrole. This is an approach that we ourselves initially considered. The authors of this work refer to the average number of electrons involved in bond formation per monomer unit as $n_{av.}$ However, it is not clear to us, how the authors have been able to calculate this parameter. They have shown that there is a difference in the numbers of electrons consumed per monomer unit, n_{av}, when the solutions are stirred compared to when they are unstirred (quiescent),

with the n_{av} values for the quiescent solutions being significantly higher than those of the stirred solutions in all cases. Similarly, they showed that n_{av} values depend upon the type of solvent. For the majority of the polymers synthesized the n_{av} values were significantly higher than 2 and therefore provide evidence of high levels of substitution and therefore imply high levels of crosslinking. For one of the polymers formed a n_{av} of 7.57 is given by the authors. This would imply that 95 % of the monomer units are completely substituted (7.57/8 x 100 %) and imply an extremely high level of crosslinking.

As stated earlier, such an approach was considered at an early stage in this work. However, it was felt that a reliable calculation of n_{av} would be difficult to achieve. This is because the charge which flows during polymerization has several sources. Not only does charge flow occur due to bond formation and oxidation of the polymer, but it also flows due to Faradic charging and can also be the result of competing (parasitic) reactions that occur within the electrochemical cell at the same time as polymerization.

It is still unclear as to how the authors of this work have calculated their n_{av} values and whether they have taken into account Faradic charging and potential parasitic charge. It is difficult to see how a 95 % level of substitution of all positions within monomer is possible on stereochemical grounds. If their measurements and calculations are correct it would provide the first truly quantitative measurement of crosslinking within the field of conducting polymers and, although their study was undertaken for polythiophene, an identical approach would also be applicable to for polypyrrole.

4.4 Other methods considered for making a direct assessment of crosslinking

4.4.1 FTIR Spectroscopy

There will be different vibrations for the pyrrole C-H bonds compared to the pyrrole C-C crosslinked/branched bonds. On this basis, it might be thought that FTIR spectroscopy might be able to reveal increased levels of substitution within the pyrrole ring (loss of C-H signal) and that this would correlate with increased levels of branching and crosslinking. This approach has not been reported in the literature. When considering the feasibility of implementing such an approach it was decided that this would be unlikely. There are a number of issues, both general and specific to the chosen system (PPy(DBS)(aq)), that make the successful implementation of such an approach very difficult to achieve.

In general the resolution possible with FTIR spectroscopy is less than that of other types of spectroscopy such as NMR. It would therefore be difficult to resolve pyrrole C-H and

C-C crosslinked/branched bonds from adjacent peaks originating from other parts of the molecule.

It was considered that the best approach would be to monitor the decrease in the pyrrollic C-H peaks that would accompany increased substitution of the pyrrole ring and hence increased branching and crosslinking. To monitor the appearance of the peaks corresponding to C-C crosslinked/branched bonds would be more difficult given the large number of substitution patterns that can exist within polypyrroles[31] in addition to the aromatic C-C bonds within the pyrrole ring itself. This would likely mean that the C-C vibrations corresponding to crosslinked/branched bonds would overlap with other C-C vibrations to form a broad complex unresolvable peak.

For the chosen system, PPy(DBS), interference from the presence of both aliphatic and particularly aromatic C-H bonds that are present within the DBS dopant, would again mean that a change in the pyrrollic C-H signal would be difficult to observe due to the presence of these interfering peaks. These difficulties would likely be compounded by the fact that C-H vibrations tend to be of low intensity compared to other functional groups and can often be "hidden" by these larger/more intense peaks.

In addition to these issues, the locations of the C-H and C-C crosslinked/branched bonds will change depending upon the oxidation level of the polymer. Given that the polymer chain can exist in either the neutral (aromatic) state or the oxidized (quinoid like) state, the vibrational frequencies of the bonds will be shifted to different frequencies. Given the fact that the polaron and bipolaron structures associated with the oxidized polymer move throughout the polymer network, this is likely to lead to further broadening and potential overlapping of peaks.

Given these issues the decision was made not did not pursue FTIR spectroscopy as a potential means to monitor structural changes to the polypyrrole network, particularly due to the fact that the planned investigation was to focus on the use of DBS as a dopant. Having said that we have noted some difference in the pyrrollic C-H region for PPy(DBS) samples prepared using different polymerization potentials.

The prospect of monitoring changes in crosslinking and branching using FTIR are more likely to be achievable using non-organic dopants such as perchlorate (ClO_4^-) and would be aided by studying the polymer in its neutral state[70] (see Section D, 1.2 Further work).

There exist the possibility of using FTIR spectroscopy to indirectly monitor changes in the levels of branching and crosslinking by using a method developed by Menon et al, capable of obtaining a qualitative measure of the conjugation length in polypyrrole[71] based upon the theoretical work by Tian and Zerbi[72,73]. Defects that interrupt conjugation include branching and crosslinking. Menon et al have used a parameter

called the effective conjugation coordinate to assess the levels of defects within template-synthesized polypyrrole tubules and fibrils. As the conjugation length is increased, the intensity of the antisymmetric ring stretching mode at 1560 cm^{-1} is predicted to decrease in its intensity relative to the symmetric mode at 1480 cm^{-1}. As a result, the ratio of these intensities can be used to obtain a relative measure of the conjugation length.

This approach could not be confidently used in this work, due to potential interference from the presence of DBS^- counter ions, which contain aromatic carbon atoms.

4.4.2 NMR Spectroscopy

Nuclear magnetic resonance spectroscopy (NMR) is arguably the most powerful technique for determining molecular structure available to a chemist. Samples are dissolved in a suitable solvent, giving a liquid sample. These samples, typically display highly resolved peaks which can be readily assigned to different parts of a molecule. Peaks within 1H NMR spectra are assigned on the basis of their location (relative to an internal standard such as tetramethylsilane (TMS)), area integrals, multiplicity and coupling constants. If peak assignment is not immediately clear, other NMR experiments can be performed to aid assignment. For example Distortionless Enhancement by Polarization Transfer (DEPT) can be used to determine the presence of methyl, secondary, tertiary carbon atoms in 13C NMR spectra. The interpretation of NMR spectra is often aided by other spectroscopic information, obtained from Fourier Transform Infrared Spectroscopy (FTIR) or from Mass Spectrometry (MS), such as the presence of specific functional groups or the molecular mass. This approach has been used in Section C, 2.2, of this thesis to confirm the structure of 3,4-dimethyl-1H-pyrrole.

When a sample is capable of being made soluble, such techniques are a powerful aid to structural elucidation and enable even subtle structural changes to be monitored. However, insoluble (intractable) samples such as polypyrroles are not amenable to such techniques. Although solid state NMR techniques exist and have developed greatly in the past decades, they yield spectra with broadened and overlapping peaks which are much more difficult to assign. To date solid state NMR spectroscopy has been used with limited success in the study of polypyrroles.

The structure of polypyrrole has been studied in the solid state using high-resolution solid-state 13C NMR spectroscopy[74]. However, it was not possible to resolve the broad aromatic 13C signal because of its complexity. This was due the presence of a number of magnetically non-equivalent aromatic carbon atoms within the polymer backbone as shown in figure 2.7.

Wehrle et al were the first to attempt to obtain structural information using 15N labeled polypyrroles in order to obtain 15N spectra with a high signal-to-noise ratio[75]. This approach offers the prospect of producing much simpler spectra than those obtained using 13C NMR spectroscopy, with an NMR line corresponding to each of the structures in figure 2.7. Unfortunately, it was not possible for them to undertake a successful analysis of the 15N cross-polarization/magic angle spinning (CP/MAS) spectra in the solid state due to insufficient resolution.

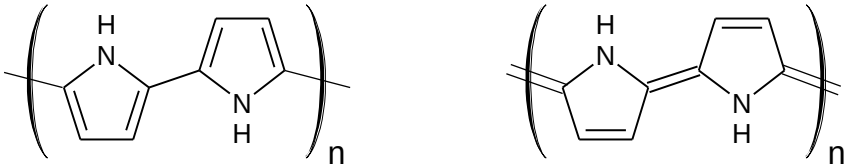

(a) (b)

Fig 2.7 PPy (a) aromatic form and (b) quinoid form.

The 15N CP/MAS NMR spectra of doped and undoped 15N-labeled polypyrroles in the solid state, prepared by electropolymerization, have been measured by high-resolution solid-state NMR[76]. The authors of this study, used computer fitting to decompose the broad 15N signal into four peaks. They also made use of a quantum chemical calculation to assist in the assignment of three of the four decomposed peaks. The major peak at 129 ppm was assigned to the nitrogen atoms in the quinoid form, whereas the other major peak at 113 ppm was assigned to the aromatic form. It was also proposed that the most likely source of the minor peak at 145 ppm was due to nitrogen atoms which are bonded to hydrogen atoms approaching other hydrogen atoms bonded to different atoms. If correct, these structural assignments would allow an alternative approach to the determination of doping levels (ratio of quinoid to aromatic) within the 15N-labeled polypyrrole films. However, as with all isotopically labeled compounds the kinetic isotope effect would be an additional complication that would need to be taken into consideration.

The assignment of NMR peaks corresponding to alpha-alpha, alpha-beta and beta-beta either directly within 13C NMR solid-state spectra or indirectly within 1H NMR solid-state spectra has not been reported in the literature. Had this information been available, along with information on the amount of end groups, it would allow an assessment of the extent of crosslinking and branching to be directly made. Unfortunately, this information is unavailable at present, and the prospect of a direct assessment of network structure (crosslinking, branching and end group) is currently out of reach.

In recent years the use of solid-state NMR relaxation techniques has been used to make an indirect assessment of the level of crosslinking within polymers. These techniques allow the levels of chain movements to be assessed, with a low degree of movement being indicative of a more rigid and more crosslinked polymer and visa versa. This approach has been successfully applied to the study of crosslinking changes in polymers, such as the curing of paints[77] and the vulcanization of tyres[78,79]. However, the success of such techniques depends upon the ability to distinguish between an NMR signal that originates exclusively from the polymer network and those that originate from the other components of the polymer matrix. For example solid-state 13C NMR relaxation of polypyrrole would be complicated by interference from other organic compounds that might be present such as the dopant e.g. NaDBS. In other words, the technique "sees" all the carbon atoms within the polymer regardless of their source. Similarly, the presence of water within the polymer either through polymerization within aqueous electrolytes or through absorption of atmospheric moisture, would be a source of interference using solid-state 1H NMR relaxation.

The successful use of solid-state NMR relaxation techniques in the assessment of crosslinking of polypyrroles has yet to be reported. However, such techniques have started to be applied to the study of crosslinking in other conducting polymers e.g. polyaniline[80]. In addition NMR imaging techniques have in recent years started to be used to assess crosslinking in polymers[81,82]. Despite the difficulties that would need to be overcome, such an approach may prove successful in the future.

4.5 Nanoindentation

In the work undertaken in this thesis two approaches have been used to monitor crosslinking levels. The first is by measuring the amount of irreversible expansion that occurs during actuation. This is the main finding from our work outlined in Section C, chapter 3, and will be discussed in-depth there. The second method that we have employed is commonly referred to as nanoindentation, which is a form of instrumented indentation. This method has been used in Section C chapter 4. Here we will review the method and outline the mathematics involved in calculating the elastic modulus and hardness using an approach known as the multiple point unloading method.

For crosslinked polymers such as polypyrrole the density of crosslinking is strongly correlated to physical properties such as strength and toughness[57]. Both the elastic modulus (E) and hardness (H) of polymer films increase with increased levels of crosslinking[64,83,84]. In keeping with this, the resistance of the polymer to plastic deformation would also be expected to increase with crosslinking. The resistance of a polymer to undergo plastic deformation can be monitored by the extent of creep[65] or the

ratio H/E^2. These materials' parameters can be determined using instrumented indentation / nanoindentation[85].

Nanoindentation allows the elastic modulus and hardness of films to be extracted from load-displacement measurements. The depth of penetration below the surface of the specimen is measured as the load is applied to an indenter. The known geometry of the indenter allows the size of the area of contact to be determined. The hardness of the specimen can then be from the area of contact and the corresponding load. The elastic modulus of the specimen can also be obtained from the "stiffness" of the contact, which is given by the rate of load and depth[86,87]. This approach, known as the multiple point unloading method or Oliver and Pharr method, is detailed in section 4.5.1.

In general nanoindentation hardness testing is undertaken with either pyramidal or spherical indenters, of which there are several different types available, each with its own relative merits. In the work undertaken in this thesis a spherical indenter has been employed as this type of indenter is particularly suitable for measuring relatively soft materials such as polymers[85].

A spherical indenter is typically constructed as a spherical tipped cone (spherocone) for ease of mounting in the instrument. Only the very tip of the indenter is allowed to penetrate the surface of the specimen. Usually, a plot of hardness versus penetration depth is made and if there is a plateau in the hardness values, then this is taken as the hardness of the film. As a general rule when measuring hardness, the penetration depth of the indenter tip is kept to less than 10% of the film, the influence of the substrate on the development of the plastic zone within the film is negligible. This "10% rule" does not apply to the modulus determination, however it is generally considered to be a good place to begin. It is best to perform a series of indentations from very low load to a reasonably high load and then plot the elastic modulus versus the penetration depth. Extrapolating the data back to "zero depth" can provide a value of the modulus for the film only[88].

Another source of interference that needs to be taken into account when analyzing data is the presence of "pile-up". The elastic equations assume that the contact circle is beneath the specimen surface (the surface "sinks in"). However, for some specimens material may be pushed upwards and be piled-up around the edges of the indentation. When this occurs more material is supporting the load than is assumed by the contact equations, with the result that the material appears harder and stiffer than it actually is. This behaviour can be corrected for during the analysis of the data and can be performed by instrument software (see section 4.5.2).

Recently, films comprising gold nanoparticles crosslinked with organic dithiols of various lengths have been synthesised[89] and studied using instrument indentation[90]. The use of instrumented indentation in this study has shown that shorter dithiol linker lengths results in an increase in both the elastic modulus and hardness of the films. This

corresponds to an increase in both the density of crosslinking and also the density of the gold nanoparticles. The increase in the elastic modulus is the result of increased crosslinking density caused by the use of shorter linker lengths. The increase in hardness with shorter linker lengths is due to the combined increase in the crosslinking density and the density of the gold nanoparticles. However, given the size of the nanoparticles, the primary source of the increase in the hardness will most likely be the increase in the crosslinking density.

Changes in density can also cause changes in the hardness of the material, with increased density leading to increased hardness. In polymers increased density can occur due to the association of linear lengths of polymer in a process known as spherulization[91]. This results in a semicrystalline polymer containing crystalline regions known as spherulites. These structures can be observed under a microscope using polarized light and typically have a "Maltese Cross" shape as shown in figure 2.8. An increase in the crystalline content of a semi-crystalline polymer can lead to a greater tendency towards brittle fracture.

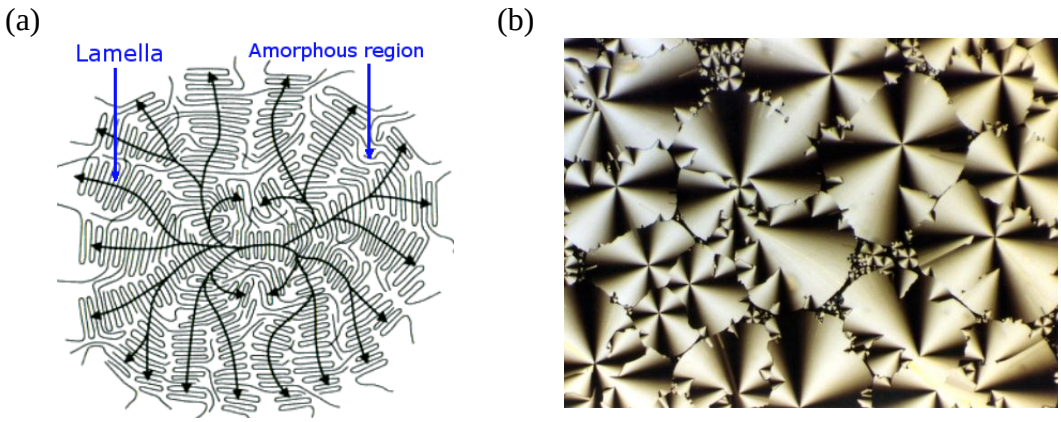

Fig 2.8 (a) Structure of a spherulite (b) Microscope image of spherulites obtained using polarized light.

The polypyrrole films that we have tested using instrumented indentation were first dried to remove absorbed water from the polymer. This was done so as to minimize any potential plasticising effects caused by the presence of water in the polymer matrix[50].

4.5.1 Multiple point unloading method

The multiple point unloading method developed by Oliver and Pharr uses the initial portion of the unloading curve to determine the hardness and elastic modulus of the specimen. Using this approach, the analysis procedure for a spherical indenter is outlined below[92].

For a given experiment comprising **n** indentation cycles there will be an associated total penetration depth $\mathbf{h_t}$ at a load $\mathbf{P_t}$ and a partially recovered depth $\mathbf{h_s}$ at a reduced load $\mathbf{P_s}$ ($\mathbf{P_s}$ would normally be 50% of $\mathbf{P_t}$). The depth $\mathbf{h_r}$ of the residual impression relative to the original surface that would be made if the indenter were fully unloaded is calculated from:

$$Hr = \frac{r.H_s - H_t}{t - 1}$$

Where:

$$r = \left(\frac{Pt}{Ps}\right)^{\frac{2}{3}}$$

The elastic component $\mathbf{h_e}$ and plastic component $\mathbf{h_p}$ of the indentation at each indentation cycle can be calculated from:

$$He = H_t - H_r$$

$$Hp = \frac{H_t + H_r}{2}$$

The radius of the circle of contact **a** in the plane of the original surface at each indentation cycle is calculated from:

$$a = \sqrt{2.R.Hp - Hp^2}$$

Where **R** is the radius of the spherical indenter.

Hardness **H**, reduced modulus $\mathbf{E_r}$, at each load step can be calculated as follows:

$$H_i = \frac{Pt_i}{A_i} = \frac{Pt_i}{\pi a_i^2}$$

$$Er_i = \frac{3}{4}\frac{Pt_i}{a_i.He_i}$$

Where: **i = 1 to n**

4.5.2 **Sinking-in and Piling-up (SIPU) analysis**

Because of possible piling-up or sinking-in around the perimeter of the spherical indenter contact, the true radius of the circle of contact $\mathbf{a_r}$ is related to **a** as determined above by the function $\mathbf{a_r = ca}$. The **c** value can be determined from plotting $\mathbf{log(Pt_i)}$ verses $\mathbf{log(a_i)}$, the slope giving Meyer's index **(2+1/n)**, thus allowing **c** to be calculated as:

$$c^2 = \frac{5}{2}\frac{2n-1}{4n+1}$$

Thus **H** and $\mathbf{E_r}$ calculated above have to be corrected by the factors $1/\mathbf{c^2}$ and $1/\mathbf{c}$, respectively.

5.0 Mechanism of electromechanical actuation

There are a number of changes that occur when polypyrrole undergoes redox switching. These include the carbon-carbon bond lengths along the polymer backbone[93-96], cis-trans isomerism[97], the angle between adjacent pyrrole units (the torsional angle) [98,99], polymer chain-solvent interactions[100], folding of the polymer backbone[101] and interchain interactions[102,98].

However, the principle mechanism by which actuation occurs is the movement of ions and solvent during redox switching. This mass transport of ions and solvent between the polymer and electrolyte is necessary in order to maintain charge neutrality within the polymer. A change in the electronic charge of the polymer must be compensated by an equivalent change in the amount of ionic charge. The polymer expands when ions and solvent (insertion) enter the polymer and contracts when they leave (deinsertion)[103-105]. It is possible for ions to move into the polymer during oxidation or reduction. There are

two possible modes by which polypyrroles can actuate. This is depicted by the equations shown in figure 2.9.

In equation (1) the ions (a^-) move into the polymer during oxidation and leave on reduction. The polymer therefore expands during the oxidation and contracts during reduction. This type of actuation occurs when the ions (a^-) are small mobile ions such as Cl^-.

Equation (2) illustrates what happens when the ions (A^-) are large immobile ions, such as DBS^-. As the polymer is reduced ($P^+ \rightarrow P^0$) cations (c^+) move into the polymer from the electrolyte to compensate the charge originating from the large immobile dopant ions (A-), causing it to expand. On oxidation ($P^0 \rightarrow P^+$) the reverse process occurs, with the large immobile ions (A^-) compensating the charge on the polymer ($P^+(A^-)$) and the small immobile cations (c^+) being expelled from the polymer, causing it to contract.

$$P^+(a^-) + e^- \leftrightarrow P^0 + a^- \qquad (1)$$

$$P^+(A^-) + c^+ + e^- \leftrightarrow P^0(Ac) \qquad (2)$$

Fig 2.9 Equations depicting two modes of actuation for polypyrrole. **Key:** P^+ = doped (oxidized) state of polymer, P^0 = undoped (reduced, neutral) state of polymer, $P^+(a^-)$ = small mobile anion (a^-) incorporated as dopant in polymer, $P^0(Ac)$ indicates that the cation (c^+, co-ion) is inserted during reduction to compensate charge on the large immobile anion (A^-).

Typically the ions that are inserted and deinserted are solvated and this increases the amount of strain compared to when the ions are not solvated. In addition, non-coordinated solvent (solvent not associated with the ions) can enter the polymer via osmosis. The movement of solvent into the polymer in this way causes it to expand (swell) irreversibly[48,49].

6.0 Techniques used in the assessment of volume change

Several different approaches have been used in the literature for the assessment of volume change in polypyrrole. However, considerable differences in the levels of strain have been reported. Estimates have ranged from less than 1 % to as much as 120 %.

Strains of up to 2% have been reported for freestanding films of polypyrrole doped with benzenesulphonate, in a direction parallel to the surface of the film[106,107]. These in-plane

strains were determined during electrochemical redox using a displacement transducer and a servo-controlled actuator.

In-plane strains have also been determined indirectly using a bending bilayer. Provided the elastic moduli and thicknesses of the bilayer are known, the degree of bending can be related to the strain by making a number of assumptions about the mechanical behavior. Using this method the in-plane strains of polypyrroles doped with a number of different anions has been undertaken[108] and values of up to 3.4% where obtained. Two studies[109, 110] have estimated the in-plane strain during reduction for polypyrrole dodecylbenzenesulphonate as being 1.7 % and approximately 2 %.

Another approach[111] that has been used to determine strains of polypyrrole films is to measure the thickness and area of the films before and after actuation. A difference of 10%, in all directions (in-plane and out-of-plane), was reported for polypyrrole perchlorate films after the first complete actuation cycle. This value is significantly higher than those reported by the other authors above. However, the volume change during the first electrochemical cycle is known to be anomalous and is typically higher than in subsequent cycles. The volume change for polypyrrole benzenesulphonate during the first electrochemical cycle was found to be more than twice as large as observed for later cycles[106].

A different approach has been the determination of the mass and density of oxidized and reduced films of polypyrrole perchlorate after their removal from the electrochemical cell and drying[112]. These authors noticed that whilst the mass increased by 35% on reduction, the density remained constant. They then concluded that the volume change must therefore also be 35%.

Other methods for making volume change estimates have been reviewed (Baughman et al). One method based on gravimetrical studies which determined the change in volume and weight of the film with charge, has given estimates of 120% for the volume change of polypyrrole[113].

Atomic force microscopy (AFM) has been used to investigate the actuation of polypyrroles. The absolute average z-piezo voltage has been monitored whilst scanning thin polypyrrole perchlorate film (620 nm) during redox cycling[114]. Their results showed a decrease in the film thickness during oxidation, a fact that is not in keeping with the known expansion of polypyrrole films employing small mobile anions such as perchlorate, during oxidation. In addition, the volume changes that they observed were not regular. These authors used the same approach to make volume change measurements on polypyrrole para-toluenesulphonate films. These results were an improvement on those undertaken on polypyrrole perchlorate films, in that the signs of the measured volume changes were in keeping with, in this case, the use of a relatively large immobile anion. They observed an initial increase of 10% during the initial reduction cycle which slowly decreased by 5%. During the subsequent oxidation cycles

they observed the volume to decrease by 5%. Again, however, the behaviour was not regular.

AFM has been used to study the out-of-plane strain of PPy(DBS)[51], where it has essentially been used as a profilometer to monitor height changes both prior to actuation and also during subsequent redox cycles. The method allowed real-time volume changes to be monitored in-situ in the out-of-plane direction. This technique showed that the thickness of PPy(DBS) increased by 35% in the reduced state compared to the oxidized state in the out-of-plane direction. This reveals that the volume change of PPy(DBS) is anisotropic, with the in-plane strain being approximately 2%, found in prior studies using the bending beam method.

This last study by Smela et al on PPy(DBS) is particularly relevant to the work presented in this thesis, also undertaken on PPy(DBS). This is not only because we have studied the same type of polypyrrole, but also because their technique like ours, determines the out-of-plane strain for films over a similar range of thicknesses.

In summary, it can be said that there have been many factors that have likely contributed to the variation in strains that have been reported in the literature for polypyrrole. One factor is the type of polypyrrole that has been studied, in particular the form of dopant that has been used, whether it is a small mobile dopant or a large immobile dopant. A second factor is whether the values reported are volume changes, in-plane strains or out-of-plane strains. This can lead to considerable differences as illustrated by the anisotropic expansion of PPy(DBS). A third factor will undoubtedly be due to the use of different techniques to obtain the reported values.

Section C Research contribution:

1. The development of laser-scan micrometry to characterize the electroactive performance of micro-actuating films

1.1 Experimental details

1.1.1 An overview of the laser micrometry setup

A laser scan micrometer (LSM) was used to make rapid, non-contact, dynamic measurements of the strain of polypyrrole films grown on a gold wire working electrode and actuated in an electrolyte. The actuations of the polymer films were controlled by means of a potentiostat (Metrohm µAUTOLAB III) and associated software (GPES). The laser scan micrometer (Mitutoyo LSM-501H) was controlled my means of a display unit (Mitutoyo LSM-6100) and the output signal was fed to the potentiostat where it was recorded simultaneously with the EC experiments. The setup is shown below in figure 1.1

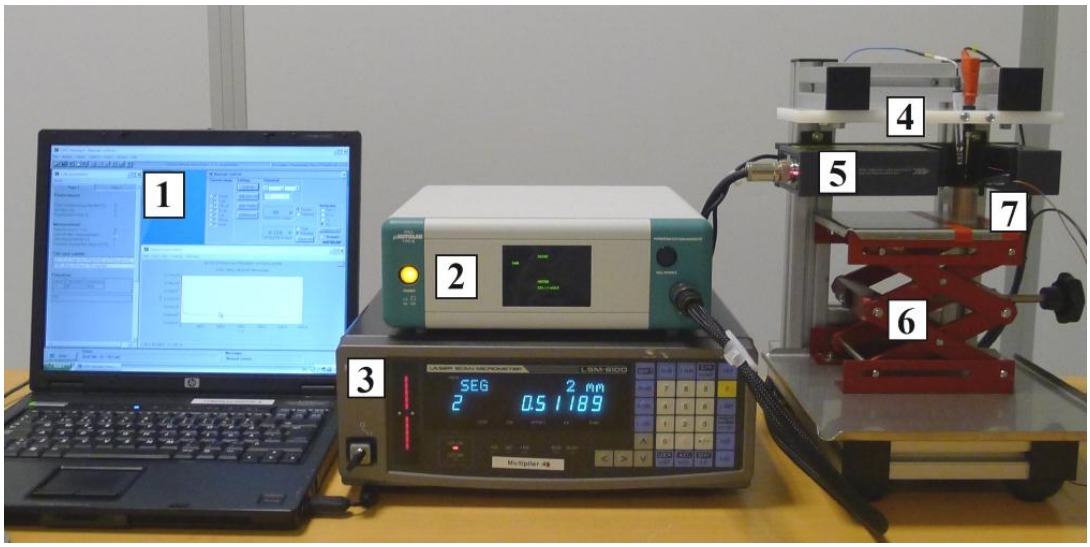

Fig 1.1 Actuation measurement equipment: 1. PC running GPES software, 2. Potentiostat, 3. LSM display unit, 4. Electrode support table, 5. LSM, 6. Lab jack, 7. Electrochemical cell.

The LSM was side mounted and securely positioned by means of a supporting frame to which anti-vibration gel feet were fitted to the base. An electrically insulating electrode support table was positioned above the LSM and also secured to the frame. This support was capable of x-y-z movement and allowed the precise positioning of the electrodes used during polymerization and actuation measurement. A lab jack was used to raise and lower the electrochemical cells facilitate their exchange.

1.1.2 The laser-scan micrometer

Unlike light emitted from a natural source, a laser provides extremely fine, rectilinear beams which do not diffuse (coherent light beams).

Using the properties of the laser beam, the LSM moves a scanning laser beam over the work piece and determines its dimensions by measuring the duration in which the beam is obstructed by the work piece. The beam not obstructed will reach the photoelectric element through the condenser lens and induce an output voltage. The output voltage will change according to the duration over which the laser beam is obstructed. Counting pulses generated during that period are used to determine the dimension of the obstructed portion.

Fig 1.2 Mitutoyo LSM-501H Laser Scan Micrometer.

The LSM employed in this work is shown in figure 1.2 and makes 1600 scans each second (6.25×10^{-4}s/scan) and can measure dimensional changes of up to 50 μm with a resolution of 0.01 μm and repeatability of ±0.05 μm.

When the LSM is used in its highest resolution setting, the measurement region is a plane with dimensions of 2 mm x 10 mm. The position of this plane is illustrated in

figure 1.3. The work piece needs to be placed within ±1 mm (optical axis) and ±5 mm (scanning direction) of the centre of the measuring region. As can be seen, the location of this region is not symmetrically located and it would be very difficult to position the work piece with accuracy without assistance from the LSM control unit. A LED display on the front left hand side of the display unit allows the correct positioning of the work piece (working electrode) in the scanning direction. When the electrode is outside the measuring region of the LSM an error message is displayed. When brought into the measuring region nine of the red LED bars are lit up, a diameter reading is displayed and the error message disappears. As the electrode is moved in the scan direction by means of the support table, different combinations of nine LED lights light up to indicate the position of the electrode with respect to the centre of the measuring region (position of most accurate measurement). Once located in the centre, all ten bars of the LED display light up and a stable and precise diameter reading is displayed. The positioning of the work piece in the optical direction was achieved by moving the electrode support table in the optical direction in conjunction with the "shift-read" mode of the LSM display unit. By minimizing the diameter reading displayed on the unit in this mode, the electrode can be located in the region of accurate measurement.

a) b)

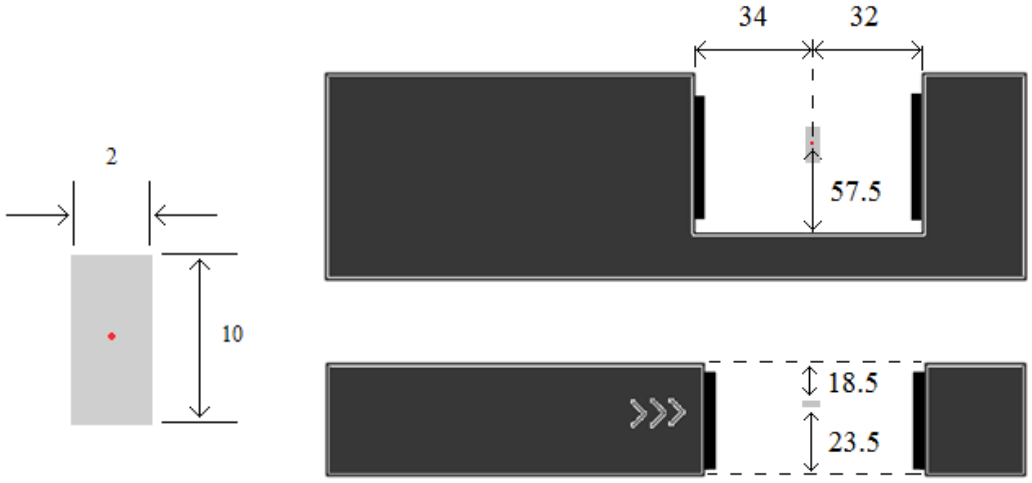

All measurements in mm

Fig 1.3 The (a) size & (b) location of the LSM's region of most accurate measurement.

The LSM was calibrated prior to use for the first time in accordance with the instructions outlined within the operating manual. This was done by means of a calibration gauge set purchased from the supplier (Part No: 02AGD120). Both the

“with-holder type” and “straight type” calibration gauges that were used are illustrated in figure 1.4. The use of two types of gauges allowed calibration at the lower and upper end of the range of the instrument. Both the known and measured diameter readings were input and stored in the calibration mode of the LSM display unit. Subsequent checks using the calibration gauge at regular intervals showed that the LSM possesses excellent stability and after the initial calibration no further calibration was necessary during the course of this work.

The LSM windows were regularly cleaned in accordance with the cleaning procedure outlined in the operator manual, to deter any debris from building up on the window and producing noise in the measurements. Dust falling into the laser during measurement can also be a cause of interference in some environments. A secondary role of the electrode support table is therefore to act as a dust cover. The sliding protective covers were kept in place at all times to protect the windows from damage during measurement and slide across the windows between measurements and when not in use.

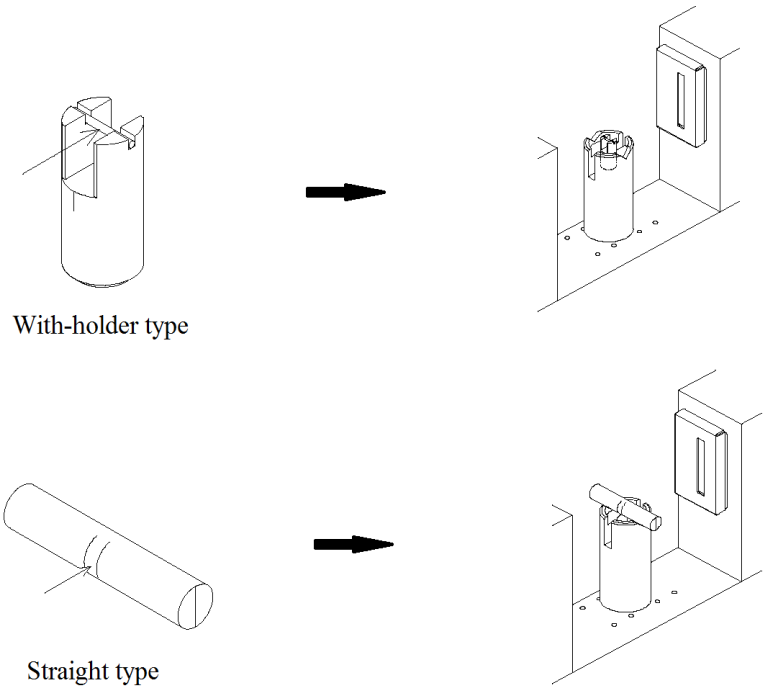

Fig 1.4 Calibration gauges used to calibrate the LSM.

1.1.3 Electrodes

1.1.3.1 Construction of working electrodes

Gold working electrodes (AuWE) were constructed using gold wire of approximately 500 μm diameter. The gold wire was electrically insulated for most of its length but had an exposed length of 10 mm towards its lower end, on which polymer films were grown (see fig 1.5(a)). In addition to providing a surface for polymer growth the gold working electrode provided a means to position the film precisely within the measurement region of the LSM.

The gold wire used in the construction of the working electrodes was obtained from Goodfellows, UK, and was supplied in the form of a coil. It was necessary to straighten the wire prior to use. A 45 mm length of gold wire was taken from the coil using wire cutters and partially straightened by carefully drawing with one gloved hand between the thumb and forefinger of your other gloved hand, so as to bend it in a direction counter to its curvature. Further straightening was achieved by rolling the wire section on a flat surface with a metal rule. Final straightening was achieved by gripping either end of the wire with a pairs of pliers and applying just enough force as to straighten the wire. Any damaged wire that had been caused by holding the ends of wire with pliers during the straightening procedure was removed using wire cutters. With care this could be limited to 2-3 mm.

Next, two pieces of electrically insulating heat-shrink coating were cut. The first piece was cut to a length of 2 mm and shrunk to fit the tip of the wire, using a hot air gun. The next piece was cut to a length of 25 mm and was positioned exactly 10 mm from the position of the first piece and shrunk to fit, so as to leave a 10 mm exposed section on which polymer could be grown. This left an additional exposed section of wire of approximately 5 mm at the end, available for soldering. The plastic coating allowed the wire to be aligned and held in place in the electrical connector until it could be more securely held by soldering. Care was taken to ensure that a good electrical contact was established. Heating the metal end of the connector by touching with the heated end of the soldering iron for 2-3 seconds prevented the molten solder from solidifying before it could fill the connector and make full contact with the exposed surface of the gold wire. If the wire moved during this procedure, the solder could be melted again by contact with the hot tip of the soldering iron and the wire repositioned to ensure it was straight. Although gloves were used at all stages during the construction, the lower half of the electrode was cleaned with TL1 wash as a precaution against contamination in accordance with the procedure outlined in section 1.1.6.

All wire electrodes were checked to ensure that they were straight using a microscope as illustrated in fig 1.5 (b). The wires were typically off the central axis of the electrode by an angle of 0.25^{o} or less.

(a) **(b)**

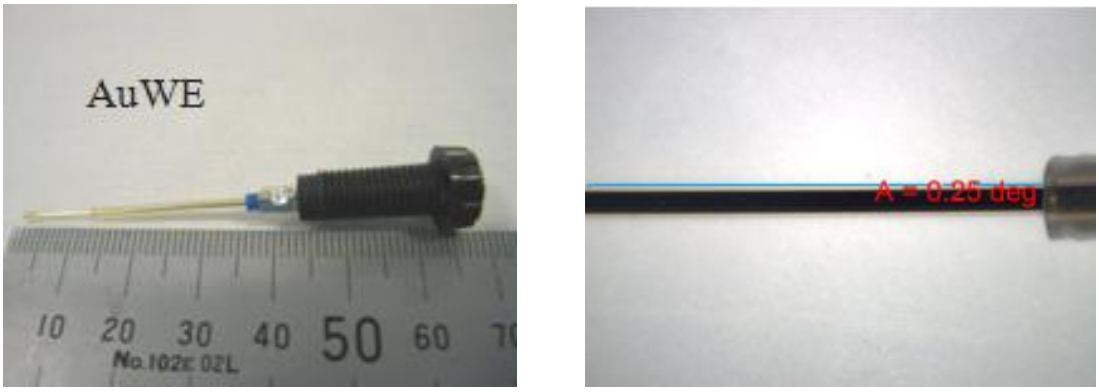

Fig 1.5 (a) A gold working electrode (AuWE) **(b)** Microscopic confirmation of the "straightness" of the AuWE.

With practice a working electrode could be constructed in approximately 30 minutes. Electrodes were reused as much as possible, not only because of the cost of the gold wire and the time taken to construct them, but also to aid in the reproducibility of the growth of films to a precise thickness. It was necessary to store the electrodes in plastic containers to prevent them from being damaged. These containers were conveniently made by cutting the end off a large plastic pipette and using the bulb end as shown in figure 1.6.

Fig 1.6 Storage of AuWE to protect from damage.

1.1.3.2 Construction of counter electrodes

A cylindrical gold counter electrode (CE) was used for the polymerization of PPy films. This shape of electrode produces a uniform coating of polymer on the wire[114].

These were constructed by first depositing a layer of chromium (30 Å) onto an acetate sheet. This formed an adhesion layer onto which gold (2000 Å) was then deposited. This flexible sheet material was cut to an appropriate size and shape and folded to form a cylindrical CE as illustrated in figure 1.7. The cylindrical CE was cut so as to exactly fit the inner surface of the polymerization cell. This design allowed the cell volume to be minimized, reducing consumption of reagents, whilst still allowing sufficient space to position both the working electrode and reference electrode at/near the centre of the cell. It also proved to be very economic alternative to the costly cylindrical gold gauze CE available commercially.

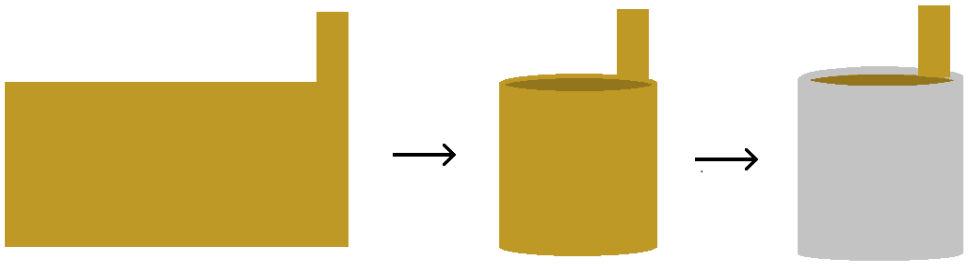

(a) Cut to correct size and shape (b) Folded into a cylinder (c) Inserted into cell

Fig 1.7 Stages in the construction of a cylindrical CE used for polymerization.

The CE used during actuation had different requirements and therefore had a different design. The electrode was obtained from Ti-shop (www.ti-shop.com) and made from platinised (2.5 μm) titanium mesh sheet. The electrode was flat and rectangular in shape and had the dimensions shown in figure 1.8(a). This allowed the CE to be positioned to one side of the actuation cell so that it did not obstruct the laser and interfere with LSM measurement.

To ensure that an accurate potential could be supplied to the electrochemical cell during both polymerization and actuation, a reference electrode was employed. The silver/silver chloride (Ag/AgCl) reference electrodes that were used were obtained from BASi, UK (see figure 1.8 (b)). Three Ag/AgCl electrodes were used. One was used exclusively for polymerization and a second used exclusively for actuation measurement. When not in use, the tips of the electrodes were kept immersed in 3M NaCl (aq). This was necessary to prevent the Vicor membrane from drying out and to

ensure the inner solution was kept uncontaminated and of the correct concentration. These electrodes have a life of 6-12 months depending upon the frequency of use and how carefully they are looked after. The third Ag/AgCl RE was kept exclusively to regularly check on the performance of the other Ag/AgCl REs.

When preparing a new Ag/AgCl RE it is important to follow the manufacturer's instructions. In particular, great care needs to be taken when removing the protective yellow coating off the end of the electrode so as to not damage the Vycor porous membrane. In addition it is important that after soaking the electrode for 24 hours, any bubbles that develop above the Vycor membrane are dislodged by tapping the base of the electrode whilst held vertically. In this way any bubbles float upwards away from the membrane.

(a) **(b)**

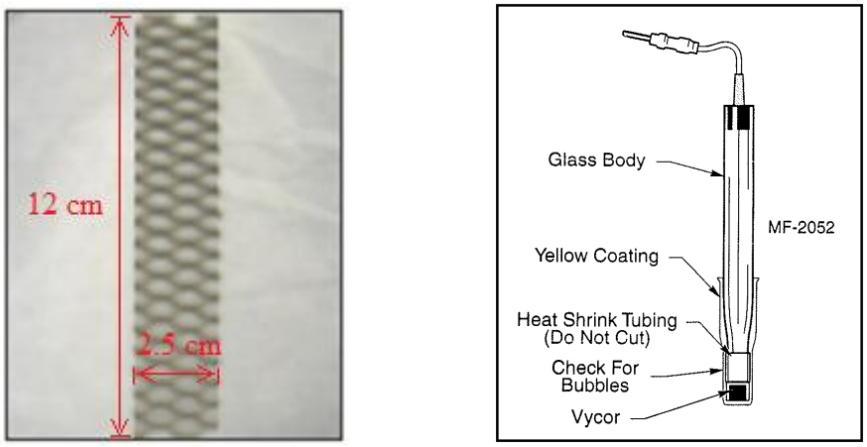

Fig 1.8 (a) Pt coated Ti gauze CE used for actuation **(b)** Ag/AgCl RE (BASi, MF-2078)

1.1.4 Reagents

Polymerization solutions were prepared using pyrrole (Py), sodium dodecylbenzene sulphonate (NaDBS) and deionized water.

Pyrrole was obtained from Sigma Aldrich (reagent grade, 98%), purified using vacuum distillation, stored under nitrogen in small amber-glass vials and kept within a freezer. Py could be kept pure in this way for a year or more. When opened to remove pyrrole, the remaining Py was stored once again under nitrogen and quickly returned to the freezer. The use of small vials is advisable as they are typical opened only 3-4 times before their contents are consumed, limiting exposure to light and air.

Two different sources of NaDBS were used. One of these was obtained from Sigma Aldrich and the other from TCI Europe. The NaDBS obtained from Sigma Aldrich was used exclusively for preparing actuation solutions as it has been shown to contain a mixture of isomers and is less suitable for use in preparing polymerization solutions[115]. The NaDBS obtained from TCI Europe was used exclusively to prepare polymerization solutions as it is of higher purity, containing more straight chain isomer as opposed to the branched.

Great skill is needed when preparing aqueous solutions of NaDBS as it foams very easily. This is particularly the case when attempting to get it to dissolve and when transferring solutions. When Py is first transferred to an aqueous solution it will typically form an immiscible layer on the surface. When transferred to a volumetric flask, this layer is broken up and largely dispersed by carefully inverting the volumetric several times. The Py was completely dissolved by sonocating for five minutes.

The 0.1M NaDBS (aq)(Sigma Aldrich) solutions prepared for use in actuating, are very stable and can be stored without decomposition for many months even at room temperature. However, polymerization solutions are more prone to decomposition because they contain Py, and were freshly prepared and used immediately. These solutions can be stored for a couple of days provided they are stored in the fridge when not in use. If the solutions are stored for longer than this they start to turn a black-green colour. In addition, cold solutions required at least half an hour with gently stirring to allow any precipitated NaDBS to re-dissolve and for the solution to warm up and reach room temperature. In this work polymerization solutions were freshly prepared when needed. Any solution remaining was safely disposed of at the end of the day.

1.1.5 Electropolymerization of polypyrrole films

Polypyrrole films were polymerized at a constant potential of 0.55 V vs. Ag/AgCl in 8 ml of aqueous electrolyte of 0.10 M Pyrrole and 0.1M NaDBS. The polymerization cell was cylindrical with a diameter of 2 cm and volume of 10 ml (see figure 1.9). The AuWE was correctly positioned so as to be within the region of most accurate measurement. The Ag/AgCl RE was rinsed with de-ionized water to remove any traces of 3M NaCl storage solution and then positioned so as to be a few millimeters away from the AuWE with its tip level with the edge of the upper insulated part of the wire. In this location the RE did not obstruct the beam of the LSM.

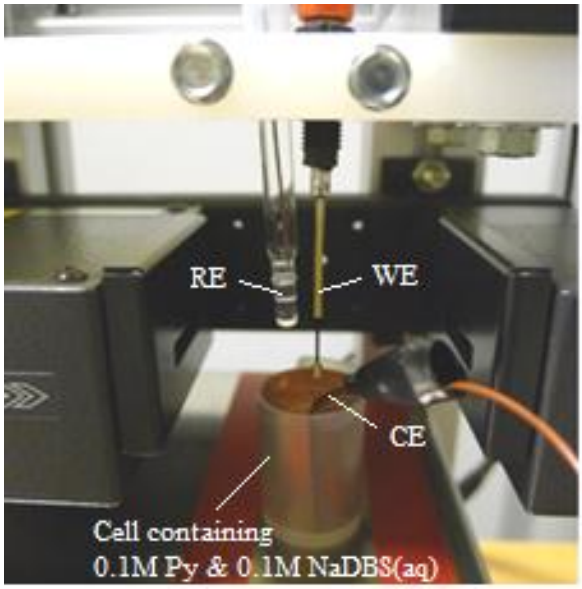

Fig 1.9 Polymerization cell (depicted in lowered position).

The thickness of the polymer films were determined by calculating the change in the radius of the gold working electrode after polymer film was grown on its surface. To ensure that the LSM beam continued to make measurements on the same part of the working electrode, the polymer films were grown *in-situ* in the instrument by immersing the working electrode into the polymerization cell by means of a lab jack. The position of the working electrode within the LSM beam remained unchanged throughout the course of the all subsequent measurements.

The growth of films to a specific thickness was done by monitoring the amount of charge that flowed corresponding to a change in thickness (radius). It was necessary to proceed cautiously when polymerizing films as it was found that the consumption of charge was only approximately linear. One possible reason for this is that part of the charge that flows is being used to charge the growing polymer layer (Faradic current). Each time the polymerization process is stopped and restarted (see next paragraph) the polymer film will undergo a charging-discharging cycle. However, a linear relationship did prove to be a useful approximation when estimating growth rates.

Initially polymerization was started and stopped after approximately 80 percent of the estimated charge had flowed to achieve the required thickness. The true thickness was then accurately determined using the LSM and was used to calculate a better estimate of the charge flow required to achieve the target thickness, based upon initial growth rate. Polymerization was restarted and paused again after 80 percent of the remaining charge had flowed to give the required thickness. The actual thickness of the film was again determined using the LSM and the growth rate re-calculated to give a more accurate

estimate of the current growth rate. This process was repeated until the target thickness was achieved. With practice, films could be precisely grown after stopping and re-starting 3-4 times.

A rinsing and drying procedure was found to be necessary to ensure that film thickness measurements made during polymerization were accurate. This involved lowering the polymerization cell by means of the lab jack (see figure 1.10), carefully removing it and replacing it with a small beaker containing de-ionized water. This was then carefully raised to re-immerse and rinse the lower portion of the working electrode supporting the polymer film. The electrode was immersed for 20 seconds in the de-ionized water before it was carefully lowered to allow the electrode to air dry prior to thickness measurement. Five minutes was used for intermediate thickness measurement and eight minutes for final thickness measurement. All timings were done by means of a stopwatch with an alarm function to ensure a consistent procedure. The Ag/AgCl RE was stored during this time in a 0.1 M NaDBS (aq) solution to prevent the Vycor membrane from drying out or developing bubbles.

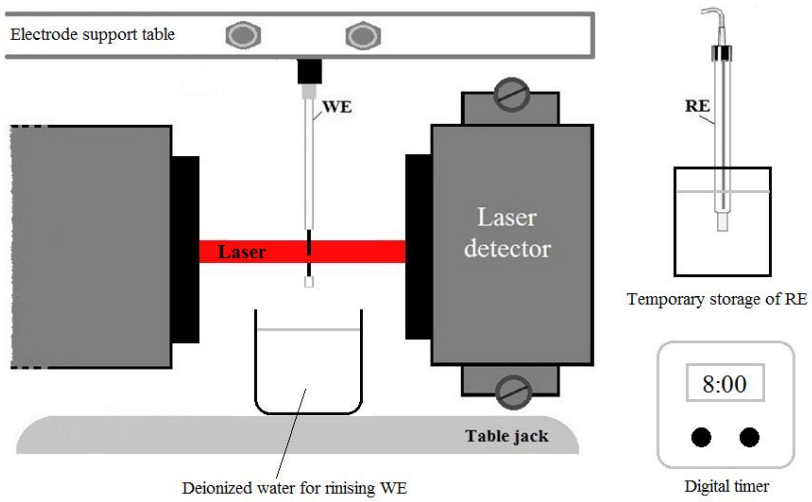

Fig 1.10 Film thickness measurement.

The RE was returned to its position in the support table, the polymerization cell placed on lab jack and carefully raised to immerse the electrodes, in preparation for further polymerization. A period equal to that used during the drying stage was allowed for the film to re-equilibrate with the electrolyte, before polymerization was recommenced.

These steps were necessary in order to prevent NaDBS deposits forming on the polymer film during the drying phase and giving too large a diameter reading. A drying period of 8 minutes was found to be optimal for stable diameter measurement as shown by figure 1.11. The rapid decrease in diameter initially observed, corresponds to surface run-off of bulk deionized water and the slower decrease to evaporation of adsorbed surface

water (1-8 min). Above 8 minutes there is a very slow decrease (less than 0.1 μm /5 min) which likely corresponds to the loss of moisture from within the polymer film. The decrease in thickness between 1-8 minutes represents a change of only 1 % for the 10 μm films shown in figure 1.11. It has been shown[51] that fully air dried PPy(DBS) films of approximately 10 μm (11.5 μm) thickness expand by 11 % on re-immersion in 0.1M NaDBS(aq). The decrease in diameter within the first eight minutes was therefore taken to represent bulk surface run-off followed by evaporation of water adsorbed on the surface and not from within the film itself.

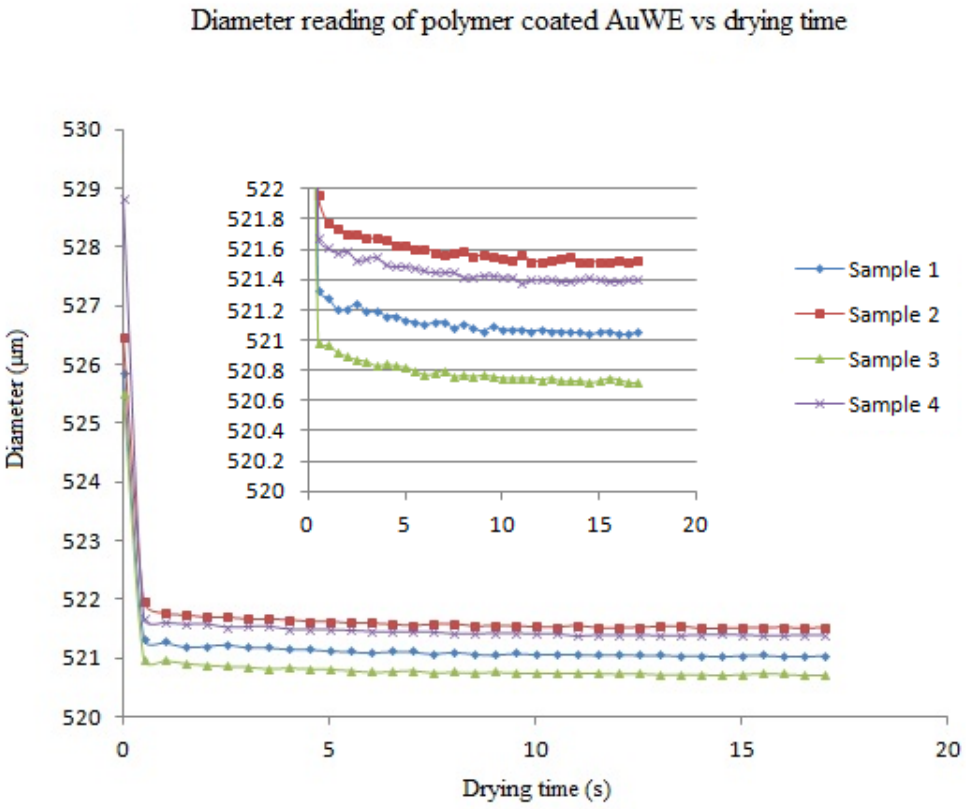

Fig 1.11 Determination of optimal air drying times for 10 μm PPy(DBS) films. Inset showing detail.

Polymer films were grown to three different thicknesses (1, 5 and 10 μm) to obtain "baseline" performance data with which different forms of polypyrrole could be compared, but this also allowed the affect of film thickness on actuation to be investigated. Three replicate samples were produced at each thickness.

Polymerization curves (current-time graphs) obtained during polymerization were used to check that no unusual behaviour had occurred during polymerization *e.g.* instability or discontinuities. A typical current-time graph is shown in figure 1.12 (a) (shown

overleaf). After an initial surge of current (double-layer capacitive charging) these curves typically display a stable period, in which there is a relatively constant current, and corresponds to the growth of good quality films. Figure 1.12 (b) is the first cyclic voltammetry scan for the electropolymerization of PPy(DBS) and indicates that polymerization starts around 0.45 V and increases linearly up to 1 V.

1.1.6 Actuation of polypyrrole films

The basic principle of how a LSM is used to measure actuation is illustrated in fig 1.13 (a). The LSM repeatedly scans a line in one direction at high speed, giving the appearance of a rectangular beam, which is received by the detector. In a sense, the polymer coated working electrode casts a shadow equal to its diameter on the LSM detector. As the polymer film expands or contracts the shadow cast on the detector changes accordingly.

The diameter of the WE is displayed on the LSM display unit and received by potentiostat by means of a second signal (voltage signal). This information is displayed as a displacement-time graph by the potentiostat's GPES software. The change in the diameter of the polymer coated wire is recorded together with the current which flows during actuation. Both sets of data are plotted on the same graph, with the current axis displayed on the left-hand-side and the second signal (change in diameter) axis being displayed on the right-hand-side.

The actuation cell had different requirements to the polymerization cell. The cell was made of transparent plastic and had a rectangular cross-section with opposite faces that were parallel (see Figure 1.13(b)). This allowed the LSM beam to be incident normally and pass through the cell without being refracted by the plastic walls of the container or the electrolyte used to actuate the polypyrrole film. It had a width of 3 cm and a volume of 50 ml. The cell was cleaned thoroughly after use with deionized water and stored appropriately. At all times fresh gloves were worn to avoid transfer of dirt and grease to the outside of the cell when handling. Great care was taken when transferring electrolyte to the cell to prevent electrolyte from making contact with the outside of the cell. The electrodes employed were the same as those used during polymerization with the exception that the counter electrode was a rectangular platinum coated titanium gauze electrode of 2.5 cm width. This was positioned to one side of the cell so as not to obstruct the LSM beam. The Ag/AgCl reference electrode was positioned near to working electrode but above the plane of the LSM beam. Actuation was undertaken in 40 ml of 0.10 M NaDBS(aq) electrolyte which was at room temperature and had been filtered through a 0.2 μm filter to remove any potential particulate matter than might be present.

(a)

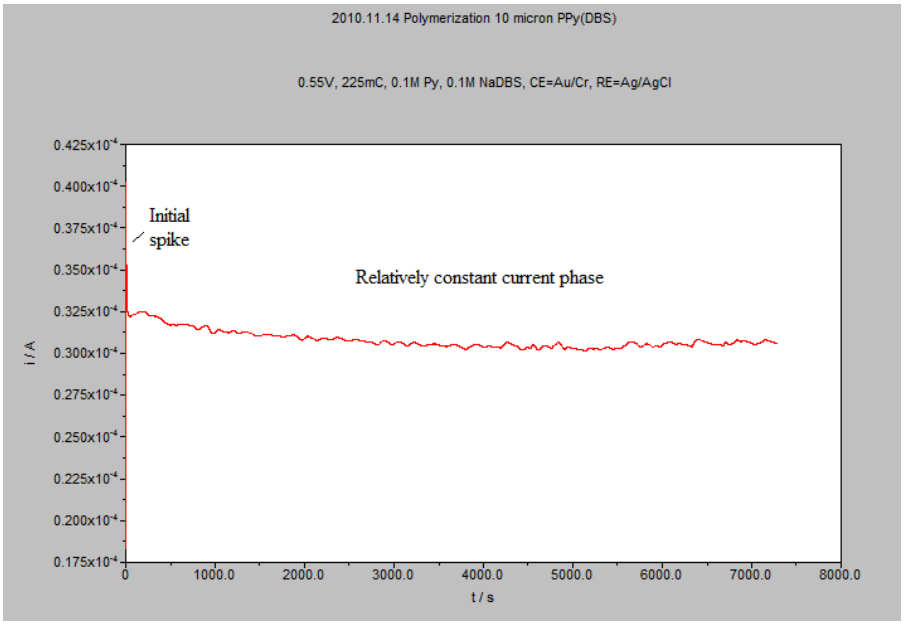

(b)

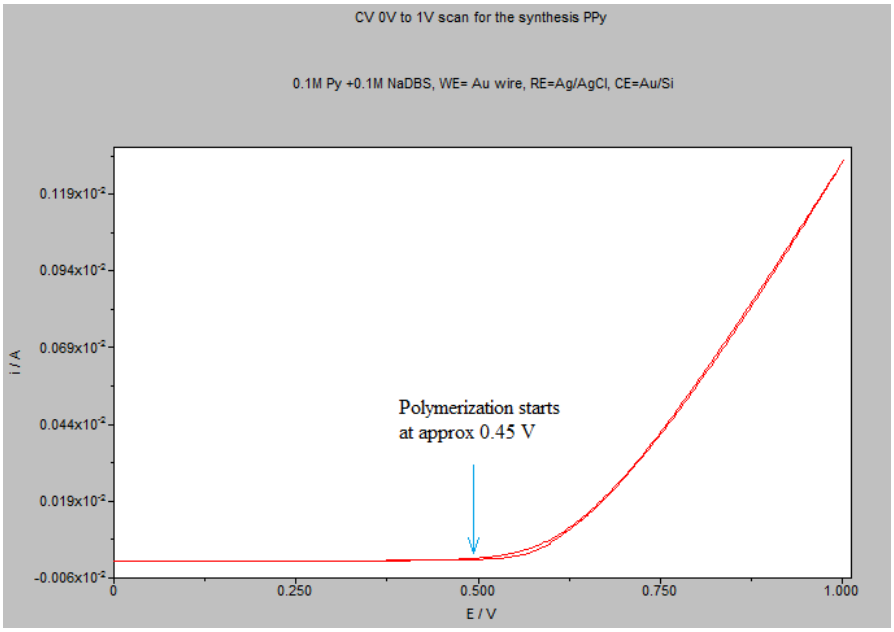

Fig 1.12 (a) A typical polymerization curve for PPy(DBS) polymerized at a constant potential of 0.55V Ag/AgCl using 0.1M Py/0.1M NaDBS(aq) to a thickness of 10 μm. **(b)** Cyclic voltammetry scan (scan 1, 0 to 1 V) for the polymerization of PPy(DBS) using 0.1M Py/0.1M NaDBS(aq).

The position of actuation cell was carefully adjusted so as to ensure that the laser is incident normally on the front and rear faces of the cell. A small rectangular set square was used to position the cell. The "shift-read" function on the LSM was then used along with fine adjustments to the cells location (by raising and lowering the lab jack) so as to minimize the diameter reading. This corresponded to the diameter reading that had previously been made in air using the LSM.

(a)

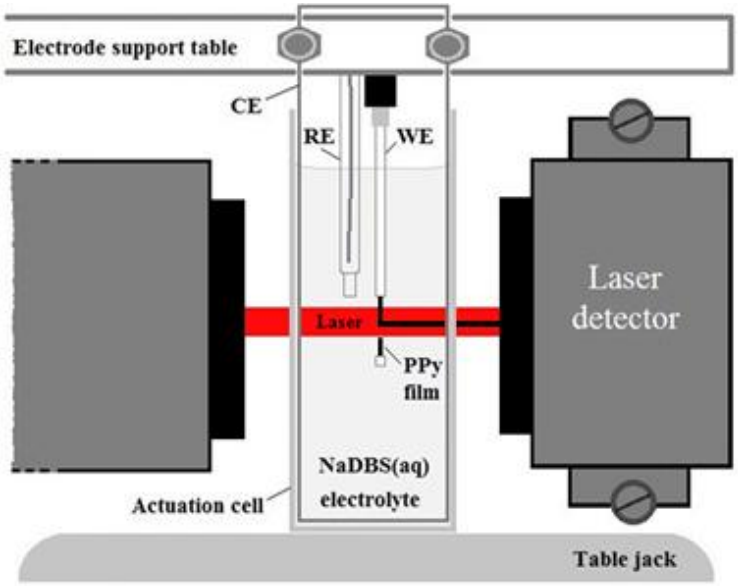

(b)

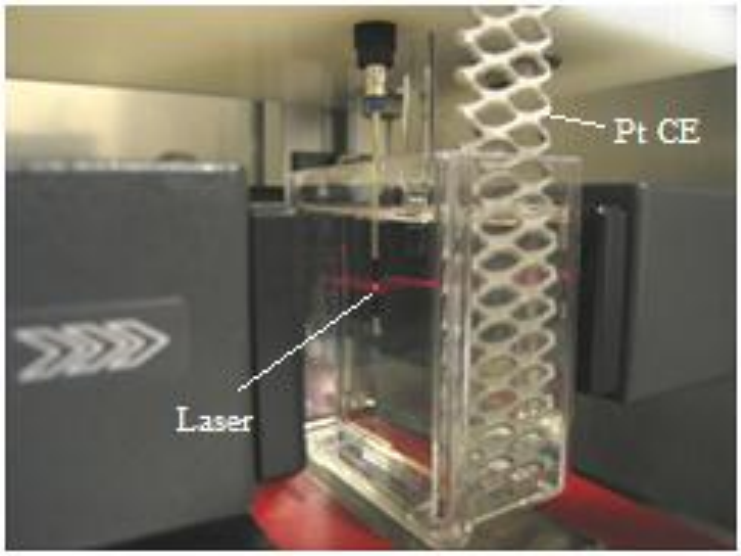

Fig 1.13 (a) Schematic of actuation cell **(b)** Photograph of actuation cell.

In order to make this process easier a specially designed actuation cell was made having a plastic base with parallel walls separated from each other the same distance as the gap between the laser generator and detector of the LSM as shown in figure 1.14 (a). This allowed the cell to be precisely located by simply sliding the cell into position within the gap as illustrated in figure 1.14 (b).

(a) **(b)**

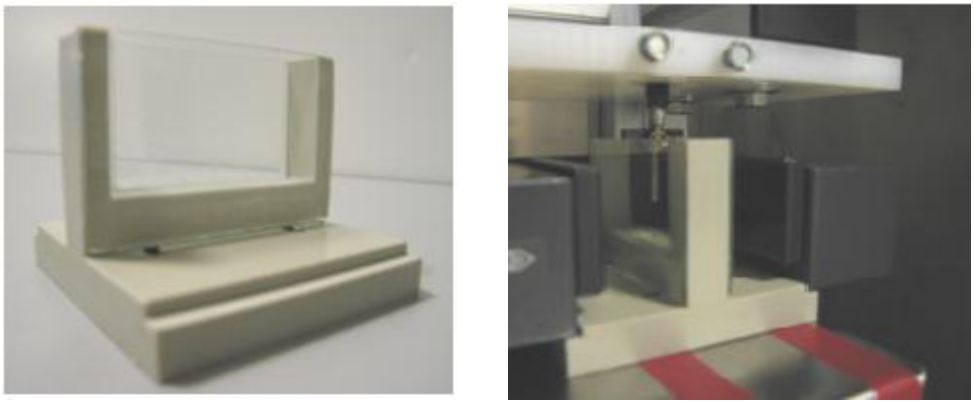

Fig 1.14 (a) Specially designed actuation cell **(b)** Actuation cell precisely located within the LSM by means of an exactly fitting base.

Cyclic voltammetry for PPy(DBS) grown in 0.1M pyrrole/0.1M NaDBS(aq) shows a reduction peak at ~ -0.70 V vs. Ag/AgCl and an oxidation peak at ~ -0.35 V vs. Ag/AgCl. A suitable switching potential of 0 V (oxidation) and -1 V (reduction) vs. Ag/AgCl was selected and used for all samples (see figure 1.15 below).

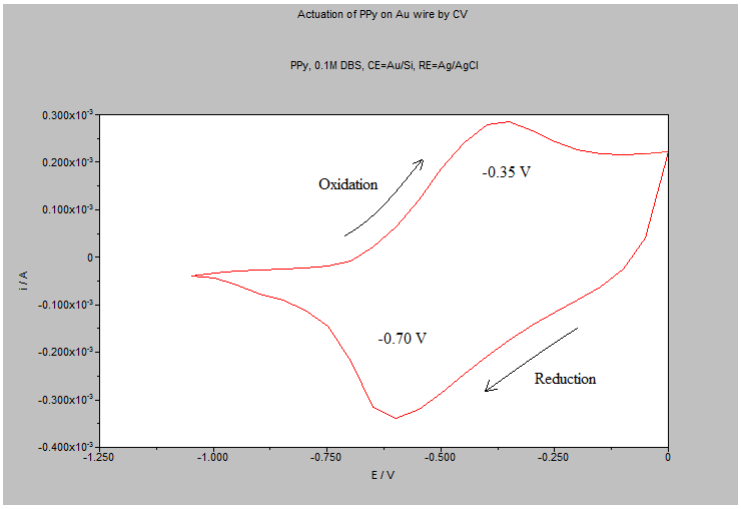

Fig 1.15 Cyclic voltammetry scan illustrating the oxidation and reduction peaks for PPy(DBS) to aid in the selection of suitable switching potentials for actuation.

Cycling times were chosen to ensure that there was enough time for maximum reversible expansion and contraction to occur. A total cycle time of 400 s (0 V (200s), -1 V (200s)) was found to be suitable for the range of films employed.

The actuations of the polymer films were controlled by means of a potentiostat (Metrohm μAUTOLAB III) and associated software (GPES).

An actuation procedure was written using the GPES software and stored so that identical conditions could be used for all samples. When reused, only the sample ID was changed so that the data could be uniquely identified and stored without overwriting previous sample data.

It was very important to ensure that the maximum number of data points (< 10000) allowed for the software was not exceeded, otherwise the data would not be stored. This was done by setting an appropriate data point interval, which was determined by calculating the total time required for the intended actuation sequence by 10000, and ensuring that the interval input into the procedure was close to, but less than this value. For long actuation sequences (hours) this means having a low sampling frequency and thus fast processes (1-2 s) could not be recorded without combining more than one procedure.

The actuation procedure was written to ensure that a potential of 0 V was initially applied to condition the polymer film and to assess the level of instability and noise prior to actuating the polymer as well as to establish a baseline of the expansion/diameter/layer thickness. The actuation procedure could be stopped and restarted at any time during this initial 200 s interval, but not afterwards as once the polymer starts to actuate it undergoes irreversible expansion and the position of the baseline will be different. This was often necessary to allow more time for the newly polymerized films to stabilize. Once actuation was started it was undertaken until the actuation profile reached a "stable state" (maximum irreversible expansion).

Prior to actuation it was very important to correctly set the LSM display unit. In particular it was necessary to ensure that a reference diameter was appropriately input and stored. This was set to a value that was expected to be in the middle of the range for the diameters determined by the LSM during the actuation sequence. This was set to be several microns above the initial diameter of the actuator at the start of the actuation sequence. For example, if the initial diameter reading was 510 μm, a suitable reference diameter would be 513 μm. If the reference was not set appropriately, the actuation sequence would risk exceeding the measurement range of the LSM. On the highest resolution setting, this range is 40 μm (mid range reference ±20 μm).

It was very important to remember to press the "continuous run" button on the LSM display unit in order to ensure that data was transferred to the potentiostat (second signal). If this is not done data from the LSM is not sent to the potentiostat for storage.

Full details of the settings for the potentiostat and LSM display unit are given in Appendix 1.

The WE was prepared for re-use by placing the lower part of the polymer coated electrode in TL1 wash (H_2O:NH_4OH:H_2O_2 = 5:1:1) maintained at 80 ^{0}C. This typically took 20 minutes with the aid of a cleaning stick to physically remove material. The electrodes were then thoroughly rinsed with deionized water to remove traces of TL1 solution and carefully dried with a nitrogen gun. The cleaning procedure did not have any adverse effect on the insulating coating.

1.1.7 Validation of the laser micrometry set-up

The LSM was calibrated as described in section 1.1.2 using the calibration gauge set supplied by the manufacturer. This calibration was undertaken by measuring the diameter of the gauges in air. However, since actuation measurements were undertaken in 0.1 M NaDBS aqueous electrolyte, it was important to determine whether the readings made by the LSM in air were the same as those made in electrolyte.

Early on in the development of the LSM set up, diameter measurements made using the LSM were compared, in both air and electrolyte, with those made using a Nikon microscope. Table 1.1 compares the typical readings made. Measurements were initially undertaken on a bare Au wire (row 1) and again after a layer of PPy had been deposited for approximately two hours.

Sample	Nikon (air) /μm	Nikon (electrolyte) /μm	LSM (air) /μm	LSM (electrolyte) /μm
Au wire	500.42	500.96	501.60	501.5
PPy coated Au wire	528.91	528.10	528.64	528.7

Table 1.1 A comparison of LSM measurements with those made using a Nikon microscope.

Although, the readings made by the LSM were in agreement within the measurement error of the microscope, the comparison was not without difficulties. Making diameter readings first with the LSM and then with the microscope required the wire to be transferred from one instrument to the other. Therefore, it was very difficult to ensure that the same cross-section of the wire was being measured and compared using both techniques. It proved very difficult to focus on the edges of the wire, particularly within an electrolyte, and to accurately position the lines either side of the wire, between which diameter measurement was made (see figure 1.16). Another issue was that the resolution and measurement accuracy of the microscope was less than that of the LSM.

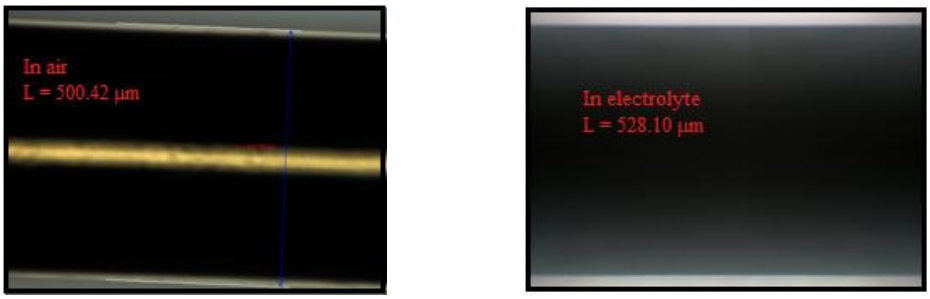

Fig 1.16 Diameter measurements made (a) in air on AuWE and (b) in 0.1M NaDBS(aq) on a polymer coated AuWE.

Having calibrated the LSM we were confidence in the LSM ability to accurately measure wire diameters in air, and we decided that it was reasonable to validate measurements made in aqueous electrolyte with those made in air, using the LSM itself.

The diameter of the AuWE was first measured within air in the absence of the actuation cell and then repeated immersed in 0.1 M NaDBS(aq) within the actuation cell. Measurements of the same cross-section of the wire were possible by positioning the electrode using the electrode support table and not moving it between air and electrolyte readings. The lab jack was use to carefully raise and lower the cell into position. Once the actuation cell had been correctly aligned, the measurements in air and electrolyte were found to be in agreement to within ± 0.10 µm.

Measurements were also made in air and electrolyte at both the start and end of an actuation sequence for comparison. A typical result is shown in table 1.2. Again these show that there was very good correspondence between the air and electrolyte measurements. However, to obtain such good agreement the actuation cell needed to be carefully aligned to ensure that the laser is incident normally at the front and back walls of the cell.

Position in actuation sequence	Diameter / μm (in air)	Diameter / μm (in liquid)
Start	512.45	512.39
End (Stable state)	526.62	526.53

Table 1.2 LSM readings made in air and electrolyte at the start and end of an actuation sequence.

1.2 Results and discussion

1.2.1 General features of actuation sequences

The typical actuation sequence for PPy(DBS) displayed in figure 1.17 reveals that the strain has both a reversible and an irreversible component. The reversible component is represented by the cyclic (up and down) movement of the actuation curve, whereas the irreversible component is evident from the upward drift of the sequence as a whole. It is the reversible component that allows the polymer to behave as an actuator. In contrast, the irreversible strain is undesirable from the point of view of an actuator and should be minimized.

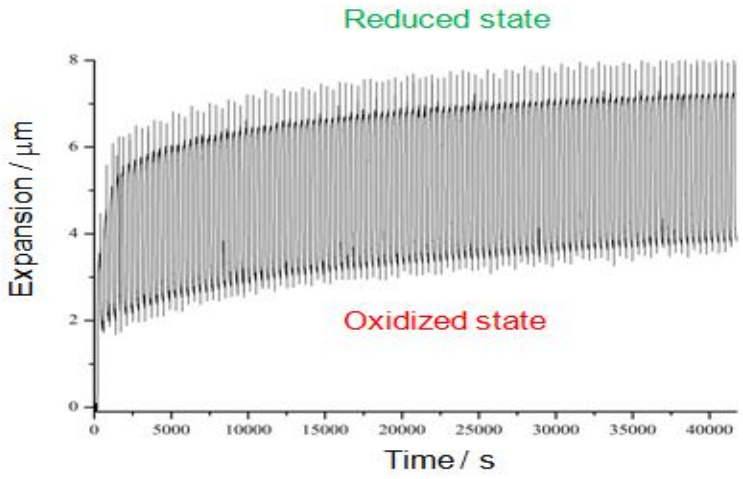

Fig 1.17 A typical actuation sequence profile.

Both the reversible and irreversible strain increase with cycle number, to a maximum stable state, but over different time scales. The reversible strain increases to a maximum value over approximately ten cycles under the cycling conditions employed in this

work. In contrast, the irreversible strain can take many tens of cycles to reach a maximum. When considering the behaviour that can be expected for an actuator in service, it is data obtained during the stable state that will be most representative of long term performance.

The greatest increase in the irreversible strain can be seen to occur during the first cycle and is well documented[116]. A hypothesis given to explain this is that water enters the film during the first reduction cycle scan and remains there during re-oxidation.

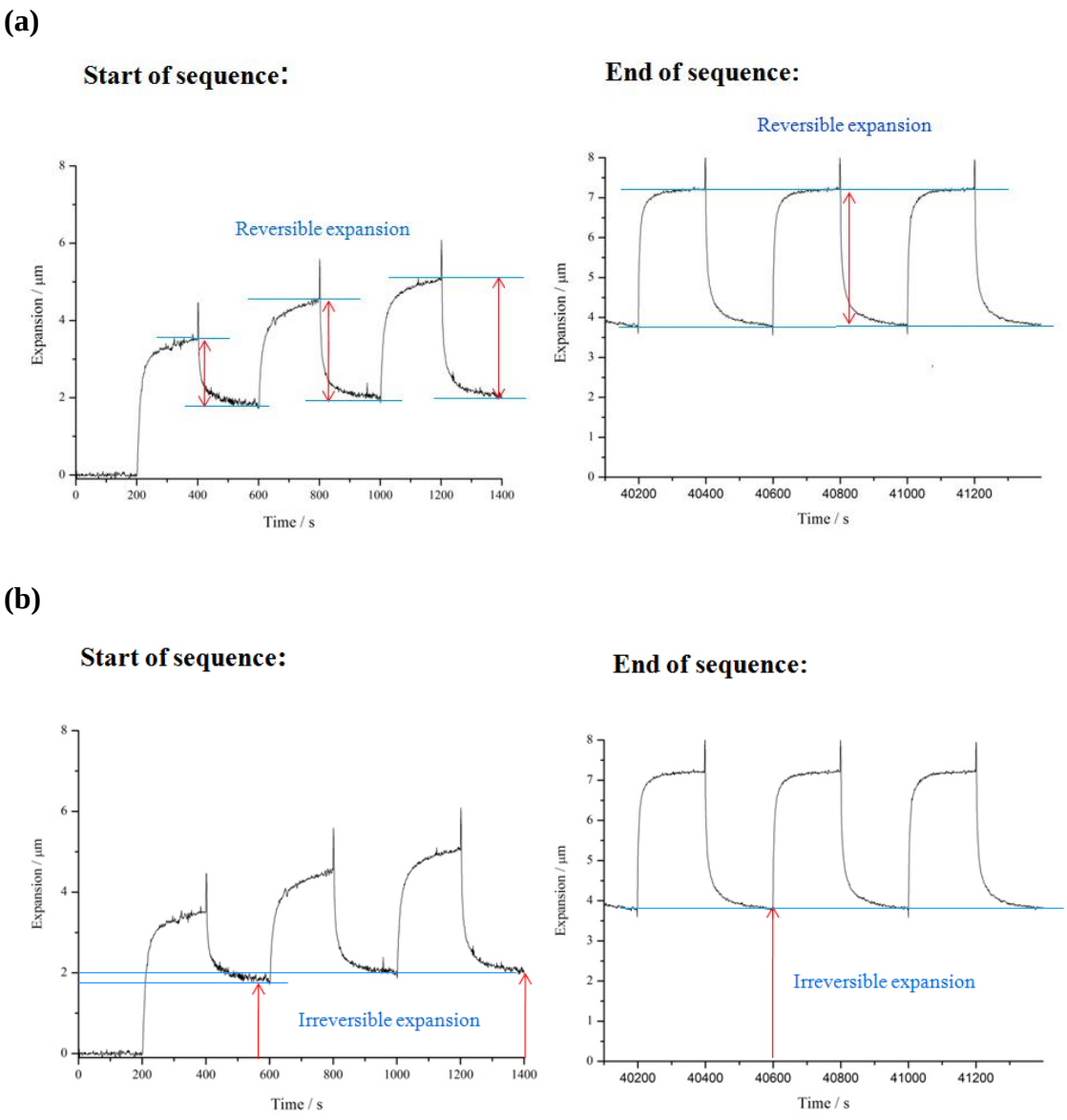

Fig 1.18 The change in (a) reversible and (b) irreversible expansion with increase in cycle number.

Another difference that can be observed between the first cycle and subsequent cycles is that considerably more charge flows during the first cycle. Figure 1.19 illustrates this, showing that the charge flow in the first reduction scan of a 5 μm film of PPy(DBS) is -9.87 mC compared to -6.16 mC in the second. It has been suggested[116] that this might be due to a fraction of the cations entering the film during the first reduction scan and remaining within the polymer during re-oxidation.

(a) **(b)**

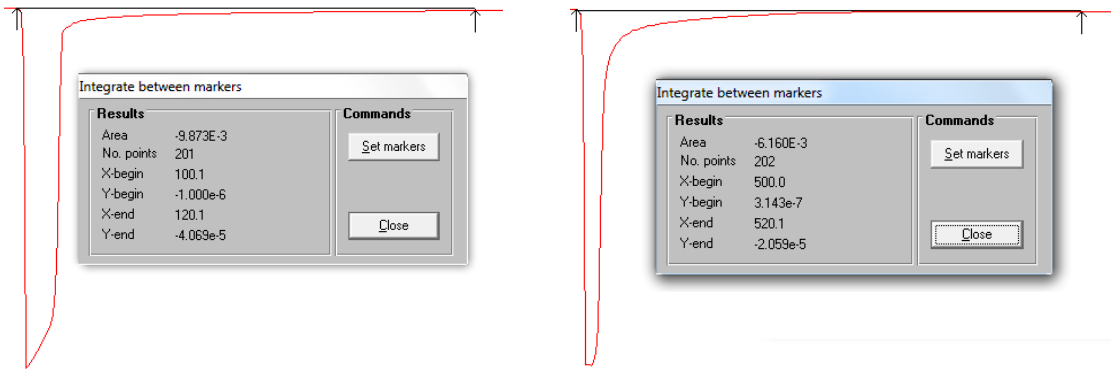

Fig 1.19 Charge flow occurring on reduction during (a) the first cycle (b) second cycle.

Figure 1.20 illustrates that the first few cycles are more prone to displaying instability; however there is a general improvement in the stability of the actuation profiles with cycle number. The shape of the actuation curves tend to become more flattened at their maxima and minima, with increasing cycle number.

(a) First four cycles **(b)** Stable state

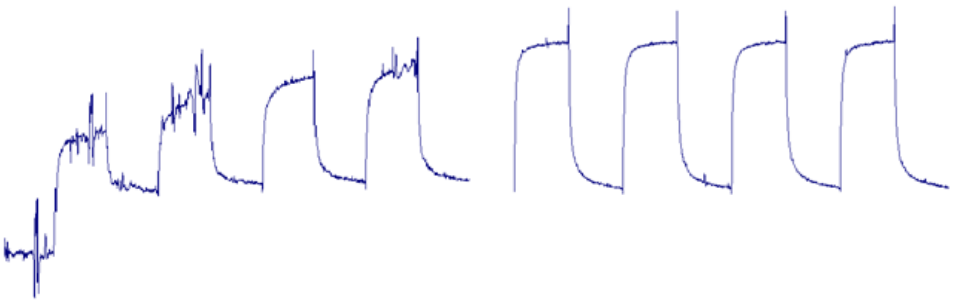

Fig 1.20 Comparison of actuation profiles at the (a) start and (b) end of the same actuation sequence for a 10 μm film of PPy(DBS).

The rate of expansion is greatest in the first part of each scan (reduction and oxidation) with 80% of the strain typically occurring within seconds. The remaining 20% of the expansion occurs much more slowly and can be of the order of minutes. This slower expansion is more prone to instability. In as sense, the quality expansion is represented by the first 80%.

An interesting feature of the actuation curves is the presence of "spikes" associated with switching the potential. An upward spike is displayed on switching to the oxidized state (-1V to 0 V) and a smaller downward spike on switching to the reduced state (0 V to -1V). It is likely that this is due to changes in the refractive index of the electrolyte near the surface of the polymer, associated with the rapid change in concentrations of sodium ions on switching the potential (see table 1.3).

Sodium chloride	
Concentration (wt %)	Refractive Index ($20^{o}C$)
5.00	1.3418
10.00	1.3505
15.00	1.3594
20.00	1.3684
25.00	1.3776

Table 1.3 Change in the refractive index of aqueous sodium chloride solutions with concentration. Source: supportive content, Mettler-Toledo International, us.mt.com.

This phenomenon has been observed elsewhere[117] and is known as the "Mirage Effect". The effect is the result of light being bent towards the normal on going from a region of lower to higher density and away from the normal, on going from a higher density to a lower density region and visa versa.

1.2.2 Actuation metrics

The expressions displayed in table 1.4 were used to calculate the expansions and strains of the films throughout this thesis and has been described in detail elsewhere[118].

Both expansion and strain quantify dimensional changes and are closely related. Expansion is a metric that expresses dimensional changes directly and therefore has units of length, micron in our work. Strain is also used to quantify dimensional changes e.g. thickness, but it relates this change to its initial thickness and is therefore a relative measure. It is a dimensionless metric, which can be expressed as either a decimal or as a

percentage. Both of these different metrics are useful to describe dimensional changes. Strain for example is a very useful metric when comparing different types of material.

In this work the initial thickness used to calculate *reversible* expansions and strains is taken as the thickness at the start of the reduction or oxidation cycle. Whereas, *irreversible* expansion and strain has been calculated using "as polymerized" film thickness as the initial condition.

State of PPy(DBS)			
As deposited	All	Fully reduced	Fully oxidized
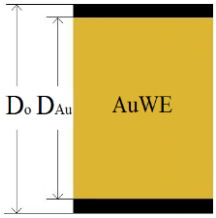	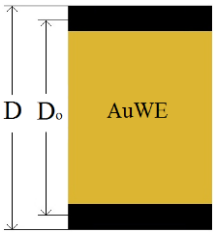	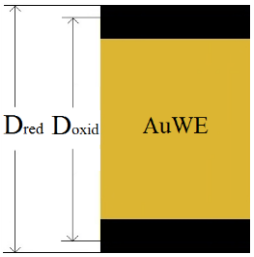	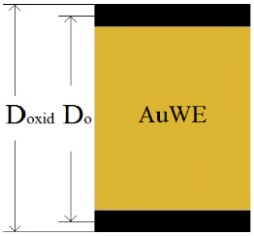
Initial film thickness: $(D_o - D_{Au}) / 2$	Expansion: $(D - D_o) / 2$ Strain: $(D - D_o) / (D_o - D_{Au})$ % Strain: $100(D - D_o) / (D_o - D_{Au})$	Reversible expansion: $(D_{red} - D_{oxid}) / 2$ Reversible strain: $(D_{red} - D_{oxid}) / (D_{oxid} - D_{Au})$ % Reversible strain: $100(D_{red} - D_{oxid}) / (D_{oxid} - D_{Au})$	Irreversible expansion: $(D_{oxid} - D_o) / 2$ Irreversible strain: $(D_{oxid} - D_o) / (D_o - D_{Au})$ % Irreversible strain: $100(D_{oxid} - D_o) / (D_o - D_{Au})$

Table 1.4 Expressions used to calculate expansion and strain. Key: AuWE (gold working electrode), D (general term for diameter), D_{Au} (diameter of AuWE), D_o (initial diameter of the "as deposited" PPy film + D_{Au}), D_{red} (diameter of the fully reduced PPy film + D_{Au}), D_{oxid} (diameter of the fully oxidized PPy film + D_{Au}).

How quickly the PPy films expand and contract was determined using a number of additional metrics. Both the maximum expansion rate and the maximum strain rate were calculated. Again, these are similar metrics, requiring that the maximum gradient in each phase (reduction and oxidation) be calculated. As has been mentioned previously, this maximum gradient or rate occurs near the start of each phase and can be located by eye. The maximum expansion rate is the maximum gradient in each phase and is

conveniently expressed in units of μm/s. The maximum strain rate was calculated by dividing the maximum gradient in each phase by the initial film thickness at the start of that specific scan and *not* the initial film thickness of the "as polymerized"/un-actuated film.

The maximum gradient can be calculated manually by drawing a tangent to the actuation curve at the position with maximum slope. Fortunately, this was made easier by making use of the linear regression function within the analysis section of the GPES software. This is illustrated in figure 1.21. This calculates both the maximum gradient and the initial starting diameter (y-begin). By subtracting the diameter of the AuWE from this initial starting diameter and dividing by two, the film thickness at the start of the phase was determined.

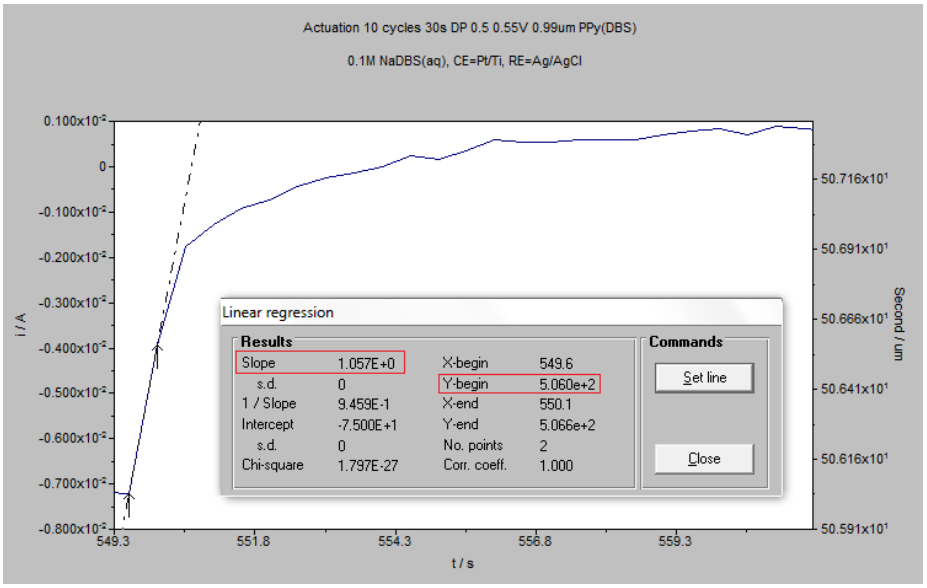

Fig 1.21 Determination of the maximum gradient (slope) using GPES. The values highlighted by red boxes, were used to determine the expansion rate (slope) and strain rate [(slope)/(("Y-begin"- D_{AuWE})/2))].

Another metric that has been used to assess how quickly the PPy films, was the time taken to reach 90% of the maximum expansion. This metric is calculated as it is phrased i.e. 90% of the maximum expansion is first determined and the time taken to reach this value from the start of the scan was determined. Again, this has been illustrated in figure 1.22. As has been mentioned previously, this region and above, is often prone to instability in the profile compared to earlier on in the scan. It was often helpful to draw and position a fitted curve by eye to aid this process. This is shown in green in figure 1.22 and it represents a form of averaging that leads to a more reliable value in the region of interest.

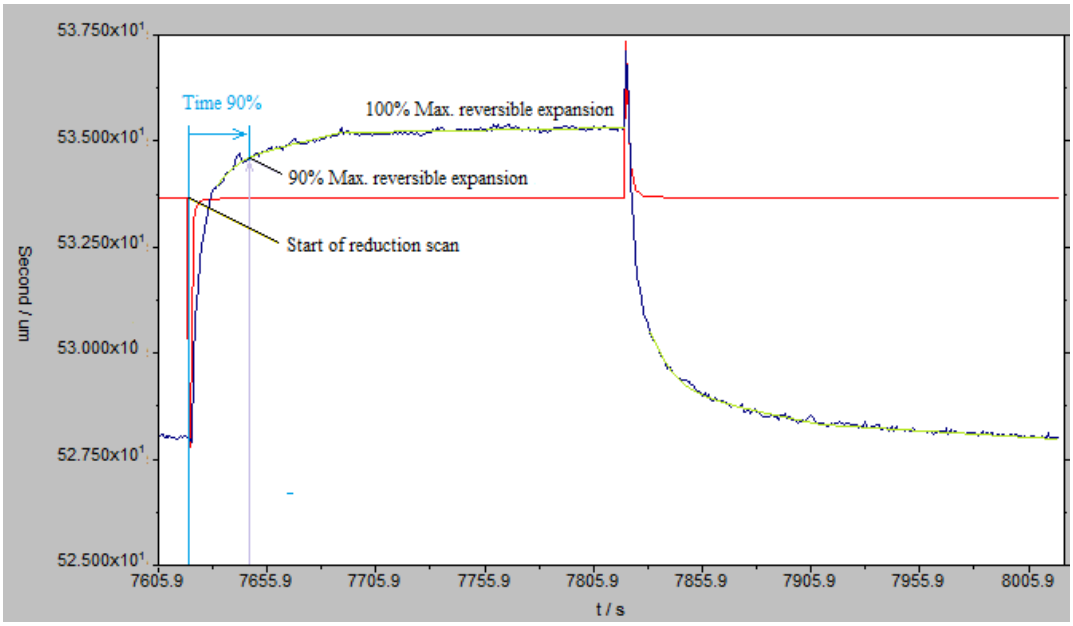

Fig 1.22 The determination of the time to 90% maximum expansion with the aid of GPES. Illustrated here, for the reduction scan of a 10 mm PPy(DBS) film in the stable state.

1.2.3 The effect of film thickness variation

When undertaking measurements on different film thicknesses, our aim was to generate base-line date, which could then be compared with the different types of polypyrrole synthesized and studied in the later sections of this thesis.

There has only been one study to date of the effect of film thickness variation on the actuation of PPy(DBS)[51] which used an atomic force microscope (AFM) to measure dimensional changes on films in the range 0.3 to 3.0 micron range. The study revealed that there was an optimal thickness (approx 1.5 μm) at which a maximum expansion occurred. Another interesting observation was that the maximum expansion observed also depended on the width of the feature, with the wider feature displaying a greater maximum expansion. These features were rectangular films with edges.

Film thicknesses of 1 to 10 microns were chosen as this leads to an absolute expansion of the PPy film that can be measured with the LSM with great accuracy, meaning that even small relative changes of the actuation performance due to a change in for example the crosslinking will lead to an absolute expansion difference larger than the measurement error. There was very good agreement between the work presented here and the previous study[51]. The values for expansion and strain were slightly higher than those given in the AFM study. This can be attributed to, amongst other things, the different cycle time employed and the different geometry of the samples. Here a 400 s

cycle (-1 V (200s), 0 V (200s), square wave) was used whereas the AFM study employed a 200 s cycle (1 V (100s), 0 V (100s), square wave). Our cycles therefore, had more time to slowly expand towards the end of each scan. The samples used in this work were formed on the surface of a cylindrical wire and, as such, had no edges. The samples in the prior study by Smela, were planar and had edges.

In the work undertaken in later sections of this thesis, it was noticed, when drying PPy(DBS) films with a nitrogen gun, that the surface of the film continues to appear dry when blown, whereas the edges of the film (which were sloping for our samples) first appear dry, but soon darken and appear moist again. It would appear that water movement is different in plane and compared to out of plane, with seepage of water being possible at the edges. This would be in keeping with the view that PPy(DBS) films have a lamella structure orientated parallel to the surface of the substrate[37]. If this is the case it would appear that water can both enter and leave the film more readily between lamellae at the edges of the film. Perhaps the difference in the expansions of the different width features studied by Smela can be attributed to the ability of the wider features to retain more solvent and expand more on actuation.

Figure 1.23 shows typical actuation sequences for both a one micron and ten micron film, which have been overlaid to aid comparison. Both the reversible and irreversible expansion is greatest for the thicker film. The time taken for the films to reach the "stable state" (maximum irreversible expansion) is greatest for the thicker film (100+ cycles) compared to the thinner film (12 cycles). The thicker film displays spikes on switching, whereas the thinner film does not.

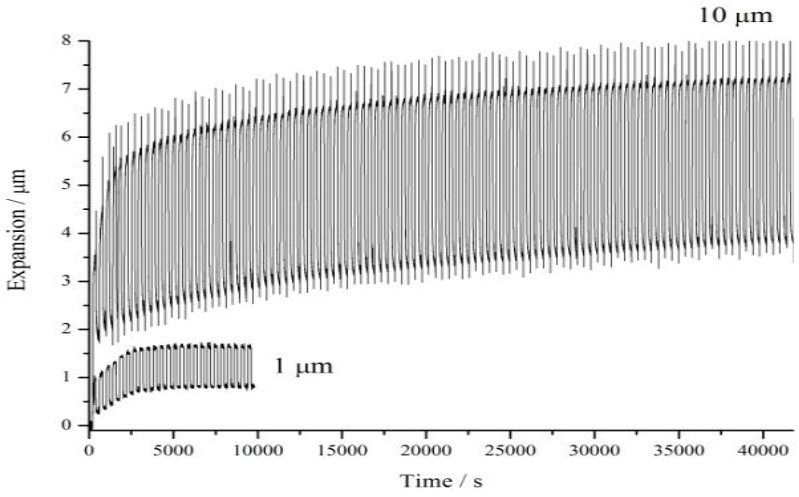

Fig 1.23 Overlay of typical actuation sequences for 1 and 10 μm PPy(DBS) films.

An overlay showing the relative proportions and shapes of the cycles displayed by the different film thicknesses is given in figure 1.24 (a) and (b). In particular figure 1.24 (b)

shows that the 1 and 10 μm films display different behaviour during the latter part of the reduction scan. This is revealed by the different peak shapes. The 1 μm film shows a maximum reversible strain earlier on which then decreases for the remainder of the scan. In contrast the reversible strain for 10 μm films (and also the 5 μm) increases to a maximum value then remains constant. This occurs towards the end of the actuation cycle.

(a)

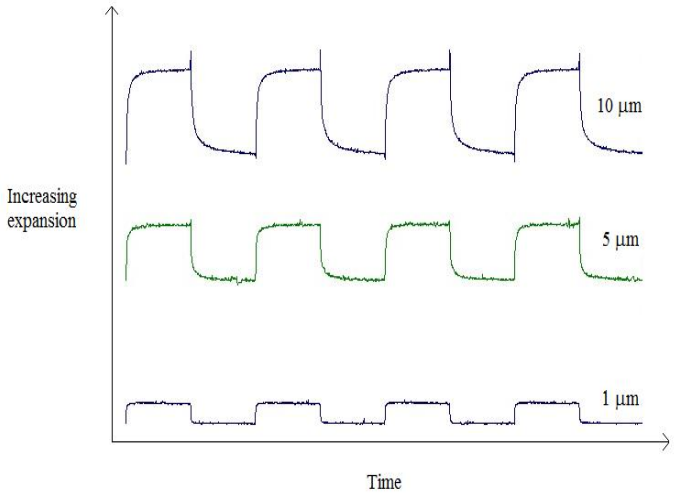

(b)

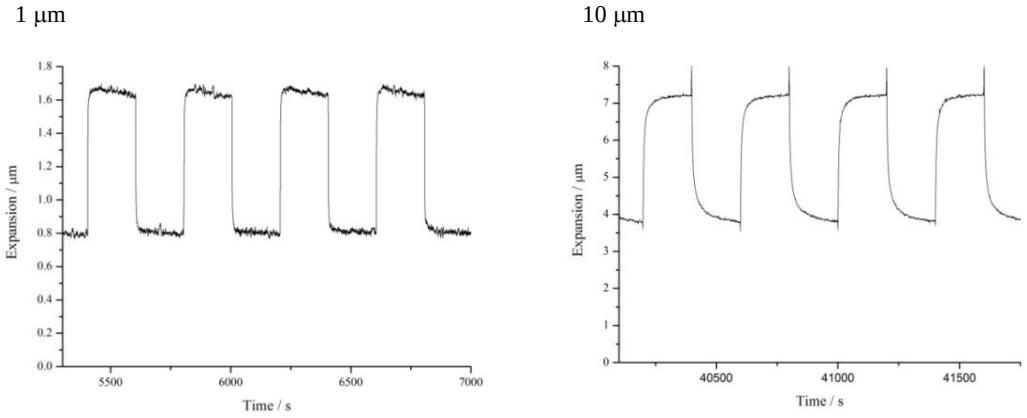

Fig 1.24 (a) Overlay of four actuation cycles for 1, 5 and 10 μm films taken during the stable state (to scale). **(b)** Actuation cycles for 1 and 10 μm films taken during the stable state showing greater detail of their respective profiles (not to scale).

The decrease in expansion observed for the 1 μm films in the latter part of the reduction scan, might be due to the loss of water that had entered the film earlier on in the reduction scan. This would be in keeping with the lower expansions observed in Smela's work for smaller width features. De-doping of the films is considered unlikely

as the performance of subsequent cycles is unaffected and this would be expected if NaDBS molecules were leaving the polymer film.

The changes that occur with thickness in the reversible and irreversible expansion are displayed in figure 1.25. Both the reversible and irreversible expansion increases on going from the 1 to 10 μm samples. The increase in the irreversible expansion is relatively large between 1 and 5 μm compared to between 5 and 10 μm. The variation between the samples (error bars = 2 SD) was relatively low, but increased with film thickness.

Figure 1.25 (b) suggests that the increase in the irreversible expansion is slowing down and potentially approaching an upper bound of a few micron. If this is the case, then it would be supportive of the notion that the expansion occurs at the surface to a depth of a few micron.

When these expansions are expressed as a percentage of their initial thickness (% strain) it can be seen that the thinner, 1 μm, films undergo a greater amount of reversible and irreversible strain in proportion to their thickness than do the thicker 10 μm films (see figures 1.26 (a) and (b)). Again, this would be supportive of the idea that actuation is occurring only within several microns of the surface. In that case most, if not all, of the thickness of the 1 μm films might be expected to be involved in actuation, whereas a much lesser proportion of the 10 μm films would be expected to take part.

The maximum reversible expansion rate during both the reduction and oxidation phases are shown in figure 1.27. During the reduction phase, this rate is reasonable constant. This again supports the idea that the actuation is occurring as the result of a near surface layer that is approximately the same size for each of the thicknesses and that below this layer the material is not taking part in the actuation process (other than to transfer charge from the AuWE).

(a)

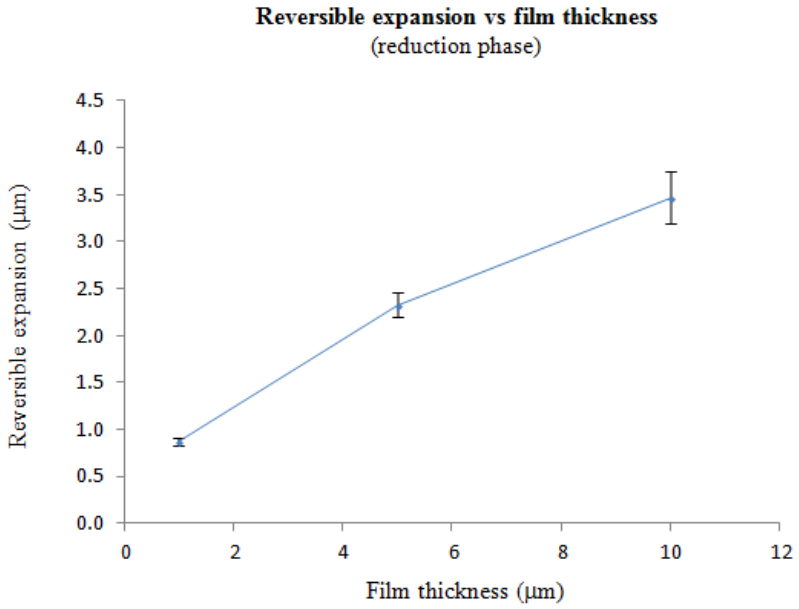

(b)

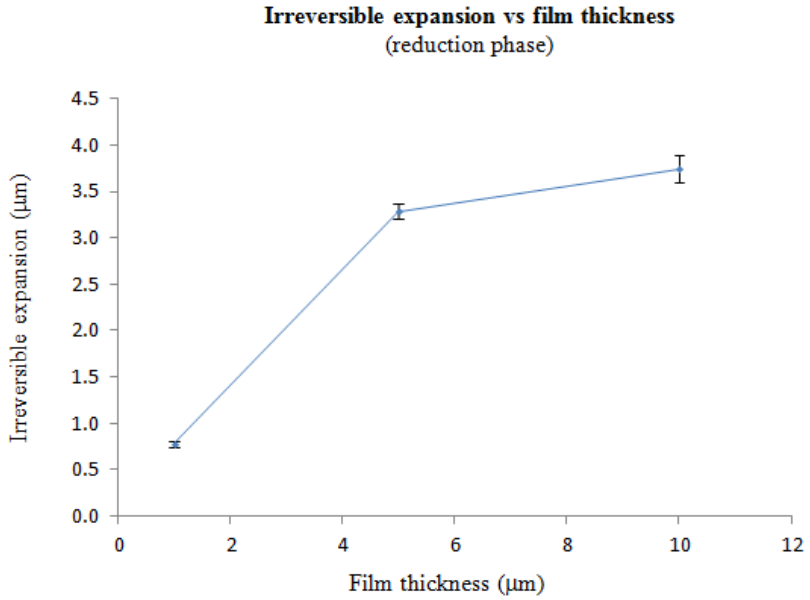

Fig 1.25 Change in (a) reversible expansion and (b) irreversible expansion with film thickness for 0.55V PPy(DBS). Error bars represent 2 SD.

(a)

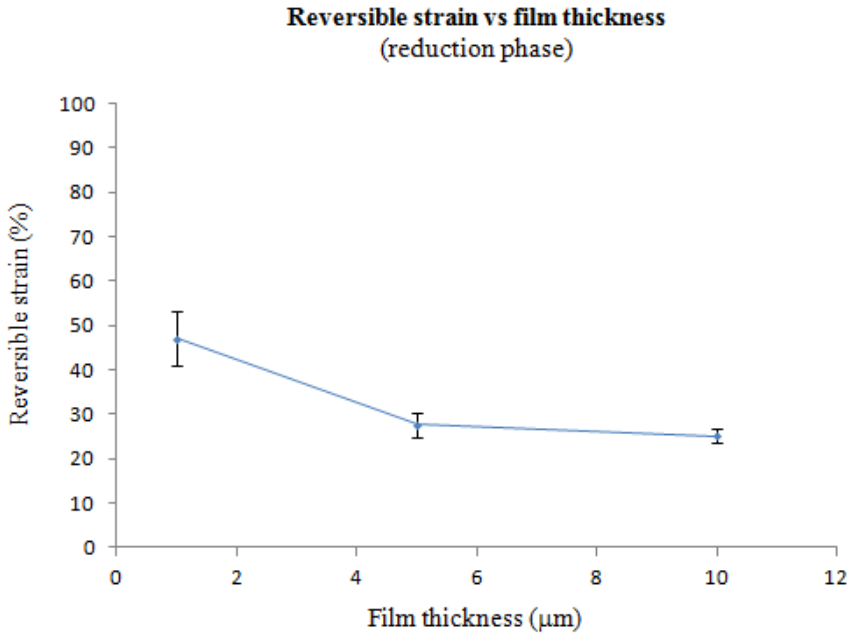

(b)

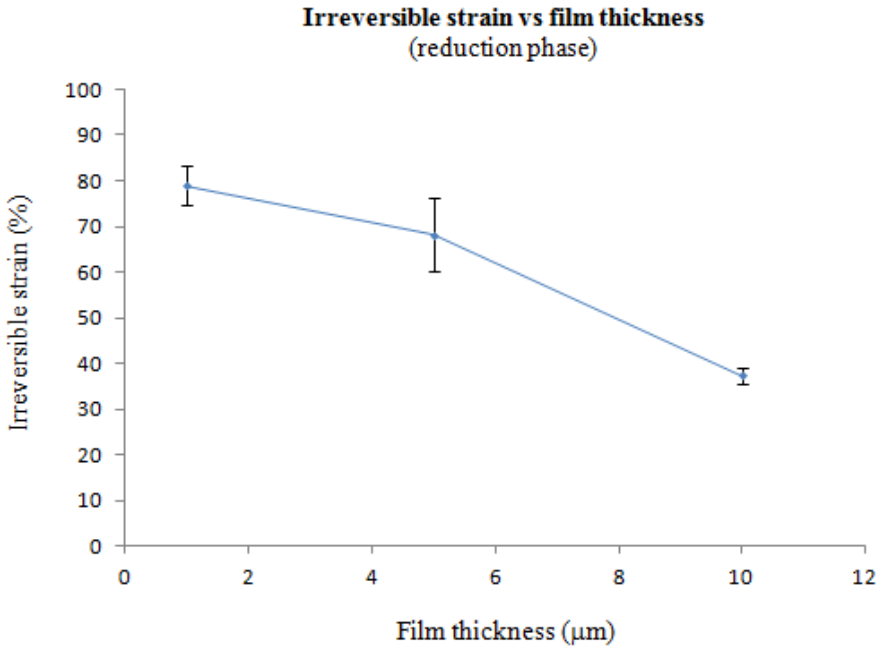

Fig 1.26 Change in (a) reversible strain and (b) irreversible strain with film thickness for 0.55 V PPy(DBS). Error bars represent 2 SD.

The maximum reversible expansion rate during the oxidation phase is however thickness dependant, with there being an increase on going from 1 to 10 μm. Once again, this increase would appear to be decreasing and beginning to level out above 5 μm.

Comparing the mean values in figure 1.27 (a) with those in 1.27 (b) we see that the reduction scan occurs more quickly that the oxidation scan for 1 μm films, but for the thicker, 5 and 10 μm films, the situation is reversed.

The maximum reversible strain rates during both reduction and oxidation are displayed in figure 1.28 (a) and (b). These graphs indicate that although the combined expansion rates increase for thicker films, it is the thinner films that will likely reach their maximum strain more quickly, since they do not have to expand as much as the thicker films to reach their maximum strain.

The time to 90% reversible expansion during both the reduction and oxidation scans are displayed in figure 1.29 (a) and (b). They clearly reveal that thicker films take longer to expand than thinner films. The total cycle time for 90 % expansion for a 1 μm film is typically less than 10 s whereas for 10 μm films this can be as much as 70 s, under the cycling conditions employed.

Comparing the variation between replicate measurements ("error" bars = 2 SD) displayed in figures 1.27 and 1.29, it can be seen that there is less variation in the measurements for thicker films when determining maximum expansion rates, whereas it is the opposite when determining times to 90% maximum expansion.

(a)

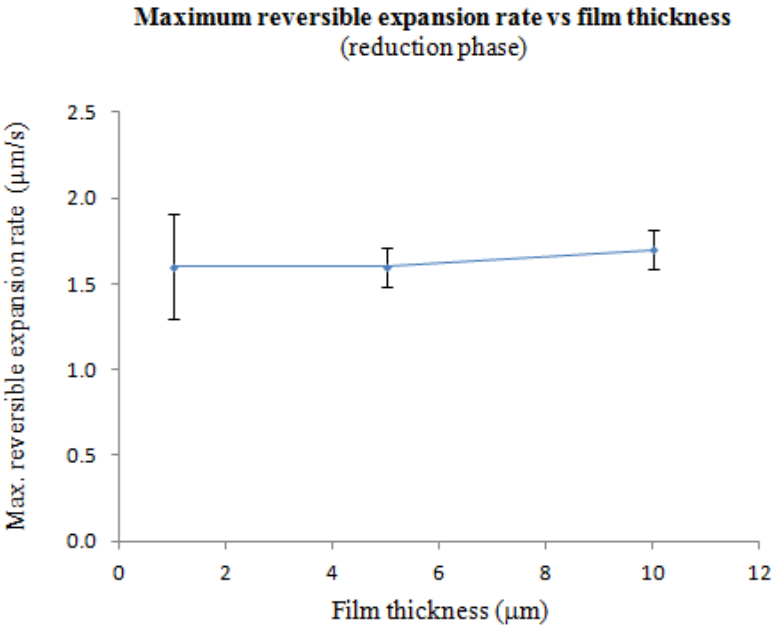

(b)

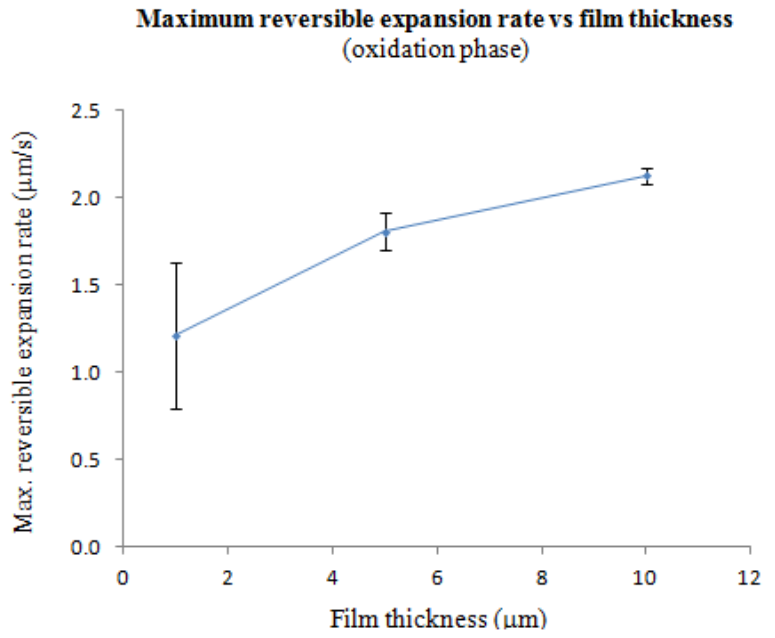

Fig 1.27 Variation in the maximum expansion rate during (a) reduction and (b) oxidation with thickness. Error bars represent 2 SD.

(a)

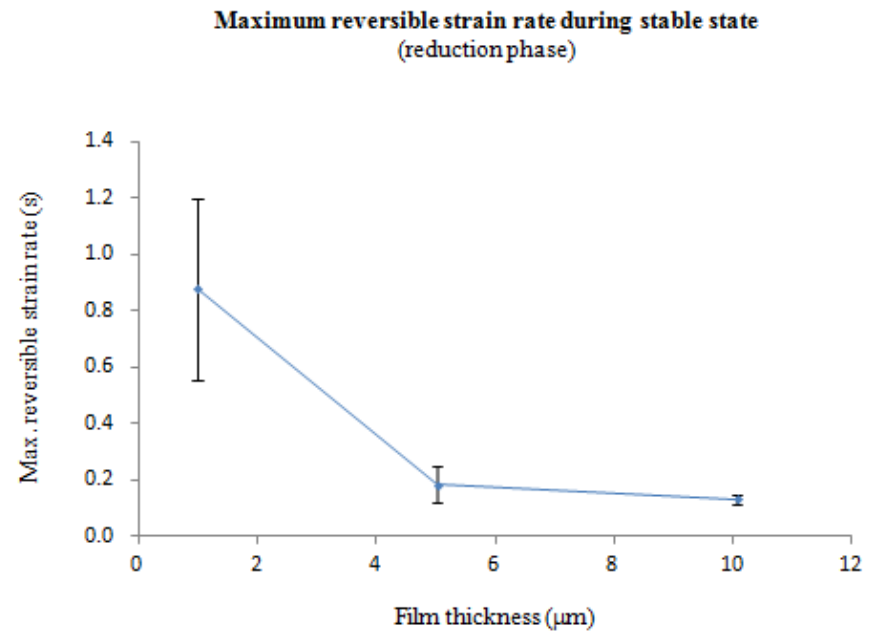

(b)

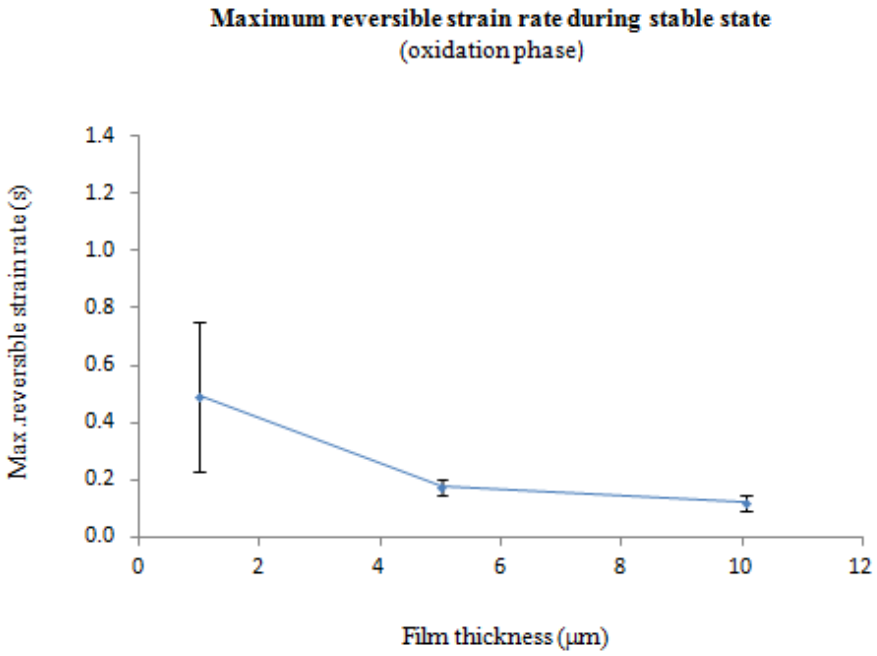

Fig 1.28 Variation in the maximum strain rate in the stable state during: (a) reduction phase (b) oxidation phase. Note: the strain rates during oxidation have been shown as positive to aid comparison. Error bars represent 2 SD.

(a)

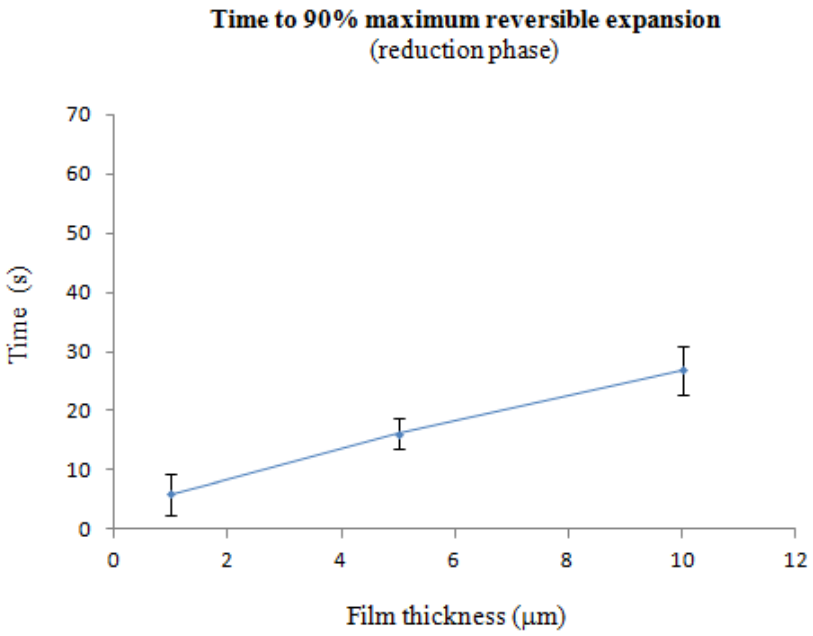

(b)

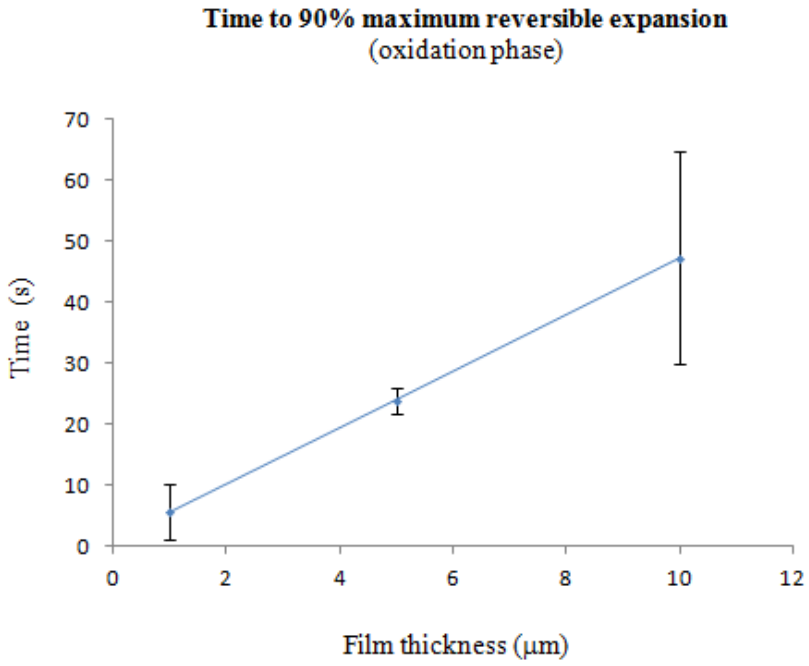

Fig 1.29 Variation in the time taken to reach 90% of the maximum reversible expansion with film thickness during: (a) Reduction phase (b) oxidation phase. Error bars represent 2 SD.

1.2.4 Apparent delay in the onset of expansion.

Another interesting observation that was made whilst undertaking measurements on films of different thickness was an apparent delay in the onset of expansion after the switching potential had been applied.

Figure 1.30 shows the typical current spikes associated with switching potential. A downward current spike is observed on switching from 0 V to -1 V and an upward spike on switching from -1 V to 0V. The shape and size of these current spikes will depend on the data point interval used during their measurement. At the scale shown in figure 1.30, no time delay in expansion is evident.

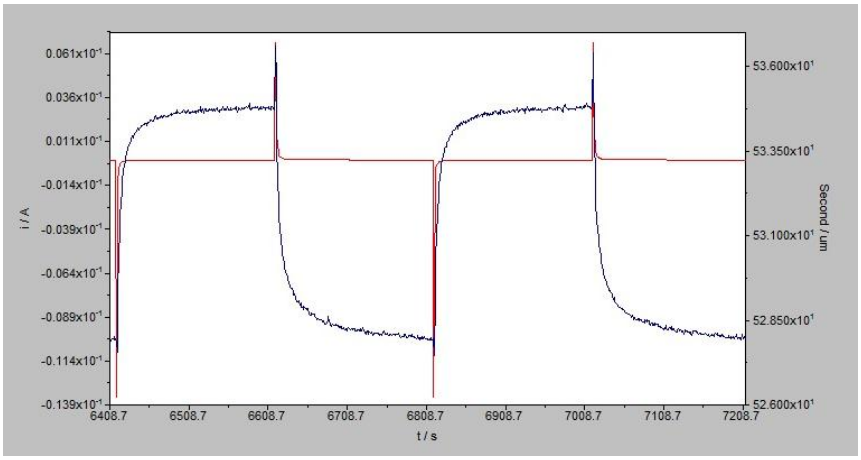

Fig 1.30 Overlay of current spikes (red) accompanying voltage switching with two actuation curves (blue).

The apparent time delay does become apparent when rescaled to zoom in on the start of each scan. Figure 1.31 (a) shows the start of the reduction scan for one of the replicate 1 μm samples. There is a 1 s time delay between the application of the switching potential and the onset of expansion. Figure 1.31 (b) shows the start of the next oxidation scan for the same sample. In this figure there is no time delay and the "expansion" occurs immediately.

Figure 1.32 (a) and (b) show similar details of the start of the reduction and oxidation scans for a 10 μm film. An apparent time delay of 2.1 s was observed on switching at the start of the oxidation scan Figure 1.32 (b) shows the detail at the start of the reduction scan for the same 10 μm film. An apparent time delay of 3.1 s was observed.

The apparent time delays between the application of the switching potential and the start of expansion and contraction could be the result of the low sampling rate employed at this stage of the work. It might be that these delays will not be evident if the work were to be repeated at a higher sampling rate. Alternatively, the delay in the onset of

expansion and contraction might be the result of interference from the "Mirage Effect" (see section 1.1.7). However, the delay might in fact be a real delay due to the time it takes for ions to move into the polymer film[116]. Given the low sampling rate employed in gathering this current data, conclusions cannot be drawn at this stage. These observations merit further investigation using a higher sampling rate.

(a)

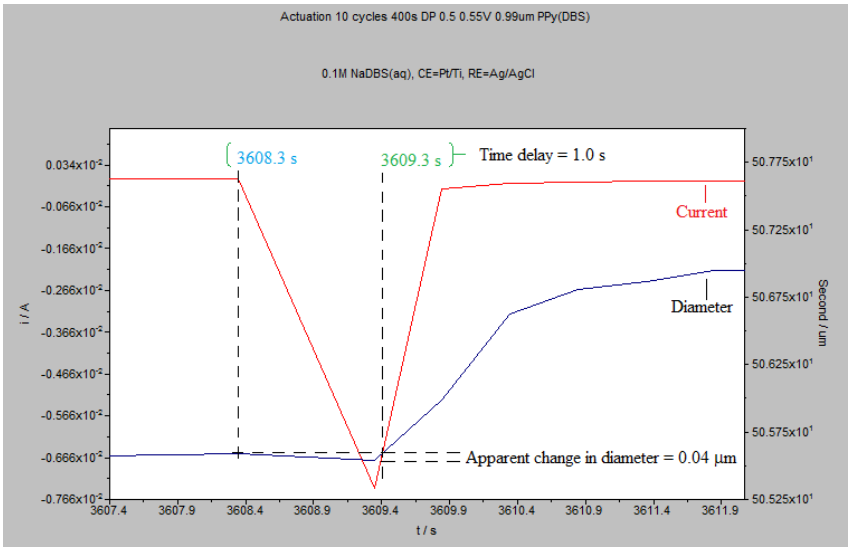

(b)

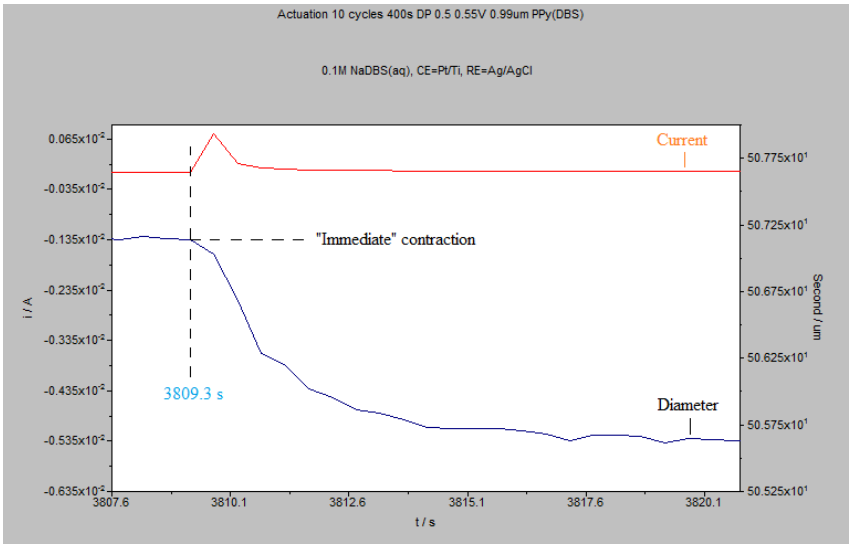

Fig 1.31 Overlays of the actuation and current curves during the first few seconds of (a) reduction and (b) oxidation scans for a 1 µm film.

(a)

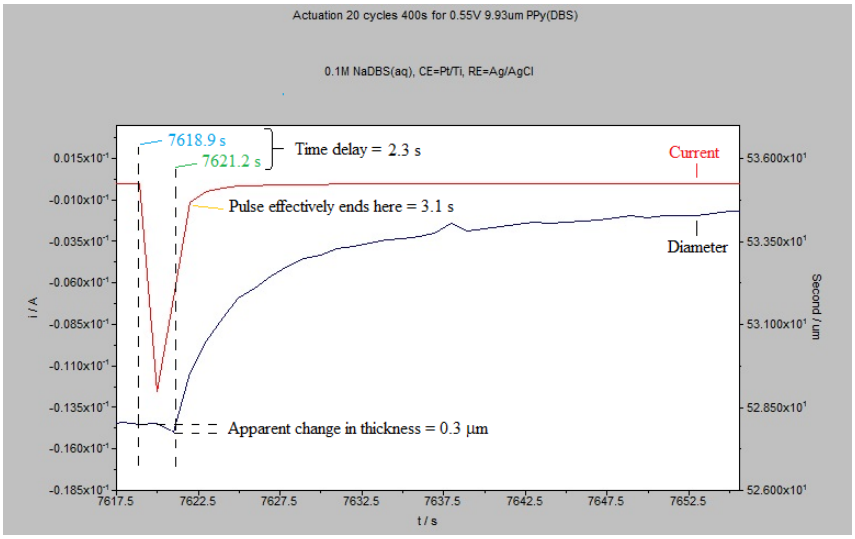

(b)

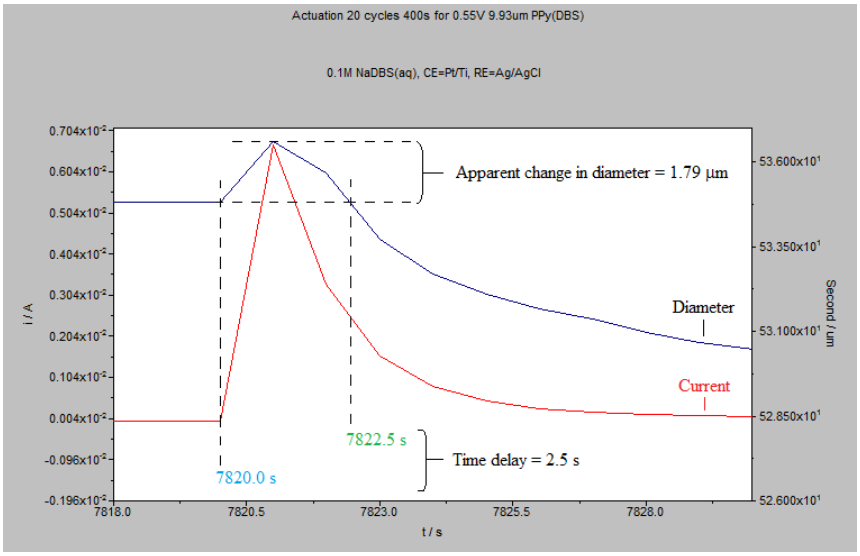

Fig 1.32 Overlays of the actuation and current curves during the first few seconds of (a) reduction and (b) oxidation scans for a 10 µm film.

1.1.5 Charge flow during reduction and oxidation

The charge which flows during oxidation and reduction is not solely used to oxidize and reduce the polymer. The charge which flows is also consumed by capacitive charging and parasitic reactions that can occur within the electrochemical cell[116]. This might explain why after the initial current spike associated with switching has decayed away, a very small constant current is observed throughout the remainder of each scan.

Because of the interest in monitoring long term behaviour (irreversible expansion) and yet being limited to using less than 10000 data points by the GPES software, out of necessity a relatively large data point interval was employed in this early work. In subsequent work, steps were taken to increase the number of data point. A comparison of the current spike profiles using a relatively large and a small data point interval are shown in figure 1.33 (a) and (b). These show that there was an under estimate of the charge which flows during the oxidation scan and an apparent over estimate of the charge flow during the reduction scan in the early work compared to the later work.

Given that it would not be possible to correctly apportion charge flow during each scan to oxidation and reduction, and having a large data point interval, no attempt was made to draw conclusions from the charge flow data.

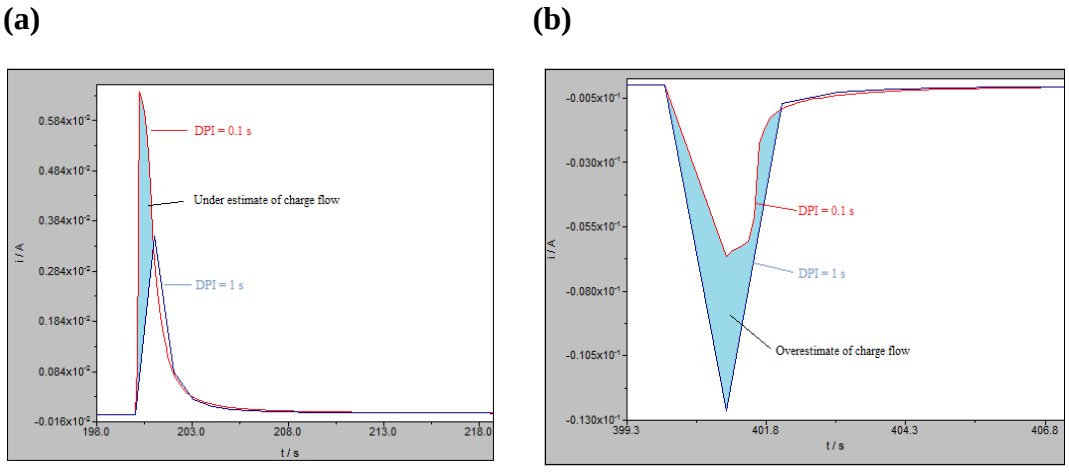

Fig 1.33 Overlays of current spikes using a relatively large (1 s) and small (0.1 s) data point interval (DPI). The oxidation spike (a) is under-estimated with a DPI of 1 s whereas the reduction peak spike (b) is over-estimated at a DPI of 1 s.

1.1.6 Different cycling conditions

During the initial stages of this work, different cycling times were investigated to aid the selection of a standard cycle time. A cycle time of 400 s was selected (200s (-1 V), 200s (0 V), square wave) in order to ensure that the complete expansion and contraction had occurred as revealed by the flattening of the upper and lower peak profiles. This was because the focus was on determining the maximum expansion in the work that we had later scheduled.

An interesting observation that was made however in undertaking this initial work was that shorter cycle times lead to more irreversible expansion and less reversible expansion. Given that this expansion is the result of mass transport, ions and solvent movement, it would appear that shorter cycle times result in more solvent and ions being retained by the polymer matrix on redox switching. An analogy might be drawn to squeezing out a sponge in a bucket of water; the less the sponge is squeezed, the more water is retained.

Given that the longer cycles shown in figure 1.35 were undertaken after the initial shorter cycles, it would appear that if one has longer cycles after shorter cycles, the "full" reversible expansion might be recovered and the irreversible expansion lowered. This merits further investigation in the future.

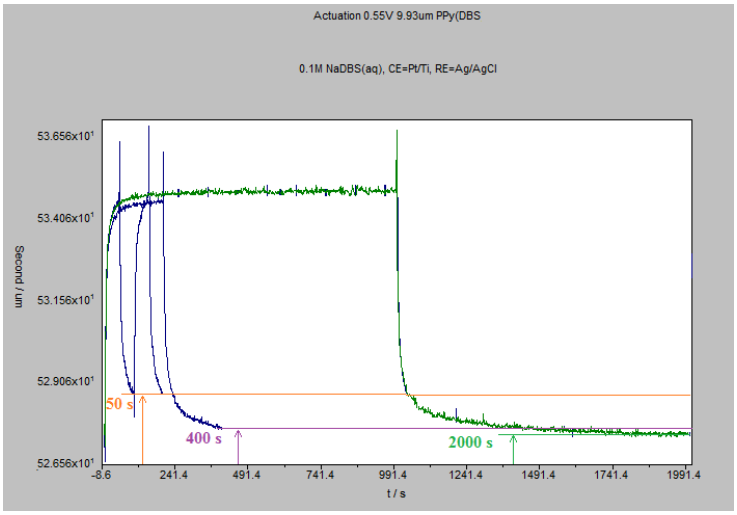

Fig 1.34 Increase in the thickness of the same PPy(DBS) film for different cycle times. Notice that the irreversible expansion (arrows) increases with shorter cycle times.

1.1.7 The "Mirage Effect"

Although the spikes observed in the diameter reading of the polymer coated wire which occur on switching have been attributed to the "Mirage Effect" we have not detailed

how we think this might be happening[117,119]. The same effect has been observed when using an AFM laser to make measurements in high salt concentrations[120].

The spikes in the diameter measurement of the wire that accompanies voltage switching is likely, in the authors view, to be due to the relative change in the refractive index accompanying the insertion and de-insertion of sodium ions at/near to the polymer surface.

An increase in the ion concentration would be expected to cause a local increase in the refractive index of the electrolyte near the surface of the polymer. This is the case at the start of the oxidation scan (-1 V to 0 V) and corresponds to an apparent increase in the diameter of the WE (upward spike) observed in the data. A local decrease in the refractive index would similarly be expected to occur when there is a decrease in the sodium ion concentration near the polymer surface. This is the case at the start of the reduction scan and corresponds to an apparent decrease in the diameter of the WE (downward spike) observed with the data.

On oxidation, the sodium ion concentration at the polymer surface is likely to first increase due to expulsion from the PPy into the solution and then decrease with time as the sodium ions are dispersed throughout the surrounding bulk electrolyte, by diffusion but possibly also through electrostatic repulsion *i.e.* classical radial diffusion of sodium ions restoring the bulk concentration near the surface.

This model was crudely tested out in a dark room with a non-transparent cylindrical object being placed at the centre of an up turned cylindrical glass, and a laser pen. The cylindrical object was taken to model the WE and the glass wall to model the increase in the refractive index of the electrolyte upon oxidation.

As illustrated in figure 1.35 the laser spot was refracted away from the wire in the radial direction. The paths of the laser could be traced as are also shown in the same figure. If this behaviour correctly models the situation that occurs upon switching from -1 V to 0 V (oxidation), it would explain the upward spike observed in the data.

The opposite effect could be expected to occur on switching from 0 V to -1 V (reduction), to produce a lower density zone at the polymer surface, depleted of sodium ions, and causing the laser to bend inwards and producing a smaller width shadow on the LSM detector. This would correspond to the apparent decrease in the diameter of the WE as represented by the downward spike observed in the data.

The absence of a spike in the diameter reading on switching the thinner, 1 μm, films is likely due to the lower numbers of sodium ions that can be exchange ("stored" and "released") by the thinner films and produce too low a refractive index change to cause the effect.

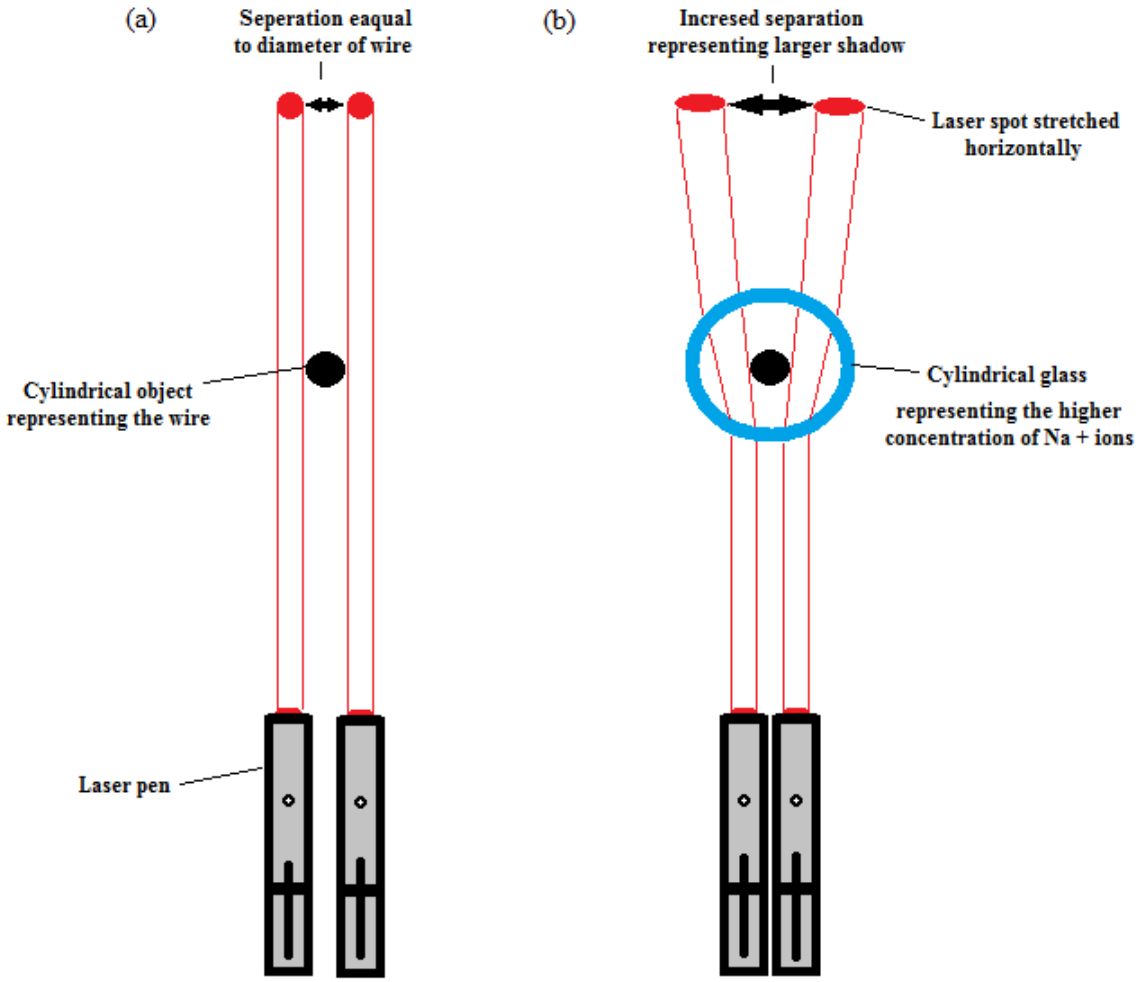

Fig 1.35 The position, size and shape of the laser spots (a) without and (b) cylindrical region of higher refractive index (a cylindrical glass).

Interestingly, a similar situation has been envisaged near the surface of a star and has been used to explain the bending of light near the surface, as an alternative to the accepted gravitational red/blue shift of light[121].

1.3 Conclusions

A method for making rapid, non-contact measurements of the actuation of electroactive films such as polypyrrole has been developed. The method is particularly suited to studying the actuation of thin films in the region of 0.5 to 5 micron, which covers the ranges of thicknesses commonly employed in the fabrication of micro-actuators. It is also suitable for studying the actuation of thicker films when they are actuated slowly,

as in this study. However, thick films actuated quickly, will be subject to measurement error in the first short period of the cycle due to the operation of the "Mirage Effect".

Once a more precise model of the out of plane movement of sodium ion has been developed and tested for the geometry of our films, the method that we have developed has the potential of being used to quantify both the amount and rate of ion flux into and out of the polymer film on switching. Not only would this lead to a better understanding of the actuation process, but it might be used to study the controlled release of chemicals/drugs that have been incorporated within the polypyrrole film during electropolymerization.

It is important to recognize that not all of the thickness of the PPy film is electroactive. Only the portion near surface of the film is active as the ions required for charge compensation are unable to penetrate the full depth of the film during the time of a typical cycle. Diffusion is typically the rate limiting step for such films and is a well-known and established fact in the field[116]. One way of demonstrating this is through the use of cyclic voltammetry performed at different scan rates (see Appendix 2).

Although the measurements that were made at different thicknesses were done to generate metrics which could then be used to compare other forms of polypyrrole against, the measurements have proved very useful in their own right. The measurements made at different film thickness, were consistent with those made using AFM[51]. The results are supportive of the view that actuation occurs at the surface to a depth of a few micron and is a diffusion limited process. For the thinnest films employed in this work (1 μm) approx. 80 % of the thickness is active and for thicker films (10 μm) this ratio drops to 25 %, which is typically an effect of diffusion. Despite using extremely long cycle times (200s (0V), 200s (-1V)), full activity of the film is not observed. In absolute numbers the active expansion increases from approx. 0.8 μm for the 1 μm to approx. 3 μm for the 10 μm films which we contribute to the film being less dense. The density of PPy films is well-known to be anisotropic[37, 51].

Two contributions to the volume change can be clearly distinguished. The fastest part is ion diffusion which in turn correlates with the current and a slower part due to the intake of solvent (osmotic flow)[49]. The thinner films are "faster" than the thicker films. In addition we have shown that quicker cycling can result in a decrease in the reversible expansion and an increased irreversible expansion.

The development of this new technology has proven very useful, not only in providing reliable actuation metrics, but also in increasing our understanding of the actuation process. In the work that is outlined in subsequent sections of this thesis, the method has been used to provide insight into how the structure of polypyrrole affects the actuation process, particularly cross-linking and branching. This is the focus of the remainder of this thesis.

2. The synthesis of 3,4-dimethyl-1H-pyrrole

2.1 Experimental details

In order to implement our strategy for controlling crosslinking in polypyrrole a supply of 3,4-dimethyl-1H-pyrrole was needed (see section 3). Unfortunately, this material is not available commercially and it therefore had to be synthesize. The synthesis of pyrroles substituted exclusively in the beta positions of the pyrrole ring is difficult to accomplish and there are few synthetic strategies available. This is because the pyrrole ring system tends to undergo substitution preferentially in the alpha positions. If substitution does occur in the beta positions it is usually accompanied by substitution in the alpha positions, resulting in multiple substitution patterns and mixed products. In addition, there is also the potential problem of substitution at the pyrrole nitrogen atom and protecting groups are often necessary to prevent this.

To produce pyrroles that have substituents exclusively in the beta positions requires that special synthetic strategies are implemented. Two strategies were selected as potentially being suitable and the detailed synthetic steps are described in section 2.1.1. The first strategy shown in figure 2.1 (a) makes use of a protecting group, which also blocks substitution at the alpha positions of the pyrrole ring[122]. The second strategy relies on the formation of the pyrrole ring by ring closure in what is a type of "Diels Alder" reaction, with the methyl groups already in place[123]. The first formed ring system in this second strategy, is a non-aromatic six-member ring. This subsequently undergoes ring reduction and aromatization to form the final product.

2.1.1 Synthetic scheme 1[122] – protecting group approach.

Step 1: Synthesis of N-(triisopropylsilyl)pyrrole (II)

Pyrrole (5.0 ml, 4.84g, 72 mmol) was added drop-wise at 0^{o}C to a mechanically stirred suspension of sodium hydride (3.17 g of a 60 % dispersion in mineral oil, 79 mmol) in anhydrous DMF (100 ml). When hydrogen evolution (foaming) had ceased (ca 1.25 h), triisopropysilyl chloride (15.3 ml, 13.9 g, 72 mmol) was then added drop-wise and stirred at 0 ^{o}C for 0.75 h. The reaction mixture was next partitioned between ether and water, the ether phase washed with water, dried over anhydrous sodium sulphate, and evaporated *in vacuo*. Vacuum distillation of the residue gave an oil (15.90 g, 99 % yield), bp 125 ^{o}C / 11 mmHg, mp 5 ^{o}C, which was indefinitely stable under ambient conditions.

Step 2: Synthesis of 3, 4-diiodo-1-(triisopropysilyl)pyrrole (III)

A solution of iodine (1.14 g, 4.48 mmol) in anhydrous dichloromethane (200 ml) was added drop-wise, over a 1 h period, to a stirred solution of N-(Triisopropylsilyl) pyrrole (0.500 g, 2.24 mmol) in dichloromethane (80 ml) containing suspended mercuric acetate (1.43 g, 4.48 mmol) at 0 ^{o}C. After a further 1 h at 0 ^{o}C, the reaction mixture was worked up as described in step 1, to give a solid (1.1 g) containing 3, 4-diiodo-1-(triisopropysilyl) pyrrole. (This solid should be purified by column chromatography on active II neutral alumina (50 g), using hexane as the eluting solvent. 3,4-diiodo-1-(triisopropylsilyl) pyrrole will be obtained as a solid (0.730 g, 69 % yield), which on crystallization from hexane will have a mp 75-78 ^{o}C)*

Step 3*: Synthesis of 3, 4-dimethy-1-(triisopropylsilyl)pyrrole (IV)

To a solution of 3, 4-iodo-1-(triisopropysilyl)pyrrole (2.375 g, 5 mmol) in anhydrous THF (25 ml) at -78 ^{o}C, add methyliodide (1.42 g, 10 mmol) and 15 min thereafter remove the reaction mixture from the cooling bath and leave to come up to room temperature. Quench with water and extract with ether. Next, dry the extract with magnesium sulphate and evaporate in vacuo. The residue should then be purified by column chromatography on silica gel using hexane-ethylacetate (4:1) to give an oil on evaporation in vacuo, of the appropriate fraction(s).

Step 4*: Synthesis 3, 4-dimethyl-1H-pyrrole (V)

Add a solution of tetra-n-butylammonium fluoride (1.00 ml of a 1 M solution, 1.00 mmol) in THF, to a stirred solution of 3, 4-dimethyl-1-(triisopropylsilyl)pyrrole (0.251 g, 1.00 mmol) in THF (3.0 ml). After 5 min at room temperature, dilute the solution with ether, and wash the organic phase with water and dried with magnesium sulphate. Remove the solvent in vacuo to give the target compound: 2, 3-dimethylpyrrole.

*****These steps were not undertaken for reasons given in section 2.4

2.1.2 Synthetic scheme 2[123] – cyclization approach

Step 1: Synthesis of 2-ethoxycarbonyl-3,6-dihydro-4,5-dimethyl-1,2-thiazine 1-oxide (III)

In a 1 litre round-bottomed flask, equipped with a large magnetic stirrer, a reflux condenser attached with a calcium chloride tube, and two 100 ml dropping funnels, were placed 27.1 g of ethyl carbamate and 150 ml of dry toluene. Pyridine and thionyl chloride were added drop-wise at the same rate with efficient stirring and cooling with cold water. A yellow precipitate was formed in the round-bottomed flask corresponding to the formation of the N-sulfinyl intermediate compound (II) (see figure 2.2 (a)). After the mixture was further stirred for one hour at room temperature, 25.0 g 2, 3-dimethylbutadiene (I) was added in one portion. The mixture was heated under mild

reflux and stirring and then allowed to stand overnight. After voluminous pyridine hydrochloride was filtered and washed with toluene, the filtrates were evaporated under reduced pressure to afford an oily residue of crude 2-ethoxycarbonyl-3,6-dihydro-4,5-dimethyl-1,2-thiazine 1-oxide (III).

Step 2: Synthesis of 3,4-dimethyl-1H-pyrrole (IV)

To the residue obtained in step 1, was added 300 ml of 10 w/w% sodium methoxide in methanol and the dark coloured mixture (see figure 2.2 (b)) was refluxed for 2 h. The solvent was removed by distillation under ordinary pressure, and the reaction mixture was steam-distilled (see figure 2.3) to give an oily substance which was extracted repeatedly with ether. The extracts were dried over anhydrous potassium carbonate, and the solvent removed by rotary evaporation under reduced pressure. Vacuum distillation of the oily residue gave 2.14 g 3,4-dimethyl-1H-pyrrole. The yield was 7.4 % based on ethylcarbamate which was lower than the published value of 62% (see section 2.4 as to why).

Scheme 1

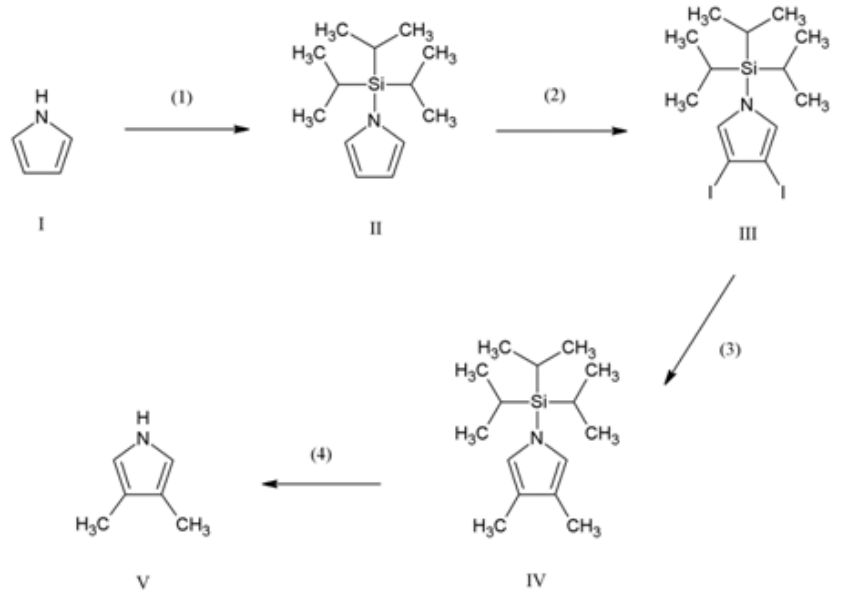

Scheme 2

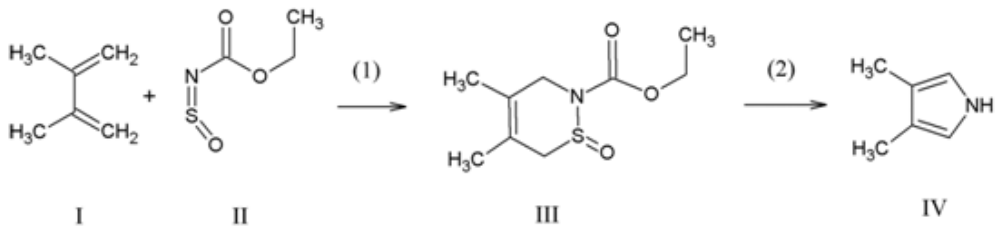

Fig 2.1 Synthetic schemes undertaken for the synthesis of 3, 4-dimethyl-1H-pyrrole.

(a)

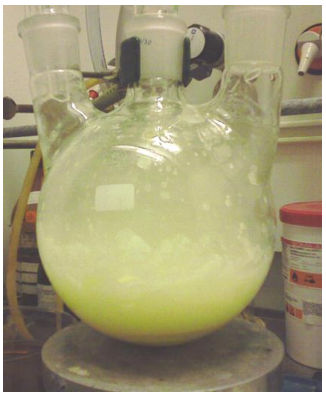

(b)

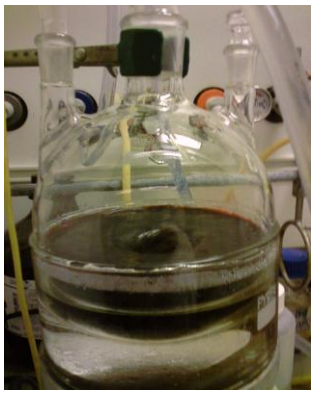

Fig 2.2 (a) Yellow precipitate of N-sulfinyl intermediate compound (III). (b) Dark coloured (intensely crimson) complex product prior to steam distillation, containing 3,4-dimethyl-1H-pyrrole.

Fig 2.3 Steam distillation of the crude product. (1) Steam generation, (2) glass tube to allow the pressure in the system to remain at atmospheric pressure and help avoid suck back, (3) glass tubing transferring steam to the distillation flask (4) distillation flask (the three necked round bottom flask used for the prior synthesis) containing the crude product, (5) water-cooled condenser, (6) flask receiving the steam distilled product (7) vent for pressure equalisation.

2.2 Structural confirmation

Proof that 3,4-dimethyl-1H-pyrrole had been synthesized was provided by a combination of techniques that are commonly used for structural confirmation in the field of synthetic organic chemistry.

The presence of both the pyrrollic ring system and methyl functionalities was confirmed using FTIR spectroscopy, with the sample in the form of a potassium bromide (KBr) disk. The FTIR spectrum and peak assignments are shown in figure 2.4 (a) and (b) respectively[124].

GCMS spectrometry was also used as part of the structural confirmation process. The mass spectrum obtained for the product is shown in figure 2.5 (a) and the gas chromatogram in figure 2.8.

The mass spectrum of the product displays a ion with the mass to charge ratio expected for 3,4-dimethyl-1H-pyrrole molecular ion (m/z = 95). A comparison was made using pyrrole, 2,4-dimethyl-1H-pyrrole and the 2,5-dimethyl-H-pyrrole isomers as being the closest matches to the synthesised product. Direct confirmation by the National Institute of Science and Technology (NIST) mass spectrometry database was not possible as the mass spectrum of 3,4-dimethyl-1H-pyrrole is not present in the database for comparison. However, contact with a company (Equinox Chemicals, USA) that has previously synthesized 3,4-dimethyl-1H-pyrrole was made and they were very helpful in providing us with a reference spectrum, which showed an excellent match for our product.

1H spectroscopy was undertaken on the product and is show in figure 2.6 (a). The 1H NMR spectrum of the product is in keeping with the 1H NMR spectrum expected for 3,4-dimethyl-1H-pyrrole. The three peaks displayed in the 1H NMR spectrum reveal the presence of three different types of protons within the molecule at 7.75, 6.53 and 2.05 ppm with corresponding area integrals in the ratio 0.15:0.35:1.06 (approx 1:2:6) (the fourth peak at approx 7.25 ppm corresponds to the small amount of trichloromethane present in the deuterated trichloromethane solvent, and is not part of the product molecule). These chemical shifts and area integrals are consistent with the types and numbers of hydrogen atoms that are present within 3,4-dimethyl-1H-pyrrolei.e. 1 x NH, 2 x ring CH and 6 x CH_3. The broadened peak at 7.75 ppm is typical of an exchangeable H-atom, and is consistent with the presence of the pyrrollic NH, which is known to be exchangeable. This broadening would also account for the area integrals not being exactly 1:2:6, particularly the area integral for the broadened peak.

(a)

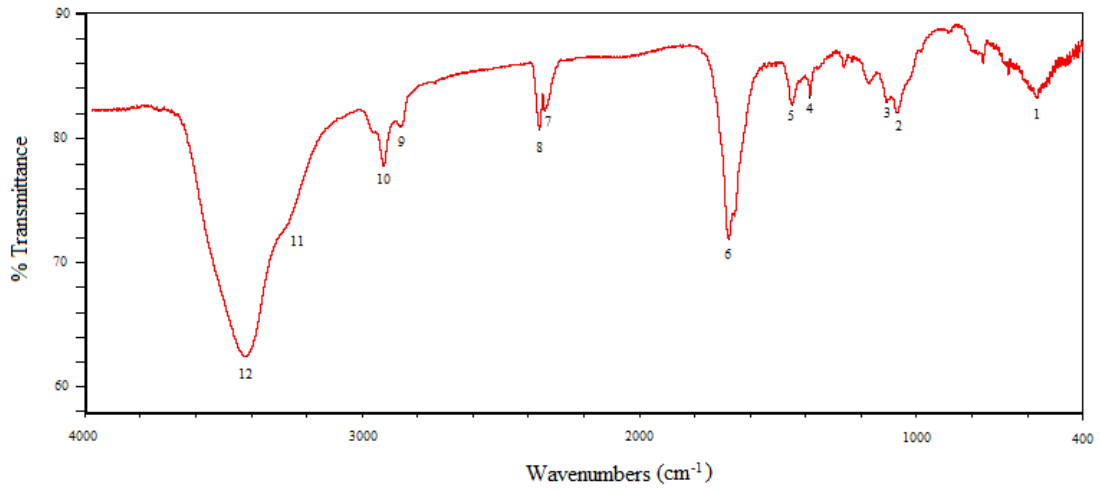

(b)

Peak Position (cm^{-1})	Peak Intensity and Description	Peak Assignments
(1) 564.57	Weak, broad	No assignment attempted.
(2) 1069.06	Weak, overlapping	No assignment attempted.
(3) 1107.54	Weak, overlapping	No assignment attempted.
(4) 1384.32	Medium	1395-1365: -CH_3 γ
(5) 1448.95	Medium	1470-1430: -CH_3 δ
(6) 1677.09	Strong, possible multiplet	No assignment attempted.
(7) 2341.24	Medium	CO_2 gas (contamination)
(8) 2360.33	Medium	CO_2 gas (contamination)
(9) 2863.05, (10) 2922.04	Medium, possible multiplet	3100: **pyrrollic CH** stretch
(11) 3250 (shoulder) (12) 3420.61	Strong Strong, broad	3400-2800: **pyrrollic NH** (H-bonded) stretch 3500-3400: **pyrrollic NH** (free) stretch

Fig 2.4 (a) FTIR Spectrum of 3, 4-Dimethyl-1H-pyrrole (KBr disc) with (b) potential peak assignments[124].

(a)

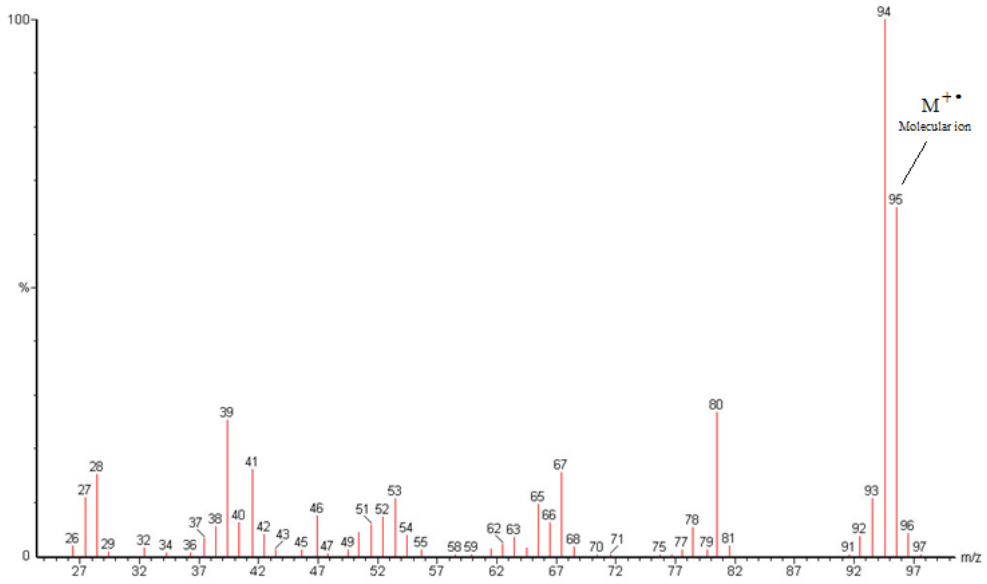

(b)

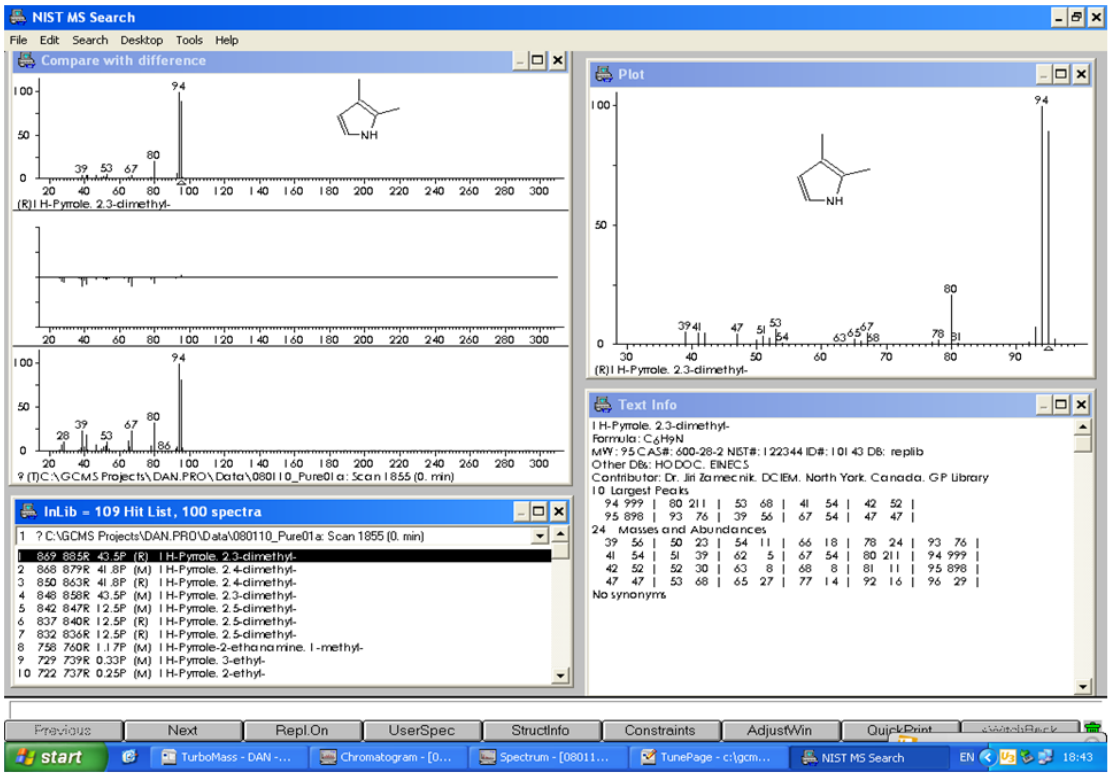

Fig 2.5 (a) Mass spectrum of 3, 4 - dimethyl-1H-pyrrole displaying the molecular ion. **(b)** NIST MS search listing three of the dimethylpyrrole isomers as the closest matches.

(a)

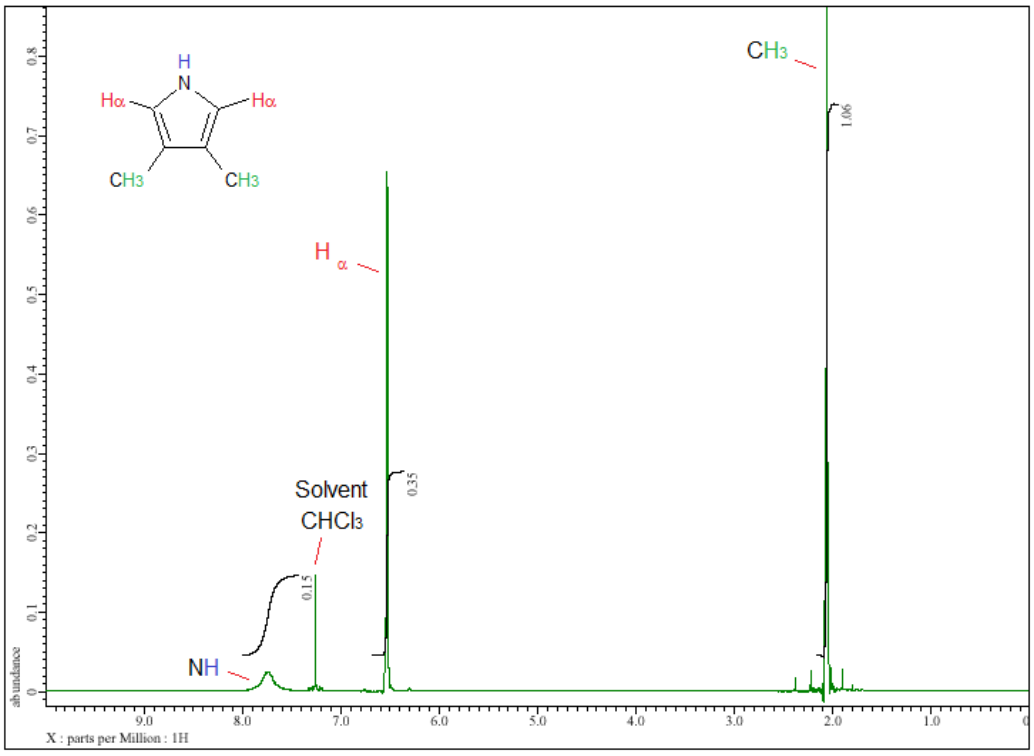

(b)

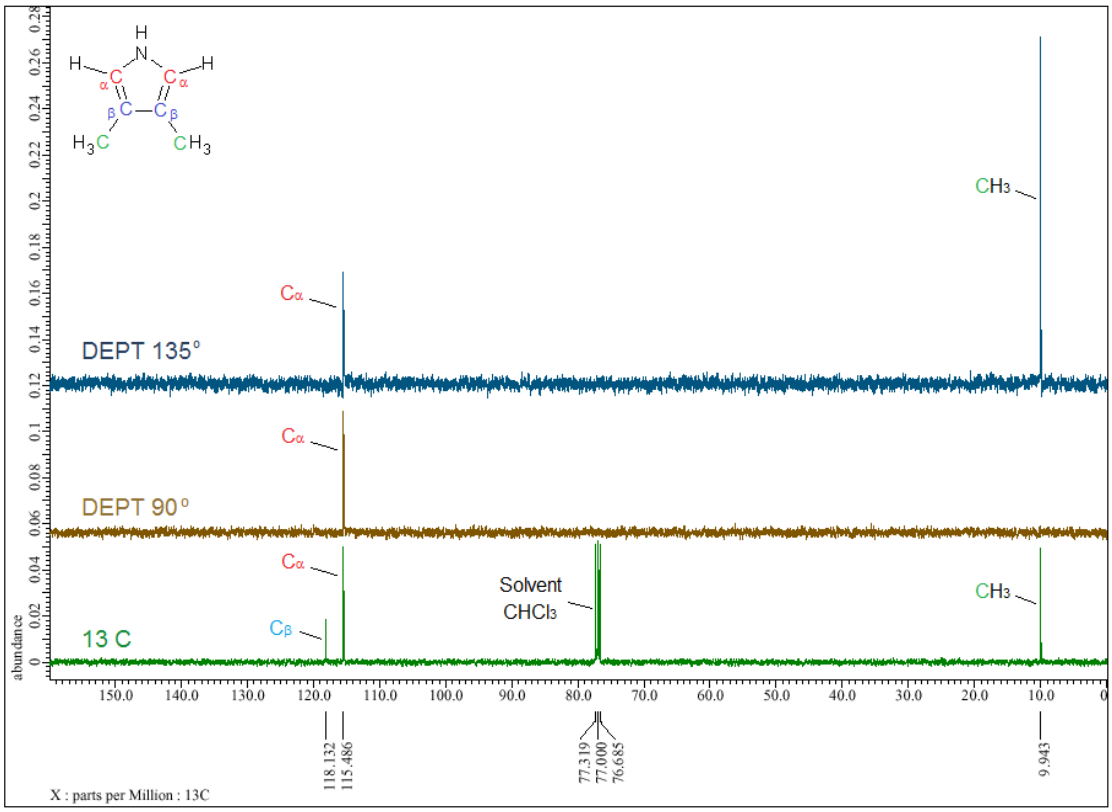

Fig 2.6 (a) 1H NMR spectrum of the product (b) Comparison of the 13C and DEPT 135^{o} and DEPT 90^{o} spectra for the product.

13C NMR spectroscopy of the product was also undertaken and is the lowest of the three spectra displayed in figure 2.6 (b). The 13 C NMR spectrum of the product displays three different peaks at 118.13, 115.49 and 9.94 ppm, due to three different types of carbon atom (the "peaks" at approx 77 ppm corresponds to the small amount of trichloromethane present in the deuterated trichloromethane solvent). Once again this is consistent with the three different carbon atoms that are present within 3,4-dimethyl-1H-pyrrole i.e. 2 x alpha C-atoms, 2 x beta C-atoms and 2 x methyl C-atoms. Unlike the area integrals in 1H NMR, the areas or heights of 13C NMR peaks should not be taken as indicative of the relative proportions of the C-atoms in the product, as area integrals are not quantitative in 13C NMR.

The two other 13C spectra displayed in figure 2.6 (b) are known as the DEPT 90^o and DEPT 135^o 13C spectra. DEPT (Distortionless Enhancement by Polarization Transfer) is a very useful method for determining the presence of primary (methyl, three attached hydrogens), secondary (CH2, two attached hydrogens), tertiary (CH, one attached hydrogen) and quaternary (C with no attached hydrogens) carbon atoms. The DEPT 90^o 13C spectrum gives only CH groups. The DEPT 135^o 13C spectrum shows CH, CH_3 in a phase (direction) opposite to CH_2. Signals from quaternary carbon atoms, and other carbon atoms with no attached hydrogens are always absent due to the lack of attached protons with which to undergo polarization transfer.

The DEPT 90^o spectrum of the product has only one peak at 115.486 ppm and reveals the presence of one type of a tertiary carbon atom (CH) within the molecule. This would correspond with the alpha carbon atoms present in 3,4-dimethyl-1H-pyrrole. The DEPT 135^o spectrum has two peaks which are in phase (both pointing upwards) and correspond to two different carbon atoms. The peak in the DEPT 135^o spectrum at 115.486 ppm corresponds to the peak at the same ppm in the DEPT 90^o spectrum; therefore this peak in the DEPT 135^o spectrum must correspond to a tertiary CH atom. The other peak at 10.08 ppm might therefore be assigned to the primary methyl carbon atoms in 3,4-dimethyl-1H-pyrrole. The locations (chemical shifts in ppm) of these peaks in the 13C spectrum are also consistent with them originating from ring CH and methyl carbon atoms. The $CHCl_3$ (solvent) signal might have been expected to be present in the DEPT 135^o spectrum in an opposite phase (downwards pointing peak) to the other two peaks, on the grounds that it contains a tertiary hydrogen atom. However, the presence of $CHCl_3$ is not observed due the very low levels that are present in the deuterated solvent ($CDCl_3$). A solvent peak for both the 1H and 13C spectra because, here, they are more sensitive to levels of 1H and 13C atoms compared to the DEPT spectra.

(a)

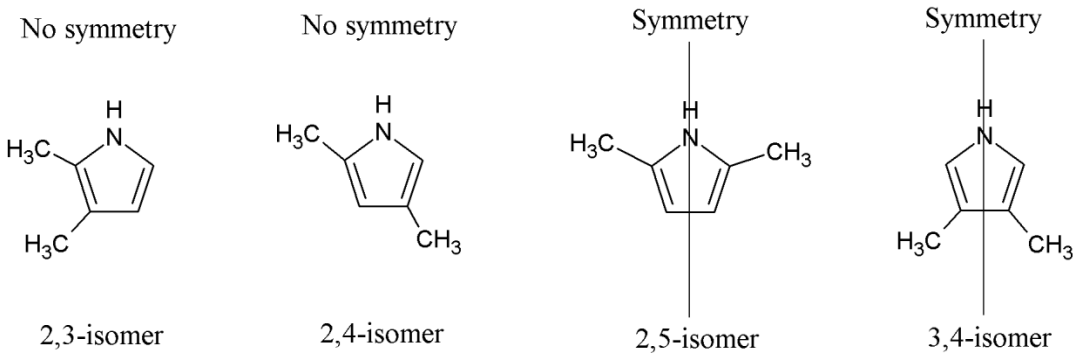

(b)

The type of non-equivalent H-atom	N-H	CH	CH_3
The chemical shifts (ppm) of the 2,5-isomer	7.10	5.57	2.13
The chemical shifts (ppm) of the product	7.75	6.53	2.04

Fig 2.7 (a) All four dimethylpyrrole isomers **(b)** Chemical shifts (ppm, TMS) of symmetrical isomers: 2, 5-isomer and the product (3, 4-isomer)).

So far it has been shown that the product has a molecular mass 95 amu, contains both pyrrollic and methyl functionalities, and has 1H and 13C NMR spectra consistent with 3,4-dimethyl-1H-pyrrole. However, very similar results would also be expected for the other three dimethyl isomers displayed in figure 2.7 (a). Fortunately, on symmetry grounds, both the 2,3-isomer and 2,4-isomer have 5 non-equivalent H-atoms and 6 non-equivalent and would be expected to give the same number of peaks respectively in their 1H and 13C NMR spectra. This still leaves the 2,5-isomer which like the 3,4-isomer, displays an axis of symmetry, with three different H-atoms and three different C-atoms. The 1H NMR spectrum for the 2,5-isomer is available for comparison. The chemical shifts of both the 2,5-isomer and our product are displayed in the figure 2.7 (b). Given that they are different we can confirm our product to be 3,4-dimethyl-1H-pyrrole.

2.3 The purity and stability

As important as confirming structure of the product as being 3,4-dimethyl-1H-pyrrole, was to confirm that it was pure. The first indication we had that our product was of high purity came from gas chromatography, which showed only one product peak in addition to the solvent (hexanes) peaks (see figure 2.8). Confirmation of the purity of the 2,3-dimethyl-1H-pyrrole that we had prepared came from CHN elemental analysis. Figure 2.9 shows the results of this analysis and reveals a difference between the measured and theoretical molecular mass of 3,4-dimethyl-1H-pyrrole of significantly less than 0.4%. This is consistent with The Royal Society of Chemistry guidelines for authors which states: "Authors are required to provide unequivocal support for the *purity* and **...** e*lemental analysis* (within ±0.4% of the calculated value) is required". We were therefore confident that we had produced a supply of high purity material.

We next wanted to determine suitable storage conditions for 3,4-dimethyl-1H-pyrrole. After being stored in an amber glass vial under nitrogen within the refrigerator (4 ^{o}C) for 3 days, GCMS was undertaken on the sample and the gas chromatogram is shown in figure 2.10. The chromatogram shows clear signs of degradation of the sample. We therefore made the decision to store freshly prepared 3,4-dimethyl-1H-pyrrole under nitrogen within amber glass vials within the freezer compartment. Even after 18 months this showed no signs of degradation as confirmed by gas chromatography (data not shown).

The lack of stability of 3,4-dimethyl-1H-pyrrole at ambient temperatures, did mean that it had to be re-synthesized when work was undertaken with this material in Sweden, rather than risk degradation of the material during shipping from the UK.

2.4 Discussion and conclusions

Of the two syntheses attempted, the ring closure synthesis, scheme 2, proved successful, albeit in a much reduced yield than was expected from the published paper[123].

The synthesis outlined in scheme 1 was only undertaken as far as step 2: the synthesis of 3, 4-diiodo-1-(triisopropysilyl)pyrrole (III). The reason why the synthesis was abandoned at the end of this stage was that thin-layer chromatography, revealed the presence of more than one closely eluting product. This meant that the synthesis did not proceed to 4-diiodo-1-(triisopropysilyl)pyrrole as the exclusive product, which had been stated in the original source of the synthesis[122]. This meant not only that we would be faced with a difficult separation to both develop and undertake, before proceeding with the remaining two steps of the synthesis, but we would also obtain a much lower yield than anticipated resulting from losses of material through co-products. Given that there was limited time (two weeks) before the material was required for the work scheduled in Sweden, we proceeded with the second synthetic approach outlined in scheme 2.

(a)

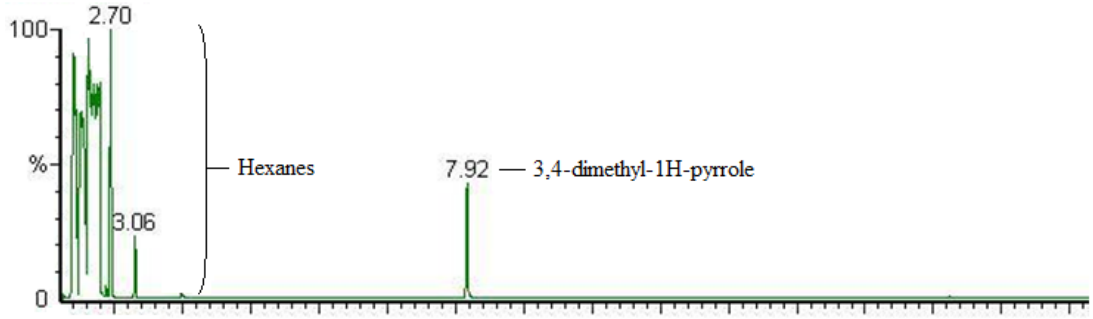

(b)

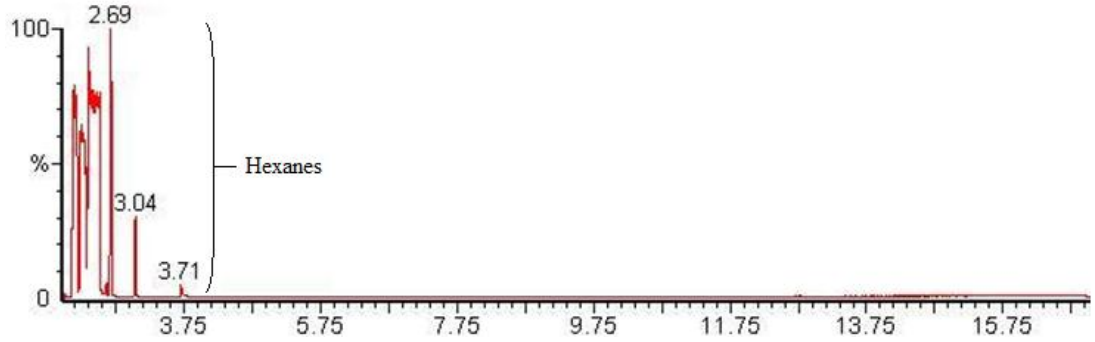

Fig 2.8 Gas chromatograms of (a) purified product in hexane(s) solvent and (b) hexane(s) solvent blank.

ELEMENT	C	H	N	∑	Difference
% Theory	75.74	9.53	14.71	100.00	N/A
% Found 1	75.74	9.52	14.90	100.16	0.16
% Found 2	75.73	9.51	14.83	100.07	0.07

Fig 2.9 Elemental analysis for 3,4-dimethyl-1H-pyrrole (undertaken by Medac Ltd., UK).

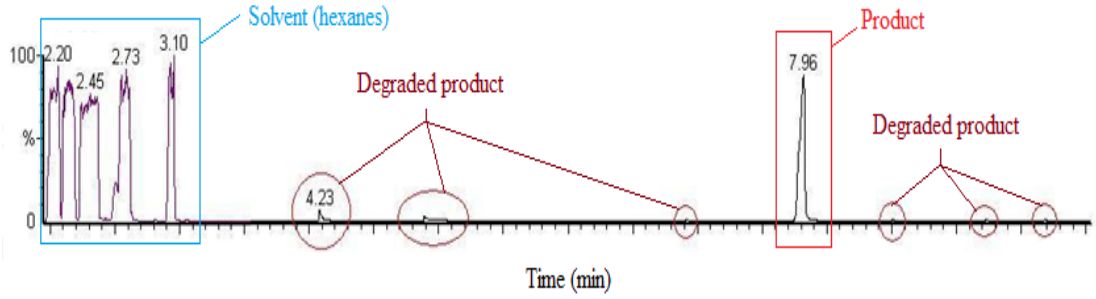

Fig 2.10 GC chromatogram showing degradation of 3,4-dimethyl-1H-pyrrole when kept in a fridge (4 ^{o}C) for 3 days.

The synthesis outlined in scheme 2 had the synthetic advantage of having only two synthetic steps. Another advantage of this synthetic approach is that the positions of the methyl groups in the final product are determined by their relative location in one of the starting materials: 2,3-dimethyl butadiene. This meant that, once the pyrrole ring was formed the methyl groups would be in the correct positions (3,4-positions or beta positions) within the pyrrole ring. This was not as certain to be the case for the synthetic approach outlined in scheme 1. In fact it is likely that one of the additional products, observed by TLC at the end of step 2 of scheme 1, was the result of only one of these positions being successfully substituted by iodine i.e. 3-iodo-1-(triisopropysilyl)pyrrole.

The yield of material by the second scheme was less than the published yield. A yield of 7.4 % was obtained compared to a yield of 62 % expected from Table 1 of the published paper (see figure 2.11). There are several reasons why this might have been the case. One might have been little experience, by the author of this thesis, in the little used procedure of steam distillation. It was necessary to make our own steam distillation apparatus to undertake this procedure as none was available within our laboratory.

Given the discrepancy between the yield obtained and that expected, contact was made with the first named author of the paper for his assistance. Prof. Ichimura was of great assistance to us. It was realised that the concentration of sodium methoxide that should have been employed was 49 w/w% and not the 10 w/w% published in the footnote of Table 1 of the paper. Given that we used 300 ml of 10 w/w% of sodium methoxide, this actually represented a value closer to 2 Mol in Table 1 of the paper. Hence, a much lower concentration of sodium methoxide was used than was ideal. Table 1 of the paper indicates that 7 Mol of sodium methoxide was required to obtain the 62% yield that had been hoped for. However, the table does indicate that lower concentrations, lead to a reduced yield of product. In fact it indicates that 4 Mol of sodium methoxide results in yields of 5-10 %. Given that we obtained a yield of 7.4 % at a concentration of close to 2 Mol, we now appreciate that under the circumstances, our synthesis proceeded well and is in agreement with what was reported in the original paper.

TABLE 1. SYNTHESES OF 3,4-DIMETHYLPYRROLE

Exp. run	R in III	Alkali[a]	Mol of alkali	Solv.	Yield (%)[b]
1	CO_2Et	NaOMe	4	MeOH	5—10
2	CO_2Et	KOH	8	MeOH	34—48
3	CO_2Et	NaOMe	7	MeOH	62
4	CO_2Ph	NaOH	5	MeOH	40
5	CO_2Ph	NaOH	5	H_2O	trace[c]
6	CO_2Ph	NaOMe	7	MeOH	59
7	$PO(OEt)_2$	KOH	8	EtOH–H_2O	22
8	$PO(OEt)_2$	NaOMe	6	MeOH	27

a) Alkali hydroxide; 20—30 w/w% in methanol or water. Sodium methoxide: *ca.* 10 w/w% in methanol. b) Based on the crude cycloadduct (III) except runs 4—6 where the purified cycloadduct was used. c) Ehrlich's test was positive.

Fig 2.11 Shows Table 1 from p 1157 of: The Synthesis of 3, 4-Dimethyl-1H-pyrrole: Kunihiro Ichimura et. al., The Bulletin of the Chemical Society of Japan, Vol. 49(4), 1157-1158 (1976).

One reason why we may have obtained a yield of 7.4 % at a 2 Mol of sodium methoxide, and not less than this, given the paper indicates that this yield would require 4 Mol of sodium methoxide, is that we did take the precaution of carrying out the synthesis under an inert atmosphere of argon. This was not done in the original paper, but is more common practice now-a-days, when dealing with potentially air sensitive materials. It would be good to repeat the synthesis at a later date using the correct concentrations of sodium methoxide, to see if a yield of greater than 62 % might be obtained by undertaking the synthesis under an inert atmosphere of argon.

Although our yield was lower than we had hoped for, we were successful in synthesizing 3,4-dimethyl-1H–pyrrole in sufficient quantities and in high purity to undertake the work outlined in the next section of this thesis.

3. The use of blocking groups to alter the structure of polypyrroles.

3.1 Introduction

Research into the effects of varying various components of the PPy matrix, such as: the type and levels of dopant, the type of solvent and the effects of various additives has been undertaken and has been presented in the literature. However, little work has been undertaken to-date on the effects of changes in the polymer network and it is likely that this will have a major influence on the polymers physical properties.

Although the primary mechanism for the actuation of polypyrroles has been shown to be the insertion and deinsertion of ions, the response of the polymer network will exert a major influence on mechanical properties such as the amount and rate of actuation. It would be a mistake to underestimate the role that the polymer network plays in the actuation process.

It is likely that there exists levels of cross-linking and branching that result in optimal actuator performance. An understanding of the relationship that exists between structure and actuation would potentially allow actuators to be designed that are capable of greater movements, operating speeds, force generation and lifetimes.

Unfortunately, the lack of an established method for monitoring levels of cross-linking and branching within polypyrroles, combined with an insufficient understanding of how to alter these levels, has been a major barrier to understanding the affect of crosslinking on the actuation of PPy and altering crosslinking levels to optimize performance.

In the absence of an established method for determining cross-linking and branching levels, we have developed a synthetic strategy which logically overcomes the need for such a method. Our approach makes use of beta-substituted pyrroles to block cross-linking and branching. It is not possible for substitution to occur at a beta-position that has been effectively blocked, and produce a branch or a cross-link.

Our strategy has been to electropolymerize pyrrole with beta-substituted pyrroles, giving polypyrroles (copolymers) with different levels of branching and cross-linking. The amount of cross-linking and branching displayed by the copolymer then depends upon the ratio of the two different types of monomer incorporated into the copolymer chain. The copolymer ratios were altered by changing the molar ratios of the two different monomers in the electrolyte used during polymerization.

In addition to exerting a blocking effect, it was recognized that the blocking group that was selected would also have the potential of exerting both an electronic effect and steric effect on the pyrrole ring and the polymer chain. The methyl group was selected in an attempt to minimize these secondary effects.

3.2 The blocking group approach

The blocking group approach allows the number of beta-positions within the polymer that are available for branching and cross-linking to be decreased relative to those present in un-blocked polymer. The approach therefore, lowers branching and cross-linking levels. By combining different ratios of blocked and un-blocked monomers, the levels of branching and cross-linking can be modulated and controlled.

Our initial hypothesis was that lower levels of cross-linking and branching would produce a polymer containing chains that have a greater degree of movement and as a consequence result in larger (increased strains) and quicker (increased strain rates) actuations. However, it was also anticipated that decreased crosslinking and branching might lead to increased non-bonding interactions such as pi-stacking which might restrict chain movement and result in a denser and harder material.

3.2.1 Blocking group selection

The methyl group was selected for use as a blocking group. Most atoms and groups that are attached to a carbon atom exert an electron-withdrawing Inductive Effect (-I effect) e.g. halogens, owing to them being more electronegative than carbon. Alkyl groups are, however, the major exception and are known to be capable of *electron-donation* (+I effect). For alkyl groups the effect is "quantitatively rather small", and depends upon the type of alkyl group[125]. The ability to donate electrons increases in the order: methyl, primary, secondary and tertiary. On this basis the methyl group will have the lowest electron donating effect. In addition, alkyl groups have the potential of displaying an effect known as hyperconjugation, which can have lead to them being slightly *electron-withdrawing* under suitable circumstances (attached to an aromatic ring). The combined effect of a weak inductive effect (electron-donating) and hyperconjugation (electron-withdrawing) makes the methyl group one of the most electronically "passive" groups that could be selected.

In addition the methyl group is one of the smallest functionalities available to a chemist, other than single atoms, and will therefore display a minimal steric effect compared to the majority of other functional groups. All single atoms that could have been selected, having sizes comparable to the size of a hydrogen atom, display larger electronic effects (both Inductive and Mesomeric) e.g. the fluorine atom, and were not suitable for selection as a blocking group.

It was also important to minimize steric effects that lead to an increase in the torsional angle between adjacent monomer units in the polymer chain. This will reduce the chains ability to take up a coplanar arrangement and thereby make polaron and bipolaron formation more difficult[24]. On the other-hand steric effects are potentially advantageous from the viewpoint of blocking e.g. 3-methyl-1H-pyrrole. In the case of singly beta-substituted pyrrole, not only will one of the positions be completely blocked with

respect to substitution (branch formation and cross-linking) but the remaining unblocked beta-position will be more crowded and likely require higher activation energy for substitution and potentially lower substitution at that position.

Two monomers were selected: 3-methyl-1H-pyrrole and 3,4-dimethyl-1H-pyrrole, shown in figure 3.1, for use in our work.

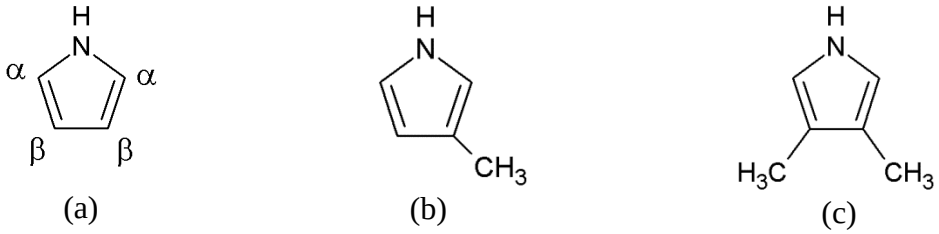

Fig 3.1 Monomers used: (a) pyrrole (Py) (b) 3-methyl-1H-pyrrole (3MPy) and (c) 3,4-dimethyl-1H-pyrrole (3,4-DMPy).

With both of the beta-positions substituted, as in 3,4-dimethyl-1H-pyrrole, blocking will be complete and branching and cross-linking will not be possible. The polymerization of 3,4-dimethyl-1H-pyrrole to form 3,4-dimethyl-1H-polypyrrole (homopolymer), will lead to "spaghetti- like" polymer chains with no branching and cross-linking. Copolymerization of 3,4-dimethyl-1H-pyrrole with pyrrole is envisaged as leading to a polymer network that will have much lower levels of branching and cross-linking compared to polypyrrole, with branching and cross-linking being possible only where there is a pyrrole monomer unit present. The possible decrease in branching introduced by a 3,4-dimethyl-1H-pyrrole monomer unit will be matched by the decreased potential for cross-linking. We would therefore expect to see both branching and cross-linking to decrease in parallel with increasing 3,4-dimethyl-1H-pyrrole content.

With just one of the beta-positions blocked, as in 3-methyl-1H-pyrrole, blocking will only be partial. However, we would expect the degree of blocking to be significant. The presence of one blocking group will decrease the number of beta-positions available for substitution by 50%. In addition, the increased steric effect caused by the beta-substituent on the unsubstituted beta-position, will further deter branching and cross-linking at this position. With this in mind, the potential for blocking branching and cross-linking can be envisaged as being considerably higher than 50% relative to pyrrole. However, although branching and cross-linking will be reduced, it will still be possible to substitute the partially blocked, 3-methyl-1H-pyrrole monomer. Polymerization of 3-methyl-1H-pyrrole to form 3-methyl-1H-polypyrrole (homopolymer) would still be expected to produce a branched and cross-linked network, albeit at much reduced levels.

The predicted order of decreasing branching and cross-linking is shown in figure 3.2. A decrease in the levels of both branching and cross-linking with increasing 3,4-DMPy

content was predicted. A similar, but smaller, decrease in the levels of branching and cross-linking with increasing 3MPy content was also expected, but the relative decrease in branching to cross-linking, would not be possible to predict. It is possible that the decrease in branching and cross-linking would not be run in parallel, as was predicted for the 3,4-DMPy monomer i.e. the decrease in branching might possibly be less than the decrease in cross-linking.

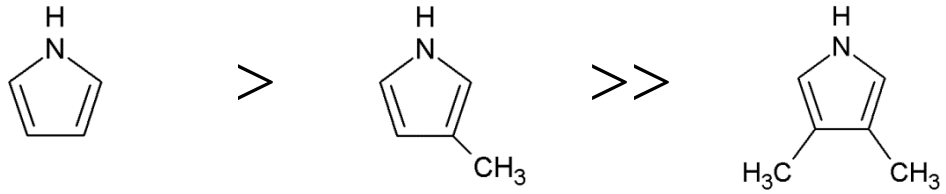

High Intermediate Low

Fig 3.2 Predicted order of decrease in cross-linking and branching displayed by the synthesized polypyrroles with monomer type.

3.2.2 Control of copolymer ratios

An issue commonly associated with polymerization involving mixed monomers (copolymerization) is that they are more difficult to both initiate and control. The ratios of the monomers present within the final copolymer will depend both on the precise conditions and the relative reactivity of the respective monomers. The ratios displayed within the monomer will be subject to both kinetic and thermodynamic control. The more readily the monomer undergoes polymerization (initiation and propagation) the more it will be incorporated within the polymer.

On the basis of the most recognized mechanism that has been proposed for electropolymerization[55,56], the initiation of electropolymerization involves the removal of an electron from two monomer units to form the two free-radical cations, which then must approach each other to initiate chain formation (chain addition and propagation). In other words, polymerization requires the approach of two free-radical cations and not the approach of a free-radical cation on a nearby neutral monomer unit.

A decreased in the concentration of a particular monomer within the polymerization solution will lead to a decrease in the amount of that monomer being incorporated into the growing polymer chain. This is based on the fact that the reactive species (free-radical cations) will find it increasingly less likely to “find” a free-radical cation of the same type as its presence in the reacting system is decreased. It will therefore be more

likely to find and react with those free-radical cations that are present in higher concentrations.

This view is based upon accepted scientific principles e.g. that an increase in the concentrations of a reacting species within a system leads to an increase in the rate at which the species reacts. Although, copolymer ratios can in certain circumstances be quantified using an analytical technique, this possibility is polymer dependant and when the monomers present within the polymer are very similar or their functionalities masked by other species present within the polymer matrix, this can become difficult to impossible to assess. For these copolymers this is likely to be the case and attempts at developing such a method might form the basis of an entire PhD.

However, as explained it is considered highly likely and reasonable that an increase concentration of a particular monomer within our system will lead to increased reaction and incorporation of that monomer into the copolymer. Using this approach copolymer ratios were changed by using different concentration ratios within the polymerization solution employed. However it was ensured that the voltage employed (0.55 V) was greater than the oxidation potential for all the monomers used, so that they are all capable of forming free-radical cations. On the basis of Diaz's mechanism the use of a polymerization potential capable of forming just one type of free-radical cation, would lead to the formation of a homopolymer and not a copolymer.

The experimental work that was undertaken developed naturally into two stages. The first stage was a development phase, in which suitable conditions were determined such as monomer ratios, polymerization potentials etc, which was necessary to undertake the work successfully. The second phase involved the application of the conditions that were developed in the first stage and represents the work that we originally set out to undertake. Although this work will be discussed in detail in later sections it is helpful at this stage, to state that that it was found to necessary to use a porous gold working electrode to successfully make actuation measurements[126].

3.3 Experimental details

3.3.1 Preparation of polymerization solutions

Aqueous solutions containing 0.10 M NaDBS and 0.10 M of the relevant pyrrole were used to prepare homopolymer films e.g. PPy(DBS), 3-MPPy(DBS) and 3,4-DMPPy(DBS).

Copolymerization solutions were prepared so as to produce a combined monomer concentration of 0.10 M and containing 0.10 M concentrations of NaDBS. This was achieved by first preparing: A) an aqueous solution containing 0.10 M β–blocked pyrrole and 0.10 M NaDBS and B) an aqueous solution containing 0.10 M pyrrole and

0.10 M NaDBS. These solutions were then combined in different volume ratios as illustrated in figure 3.3. This figure shows the preparation of a solution of mixed monomers having a combined concentration of 0.10 M, formed from 1 ml of 0.10 M solution A and 24 ml of solution B.

In this work copolymers formed using solutions prepared with 1ml of 0.10 M β–blocked pyrrole are termed "1 ml copolymers". Similarly, other copolymers are referred to as being "0.75 ml copolymers", "0.50 ml copolymers", etc. depending upon the volume of 0.10 M β–blocked pyrrole used to make up the polymerization solutions from which they were made.

For 3MPPy-co-PPy(DBS), the copolymers synthesized and actuated in the final section of this work, were: "0.5 ml copolymer", "0.75 ml copolymer" and "1 ml copolymer". Similarly, "0.5 ml copolymers", "0.6 ml copolymers" and "0.7 ml copolymers" were prepared for 3.4-DMPPy-co-PPy(DBS) and their actuation studied.

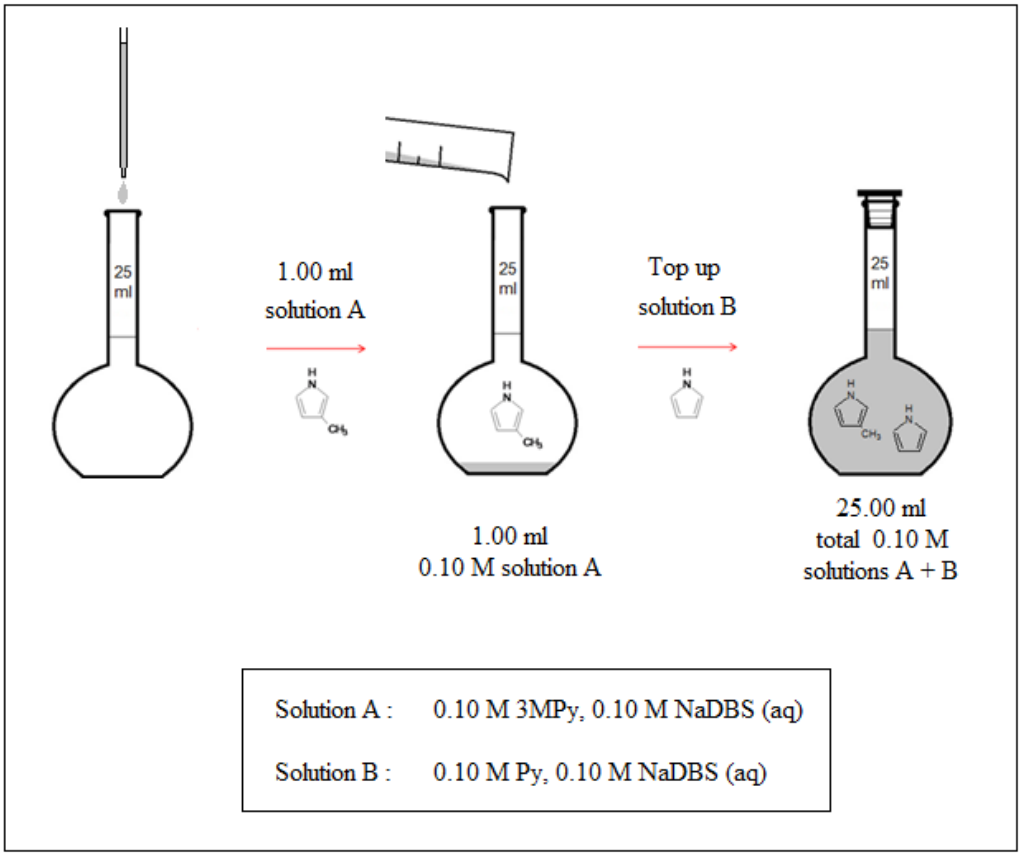

Fig 3.3 Preparation of copolymer polymerization solutions, illustrated for 3MPy.

Unfortunately, these solutions were not suited to storage, even when stored in the laboratory freezer compartment of the fridge. When this was done, solutions darkened and within 24 hours, with black suspended particulates typically seen with pyrrole solution after several days storage. This was unfortunate as solutions were time

consuming and difficult to prepare due to the tendency of NaDBS (aq) solutions to foam on transfer and making up of solutions. This meant that solution had to be freshly prepared and used immediately to polymerize films.

3.3.2 Preparation of porous gold working electrodes (pAuWE)

As was stated earlier it was found to be necessary to use porous gold working electrodes to successfully undertake this work[30]. These electrodes were formed using a standard AuWE, whose preparation has been described in detail in Section 1.1.3.1, and electroplating a layer of porous gold on to the existing gold surface of the AuWE. The exact conditions are given in table 3.1.

The surface of the AuWE was first "cleaned" by heating in "Piranha solution" (H_2SO_4:H_2O_2:H_2O = 1:2:4 volume ratio) at approximately 70 ^oC for 5 minutes and thoroughly rinsed with deionized water prior to electroplating to prepare the gold surface (Note: Piranha solution is hazardous, particularly when hot and should not be used without first undertaking a full COSHH assessment and training to cover safe use and disposal. In particular it should never be disposed of with organic solvents as there is a risk of explosion).

Electroplating was undertaken using a dilute aqueous mixture of two types of commercially available gold electroplating salt (Neutronex 309 A and 309 B) and conditions commonly used at Linkoping University, Sweden. The electroplating conditions first allowed an initial "seeding" period followed by a "growth" period. A used a porous gold layer of five microns was used.

The same pAuWE was employed throughout the work so as to ensure a fare comparison was made between the different films. The pAuWE electrode was "cleaned" after use to remove all traces of the prior polymer films by heating in TL1, as describe in Section 1.1.6.

Electroplating solution:	**Electroplating conditions:**
A solution low Au concentration stock containing Neutronex 309A, Neutronex 309B and deionized water in the ratio: 10 ml: 300 ml: 190 ml	1) Seeding period: -0.7 V for 120 s 2) Growth period: -0.9 V for 390 s (for a 5 micron layer)

Table 3.1 (a) Electroplating solutions and (b) electroplating conditions used to form porous gold working electrode.

3.3.3 Polymerization conditions

All polymer films were polymerized as described in Section 1.1.5 using potentiostatic conditions of 0.55 V vs. Ag/AgCl, using 7 ml of 0.1 M monomer(s), 0.1 M NaDBS(aq) solutions at room temperature to a thickness of five microns.

Films were actuated as described in Section 1.1.6 using an initial conditioning period of 0 V (100s) followed by a square wave potential of -1 V (200 s) and 0 V (200 s). Actuation was continued until the actuation profiles could be seen to have reached their fully irreversibly expanded state. This "stable state" (end cycles) is representative of the long term performance of the polymer. This typically can be anywhere between 20 to 100 cycles and under the conditions we have employed, is dependent upon the type of polymer film being actuated.

3.4 Results and discussion

3.4.1 Initial results

The polymerization of *homopolymer* films of 3-MPPy(DBS), at 0.55 V vs. Ag/AgCl, occurred readily, at growth rates considerably faster than that of PPy(DBS). Unfortunately, the actuation of these films all resulted in failure, after a small number of cycles, via fracture and delamination. Figure 3.4 shows the typical appearance of these films before and after actuation. Prior to failure the films displayed very large irreversible expansion which continued right up to failure. Failure was evident from the sudden change in the actuation profiles.

(a) (b)

Fig 3.4 A 5 μm film of 3MPPy(DBS) both (a) before and (b) after actuation. Fracture and delamination was evident during actuation of these films even when a porous gold working electrode was used.

It would appear that blocking of cross-linking and branching in these 3-MPPy(DBS) homopolymer films is too great, resulting in a polymer that undergoes large irreversible

expansion and has poor mechanical strength. We tried polymerizing 3-MPPy(DBS) films at higher polymerization potentials in an attempt at increasing substitution in the unblocked-beta position (4-position) and produce an increase in cross-linking, but all are attempts failed to produce a form of polymer that could continue to be actuated for more than a few cycles even when a porous gold working electrode was employed.

Given the failure of these films, we expected to see similar behaviour for homopolymer films of 3,4-DMPPy(DBS) when actuated, given that the degree of blocking in this polymer would be complete, producing a totally un-branched and non-crosslinked polymer. This was the case and these films very quickly failed by fracture and delamination upon actuation.

The lack of branching and cross-linking in homopolymer films of 3,4-DMPPy(DBS) was evident during cyclic voltammetry measurement made on 0.1 M 3,4-DMPy, 0.1 M NaDBS (aq) solutions. On cycling between 1 V and -1 V, a black adherent film was formed on the AuWE, which on removal from the polymerization solution could be seen to be covered with a relatively thick film of gel as shown in figure 3.5. This revealed two things, first that the absence of cross-linking and branching in these films results in very large solvent swelling leading to gels. Secondly, due to the presence of a black polymer layer on the Au substrate, it illustrates that these films, although un-branched and non-crosslinked, are capable of forming what appeared to be dense polymer films. This might be explained through the operation of a form of non-bonding interaction such as pi-stacking[33] and chain entanglement.

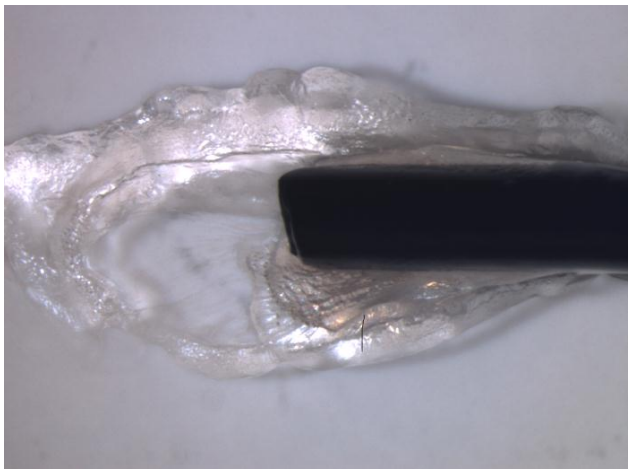

Fig 3.5 The formation of a black adherent polymer film on the surface of the AuWE, surrounded by a very large and soft layer of gel. These films were formed during cyclic voltammetry measurements using 0.1 M 3,4-DMPy, 0.1 M NaDBS (aq) solutions on cycling between 1 V and -1 V.

Given the failure of all the homopolymer films that were polymerized and actuated, copolymer films were next synthesized and actuated. These films could be expected to

demonstrate levels of branching and cross-linking between those of the beta-substituted homopolymers (3MPPy(DBS) and 3,4-DMPPy(DBS)) and polypyrrole (PPy(DBS)).

Once again it was found that the actuation of copolymer films formed using relatively high concentrations of beta-substituted pyrroles, lead to films that underwent large irreversible expansions prior to failure by fracture and delamination. Eventually it was possible to actuate copolymer films for extended periods prior to fracture, by forming copolymer films using polymerization solutions containing low concentrations of beta-substituted pyrrole. Figure 3.6 shows a typical actuation profile for "1.5 ml to 5 ml copolymers". These films typically undergo large irreversible expansion (region A) from the onset of actuation and then enter a period of rapidly increasing irreversible and reversible expansion (region B), which we believe to be the result of plastic deformation, followed by fracture and delamination occurring at point C.

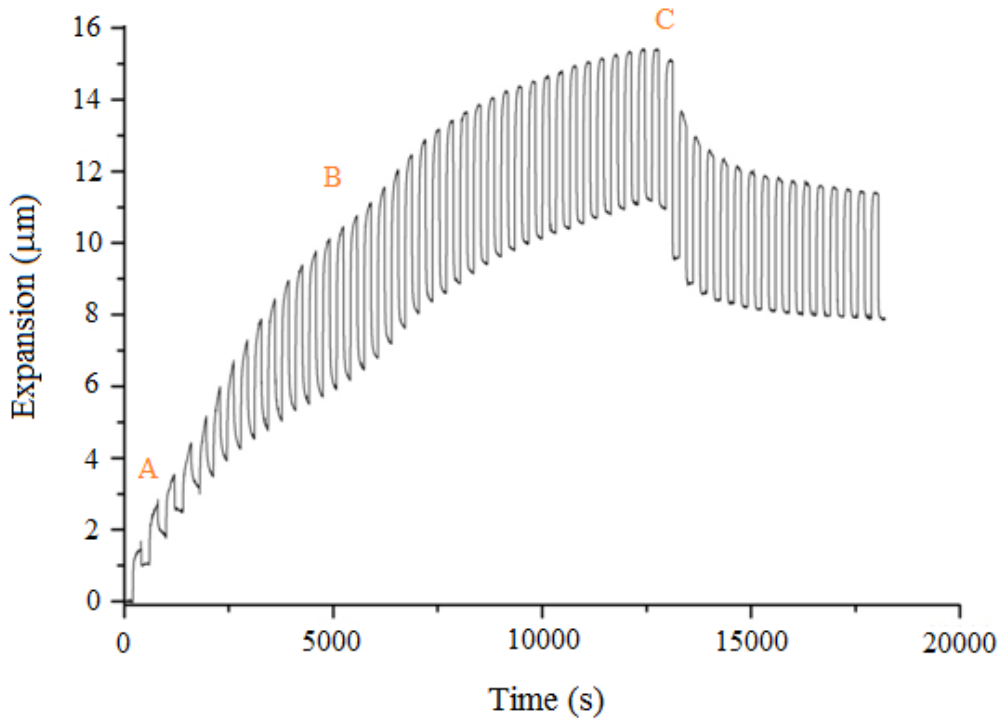

Fig 3.6 The actuation profile obtained for 1.5 ml 3MPPy-co-PPy(DBS).

Examination of these films post-actuation revealed not only regions of fracture, but also regions of what appeared to be plastically deformed polymer, in the form of rings and ripples. The typical appearance of these plastically deformed regions is shown in figure 3.7.

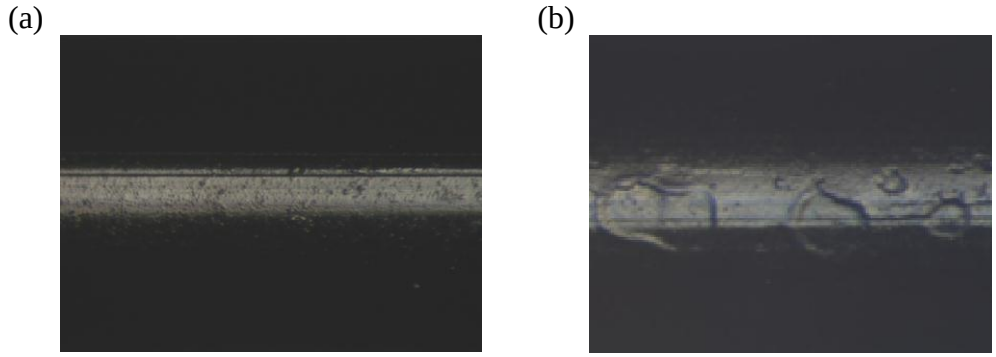

Fig 3.7 Microscope images of 1.5 ml 3MPPy-co-PPy(DBS) films (a) before and (b) after actuation. Image (b) shows rings and ridges that were typical for 3MPPy-coPPy(DBS) films formed using a couple of ml or more of 3MPy in the polymerization solutions.

The levels of 3MPy in the 3MPPy-co-PPy(DBS) copolymer were lowered further by using smaller volumes of 3MPy in the polymerization solutions. This is illustrated in figure 3.8, which shows an overlay of the first few actuations of 0.75 ml to 2.50 ml 3MPPy-co-PPy(DBS) copolymer films. The figure nicely illustrates that there is a transition in behaviour above 1 ml 3MPPy-co-PPy(DBS) with the large and unstable irreversible and reversible expansions that occur above the 1.5 ml 3MPPy-co-PPy(DBS) copolymer are no longer evident. For films containing levels of blocked monomer at or below the 1 ml level, no plastic deformation was observed in microscopic images of the films post-actuation or from the appearance of the actuation profiles. Films in this range were capable of undergoing sustained reversible actuations for long periods without failure and reached a "stable end state" corresponding to a maximum level of irreversible expansion and typical of the behaviour of PPy(DBS) films actuated in earlier sections of this thesis.

Through the combined use of a pAuWE and low levels of blocked pyrrole monomer a range of 3MPPy-co-PPy(DBS) copolymers suitable for investigation could be formed using polymerization solutions prepared using: 0 ml < x ml ≤ 1 ml 3MPPy-co-PPy(DBS). By the same approach it was possible to identify a similar range for the 3,4-MPPy-co-PPy(DBS) to be 0 ml < x ml ≤ 0.7 ml 3,4-MPPy-co-PPy(DBS).

Figure 3.9 shows an overlay of two full actuation sequences, one for 1 ml 3-PPy-co-PPy(DBS) and the other for PPy(DBS). Both actuation sequences show similar shaped profiles, and demonstrate the ability to undergo sustained reversible actuations in their stable states without the deterioration of performance typically associated with either deformation or fracture and delamination.

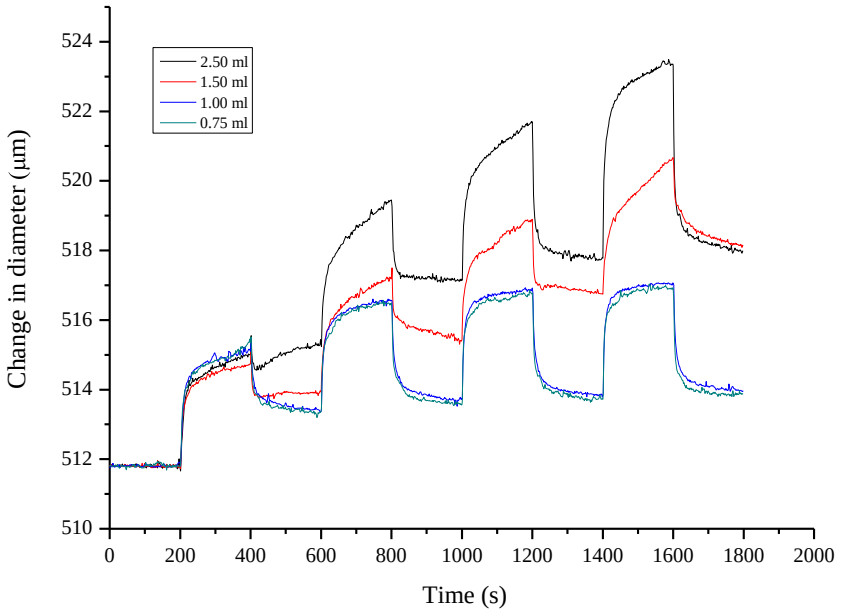

Fig 3.8 An overlay of the first four actuation cycles of 3MPPy-co-PPy(DBS) copolymers containing decreasing levels of 3MPy monomer. The sequences illustrate that there is a transition in behaviour in the region of the 1.5 ml 3MPPy-co-PPy(DBS) copolymer.

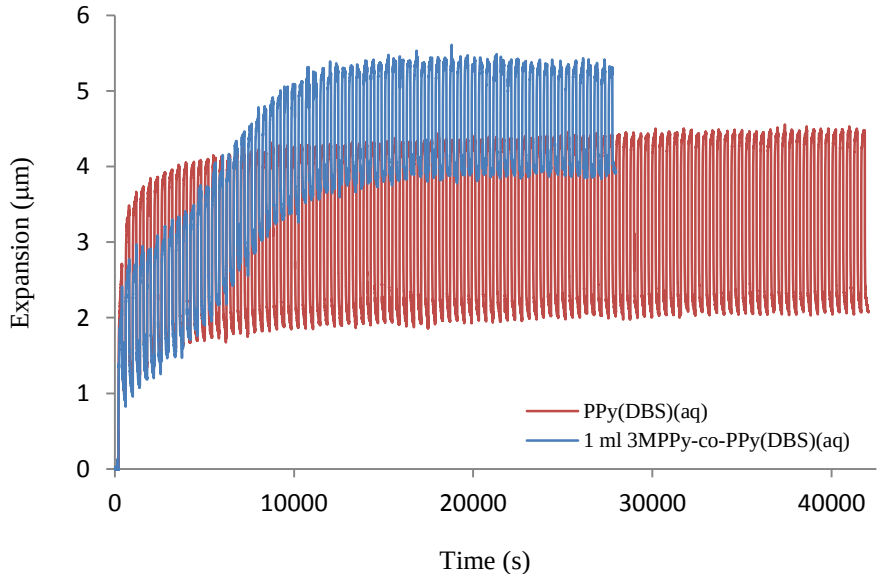

Fig 3.9 An overlay of the actuation sequences for 5 µm films of 1 ml 3MPPy-co-PPy(DBS) and PPy(DBS).

At this stage it can be concluded that high levels of blocking leading to low levels of cross-linking and decreased branching and results in polypyrrole films that have poor actuating properties and low mechanical strength. The large increase in irreversible expansion is likely the result of increased solvent swelling. The formation of a gel like polymer for 3,4-DMPPy(DBS) during cyclic voltammetry measurements is an extreme case of solvent swelling resulting from low cross-linking levels.

The next section shows the results of an investigation of the two suitable ranges identified by the preliminary work for 3MPPy-co-PPy(DBS) and 3,4-DMPPy-co-PPy(DBS) i.e. 0.5-1 ml and 0.5-0.7 ml respectively.

3.4.2 Main results and discussion

In this section the actuation performance of 3MPPy-co-PPy(DBS) and 3,4-DMPPy-co-PPy(DBS) are compared with PPy(DBS). The films all have a thickness of five microns and were synthesized and actuated under the same conditions e.g. all films were actuated on the same pAuWE. Each point represents the mean of three replicate measurements and the error bars are ± 1SD. Unless stated otherwise the measurements are for the reduction scan in the "stable state" (fully irreversibly expanded state; end cycles).

Figure 3.10 shows the reversible expansion of the films as a function of increasing blocked monomer content. The first thing to note is that the reversible expansion of the copolymers is less than that of the PPy(DBS). Therefore the actuating performance of the copolymer films is decreased by the presence of the blocking groups and corresponds to a decrease in cross-linking and branching. This decrease in performance is not in keeping with the initial hypothesis, in which we predicted that there would be an increase in the reversible expansion with a decrease in the levels of cross-linking.

The trend within the polymers series is another interesting feature to note. There is a clear increase in the reversible expansion with increasing blocked monomer content for 3,4-DMPPy-co-PPy(DBS) and corresponds with a decrease in both cross-linking and branching. This trend, within the copolymer series (0.5 to 0.7 ml) is in keeping with the initial hypothesis. There is a slight decrease in the reversible expansion observed between 0.5 ml and 0.75 ml for 3MPPy-co-PPy(DBS). Between 0.75 ml and 1 ml there is essentially no change in the reversible expansion. Given the size of the change observed between 0.5 ml and 0.75 ml and the size error bars it is difficult to say if the decrease in the mean value in this range represents an actual trend or is due to the variation in the level of reproducibility for the replicate measurements.

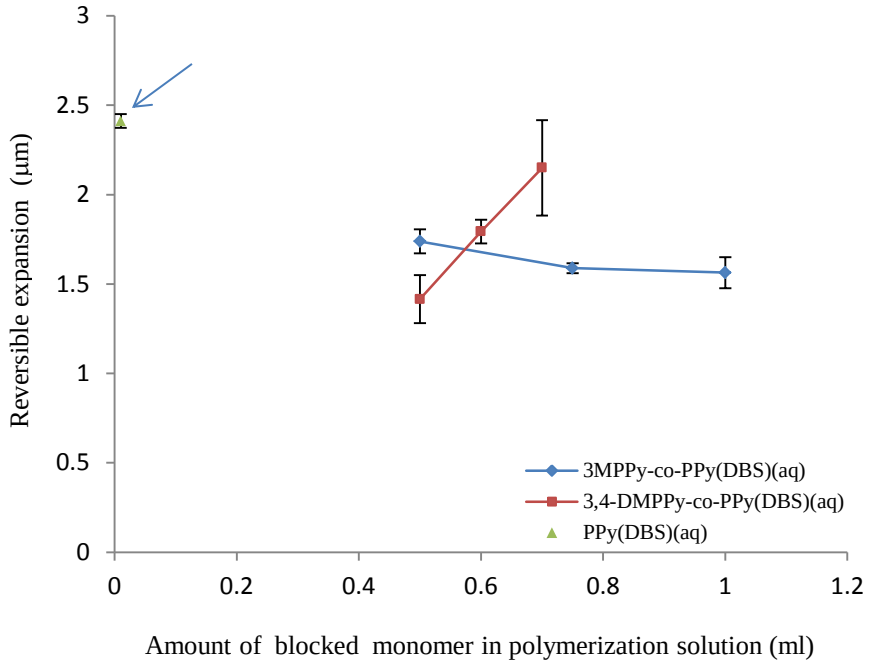

Fig 3.10 An overlay showing the differences between the reversible expansions of the copolymer films and PPy(DBS) in the stable state. In addition, the overlay reveals changes in the reversible expansion that occur "within" the individual copolymer series. Note: the plotted point for PPy(DBS) is shown slightly displaced to the right hand side of the y-axis for ease of illustration (as indicated by the blue arrow).

Figure 3.11 represents one of the most important findings of the work. It shows the change in irreversible expansion for the copolymers compared to PPy(DBS) with increasing blocked monomer content. There is a clear correlation between the irreversible expansion and increased levels of blocking. This represents a correlation between decreased levels of cross-linking and branching and irreversible expansion. There is an increase in the mean irreversible expansion for all the copolymers compared to PPy(DBS).

It is interesting to note that the irreversible expansion of 3,4-DMPPy-co-PPy(DBS) series is less than that of the 3MPPy-co-PPy(DBS) series, for most of its range. It is only the 0.7 ml 3,4-DMPPy-co-PPy(DBS) that is within the same range of irreversible expansions for 3MPPy-co-PPy(DBS). However, the 3,4-DMPPy-co-PPy(DBS) series does have a narrower range. In addition the gradient is of the 3,4-DMPPy-co-PPy(DBS) series is significantly steeper than the 3MPPy-co-PPy(DBS) series. If extrapolated to 1 ml, the 3,4-DMPPy-co-PPy(DBS) series would have a significantly higher irreversible expansion. This is in line with the earlier findings that 1 ml 3,4-DMPPy-co-PPy(DBS) was not capable of being successfully actuated long term without failure associated with large irreversible expansions.

The greater irreversible expansion of 3MPPy-co-PPy(DBS) in the range 0.5ml to 0.75 ml compared to 3,4-DMPPy-co-PPy(DBS), might be the result of the differences in relative increases in cross-linking and branching that occur within the copolymers with increasing blocked monomer content i.e. the ratio of branching: cross-linking. As the levels of 3,4-DMPy increase within 3,4-DMPPy-co-PPy(DBS) there would be expected to be a near equal decrease in both cross-linking and branching. Whereas this might not necessarily be the case for 3MPPy-co-PPy(DBS) with increasing 3MPy content. It is possible that the decrease in cross-linking is greater than the decrease in branching. The differences in the irreversible expansion of the copolymers in the range 0.5 ml to 0.75 ml might be due to the differences in branching i.e. that a combination of low cross-linking and relatively high branching lead to the largest expansions. An increase in branching without an increase in the levels of cross-linking would not increase the connectivity within the network and would tend to increase the distances between adjacent branched sections, leading to less rigid a lower density network.

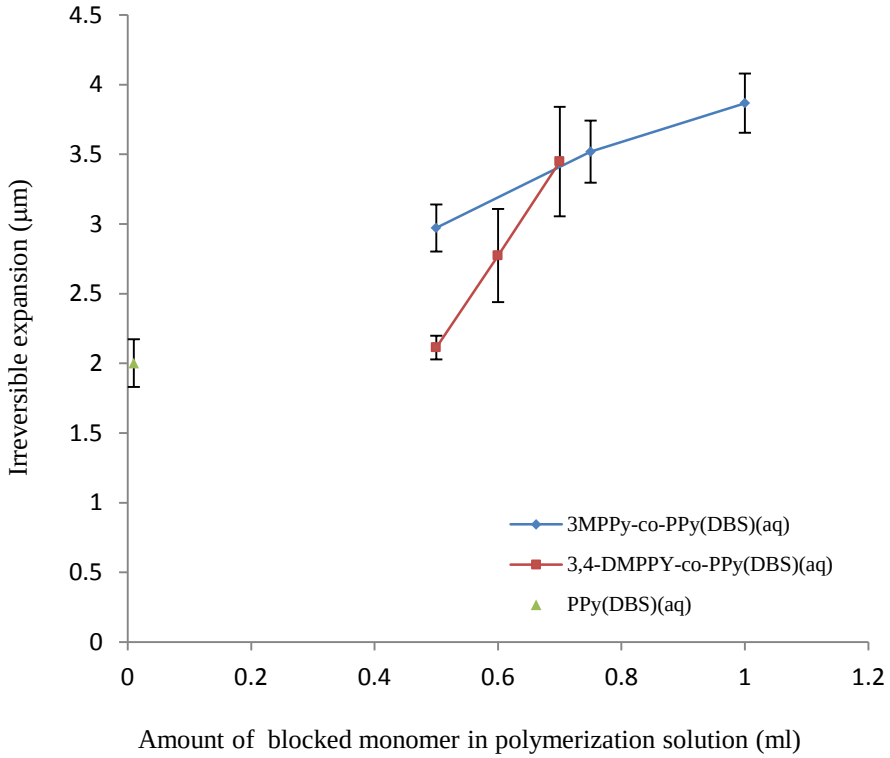

Fig 3.11 An overlay showing the difference in the irreversible expansions of the copolymers compared to PPy(DBS) and also the variation in the irreversible expansion with increasing blocked monomer content in the stable state.

Figure 3.12 compares the maximum reversible expansion rates for 3MPPy-co-PPy(DBS) and PPy(DBS), during the reduction and oxidation scans in the stable state. One of the first things to observe is that the expansion rates are slower for all of the 3MPPy-co-PPy(DBS) copolymers compared to PPy(DBS). In addition it is evident that the rate of actuation during reduction (blue line) is always greater than the rate during oxidation (red line) for both the 3MPPy-co-PPy(DBS) copolymers and PPy(DBS). Comparing the expansion rates across the series of 3MPPy-co-PPy(DBS) copolymers, there is little change discernible, this might be due to the relatively large variation in the values of the replicate measurements, as indicated by the large error bars.

As has been discussed in previous sections of this thesis, the maximum expansion rate usually occurs very early on in each scan, typically within the seconds just after switching. Therefore the time it takes for the samples to undergo 80 % of their maximum reversible expansion was also used as a metric for speed for both the copolymers and PPy(DBS), which are displayed in figure 3.13.

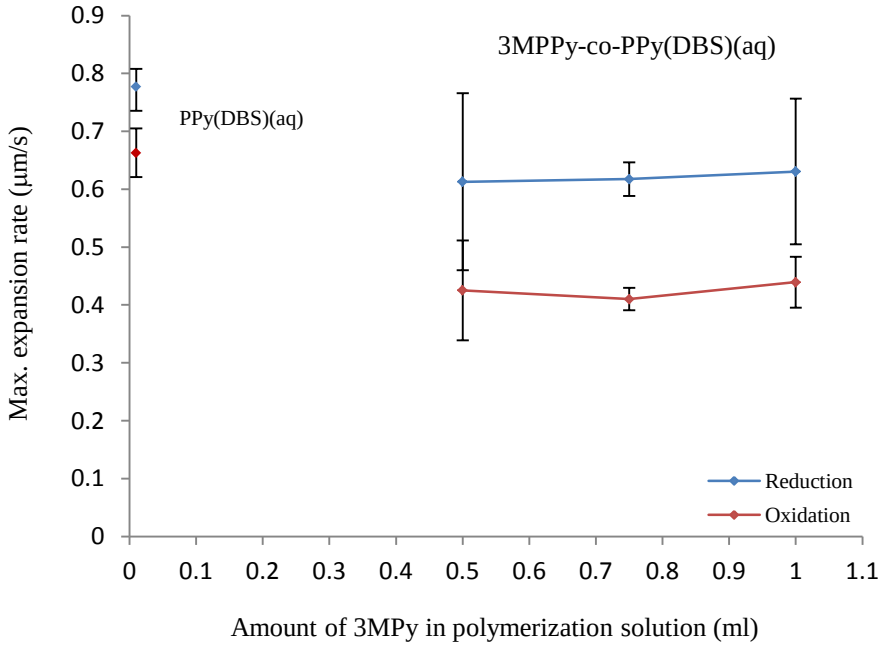

Fig 3.12 Maximum expansion rates for 3MPPy-co-PPy(DBS) and PPy(DBS) in the stable state during the reduction and oxidation scans.

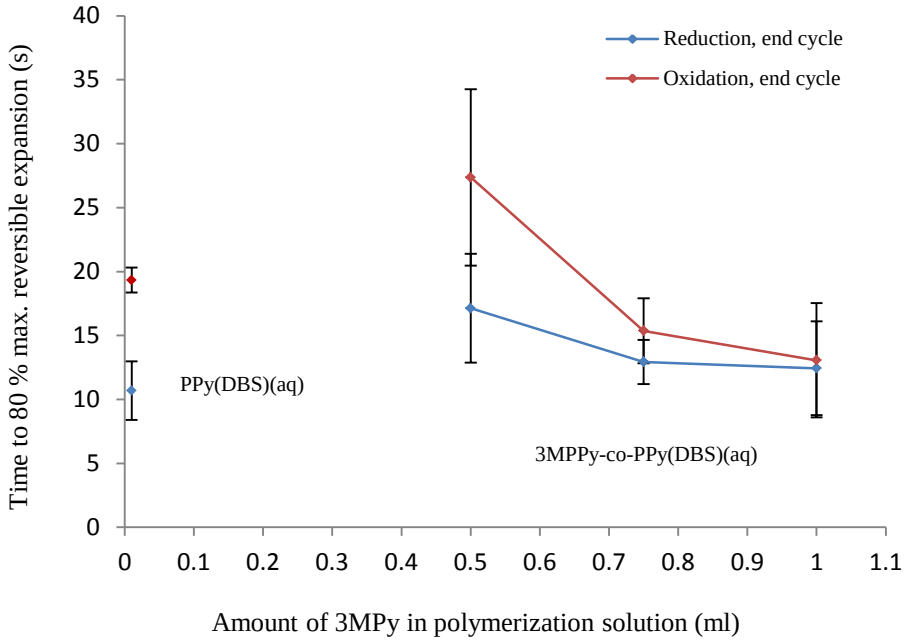

Fig 3.13 An overlay comparing the mean times taken to reach 80% maximum reversible expansion during the reduction scans and in the stable state for 3MPPy-co-PPy(DBS) and PPy(DBS).

Figure 3.13 again reveals that actuation occurs more quickly during reduction compared to oxidation. The time taken to reach 80% maximum expansion is greater than PPy(DBS) for 0.5 ml 3MPPy-co-PPy(DBS) but less for both the 0.75 ml and 1 ml 3MPPy-co-PPy(DBS). There is also a decrease in the expansion times for the copolymer series on going from the 0.5 ml to 1 ml 3MPPy-co-PPy(DBS) copolymer. However, caution needs to be exercised in interpreting this change as the expansion times correspond to percentage changes. Given that there is a slight decrease in the reversible expansions on going from 0.5 ml to 1 ml 3MPPy-co-PPy(DBS) copolymer (see figure 3.10) the decrease in expansion times might be due to the lower reversible expansion displayed for the 0.75 ml and 1 ml copolymers compared to the 0.5 ml copolymer.

Figure 3.14 shows the data used to produce figure 3.13 displayed in a different way and shows the individual replicate measurement and not their means. The heights of the columns show the combined totals of the reduction and oxidation expansion times. Again there is a decrease in the expansion times between the 0.5 ml and 0.75 ml copolymers.

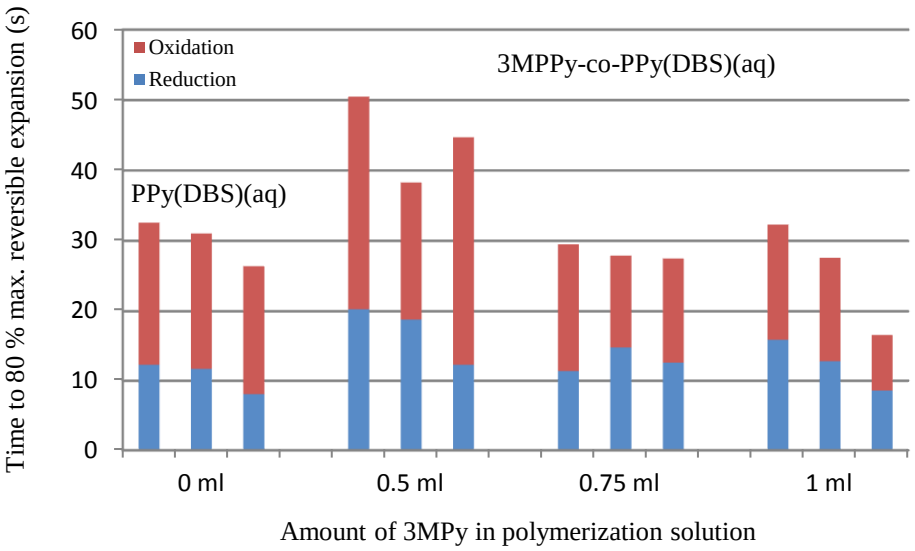

Fig 3.14 Combined (reduction + oxidation) times to 80 % maximum reversible expansion of 3MPPy-co-PPy(DBS) and PPy(DBS) for each of the replicate measurements in the stable state.

Figures 3.15 and 3.16 for 3,4-DMPPy-co-PPy(DBS) similarly show that the expansion times during reduction are less than those during oxidation. Figure 3.16 shows that there is a decrease in the expansions times on going from 0.5 ml to 0.7 ml 3,4-DMPPy-co-PPy(DBS). In fact it would appear that the expansion times for both 0.6 ml and 0.7 ml 3,4-DMPPy-co-PPy(DBS) are on average less than for PPy(DBS). As mentioned previously, the time to 80 % expansion deals with percentages and any decrease in the expansion time might be the result of a decrease in the magnitude of the maximum reversible expansion and not due to a real increase in the expansion times. However, in this case the decrease in the time to 80 % maximum expansion is a real decrease as it corresponds with an increase in the maximum reversible expansion from 0.5 to 0.7 ml (see figure 3.10). So there would appear to be an increase in actuation speed for the 3,4-DMPPy-co-PPy(DBS) copolymer with increasing blocking and decreasing branching and cross-linking.

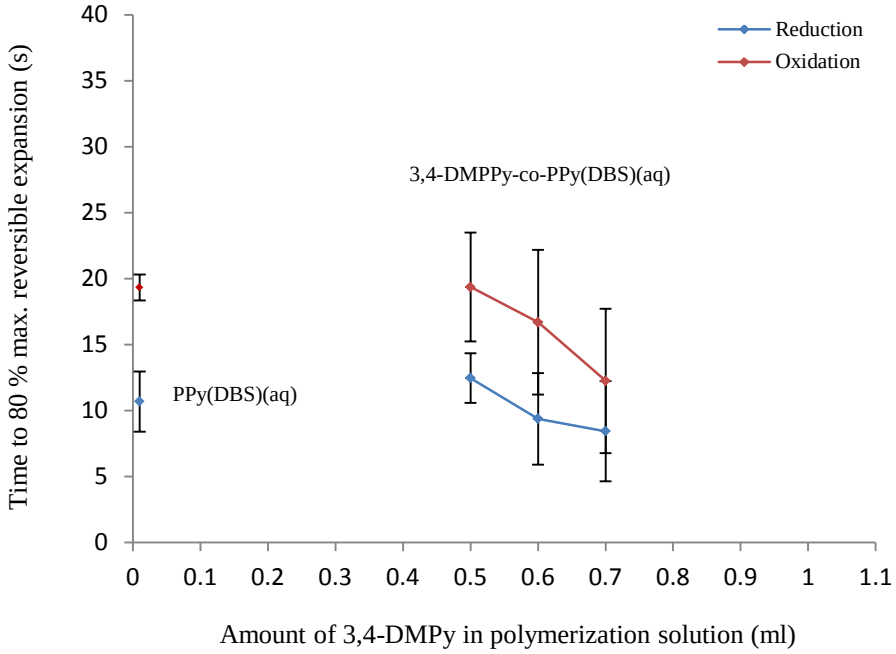

Fig 3.15 The mean times to reach 80% maximum reversible expansion for 3,4-DMPPy-co-PPy(DBS) and PPy(DBS) in the stable state.

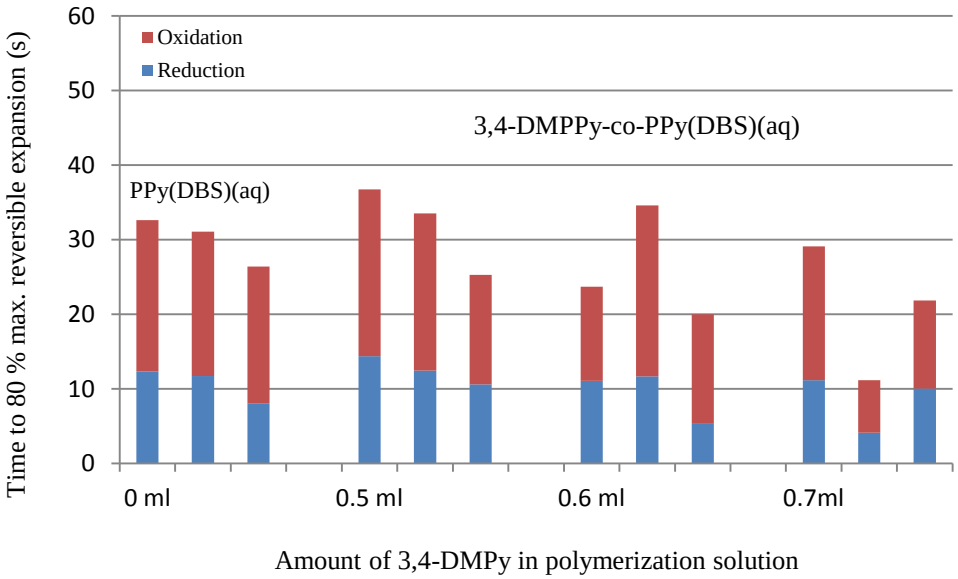

Fig 3.16 Combined (reduction + oxidation) times to 80 % maximum reversible expansion of 3,4-DMPPy-co-PPy(DBS) and PPy(DBS) for each of the replicate measurements in the stable state.

Figure 3.17 shows that there is a decrease in the charge which flows during redox switching of the copolymers compared to PPy(DBS). This might partly explain why the reversible expansion of the copolymer films is less than the PPy(DBS) films. As explained in section 3.2.1, the methyl blocking group will have an electronic and steric influence on the pyrrole ring and the polymer chain. These electronic and steric effects if significant would be expected to reduce the number of polarons and bipolarons within the polymer and decrease its electroactivity.

(a)

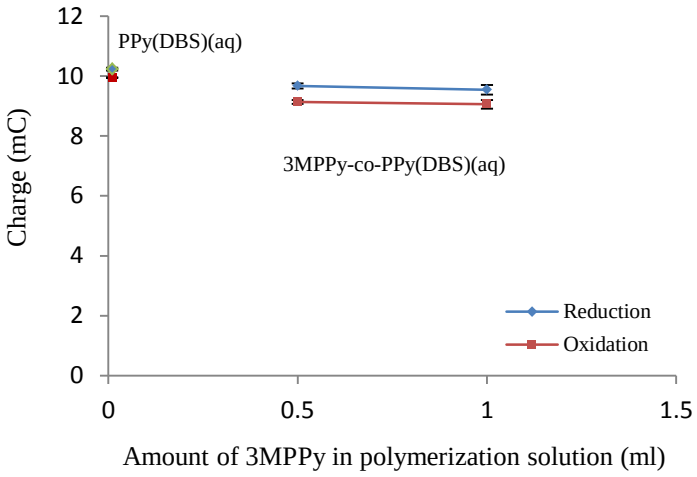

(b)

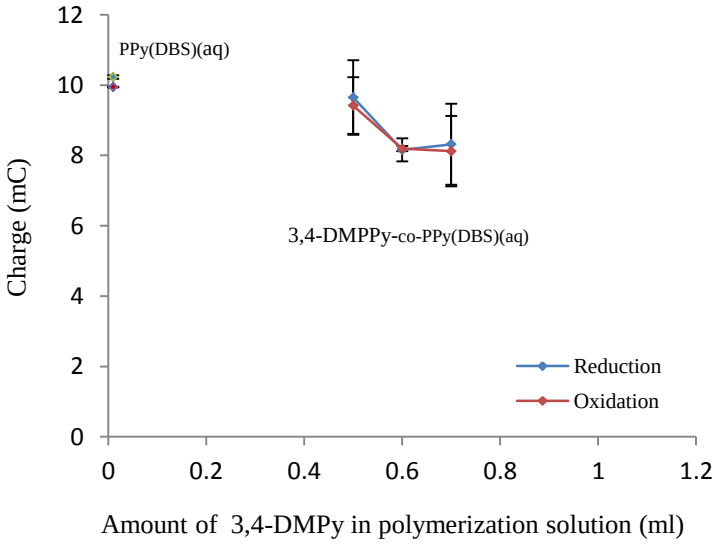

Fig 3.17 Charge flow that occurs during switching for (a) 3MPPy-co-PPy(DBS) and (b) 3,4-DMPPy-co-PPy(DBS) relative to PPy(DBS).

However, it does not account for the increase in the reversible expansion observed for 3,4-DMPPy-co-PPy(DBS) with increasing levels of blocked monomer i.e. on going from 0.5 to 0.7 ml 3,4-DMPPy-co-PPy(DBS). This increase must therefore originate from some other source such as increased freedom of movement of the polymer chains associated with decreased levels of crosslinking.

3.5 Further discussion

In the preliminary work (section 3.4.1) it has been shown that the blocking group approach to changing cross-linking and branching results in huge and unstable irreversible expansions and reversible expansions. This behaviour is typically observed for 3MPPy(DBS) and 3,4-DMPPy(DBS) and their copolymers with PPy(DBS), containing high levels of blocked monomer e.g. several ml or more of blocked monomer in the polymerization solution. These polymers undergo failure by delamination and fracture after a small number of cycles (see figure 3.4). At lower levels of blocked monomer e.g. 2-3 ml the copolymers are more amenable to actuation and can be actuated for longer periods prior to undergoing failure, this time by deformation rather than fracture (see figure 3.7). Deformation in this range is likely the result of creep and an indication of plastic deformation. Both deformation and fracture is clearly visible in the profiles of the actuation sequences for these films. At lower levels of blocked monomer the copolymer films were capable of being successfully actuated to their fully irreversibly expanded state ("stable" or "end" state). These ranges were below 1 ml and 0.7 ml respectively for 3MPPy-co-PPy(DBS) and 3, 4-DMPPy-co-PPy(DBS). In this region the behaviour is elastic in nature and actuation could be sustained long term without failure of the films. This transition from elastic to plastic to brittle failure is reminiscent of what is seen during a "tensile test" and it would appear that the actuating polymer is in a sense performing a "tensile test on itself" as it actuates.

Another very interesting observation that was made of the "spaghetti like" 3,4-DMPPy (aq) homopolymer, which is incapable of cross-linking and branching, was that it can exist in two very different physical forms. The first being a very adherent black polymer film that was formed initially next to the AuWE. This homopolymer was much more resistant to removal from the AuWE when heated with hot TL1 wash compared to the copolymer films that we prepared. The material appeared denser than the copolymer films. The second form of this material was a very soft gel which formed on the outer surface of the first form. This appeared after being left in contact with aqueous electrolyte for approximately half an hour after the end of the cyclic voltammetry measurements.

This material demonstrated that linear un-branched and non-crosslinked chains can form both adherent solid films initially and soft gels when swollen. The first formed adherent

layer strength can only be explained the operation of some non-bonding interaction. This type of bonding would appear to be readily overcome by the penetration of the surrounding solvent, in the case where no branching and cross-linking is present.

The main work here has shown that there is a strong correlation between the amount of blocking of the beta-positions in the polymer chain and the size of irreversible expansion that polypyrrole films undergo upon actuation. This can be explained by the decreased levels of cross-linking and branching introduced by the blocking group, in-line with the initial hypothesis. This correlation between irreversible expansion (solvent swelling) is recognized and commonly used within the polymer industry, where the phenomenon is described as "solvent swellability" and it measurement which can take several weeks to perform, as "swelling studies". Solvent swellability is used as a standardized way of assessing crosslinking (e.g. American test standard: ASTM F2214-02(2008)). In this sense, the actuation sequences obtained here for the polymer films form a type of "dynamic" swelling study.

It was noted that the size of the irreversible expansion for the 3MPPy-co-PPy(DBS) series was generally larger than that of the 3,4-DMPPy-co-PPy(aq) series. Initially this was a surprise as we expected the 3,4-DMPPy-co-PPy(aq) series of copolymers to display a larger irreversible expansion due to the presence of blocking groups in both of its beta-positions compared to just one, in the 3MPPy-co-PPy(aq) series of copolymers. This might be explained by the fact that the 3,4-DMPPy-co-PPy(aq) series was a narrower range series (0.5 to 0.7 ml) compared to the 3MPPy-co-PPy(aq) series. However this does not explain why the 3MPPy-co-PPy(aq) series still displays a higher irreversible expansion in the shared range (0.5 to 0.7 ml). This could be explained by the increased levels of branching that will likely be present within the 3MPPy-co-PPy(aq) series.

On this basis, not only would a decrease in branching cause an increase in irreversible expansion, but the combination of low levels of cross-linking with a relatively high level of branching, increases this effect further. Certainly, increased levels of branching will result in a more open and lower density network compared to one with lower levels of branching, whose chains can be packed more closely together.

From the point of view of performance it was unfortunate that the presence of the blocking group resulted in decreased levels of reversible expansion relative to the unblocked polymer. This decrease relative to the unblocked polymer is most likely the result of electronic and steric effects introduced by the blocking group. However, the changes that occur in the reversible expansion *within* the blocked polymer series cannot be explained by electronic and steric effects. For example, it has been shown that there is an increase in the reversible expansion occurs across the 0.5 ml to 0.7 ml 3,4-DMPPy-co-PPy(DBS) series which corresponds with a decrease in the charge flow that occurs during switching. Therefore, what is noted is an increase in the reversible

expansion alone with an apparent decrease in the levels of polarons and bipolarons within the film. Such a decrease would be expected to cause a decrease in the reversible expansion of the film and not an increase. The most probable explanation for this increase in reversible expansion is the decrease levels of cross-linking, introduced by the blocking groups, allowing the polymer chain to move more freely. This is intuitive and is in keeping with the initial hypothesis.

For the majority of the copolymers studied, the actuation speeds appear to be less than PPy(DBS), as revealed by the expansion times. In addition, actuation was seen to be slower during the oxidation scan than during the reduction scan for both the copolymers and PPy(DBS) and is consistent with normal polypyrrole (see figures 3.12 and 3.13).

Also noted is an apparent increase in actuation speed across both series of copolymers. However, the measurement of expansion rates and times has been made difficult by the use of a relatively large data point interval. This was out of necessity, due to the software restriction of using less than 10000 points in a single procedure. Given the relatively larger data point intervals, the times to 80 % maximum expansion did appear to be a more reliable and sensitive indication of the changes that occur in the speed of actuation within the copolymer series (compare figures 3.12 and 3.13). On this basis the actuation times decrease with increasing blocked monomer content for both series of copolymers. In the case of the 0.7 ml 3,4-DMPPy-co-PPy(DBS) expansion time is lower than for PPy(DBS).

3.6 Conclusion

The research has shown that a “blocking approach” using substituted monomers can be successfully used to change the levels of cross-linking and branching within polypyrroles and thereby influence both the reversible and irreversible expansion.

The main finding has been that there exists a strong correlation between cross-linking and irreversible expansion, with decreasing levels of cross-linking, producing a large increase in the irreversible expansion.

By using two different types of blocked monomer (3MPy and 3,4-DMPy) data has also been obtained that suggests that under certain circumstances a combination of relatively high levels of branching and low levels of cross-linking can produce larger increases in irreversible expansion than decreasing levels of cross-linking on its own.

The reversible expansion of all the copolymers prepared in this work have been lower than PPy(DB)(aq) and this combined with an increase in the irreversible expansion, results in films with a lower actuating performance.

This decrease in reversible expansion relative to PPy(DBS) is most likely the result of a combination of changes due to electronic and steric effects caused by the blocking group, as well as crosslinking and branching. In addition, there was an increase in reversible expansion corresponding with decreased levels of cross-linking *within* the 3,4-MPPy-co-PPy(DBS) series of copolymers. This was in keeping with the initial hypothesis that decreased cross-linking would lead to increased reversible expansion. The magnitude of the reversible expansion would appear to depend upon the balance between the blocking effect and electronic and steric effects. Unfortunately, the increase in reversible expansion seen for the 3,4-MPPy-co-PPy(DBS) series of copolymers coincides with an increase in the irreversible expansion and therefore there is little to no increase in strain performance.

It has been shown that there is an increase in actuation speeds within the 3,4-DMPPy-co-PPy(DBS) copolymer series, with increasing levels of blocked monomer and corresponding with decreasing levels of crosslinking. In fact the 0.6 ml an 0.7 ml 3,4-DMPPy-co-PPy(DBS) copolymer films are faster actuating films. In this respect there has been a slight boost in performance of these films over 0.55V PPy(DBS).

The work has shown that very low levels of cross-linking result in very poor actuating films that undergo failure after a small number of cycles by brittle fracture or deformation, depending upon the amount of blocked monomer. In fact none of the blocked homopolymers could be successfully actuated for more than a few cycles before failure.

By undertaking this work it has been demonstrated that changes in irreversible expansion can be used to monitor cross-linking changes. It is now possible to monitor cross-linking changes within polypyrroles without the necessity of employing a blocking-group. This represents a major advancement in the study of polypyrrole films made possible through the application of a blocking-approach.

4. The effect of polymerization potential on the structure and actuation performance of PPy(DBS)

4.1 Introduction

When we first embarked upon the work outlined in the previous section of this thesis, it was anticipated that a decrease in crosslinking would result in an increase in the reversible strain, producing a better actuating material. Our reasoning was that with lower levels of crosslinking, the polymer chains would be less restricted and capable of greater movement, resulting in greater reversible strains. However, although an increase in irreversible strain with decreasing levels of crosslinking was observed, a decrease in the reversible strain was also observed.

In the earlier work a blocking approach was used to change the degree of branching and crosslinking in polypyrroles. In addition to their blocking effect, beta-substituents have the potential of exerting both an electronic and steric affect. For example, methyl substituents in the beta-positions of the pyrrole ring have a greater tendency to donate electrons compared to hydrogen substituents, due to the Inductive Effect. In addition they might be expected to increase the torsional angle along the polymer backbone and potentially disrupt polaron and bipolaron formation.

Although the copolymers that were synthesized and studied in the earlier work were polypyrroles, they were not polypyrrole in the strict sense i.e. polypyrrole homopolymer. We therefore wanted to see if similar effects accompanying crosslinking changes in the homopolymer are observed. In addition, it was of interest to see if the unexpected decrease in reversible strain observed for the beta-substituted polypyrroles was observed in the homopolymer. If not, then the decrease in the reversible strain observed for the copolymers with increasing beta-substitution might be the result of electronic effects.

We decided to monitor changes in crosslinking indirectly through changes in the degree of irreversible strain (swellability). The use of swelling studies to monitor crosslinking changes in polymers is a standard approach used in the polymer industry (e.g. American test standard: ASTM F2214-02(2008)). In a sense the irreversible strain measurements that were made in the earlier work are a “dynamic swelling study”. By using a blocking group approach we identified a means of monitoring crosslinking changes in polypyrroles. In support of this view, an alternative approach to monitoring crosslinking changes was also used, one that is recognized within the field of conducting polymers, to act as a secondary method in support of approach.

In addition to the use of solvent swellability to monitor the density of crosslinking, it is recognized that there is a strong correlation between crosslinking density and physical properties such as strength and toughness[26]. That this is indeed the case is clearly

illustrated in figure 4.1 where polypyrrole films with high levels of beta-substitution in the polymer backbone break after a few actuation cycles. We have also noted that these films are more easily removed from their AuWE using TL1 wash, even when they had not been actuated. Therefore it was decided to monitor changes in the physical properties of the polypyrrole films alongside the actuation measurements. Nanoindentation was selected as suitable method for monitoring changes in the physical properties of the thin films of polypyrrole. A decision was made to monitor changes in the Young's modulus of elasticity, hardness and creep.

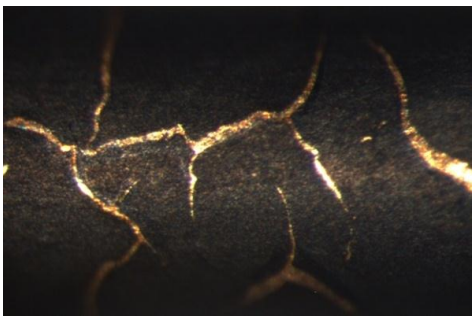

Fig 4.1 Fracturing of a 5 μm layer of 3-methylpolypyrrole dodecylbenzenesulphonate (aq), polymerized on a AuWE, after just a few actuation cycles.

However, in order to monitor changes in polypyrrole homopolymer, an alternative approach to changing the degree of crosslinking in polypyrrole was needed. Both the electrical potential[30] and temperature[32] employed during polymerization were identified as potentially being simpler means of altering the crosslinking.

Although discussion of the issue of branching and crosslinking in polypyrrole in the literature was limited, we did find some. One excellent paper[32] did show that an increase in temperature during synthesis likely results in an increase in branching and crosslinking. It is also considered likely that higher polymerization potentials yield a higher degree of cross-linking (a tighter network), and thus the ability of the polymer to strain is reduced[30].

Higher polymerization temperatures and electrical potentials will likely increase the energy that is available within the system during electropolymerization, allowing more of the processes that require higher energy, such as beta substitution compared to alpha substitution, to take place compared to when there is less energy available to the system.

Given the difficulties (temperature dependence) in operating reference electrodes such as the Ag/AgCl electrode at temperatures significantly above or below room temperature, and given the large variation in the solubility of NaDBS in aqueous solutions at temperature below room temperature and 1^{o}C, it was decided to use polymerization potential as the means to investigate crosslinking changes.

4.2 Synthesis of PPy films

PPy(DBS) films were polymerized at constant potential in the range 0.50 V to 0.90 V. A potential lower than 0.50 V was not employed as this would lead to very long polymerization time for the film thickness that was planned to synthesize (5 μm for actuation measurement and 30 μm films for nanoindentation measurement) as this potential is very close to the oxidation potential of pyrrole. Figure 4.2 shows the huge variation in polymerization times recorded for the polymerization of the 5 μm films prepared for actuation measurement over this potential range.

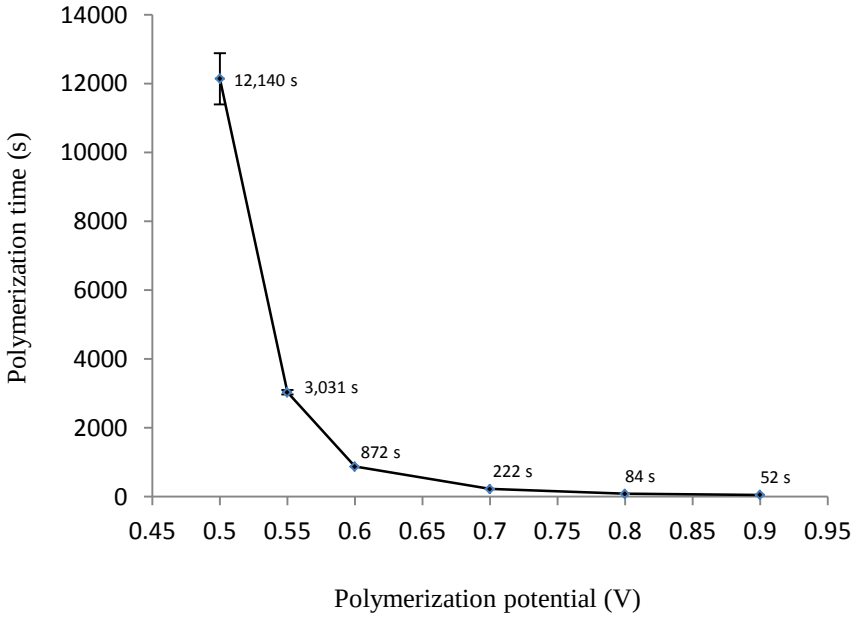

Fig 4.2 Polymerization times for the preparation of 5 μm PPy(DBS) for actuation. Error bars are 1 SD and are only shown for the first two points as they are very small for the other points and impractical to use.

Polymerization potentials greater than 0.90 V were not employed; firstly because the growth at this potential is very rapid and the thickness of the films becomes increasingly difficult to control and secondly that the over-oxidation of the polymer films becomes more likely. This type of decomposition leads to the formation of C=O, -O-H and CO_2 groups/molecules and loss of aromaticity within the polymer and can be seen using FTIR spectroscopy and is depicted in figure 4.3.

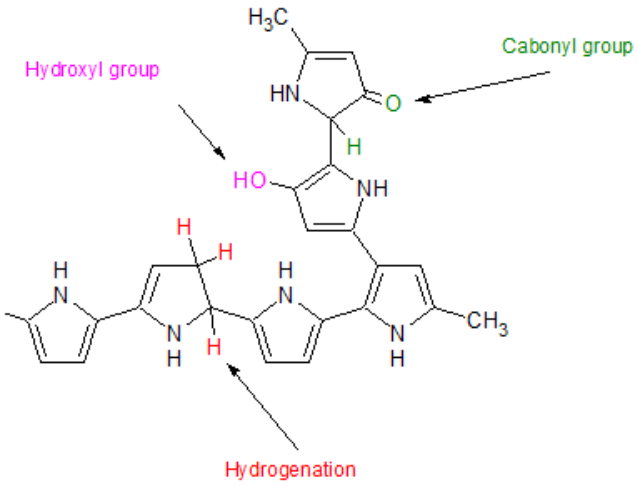

Fig 4.3 Functionalities characteristic of over-oxidation of polypyrroles.

4.3 Experimental details

4.3.1 Preparation of samples for actuation

Py(DBS)(aq) films were grown to a thickness of 5 μm under potentiostatic (constant potential) conditions in an manner identical to that described in section 1 of this thesis. The only difference being that six different potentials were employed to cover the range 0.50V to 0.90 V i.e. 0.50 V, 0.55 V, 0.60 V, 0.70 V, 0.80 V and 0.90 V, with three replicate samples being produced at each thickness, to give a total of 18 samples for actuation measurement.

When growing the first sample at a new potential, particular care needs to be taken, as each new potential produces a different growth rate. Once the initial sample has been produced the second and third replicates are more easily formed as the growth conditions are then better known.

Steps were taken to ensure all other variables were kept constant during the preparation of all of the samples, such as using the same Ag/AgCl RE throughout and ensuring the ambient temperature was constant (in the lab the temperature control was consistently in the range: 20.5 to 21.5 ^{o}C).

4.3.2 Preparation of samples for nanoindentation

The samples prepared for nanoindentation had different requirements and had to be produced in a different way and form to those produced for actuation measurements. The sample films needed to be planar and relatively thick (30 μm) to avoid interference from the substrate during nanoindentation measurements.

Polymer films were grown onto a working electrode (WE) which had been cut from a silicon wafer with a layer of gold evaporated onto one of its sides (1000 Å Au and 50 Å Ti). Four WE could be formed in this way from each wafer as depicted in figure 4.4 (a).

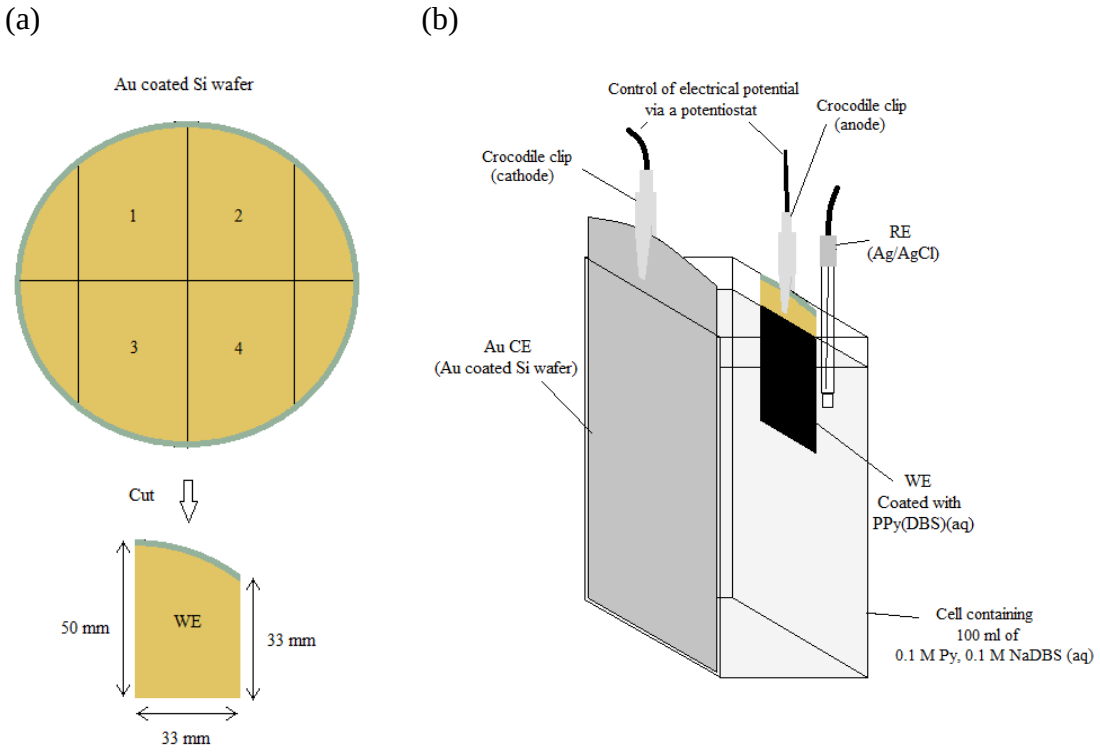

Fig 4.4 (a) Formation and dimensions of AuWE for use in preparation of nanoindentation samples (b) Polymerization cell setup used to polymerize 30 μm films for nanoindentation.

The cell arrangement used to synthesize the films for nanoindentation is shown in figure 4.4 (b). As with polymerization of the films for actuation measurement, polymerization to a precise thickness of 30 μm required the films to be polymerized in stages, being stopped to have their thickness determined and the growth rate calculated, before polymerization was recommenced. The growth of precise film thicknesses typically required stopping polymerization, measuring the thickness, recalculating growth rates and restarting polymerization, three or four times. The polymerization times varied greatly, depending upon the electrical potential employed, and are shown in Figure 4.2.

Thickness measurement was undertaken using a Dektak profilometer. A diagonal scratch was made in a lower corner of the sample film, using the tip of a pair of tweezers, so as to just reveal the surface of the underlying gold substrate. Three Dektak scans across this scratch were used to obtain the average thickness of the film. The final thicknesses were accurate to 30 ± 0.5 μm. A degree of uniformity of the film was

assumed and nanoindentation measurements were undertaken as near to these scratches as possible.

In order to obtain representative data from the samples indentations were carried out in a systematic way. Indentations were undertaken in the form of a 5 x 5 matrix, with each point being indented to the 5 depths. This generated 125 measurements for each replicate sample, giving a total of 375 measurements on polymer polymerized at each potential of our chosen potentials. This approach was used to generate both the reduced Young's modulus and micro-hardness data. In addition, creep testing was performed on each replicate sample, with 5 measurements being performed and used to obtain an average value.

4.4 Results

4.4.1 Polymerization

FTIR spectra were obtained for 30 μm films polymerized at 0.50 V, 0.70 V and 0.90 V using a FTIR microscope and these spectra are shown staggered in the overlay in figure 4.5.

The first thing to note is that there is little difference in the spectra recorded for the samples covering the 0.50 to 0.90 V range. However, this reveals something very useful i.e. that the PPy(DBS) films do not show signs of decomposition via over-oxidation occurring at higher polymerization potentials 0.70 and 0.90 V relative to the 0.50 V sample. There are no differences in the samples in the regions typically indicating overoxidation i.e. 1720 cm^{-1} (C=O) or 3615 cm^{-1} (non-hydrogen bonded –OH)[127]. Although there are CO_2 peaks observed in all three of the spectra, which can be a sign of overoxidation, it is most likely that this has come from atmospheric CO_2 being present within the FTIR microscope chamber. (If the source of this CO_2 was taken to originate from the overoxidation occurring within the polymer, the intensity of the CO_2 peak would be expected to be greatest at 0.90 V, which it clearly is not. Also, over-oxidation forming CO_2 should not be occurring at all at 0.50 V).

Although there is little difference observed in the spectra, this should not be taken to indicate that there has not been any change occurring within the polymer network, as it would be expected that these changes would be very subtle and difficult to observe using FTIR spectroscopy, especially given the interference that comes from the presence of peaks due to the DBS dopant within the polymer matrix.

The only notable difference in the FTIR spectra, which was identified occurs at 668 Hz, and is shown (expanded) in the insert in figure 4.5. There is a relative increase in the intensity of peak on going from 0.50 V to 0.55 V, which then decreases again on going from 0.55 V to 0.90 V. This peak lies within the CH ring bending region and might

possibly be due to an increase presence of CHα bonds present within end groups at 0.70 V and would correspond to increased levels of branching[128,72,73].

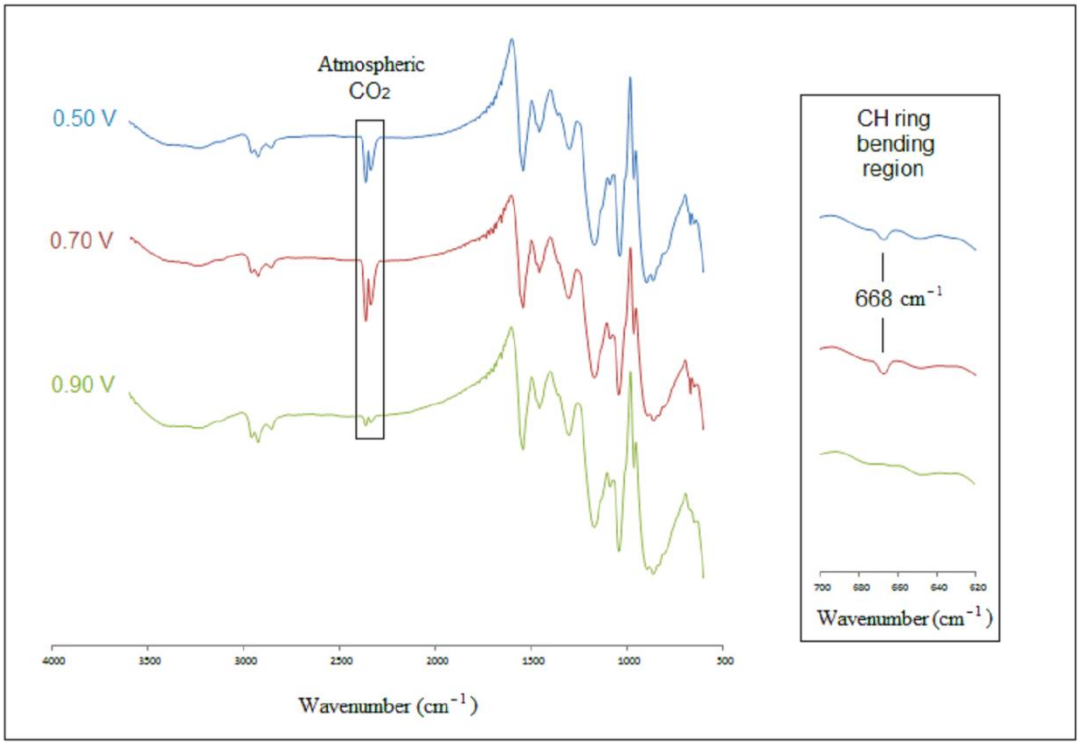

Fig 4.5 Overlay of FTIR spectra for three samples covering the whole of the polymerization potential range used to synthesize the samples in the investigation (shown staggered).

The charge consumed during polymerization of the 5 μm films is shown in figure 4.6. There can be seen to be a general decrease in the charge consumed during polymerization with increasing polymerization potential, with the greatest decrease occurring between 0.55 V and 0.60 V. However, there would appear to be an increase in charge consumption occurring in the range 0.70 V to 0.90 V.

Charge flow during polymerization can occur for a number of reasons. The first and most obvious way is due to the formation of bonds e.g. chain growth, branching and crosslinking. Charge will also be produced through the oxidation of the polymer to give polarons and bipolarons. In addition charge can also flow due to faradic charging of the polymer and also due to the presence of parasitic reactions. The fact that charge can flow for reasons other than the direct formation (Faradic and parasitic currents) of the polymer network, makes it very difficult to draw firm conclusions from charge flow data.

However, a general decrease in the polymerization charge with increasing polymerization potential might be expected to occur as the polymer chains become more branched and less densely packed. A lower density of material would mean that

there would be less charge needed to polymerize the same thickness of material. In addition increased branching and crosslinking would be expected to decrease the ability of adjacent monomer units to forming the network to take up a favourable orientation (coplanar) to form polarons and bipolarons. Hence increased numbers of these "defect" (branching and crosslinking) would be expected to reduce charge released during polymerization due to the decrease in the numbers of polarons and bipolarons.

The increase in charge flow that occurs between 0.70 V and 0.90 V could be due to an increase in crosslinking in that potential range, possibly resulting in a re-densification of the polymer network.

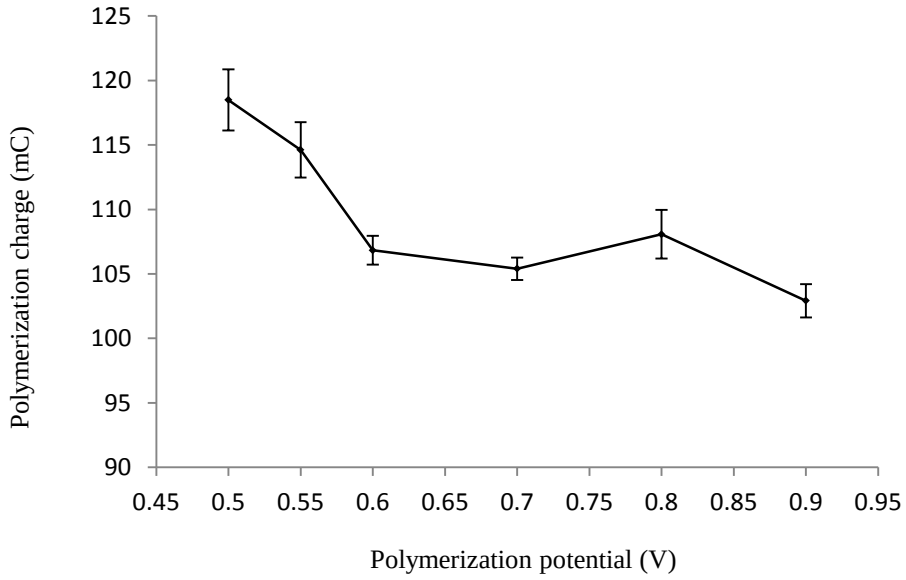

Fig 4.6 Charge flow during polymerization of 5 μm PPy(DBS) films vs polymerization potential. Error bars = 1SD.

4.4.2 Actuation performance

In assessing the actuation performance of the PPy(DBS) in the potential range 0.50 V to 0.90 V, focus was on the amount (expansion and strain) and speed of movement of the films (time to 90 % maximum reversible strain).

Figure 4.7 shows the mean maximum reversible expansion during the reduction phase for the end cycle. The maximum reversible expansion occurs in region 0.45 to 0.65 V with the mean maximum reversible expansion corresponding to the 0.55 V for the samples. A relatively large decrease in the mean maximum reversible expansion occurs between 0.55 V and 0.90 V. The greatest variation in the replicate measurements

correspond to the region in which the maximum reversible expansion is changing most rapidly i.e. the region with greatest gradient: 0.70 V.

The value at 0.90V does not have any error bars as it represents just one value. Three replicate measurements were made on polymer films synthesised at this potential, but only the one shown was successfully actuated. The other two samples were actuated, but underwent delamination. This vulnerability towards delamination is likely to be related to the structural changes that are taking place in the polymer films at the polymerization potential. It is possible that the increased stiffness in the polymer is causing increased stress at polymer substrate interface resulting in delamination.

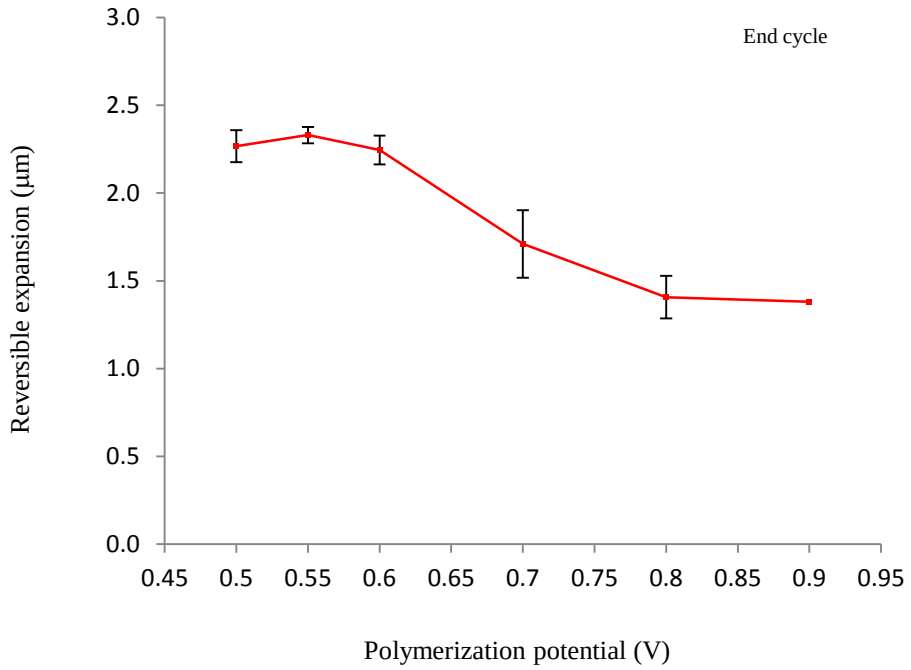

Fig 4.7 Variation in the mean maximum reversible expansion with polymerization potential for a 5 μm films of PPy(DBS) during the reduction phase and in end cycle (stable state). Error bars = 1 SD.

When the profiles are compared for the 10th and end cycle sets of data shown in figure 4.8 they are very similar. The end cycle profile is shifted downwards relative to the 10th cycle, in the direction of higher reversible expansion between 0.50 V and 0.80 V, showing that there is a decrease in the maximum reversible expansion on reaching the end cycle. The greatest change in the reversible expansion on going from cycle 10 to the end cycle corresponds to a polymerization potential of 0.55 V. Above 0.80 V the curves essentially coincide, with there being little to no change in reversible expansion above the tenth cycle.

Figure 4.9 (a) shows the changes in the irreversible expansion with polymerization potential. The profile largely mirrors that seen for the reversible expansion. However, the magnitude of the irreversible expansion is greater than the reversible expansion. There is a relatively large decrease in the mean maximum irreversible expansion on going from 0.55 V to 0.90 V, with the greatest change occurring in range 0.70 V to 0.80 V. The variation between replicate samples is greatest at 0.50 V, as indicated by the error bars (1 SD).

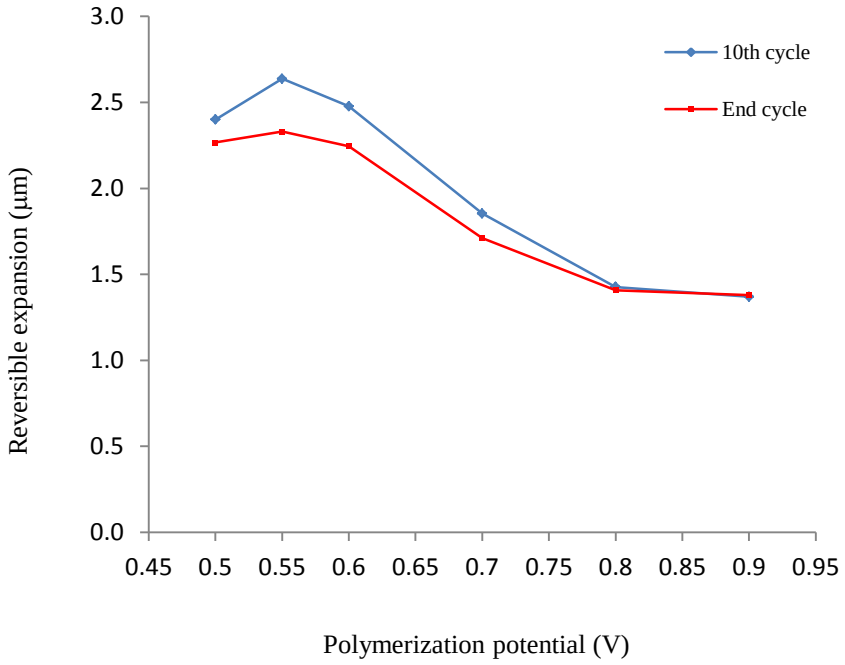

Fig 4.8 Comparison of the mean maximum reversible expansion vs. Polymerization potential for the 10th cycle and the end (stable state) cycle during the reduction phase. Error bars have not been shown to aid comparison.

A comparison of the changes occurring in the irreversible expansion with polymerization potential at the 10th cycle with those during the end cycle, are shown in the overlay in figure 4.9 (b). The changes that occur with polymerization potential are very similar, but the magnitude of these changes increases considerably between 0.50 V and 0.80 V on going from cycle 10 to the end cycle. The values displayed at 0.90 V essentially correspond, showing little to no change in irreversible expansion beyond cycle 10. However, the data for this point represents only one measurement and not the mean of three replicate, for the reasons previously described.

(a)

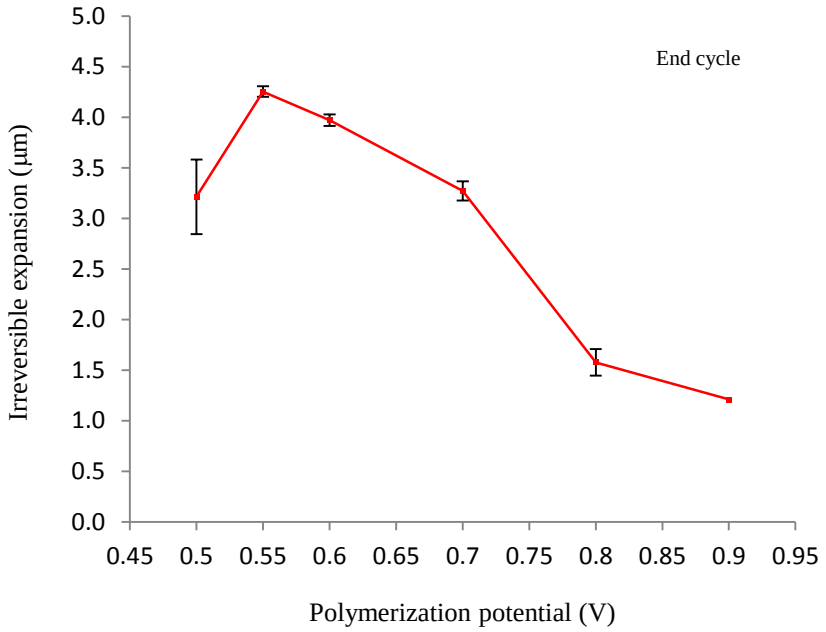

(b)

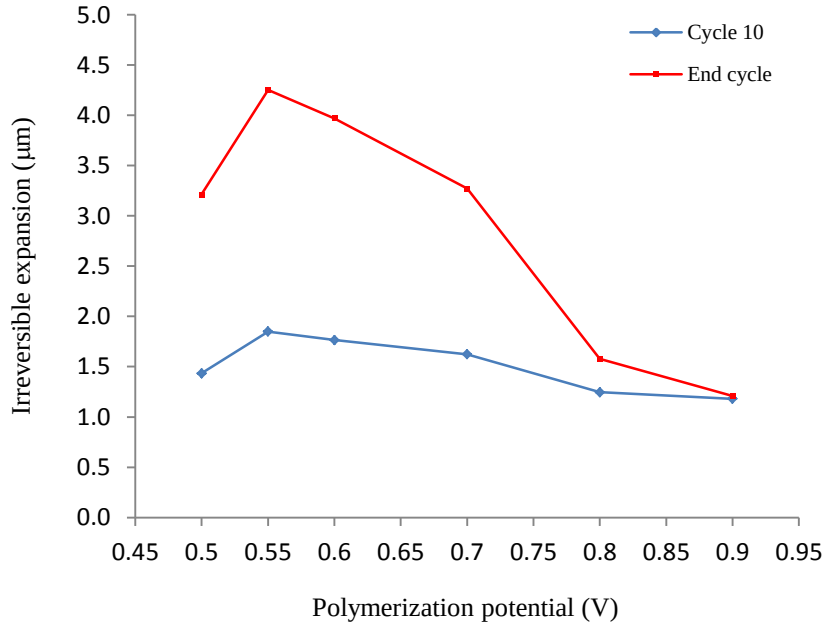

Fig 4.9 (a) The change in the mean maximum irreversible expansion with polymerization potential during the reduction phase and at the end cycle for 5 µm films of PPy(DBS). Error bars = 1 SD. **(b)** A comparison of the change in the mean maximum irreversible expansion with polymerization potential for the 10th and end cycles during the reduction cycle.

An overlay of the mean maximum *reversible* and *irreversible* expansions during the reduction phase at the end cycle is shown in figure 4.10. This shows that the irreversible component of the expansion is larger than the reversible component for most of the potential range. However, at 0.90 V the mean maximum irreversible expansion is less than the corresponding reversible component. Another important change that can be seen occurs in the region 0.50 V to 0.90 V. Here there is a significant decrease in the irreversible expansion on going from 0.55 V to 0.50 V.

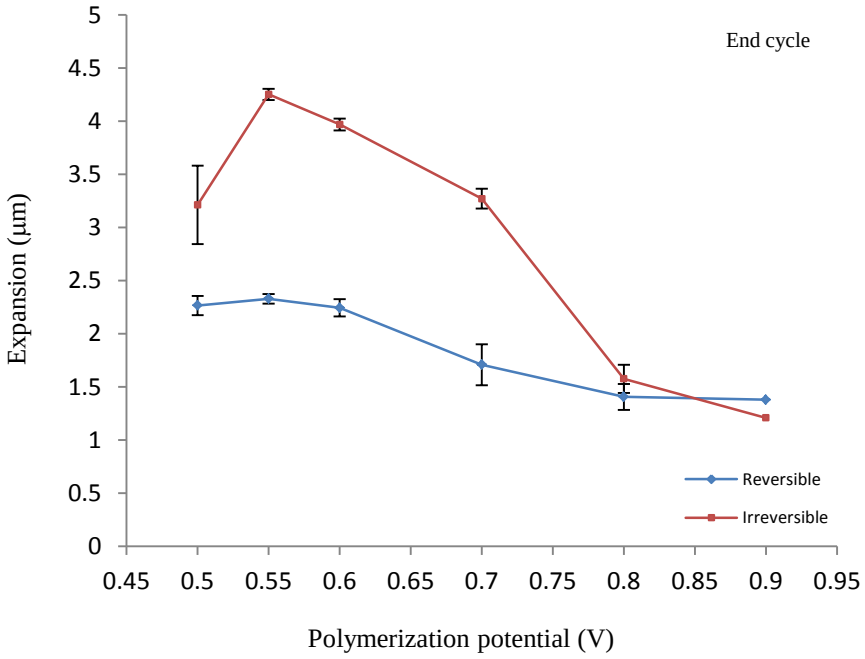

Fig 4.10 An overlay of the mean maximum reversible and irreversible expansions during the reduction phase at the end cycle for 5 µm PPy(DBS). Error bars = 1 SD.

The changes occurring in the calculated reversible *strain* with polymerization potential are shown in figure 4.11 for both the 10^{th} and end cycles. The changes occurring in the reversible *strain* for the 10^{th} cycle are similar to those observed for the reversible *expansion*, as evident from their similar profiles. There is a decrease in the reversible strain on going from cycle 10 to the end cycle for all the polymerization potential with the exception of that at 0.90 V. The maximum reversible strain for cycle 10 corresponds to 0.55 V, whereas the maximum for the end cycle occurs at 0.50 V. The differences in the magnitude and trends in the reversible strain compared to those of the reversible expansion are in part due to the differences in how these metrics are defined and calculated. Both the reversible expansion and reversible strain are influenced by the irreversible changes that are taking place. The reason why there are increases in the end

cycle reversible strain (red line) in on going from 0.55 V to 0.50 V and 0.70 V to 0.90 V, is due to the corresponding decrease in the irreversible component that is occurring at the same time.

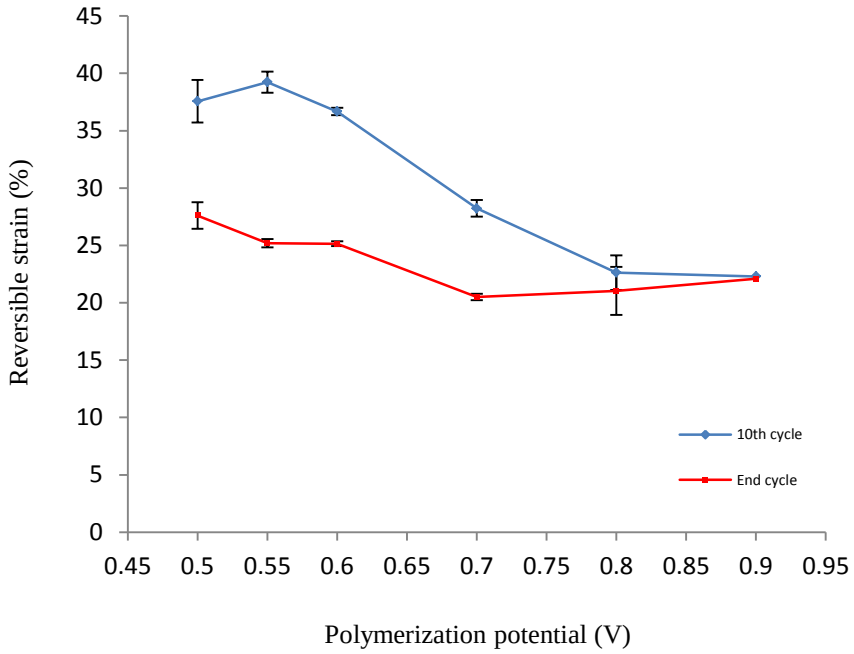

Fig 4.11 Overlay of the mean maximum reversible strain during the reduction cycle for the 10th and end cycles. Error bars = 1 SD.

How quickly the films are able to actuate has been assessed using the time it takes for the films to reach 90% of their maximum reversible expansion. A small time therefore corresponds to a quicker actuating film and visa versa. The variation in these times with polymerization potential, for both the reduction and oxidation phases of the end cycles, are shown in figure 4.12. In addition, the total time (reduction + oxidation cycle times) is also shown in the same overlay, as an estimate of the minimum cycle times required to obtain 90% maximum reversible strain under the cycling conditions employed.

Considering the total cycle time (red line), there is a decrease in the time taken to reach 90% maximum reversible expansion on going from 0.50 V to 0.60 V and a much greater increase on going from 0.60 V to 0.90 V. The minimum time to reach 90% maximum reversible expansion for the samples occurs at 0.60 V, representing the quickest actuating films that were prepared.

Comparing the reduction and oxidation phases, the reduction phase is essential always faster actuating than the oxidation phase, taking less time to reach 90% maximum reversible expansion. The shapes of both the reduction and oxidation curves are similar and therefore combine to give a total with a similar profile. Both the reduction and oxidation phases display a minimum time to 90% reversible expansion at a polymerization potential of 0.60 V.

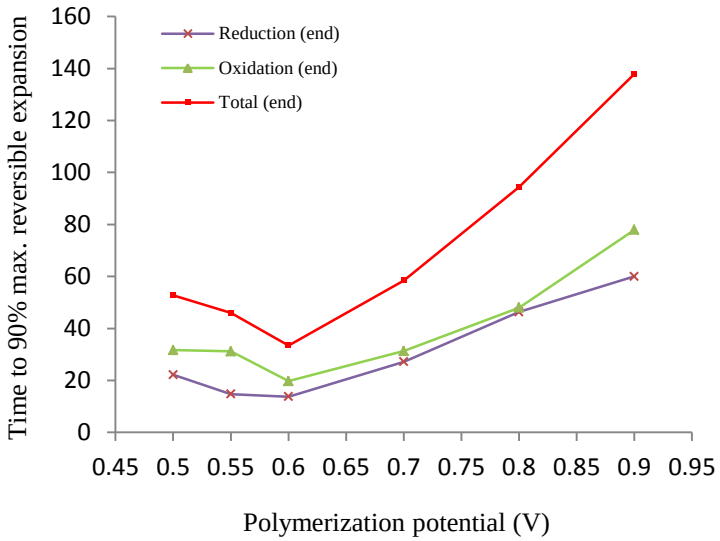

Fig 4.12 Overlay of the times to 90% of the mean maximum expansion for the end cycles during the reduction and oxidation phases. The total (reduction + oxidation) times are also shown as an estimate of the corresponding overall cycle times.

The times to 90% maximum reversible expansion for cycle 10 are shown in figure 4.13. Once again the reduction, oxidation and total times are at a minimum in the region of 0.60 V. There is also a similar decrease in the times on going from 0.50 V to 0.60 V and a larger increase in from 0.60 V to 0.90 V. As with the end cycles the reduction cycle is always faster actuating than the oxidation cycle, with the exception of the one value recorded at 0.90 V.

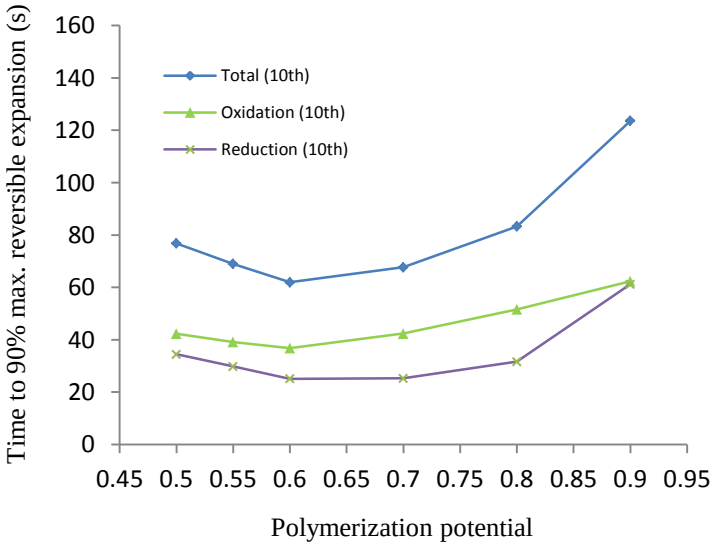

Fig 4.13 Overlay of the times to 90% of the mean maximum expansion for the 10th cycle during the reduction and oxidation phases. Again, the total (reduction + oxidation) times are shown as an estimate of the corresponding overall cycle times.

It is useful to overlay the totals for cycle 10 and the end cycle for comparison (see figure 4.14). This overlay reveals that the total cycle time is less and the speed of actuation increases on going from cycle 10 to the end cycle (stable state) in the range 0.50 V to 0.70 V, but in the range 0.70 V to 0.80 V cross over occurs, so that the total cycle time is more and the rate of actuation slower for the end cycle compared to the 10^{th} cycle in the range 0.80V to 0.90V.

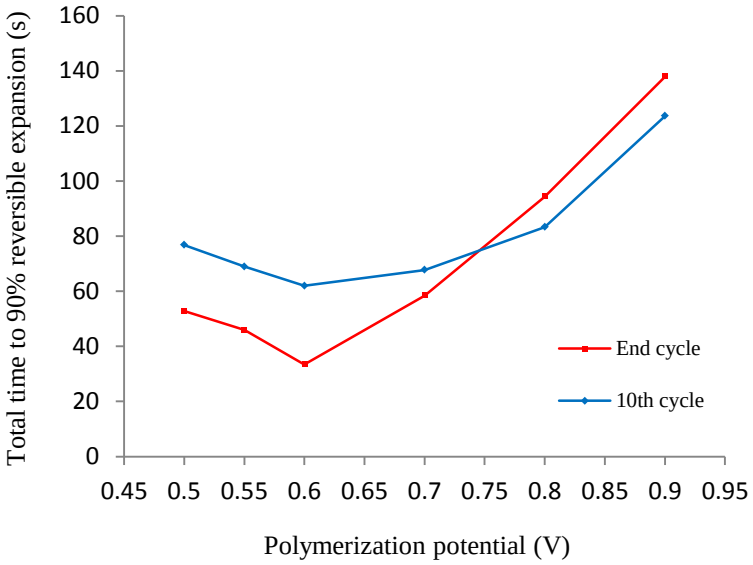

Fig 4.14 Overlay of the total times to 90% mean maximum reversible expansion for 10^{th} and end cycles.

In summary, the result of the actuation measurements have shown that the expansion (and strain) and speed depend upon the polymerization potential. It appears that there is a slight maximum (although not statistically sound since it is within the error bars) of the expansion around 0.55 V, after which both the reversible and irreversible expansion decrease between 0.55 V and 0.90 V. The reversible expansion decreases and the irreversible expansion increases on going from cycle 10 to the end cycle. The reversible expansion is less than irreversible expansion for most of the polymerization potential range investigated, except towards the higher potential end (0.80 – 0.90 V) where they have approximately the same magnitude. The speed at which the films actuate was found to be quicker during the reduction scan than the oxidation scan. In addition the speed of actuation increases on going from the cycle 10 to the end cycle over most of the polymerization potential range, except above approximately 0.75 V, were the cycle 10 is quicker than the end cycle. For the samples the maximum expansion corresponded to films polymerized at 0.55 V, whereas the maximum strain corresponded to films polymerized at 0.50 V. The fastest actuating films were formed at a polymerization potential of 0.60 V.

4.4.3 Nanoindentation

The variation in the physical properties of films prepared in the range 0.50 V to 0.90 V has been determined using nanoindentation. The physical properties monitored were the reduced Young's modulus of elasticity (Er), the micro-hardness (H) and creep, as these were considered likely to correlate with changes in the crosslinking.

On the recommendation of Prof Nicholls (Cranfield University, UK) the decision was made to undertake indentations over a range of depths (5 depths) in the form of a matrix (5 x 5) giving a data set of 125 measurements for each of the three replicate samples that were prepared at each polymerization potential. This is illustrated in figure 4.15 which uses just one replicate at each polymerization potential and shows the changes that occur in Er with both polymerization potential and depth.

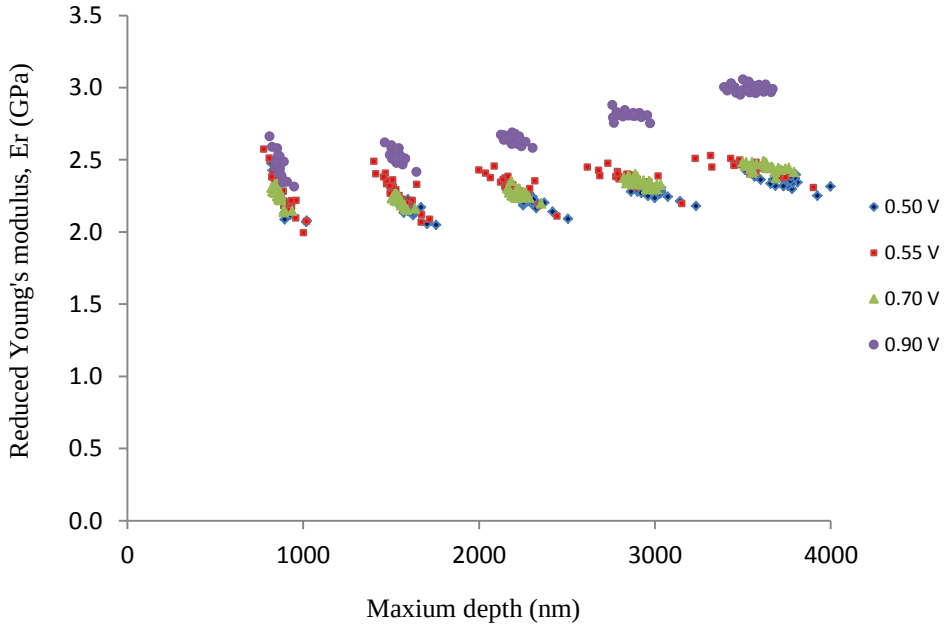

Fig 4.15 Er values recorded at five different depths for films polymerized at 0.50 V to 0.90 V. Note: Only values for one replicate at each polymerization potential are shown for clarity.

The changes observed in the mean values for the reduced Young's modulus of elasticity (Er) of the films with polymerization potential are shown in figures 4.16 (a) and (b). The first of these graphs displays the mean of all the indents for the three replicates samples at each polymerization potential The second of these graphs shows the mean of just the deepest indents (5^{th} indents).

Both graphs show that there is a general increase in Er between 0.50 V and 0.90 V, with there being a relatively large increase in Er of the films between 0.70 V to 0.90 V. In addition the mean values for both graphs provide evidence of a slight increase in the range 0.50 V to 0.55 V. Although the range of the error bars for these two adjacent

points overlap to an extent, the means are calculated from over 300 values for graph (a) and approximately 75 values for graph (b), and the change would therefore appear to be representative of the two adjacent sets (0.50 V and 0.55 V) of samples. No change in the mean Er in the range 0.55 V to 0.70 V was observed.

(a)

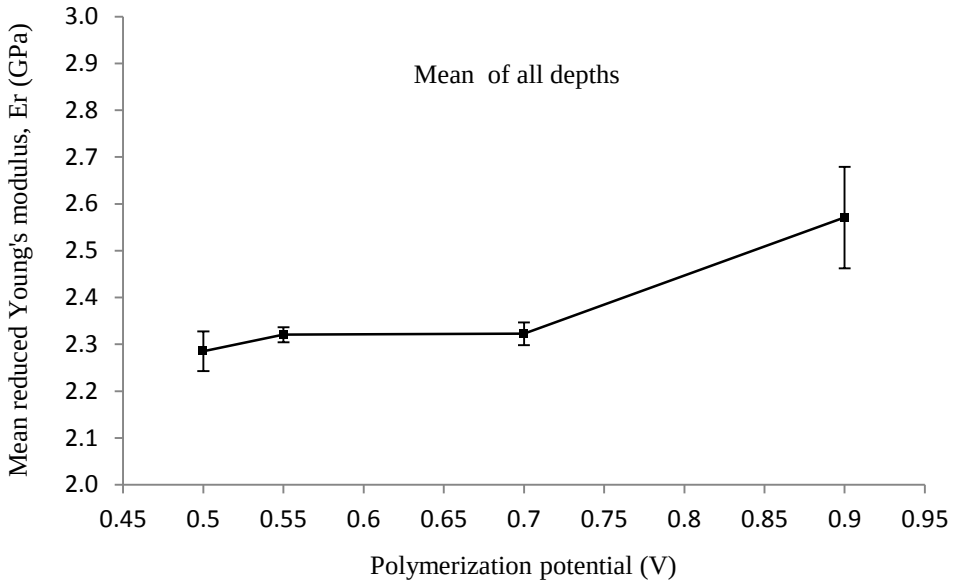

(b)

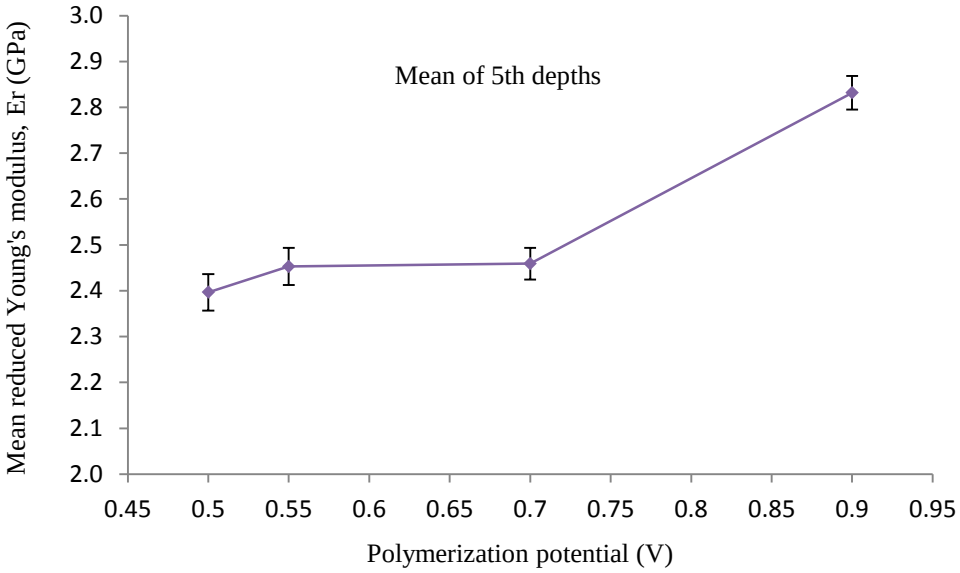

Fig 4.16 (a) Variation in the mean Er with polymerization potential - means calculated using the values at all depths (b) Variation in the mean Er with polymerization potential – means calculated using only values measured at the deepest (5^{th}) indent.

The mean Er values in figure 4.16 (a) are always less than the corresponding values displayed in figure 4.16 (b). This is also evident in figure 4.17, which displays the change in mean Er with depth at each polymerization potential. In all cases the Er values increase with depth from the second to the fifth indent. However, the mean Er of the first indent would appear to be higher than the second, with the exception of that at 0.90 V.

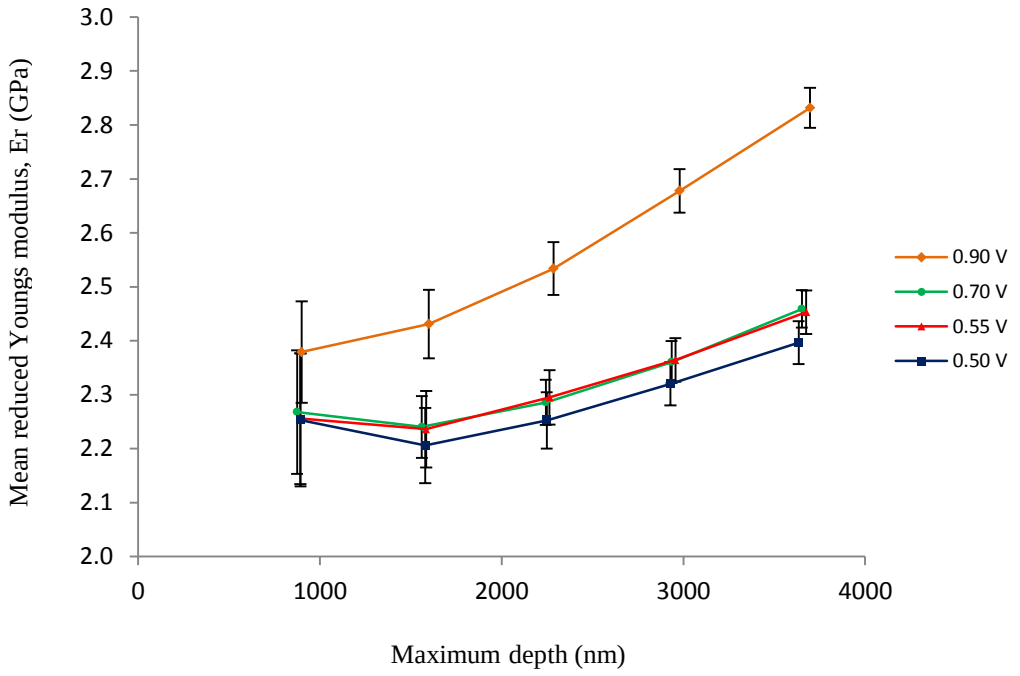

Fig 4.17 Variation in Er with depth for the four different polymerization potentials employed in the synthesis of the films. Error bars = 1 SD.

The micro-hardness data obtained for the films is shown in figure 4.18 for one replicate for clarity. The there is little difference discernible in the hardness values at the shallowest indent, but the difference between the indents on polymer films synthesized at different potentials becomes greater with indentation depth. By the deepest indent (5^{th}) there is a significant difference in the micro-hardness values for the films polymerization at different potentials.

The variation in the mean micro-hardness values with polymerization potential is shown in figure 4.19. The mean micro-hardness decreases on going from 0.50 V to 0.70 V and increases again from 0.70 V to 0.90 V. The minimum mean micro-hardness for our samples occurred at 0.70 V and was 0.083 GPa. The range of micro-hardness values for our samples was approximately 0.07 to 0.11 GPa.

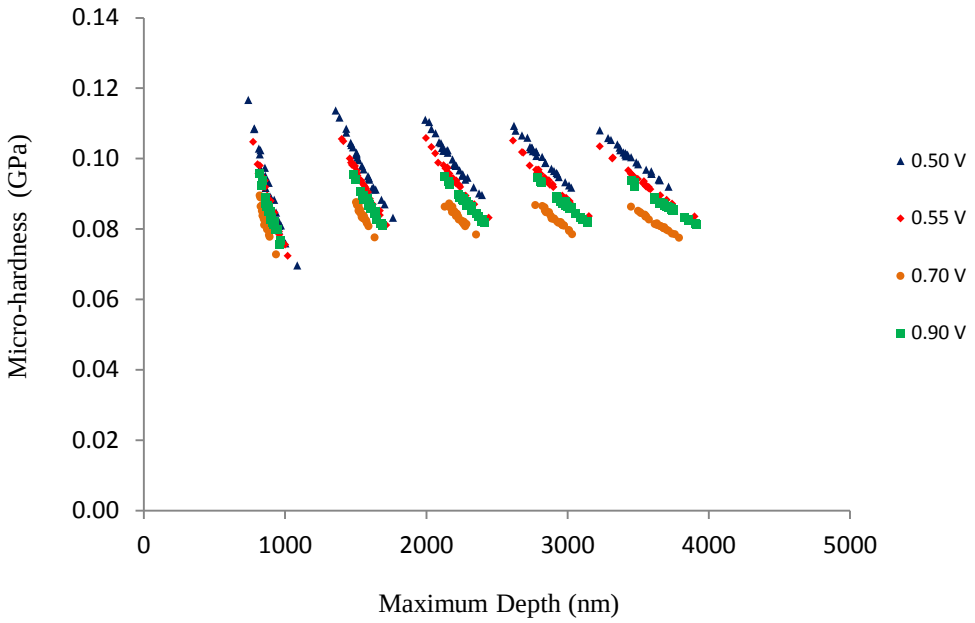

Fig 4.18 H values recorded at five different depths for films polymerized at 0.50 V to 0.90 V. Note: Only values for one replicate at each polymerization potential are shown for clarity.

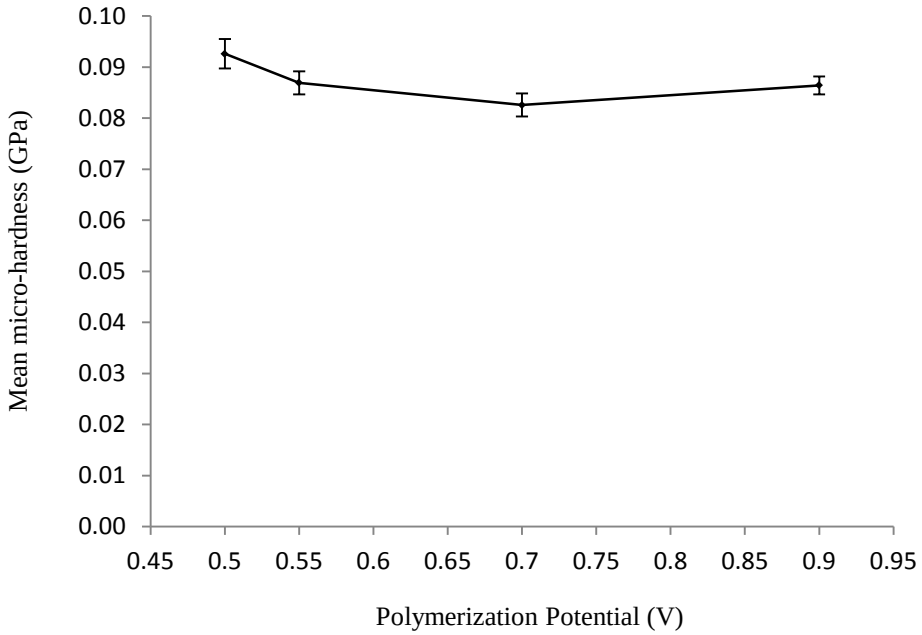

Fig 4.19 Variation in mean micro-hardness, H, with polymerization potential – means calculated using only the values recorded at the deepest (5^{th}) indent. Error bars = 1 SD.

Figure 4.20 reveals that although there is little variation in micro-hardness with depth there is a systematic trend in the profile of the mean micro-hardness values. The greatest difference in the mean micro-hardness values occurs between the first and second depth indent with a maximum occurring at either the second or third depth indent.

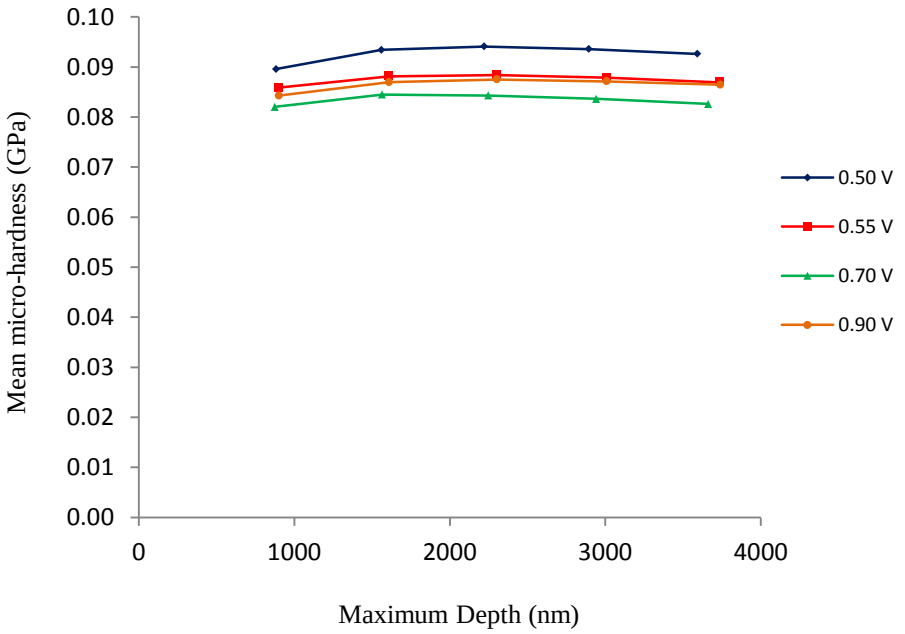

Fig 4.20 Variation in mean H values with depth and polymerization potential. Error bars are omitted to improve the clarity of the overlay.

Creep is the ability of a material to undergo plastic deformation under a sustained load. Large differences in the amount of creep could potentially be one explanation as to why there are large differences in the irreversible expansion of the films with polymerization potential. In addition, creep is a phenomenon that would be expected to correlate with crosslinking changes, decreasing with increasing crosslinking.

Creep testing was undertaken on the films, but not with the same number of measurements that were undertaken for the Er and H measurements. In fact each film had only five repeat measurement made.

Figure 4.21 shows that although the films underwent creep, there was little variation in amount of the creep observed with polymerization potential. The creep data for the films produced at different polymerized potentials gave similar mean values. The error bars (1 SD) for the means are very similar in size to the difference between the maximum and minimum mean values and a line drawn parallel to the horizontal axis could be drawn so as to pass through all the error bars associated with the data set.

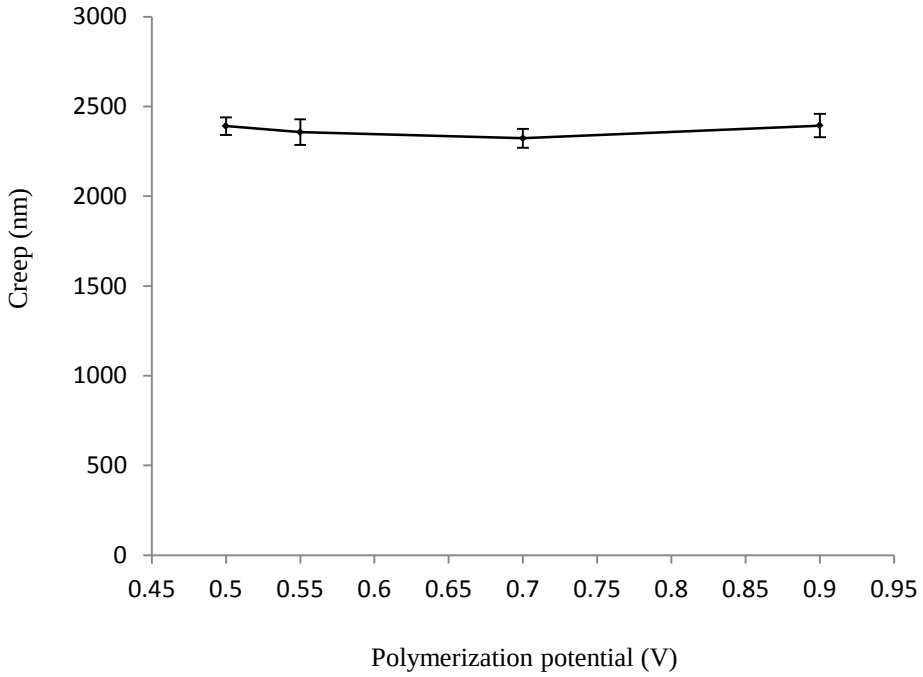

Fig 4.21 The mean creep determined for the films synthesized with polymerization potentials in the range 0.50 V to 0.90 V. Error bars = 1 SD.

An alternative way to measure a materials resistance to plastic deformation is the parameter of materials performance: H/E^2 (Fischer-Cripps, A., Nanoindentation, 3rd Ed, p94). The use of this parameter for the samples allows use of the much larger data set that has been gathered for Er and H to make an alternative assessment of the changes in the ability of our films to resist plastic deformation with polymerization potential.

Figure 4.22 shows the variation in H/E^2 with polymerization potential for the films. An increase in the materials ability of the films to resist plastic deformation with increasing polymerization potential is evident from the decrease in the ratio: H/E^2 with increasing polymerization potential. The greatest decrease in the H/E^2 occurs in the ranges 0.50 V to 0.55 V and 0.70 V to 0.90 V. There is therefore an increase in the ability of the films to resist plastic deformation with increasing polymerization potential, with the greatest increase being in the ranges 0.55 V to 0.70 V and 0.70 V to 0.90 V, which is consistent with the results found earlier for Er.

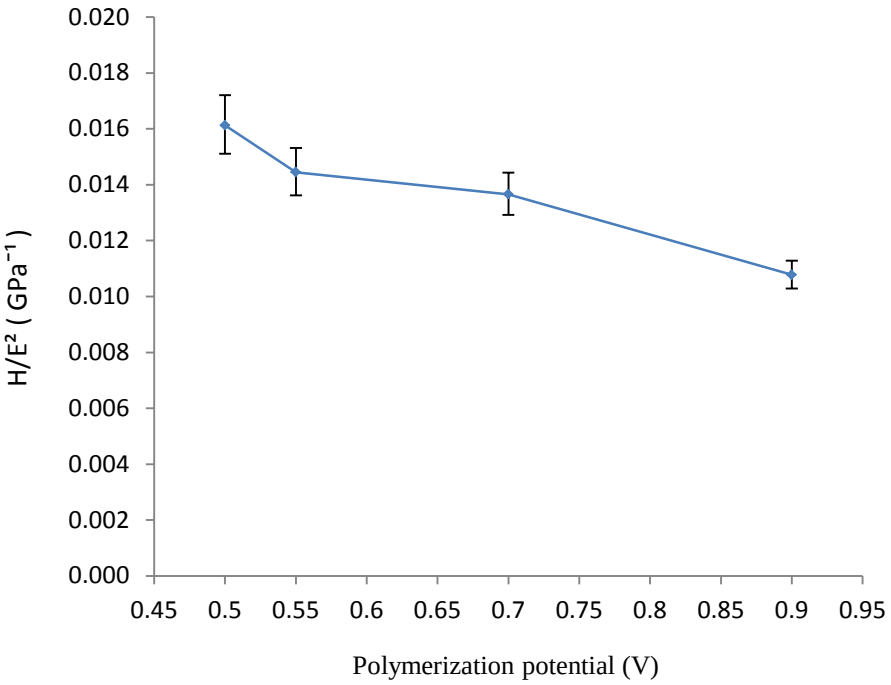

Fig 4.22 Variation in H/E^2 with polymerization potential. Note: (i) A decrease in H/E^2 indicates an increase in the films ability to resist plastic deformation. (ii) Error bars have been constructed so as to give the maximum possible variation from the mean using the error bars for H and Er, and are equivalent to 1 SD.

In summary, the nanoindentation measurements have shown that there is an increase in Er with increasing polymerization potential, particularly in the range 0.70 V to 0.90 V. It has also shown that the micro-hardness decreases from 0.50 V to 0.70 V, increasing again in the region 0.70 V to 0.90 V. Creep measurements made using a relatively small sample size showed that the films undergo creep, but that the variation between replicate measurements made at the same polymerization potential were comparable to the differences in the mean creep measured at different polymerization potentials. The use of the parameter of materials performance, H/E^2, calculated using a much larger data set, revealed that there is an increase in the ability of the films to resist plastic deformation with increasing polymerization potential. There would also appear to be an increase in Er with increasing depth for all the films investigated. However, an exception was seen on going from the first (shallowest) to the second indents, which tended to show a slight decrease in Er. In contrast, the micro-hardness was found to be essentially constant with indentation depth. However, once again there was consistently observed a difference between the first and second depth indent, which in this case showed a slight increase.

4.5 Discussion and conclusions

A primary aim of the research undertaken in this thesis, has been to investigate and understand the relationship between the structure of the polymer network and actuation of PPy(DBS) films. Investigating the impact of crosslinking and branching has been of particular interest.

Significant advancement in the understanding of the mechanism by which polypyrroles actuate has been gained in recent decades as discussed in the introduction to this thesis. In particular, it is now understood that the primary actuation mechanism is the insertion and de-insertion of ions and associated solvent. Efforts aimed at increasing the amount of ions that enter and leave the polymer during actuation are likely to lead to increased strains. However, it is important to recognize that the response that the polymer network makes when ions are inserted and de-inserted, will have a major influence on the strains that are achievable. Although the polymer films have a matrix consisting of polypyrrole chains, dopant molecules and solvent molecules, it is the polymer network that is generally viewed to be the polymer, and on which a major part of its physical and mechanical properties depend.

In general, branching precedes crosslinking and an increase in branching increases the opportunities for crosslinking. In a sense, branching is a natural predecessor of crosslinking and the two processes are intimately related. The ratio of branching to crosslinking will have an important impact on the physical and mechanical properties of the polymer and its microstructure.

The films show no signs of the presence of the functionalities that typically accompany overoxidation through the use of FTIR spectroscopy. The changes that occur within the polymer films cannot therefore be attributed to decomposition accompanying the use of increasing electrical potentials during synthesis.

The work presented in this section of the thesis, reveals that there is an increase in the stiffness of the polymer films (increased Er) and their ability to resist plastic deformation (decreasing E/H^2), with increasing polymerization potential. This is supportive of the view that the polymer films undergo increased crosslinking as the polymerization potential is increased. In addition it has shown that there is a decrease in the irreversible expansion with increasing polymerization potential in the range 0.55 V to 0.90 V. This is consistent with the major result that was obtained from the earlier work in section 3 of this thesis i.e. that an increase in crosslinking results in a decrease in the irreversible expansion of the polymer. Interestingly, the greatest decrease in the irreversible expansion that occurs above 0.55 V, occurs in the region 0.70 V to 0.80 V and corresponds with the increase in charge flow observed during polymerization in the same potential range (compare figures 4.6 and 4.9 (a)). It is therefore possible that this increase in charge corresponds to a surge in crosslinking in this potential range.

The research has also shown, however, that there is a relatively large decrease in the irreversible expansion of the films between 0.55 V to 0.90 V, with a possible peak in the region of 0.55 V. The apparent increase in the mean irreversible expansion observed on going from 0.50 V to 0.55 V, is contrary to the initial hypothesis that increasing polymerization potentials result in increased crosslinking. On this basis it would have been predicted that there would be an increase in the irreversible and reversible expansions on going from 0.55 V to 0.50 V, corresponding with decrease in crosslinking and not the opposite. This might be explained by modifying the initial hypothesis to include branching.

As stated previously, the decrease in the irreversible expansion on going from 0.55 V to 0.90 V was attributed to an increase in crosslinking, as evidenced by an increase in the stiffness of the films (increase in Er) and a decrease in the materials ability to undergo plastic deformation (decrease in E/H^2). However, it has also been pointed out that crosslinking is intimately related to branching. A branched structure, as it becomes more crosslinked will become less branched and visa versa. The ratio of branching to crosslinking will therefore be an important consideration for the polymers. The decrease in the irreversible expansion observed on going from 0.55 V to 0.90 V might be explained by the decrease in branching that accompanies the increase in crosslinking i.e. the ratio of branching to crosslinking decreases. It is likely that an increase in branching over crosslinking will produce a lower density polymer that is more open and porous. A more open and porous structure would allow more solvent to enter and swell the polymer and produce an irreversible expansion of the polymer. The increase in the reversible expansion on going from 0.55 V to 0.90 V would therefore be explained by an increase in branching that accompanies the decrease in crosslinking, leading to a less stiff, lower density polymer, capable of increased irreversible expansion through solvent swelling.

A polymerization potential of 0.50 V is very close to the polymerization potential of PPy(DBS), as indicated by the much slower polymerization times (see figure 4.2), and will likely contain longer length of un-branched (straight chain) polymer. This is a generally accepted idea within the field of conducting polymers i.e. that lower polymerization potentials (and temperatures), result in more ordered linear chains containing lower levels of "defects" (branches and crosslinks)[30,134].

Returning to the observation that there is an increase in both the irreversible and reversible expansion occurring on going from 0.50 V to 0.55 V, this now might be explained as being the result of increased levels of branching of the polymer at 0.55 V compared to the polymer at 0.50 V. There will no doubt be an increase in the levels of crosslinking on going from 0.50 V to 0.55 V, as evidenced by the increase in Er and decrease in E/H^2, but the increase in branching must be greater and have a greater impact on the physical and mechanical properties in the region of 0.55 V i.e. the ratio of branching : crosslinking is greater than, for example, that in the region 0.70 V to 0.90 V.

The lower levels of defects within the polymer synthesized at 0.50 V, means that there will be both more and longer linear chain sections. These linear chains will have a greater ability to pack more densely and undergo non-bonding interactions such pi-stacking[33]. Again, this is a generally accepted idea within the field of conducting polymers and is illustrated in figure 4.23. This increased packing density and ability of pi-stacking might explain why there was an increase in H observed on going from 0.70 V to 0.50 V accompanying a decrease in Er i.e. that H is more affected by the increase in the density and the decrease in branching on going from 0.55 V to 0.50 V, than the decrease in crosslinking. Similarly, the increase in H, observed on going from 0.70 V to 0.90 V, might be explained by the decrease in branching and an increase in crosslinking, resulting in a re-densification of the polymer relative to that at 0.70 V.

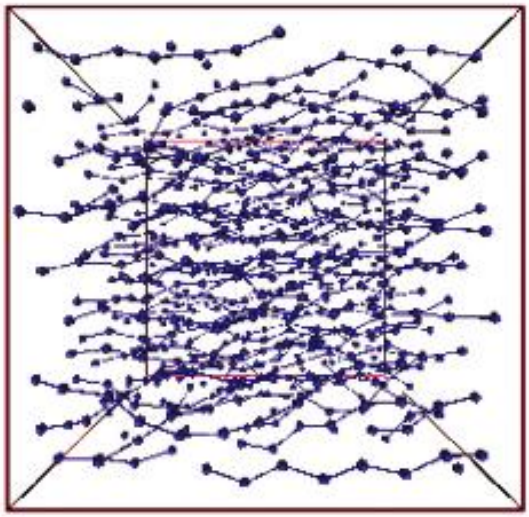

Fig 4.23 An increase in density of polypyrrole with increasing straight chain length has been demonstrated using a model developed by Y. Dai and E. Blaisten-Barojas[33]. This has been explained by the ability of straight chains to pack closely and to undergo increasing pi-stacking interactions with increasing chain lengths. A similar situation occurs in pherualites[91] and the lamella structure proposed for PPy(DBS)[37].

At this stage in the writing of this thesis, the samples have submitted, synthesized at different polymerization potentials, for skeletal density analysis by gas intrusion. Porosity measurements are also a possibility, using mercury intrusion, but it is likely that our sample size is insufficient for this technique. We hope to re-synthesize sufficient material to undertake this work (see the further work section later in this thesis).

Results suggesting a decrease in density of our films in the range 0.50 V to 0.55 V (see figure 4.24) have been obtained. This has come from measuring the nitrogen (N) signal from a fixed area of our polymer samples, using EDX spectroscopy. These measurements gather the N-signal over a fixed area and approximately similar depths, and therefore sample similar volumes of the polymer film. The N-signal from a fixed

volume will be proportional to the density of the polymer network, since the polymer network is the only part of the polymer matrix containing N-atoms, and the distribution of the N-atoms within the polymer network is regular (1 N-atom per pyrrole monomer unit). Figure 4.24 shows that there are changes occurring in the density of the films with polymerization potential and that the minimum density corresponds with the maximum irreversible and reversible expansion i.e. 0.55 V. More detailed EDX measurements are planned for the future.

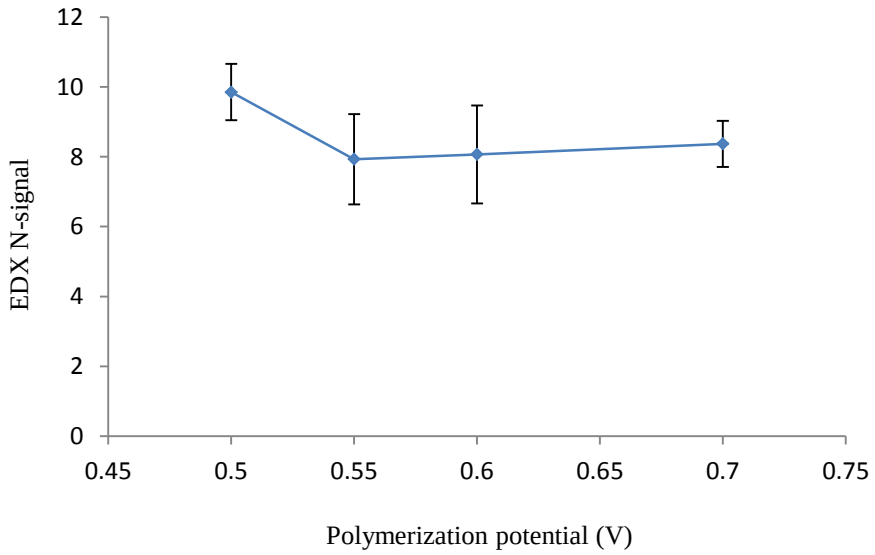

Fig 4.24 Variation in the density of N-atoms with polymerization potential within our films. Error bars = 1 SD.

Measurements of the charge flow that occurs during reduction and oxidation show that there is a decrease in the charge flow that occurs during both the oxidation and reduction scans with increasing polymerization potential. This is illustrated in figure 4.25 for both the 10^{th} cycle and end cycle during the oxidation phase. It is also interesting to note that the charge flow decrease on going from cycle 10 to the end cycle. A similar trend was observed in the reversible expansion (see fig 4.8).

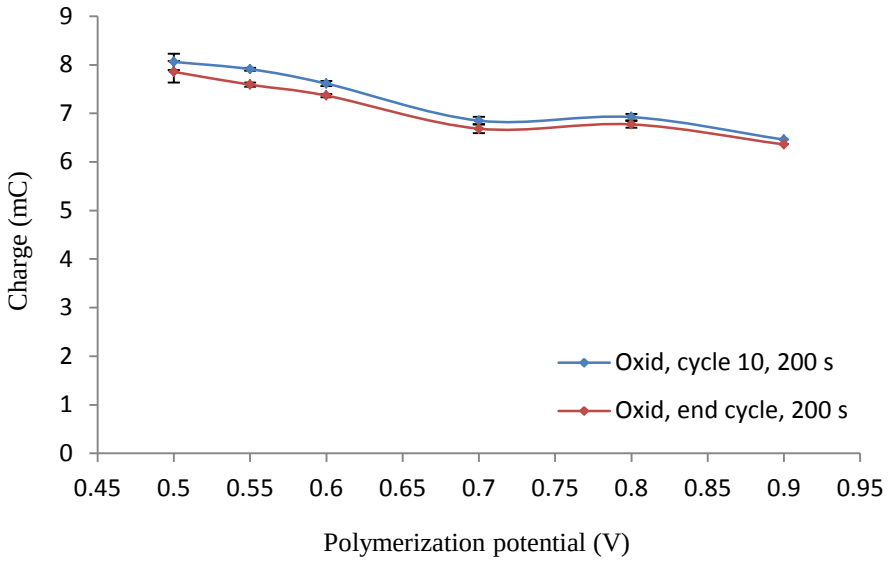

Fig 4.25 Variation in the amount of charge which flows during the oxidation phase with polymerization potential for our 5 μm films of PPy(DBS). Error bars = 1 SD.

This decrease would be something that would be expected to correspond with lower levels of charge carriers (polarons and bipolarons) within the films i.e. the density of charge carriers. The density of charge carriers associated with the polymer network will be related to both the density of the network and also the structure of the network i.e. the ratio of linear: branched: crosslinked sections present within the network. The decrease in the charge flow during oxidation and reduction is likely due to both the reduction in the density and the number of charge carriers which naturally occurs on going from a network containing long linear section with a greater ability to pack and form polarons and bipolarons to one containing more branched chains with a lower ability to pack closely alongside adjacent chains and which contains fewer polarons and bipolarons.

It has been that there is a decrease in both the reversible expansion and irreversible expansion on going from 0.55 V to 0.90 V. This decrease in the irreversible expansion is again consistent with there being an increase in crosslinking on going from 0.55 V to 0.90V. In addition, the decrease in the reversible expansion on going from 0.55 V to 0.90 V is consistent with the findings for the 3,4-DMPPy-co-PPy(DBS) series. The results presented in this section are consistent with the findings of the copolymer work and supportive of the initial hypothesis that decrease in crosslinking would lead to an increase in reversible expansion, due to greater freedom of movement of the polymer chains. The results presented in this section are therefore consistent with this hypothesis.

It is therefore likely that the decrease in reversible expansion, observed with the copolymers of section three, with increasing blocking (substitution) of the beta positions in the pyrrole ring system, is the result of electronic and steric effects caused by the

presence of the blocking (methyl) group. The presence of beta-substituents is known to increase the torsional angle along the polypyrrole chain and make it more difficult for adjacent pyrrole units to take up a coplanar arrangement. This has been shown to be the case for 3, 4-dimethylpolypyrrole homopolymer[24]. The ability to take up a coplanar arrangement is necessary in order for polarons and bipolarons to form. Hence beta substituents likely decrease the numbers of polarons and bipolarons and reduce both the conductivity and electroactivity (reversible expansion) of the polymer. However, this steric effect is likely off-set by the reduction in the amount of cross-linking that that accompanies increased beta-substitution, as crosslinking might also restrict the movement of polymer chains in the region of the crosslinking and lower the chains ability to take up a coplanar conformation and form polarons and bipolarons. The inductive (+M) effect of the methyl substituents in the pyrrole ring are also more capable of delocalizing charge within a polaron compared to a hydrogen substituent and might therefore lower the numbers of counter ions needed for charge compensation. Increased doping levels have been reported for 3,4-difluoropolypyrrole[129]. Here the fluorine substituents have a very strong electron withdrawing effect (-M effect) and this will decrease the charge density within the pyrrole rings of the polymer network and could potentially promote the oxidation of the pyrrole ring system and hence increase the ease with which polarons might be formed. Both an increase in the numbers of polarons and bipolarons and also a general increase in the polarity of pyrrole ring system, would explain why increased levels of counter ions have been observed in this polymer.

An increase in the stiffness of the material (Er) with indentation depth was observed. This suggests a change in structure over the depth range tested. This is in agreement with reports that the structure of PPy(DBS) changes after the first 60 mC/cm^2, or approximately 0.33 μm is deposited[130]. It has been observed that thin films used in microactuators that have delaminated from the gold backing, bend upon electrochemical cycling, which would not occur if the films were homogeneous. The side originally facing the gold electrode was on the exterior of the curve, showing that it underwent less contraction or is denser, de facto forming a bilayer configuration[51].

It has also been observed that the first (shallowest) indent had a higher Er that the second indent, resulting in a slight decrease in Er on going from the first to the second indent. This behaviour has also been observed during the nanoindentation of other polymer films[131].

It is now appropriate to explain the changes that occur with polymerization potential using a model that is in keeping with our findings and the general ideas prevailing within the field of conducting polymers. Our model is shown in figure 4.26 (a) along with a summary (b) of the supportive evidence.

(a)

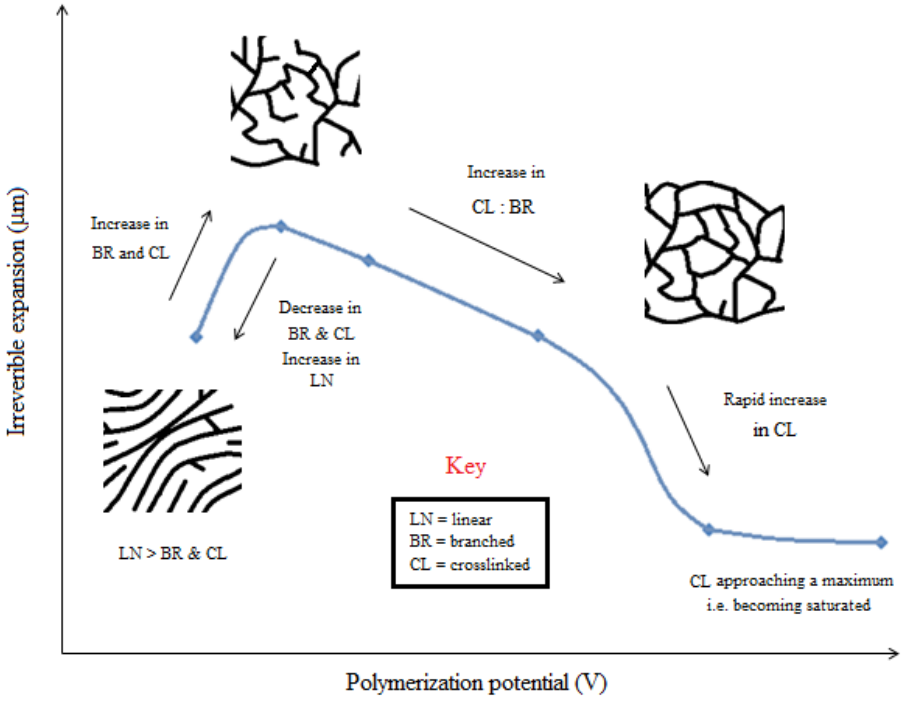

(b)

0.50 V	0.55 V- 0.70 V	0.90 V
High irreversible expansion	Max irreversible expansion	Min irreversible expansion
High reversible expansion	Max reversible expansion	Min reversible expansion
Intermediate time to 90% expansion	Min time to 90% expansion	Max time to 90% expansion
Min Er	0.50 V < Er < 0.90 V	Max Er
Max Er/H^2	0.50 V > Er/H^2 > 0.90 V	Min Er/H^2
Max H	Min H	
Max density	Min density	

Fig 4.26 (a) A model explaining the changes that occur in the irreversible expansion with polymerization potential. **(b)** Evidence in support of our model.

5. The use of elemental analysis for the quantitative determination of the levels of crosslinking in polypyrrole.

5.1 Introduction

The quantitative determination of the different types of atoms present in a sample can be undertaken using combustion analysis or optical emission spectroscopy. Elemental analysis is typically used to determine the purity of a compound but it can also be used to help in the determination of structure i.e. once the number of moles of each element is known an empirical formula of the original material can be calculated.

The global polymerization reaction for the electropolymerization of polypyrrole indicates that there will be a decrease in the total hydrogen content on going from the starting material (pyrrole monomer) to the final product (polymer). Whereas, both the number of nitrogen and carbon atoms remain constant. The moles of nitrogen or carbon present within the polypyrrole network can therefore be used to determine the number of monomer units present within the network. The ratio of N:H will decrease during polymerization from a value of 1:5 in the pyrrole monomer. Similarly, there will also be a decrease in the C:H ratio of the polymer from a value of 4:5 in the pyrrole monomer. However, the use of the H:C ratio will be more likely to be prone to interference from sources of carbon not originating from the polymer network e.g. organic contaminants or dopant anions such as DBS^-.

A pertinent question to now ask is: can the N:H ratio of polypyrrole be used to reveal anything usefully about the polymer network structure? Specifically, can it be used to reveal information about the extent of crosslinking? An answer to this question is not immediately obvious given the huge number of ways in which a polymer network, containing several million monomer units, can combine.

These questions have to our knowledge, not been addressed within the literature on polypyrrole, despite a extensive search. The author of this thesis has thought hard about these questions and it has taken considerable time to arrive at possible answers. This has been due to the difficulty in visualizing the effect of changes in the connectivity of the pyrrole monomer units on the overall network structure. In this context, the expression that one “cannot see the wood for the trees” is highly appropriate.

Given the relevance of such questions to the subject of this thesis, the author would like to discuss and propose answers to these questions, which will might allow the levels of crosslinking of the polymer network to be determined using elemental analysis.

5.2 The change in total hydrogen content with crosslinking

The number of hydrogen atoms present within a linear polypyrrole chain is given by the relation: H = 3(n) +2 (equation 1), where n represents the number of monomer unit. Since the number of monomer units is also equal to the number of nitrogen atoms present in the polymer, this relation can also be expressed as 3(N) +2, where N represents the number of nitrogen atoms. The validity of this relation is illustrated in figure 5.1 where it has been used to determine the N:H ratios for a linear chain containing six pyrrole units.

Structure	N:H
(a) 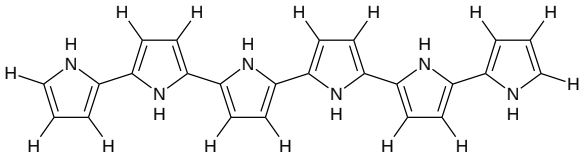	Linear: 6: 3(6) + 2 = 6: 20 = 3:10 = 1: 3 $^{1}/_{3}$
(b) 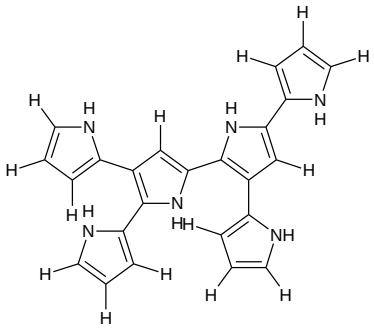	Branched: = 6: 20 = 3:10 = 1: 3 $^{1}/_{3}$

Fig 5.1 The N:H ratio for (a) linear and (b) a branched oligomers containing six pyrrole monomer units (sexipyrrole).

Consider figure 5.2 as a further illustration of the applicability of the relation 3N + 2 to branched structures. The structure displayed in figure 5.2 is a single, purely branched chain containing 41 monomer units. The number of H-atoms in the polymer network is

125, which can be seen by carefully counting the number of H-atoms within the network. Applying the formula: H = 3N +2 to this structure gives H = 3(41) + 2 = 125.

Figures 5.1 and 5.2 show that the relation: 3N + 2, applies to both linear and branched structures.

At first this might appear surprising, but similar situations occur within organic chemistry such as the homologous series of alkanes which share the same empirical formula: C_nH_{2n} +2, whether linear or branched.

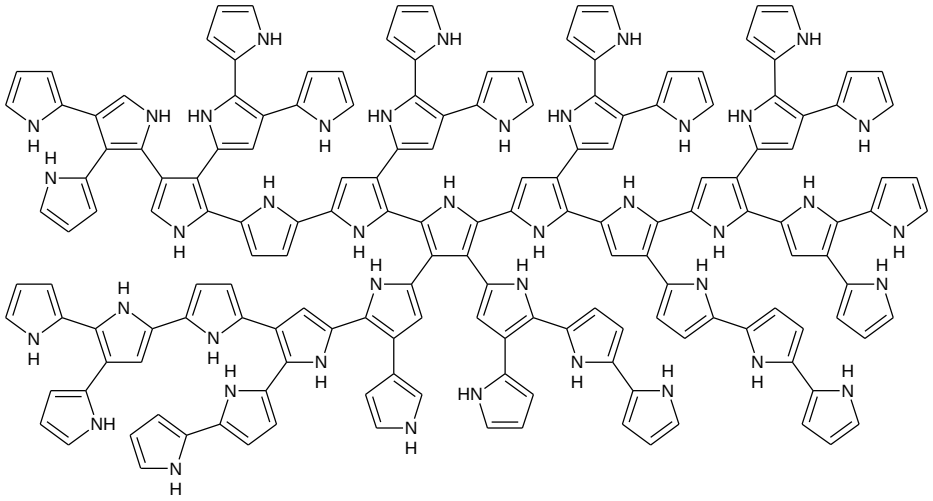

Fig 5.2 A highly branched non-crosslinked PPy structure.

Whenever a pyrrole monomer unit is coupled in three positions, leading to a branch, it "looses an extra hydrogen atom" at the ring. However, the branch that is formed goes on to form a chain ending in an additional "end group" which is coupled in just one position. Therefore, there is no net loss in the number of hydrogen atoms and both linear and branched structures containing the same number of pyrrole units (structural isomers) have the same N:H ratio. On this basis the N:H ratio cannot be used to distinguish between these structural isomers. However, if a method for determining the number of end groups could be developed, then a distinction could be made, since each branch produces one end group. End group analysis is a technique that can be performed on other types of polymer.

Differences in the N:H ratio between structures containing different numbers of monomer units will occur however. This difference is most pronounced during the early stages in the growth of the polymer chain. For example the N:H ratio, on going from monomer to dimer, will change from 1:5 to 1:4. On going from the trimer to the dimer the ratio will change to 1: 3 $^{2}/_{3}$. As the chain grows the ratio quickly converges to a

limiting value of 1:3. This can be seen from the expression: 3(N) +2 where as N → ∞, 3(N) +2 → 3(N). This is illustrated by the graph of 3(N) +2 vs N shown in figure 5.3. Therefore, the N:H ratio for totally linear chains, branched chains or any mixture of the two, cannot take a value of less than 1:3 (using allowable valences and bond angles for the atoms involved).

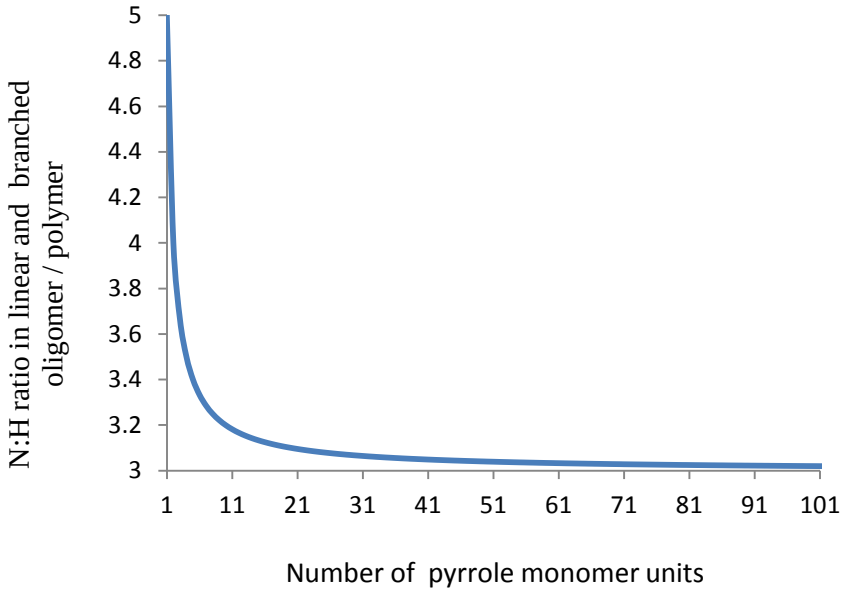

Fig 5.3 The variation in the ratio of the number of nitrogen to hydrogen atoms, N:H, with the number of pyrrole monomer units for linear and branched oligomers/polymer chains.

Considering next: crosslinked structures, we need to first recognize that a structure like that shown in figure 5.4(a), which might appear to contain a crosslink, is in fact branched. This can be seen by redrawing the structure as illustrated in figure 5.4(b).

Only when a "second connection" is made to form a "loop" structure can a crosslink be considered to be formed as shown in figure 5.5. Cutting one just one C-C bond between coupled monomer units within this "loop" structure would result in a single purely branched chain. This structure therefore contains a one crosslink.

Structure	N: H
(a) 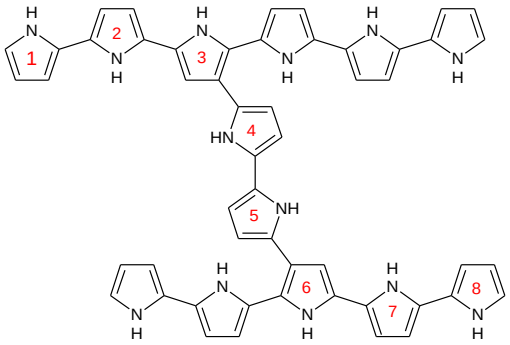	Single Crosslink? 13: 41 = 1: 3.154
(b) 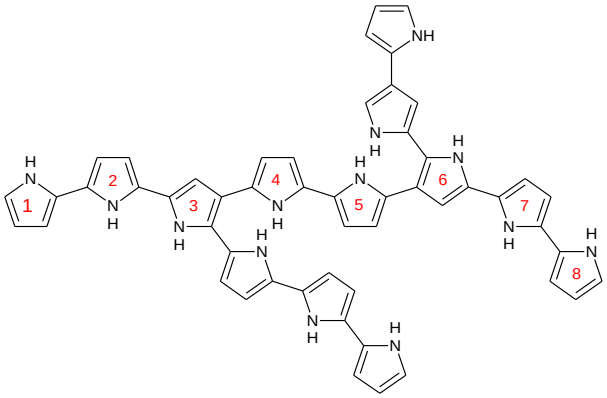	Branched (same structure): 13: 41 = 1: 3.154 Linear equivalent: 13: 3(13) + 2 = 13:41 = 1: 3.154

Fig 5.4 Structure (a) is actually branched and identical to structure (b).

Structure	N: H
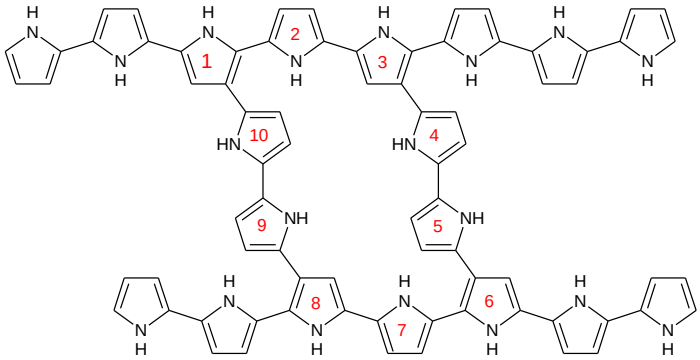	Single crosslink: = 19: 57 = 1: 3 Linear equivalent: 19: 3(19) + 2 = 19:59 = 1: 3.105

Fig 5.5 The presence of "loop" structure is indicative of a crosslink.

The presence of crosslinking can therefore be tracked by the number of loops present within the structure. Confusion can occur when considering the number of crosslinks in a drawn structure by counting the number of linkers and not the number of loops. The number of crosslinks is equal to the number of loops that would need to be "cut" in order to reduce the original structure to a single purely branched/linear chain. This is illustrated in figure 5.6 which contains six loops and therefore six crosslinks. Cutting just six C-C coupling bonds (one in each loop) leads to a single purely branched chain. The number of loops can therefore be seen to be equivalent to the number of crosslinks.

Consider next the N:H ratio for the crosslinked structure shown in figure 5.6 (a). This structure contains six crosslinks (loops) and 38 pyrrole units. The number of hydrogen atoms in this structure is 104, giving a N:H ratio of 38:104 = 1:2.7368 (to 4 d.p.). Crosslinking can therefore lead to N:H values below 1:3.

The N:H ratio therefore serves as a means of distinguishing between crosslinked and linear/branched structures, with N:H values less than 1:3 being evidence of crosslinking. The lower the N:H the higher the degree of crosslinking will be.

For all the structures that are drawn, the number of crosslinks (CL) can be calculated from the difference in the number of hydrogen atoms present within the polymer network (H_{obs}) and the number of hydrogen atoms that would be present in a totally

linear/branched network containing the same number of monomer units ($H_{Lin/Br}$) using the simple equation (2):

$$CL = \frac{1}{2}(H_{Lin/Br} - H_{obs})$$

$$\therefore \quad CL = \frac{1}{2}[(3N + 2) - H] \quad \text{..... (equation 2)}$$

Where: N = number of nitrogen atoms and H = number of hydrogen atoms.

Applying this equation to the structure shown in figure 5.7, which contains both linear, branched and crosslinked sections leads to the correct calculation of the number of crosslinks, as show below:

$$\text{For } H = 104 \text{ and } N = 38, \; CL = \frac{1}{2}((3(38) + 2) - 104) = 6$$

This can again be seen to be the case by cutting bonds between monomers in the structure shown in figure 5.7 (a) until it is reduced to a single purely branched chain as shown in figure 5.7 (b).

The reader is invited to draw more structures, using the rules of valences and allowable bond angles, and apply equation (2) to calculate the number of crosslinks. Comparing the value obtained using equation (2) with the number of C-C coupling bonds that would be required to be cut to reduce the network to a purely branched/linear structure, gives the same values.

Although the representations that have been show so far have been planar, it is still possible to appreciate that the structure of the polymer network will impact upon the density and porosity of the polymer. Figure 5.8 (a) shows a close packed network with just two crosslinks. The close packing and relatively long linear chain segments would be more likely to be subject to non-bonding interactions such as pi stacking. The close packing and possibility of pi stacking would be expected to result in both a denser and harder material than the highly branched structures figure 5.8(b). This structure contains the same number of monomer units, five crosslinks and occupies a greater “space” (more “spread out”). This would be expected to be less dense, more porous structure with lower hardness (based on density). However, due to the increased levels of crosslinking, it would be expected to have a greater rigidity and hence Young’s modulus of elasticity.

(a)

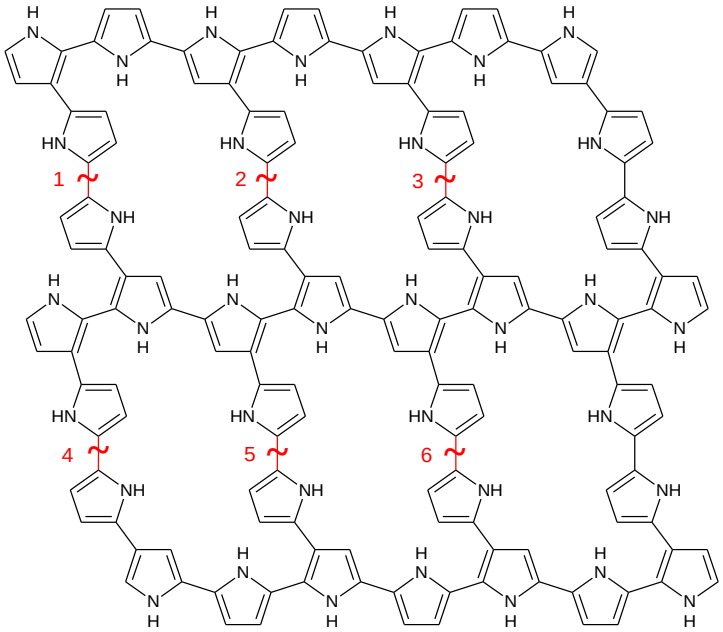

(b)

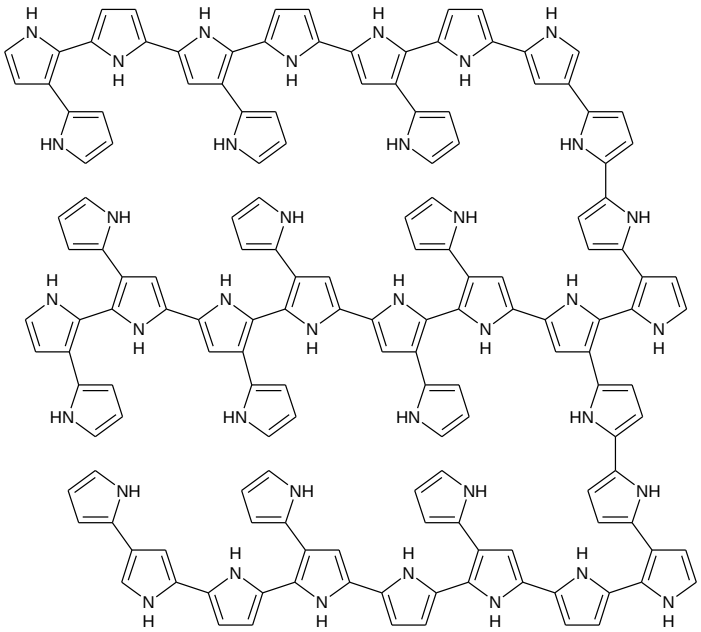

Fig 5.6 (a) A highly crosslinked structure and (b) the single purely branched chain obtained from structure (a) by "cutting" the six bonds shown in red.

(a)

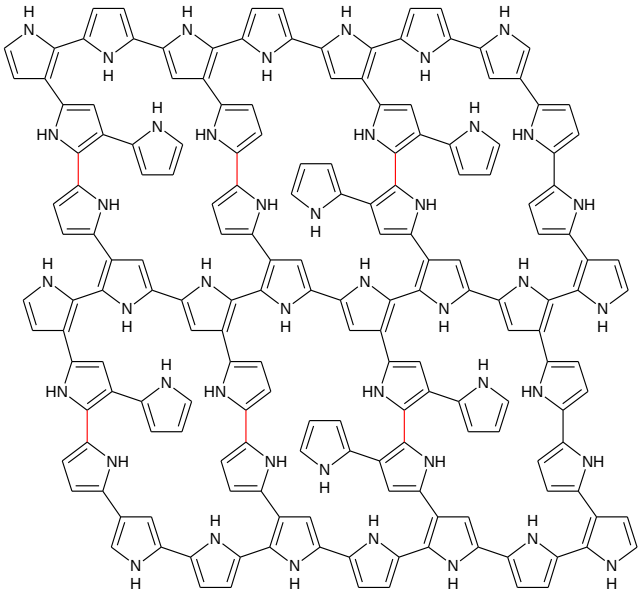

(b)

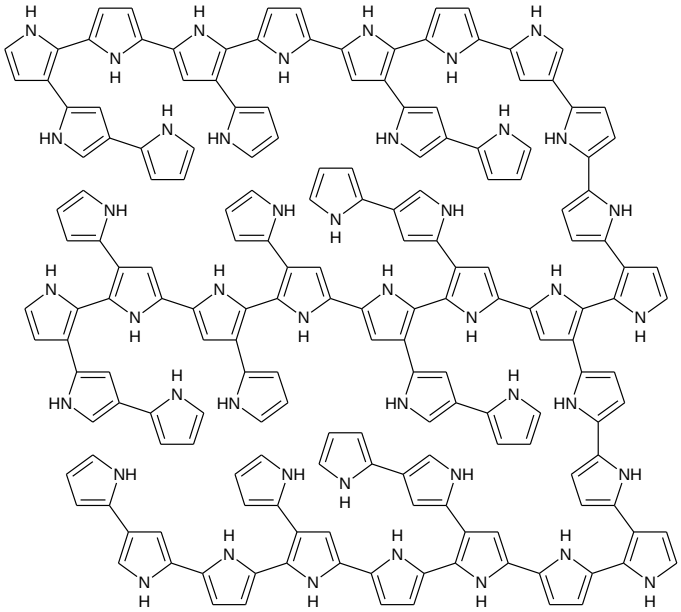

Fig 5.7 (a) A highly crosslinked and branched structure and (b) the single, purely branched chain obtained from structure (a) by "cutting" the six bonds shown in red.

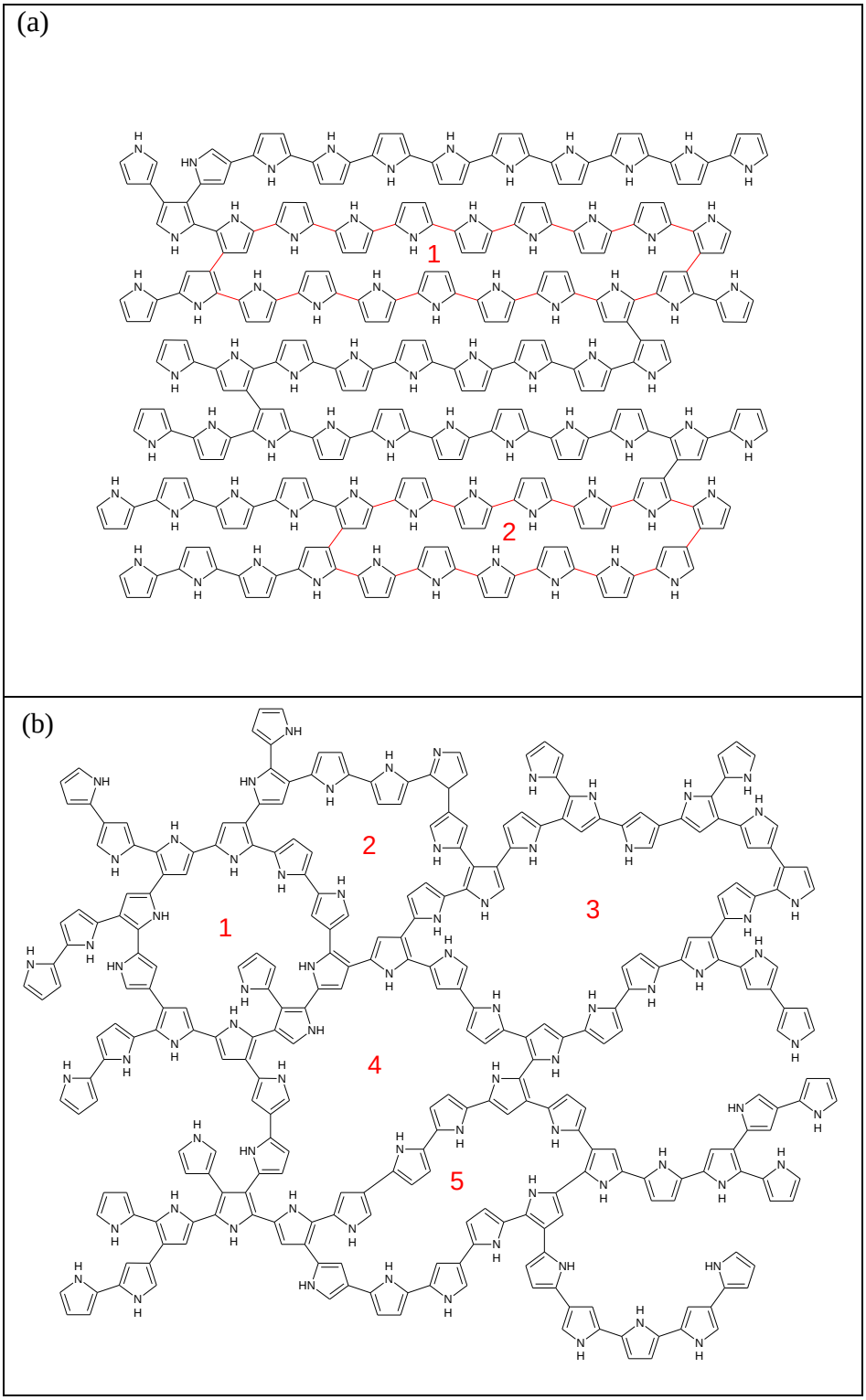

Fig 5.8 Two PPy structures containing the same number of monomer units. Structure (a) contains highly "linear", densely packed chains with just two crosslinks (loops). Structure (b) is a highly branched, less densely packed structure with five crosslinks (loops).

Using the structure in figure 5.7 to illustrate this approach:

$$CL = [(3N + 2) - H)/N] \times 100\ \%$$

$$= [(3(38) + 2 - 104)/ 38] \times 100\ \%$$

$$= (12/38) \times 100\% = 31.58\ \%$$

So, 12 monomer units out of 38 in the structure are involved in crosslinking, which represents 31.58 % of the monomer units in the network (**Note:** the expression 3N+2 was not approximated here to 3N as the structure is not very large).

5.3 Practical difficulties

A number of practical difficulties will need to be overcome if the number of hydrogen atoms within the polymer network is to be determined accurately. These difficulties will be due to the presence of hydrogen within the polymer matrix from sources other than from the polymer network, such as the dopant, water or organic contaminants.

The presence of hydrogen that originates from the dopant could be overcome either by using a non-hydrogen containing dopant or by making corrections to account for this. DBS could be used given that it its elemental composition will remain constant during polymerization and incorporation into the growing polymer matrix, and by the fact that it contains a sulphur to hydrogen ratio of 1:29. If the moles of sulphur (S) atoms present within the polymer is known, the moles of hydrogen (H) atoms from this source can be accounted for i.e. moles of H atoms from dopant = 29 x moles of S atoms present. This would be possible as elemental determination via combustion analysis is commonly used to determine S atoms as well as CHN atoms.

The presence of H atoms which originate from water is perhaps a more difficult issue to overcome as even if an organic electrolyte were to be used during polymerization, as opposed to an aqueous electrolyte, polypyrrole films can absorb water from the atmosphere. The obvious solution to this would be to remove the water by placing the polypyrrole sample in a vacuum oven at a suitable temperature (so as not to decompose the polymer) and for sufficient time to remove all traces of water. The sample would then need to be stored in a dry inert atmosphere such as argon prior to analysis. Another possibility might be to use a deuterated solvent, but it would be necessary to ensure that the technique used to determine the elemental composition of the sample, could distinguish between deuterium and hydrogen atoms.

Sources of H atoms that originate from organic contaminants could be eliminated through using pure reagents (pyrrole, dopant and solvent) and clean equipment used in the preparation of the polymer and careful handling.

5.4 Conclusion

Recognition that elemental composition could potentially reveal crosslinking levels in polypyrroles is through the work completed here. This has taken time and we are unable to practically check the validity of the approach outlined above at the time of writing this thesis.

However, the theoretical basis by which it should be possible to make direct and quantitative determination of crosslinking levels in polypyrrole has been outlined. In addition it has been possible to discuss how structural changes to the polypyrrole network would likely lead to changes in density, porosity and strength. This discussion gives further support to the experimental observations presented in other sections of this thesis.

If a method were to become available for determining the number of end groups within the polymer, it would allow the determination of the levels of branching within the polymer, since one branch produces one end group. If both the levels of crosslinking and branching could be quantified this would allow full characterization of the polypyrrole network.

Section D: Overview

1.1 Overall discussion

Throughout this thesis the impact that changes in the polymer network of PPy(DBS) have on its actuation performance has been investigated. In particular the focus has been on the impact of crosslinking.

In order to characterize the actuation performance of polypyrrole films a new technique has been developed which makes use of a laser scanning micrometer to make non-contact measurements of the actuating films. The technique is relatively simple to perform and can be used to study the long term stability and operational failure of the films, the effects of synthesis conditions and to optimize of actuator performance.

This new technique clearly shows that there are two components to the overall expansion: a reversible and an irreversible component, which operate over different time scales. The reversible component increases with cycle number quickly reaching a maximum stable value after 5-10 cycles. However, the irreversible component takes longer to reach a maximum stable value. Typically this can be between 20-100 cycles. For all actuation sequences the first cycle shows the greatest increase in irreversible expansion, after which there is a smaller more gradual increase until it reaches a maximum value ("stable state"). The first few cycles have a greater tendency to display unstable behaviour but in general the stability of the actuation profiles increase with cycle number.

By investigating the actuation of films of different thickness (1, 5 and 10 μm), it has been shown that although there is an increase in both the reversible and irreversible expansion on going from thinner to thicker films, there is a decrease in the reversible strain with increasing film thickness (Fig. 1.26 (b)). Thinner films therefore produce more efficient actuators compared to thicker films. In addition the research has shown that thinner films actuate more quickly than thicker films once they have reached their stable state (Fig. 1.28 and 1.29).

A possible delay in the onset of expansion has been observed on switching the potential. This might not be a true delay, but the result of a slow sampling rate. However, it could represent a real delay due to the time it takes for the Na^+ ions to enter the polymer film during the reduction scan to compensate the immobile DBS^- ions[116]. This merits further investigation using a higher sampling rate.

A "spike" has been observed in the measured expansion associated with switching the potential. This has been attributed to ions entering and leaving the polymer film causing the refractive index to change rapidly close to the surface of the polymer film, bending the LSM laser to produce a virtual movement. This behaviour has been observed elsewhere in the literature and is referred to as the "Mirage Effect". The spike observed

on switching from -1 V to 0 V (reduced to oxidized state) is an “upward spike” whereas the spike observed on switching from 0 V to – 1 V (oxidized state to reduced state) is a smaller “downward spike”. For the thin PPy(DBS) films e.g. 1 μm these spikes are not observed, whereas they are for 5 and 10 μm PPy(DBS) films. This suggests that the increase in concentration of the ions at the polymer surface on switching has to be greater than a threshold value to be observed (see Fig. 1.24). The films act as an “ion reservoir” with the thicker films being capable of storing more ions than the thinner films. A better understanding of the physics of this effect could allow it to be used in the study of ion movements during actuation and potentially allow the study of PPy films for use in applications such as the controlled release of chemicals/drugs.

The cycling condition employed, have been shown to result in different reversible and irreversible expansions. Shorter cycle times result not only in lower reversible expansion but also larger irreversible expansions (Fig. 1.34). The observations suggest that larger reversible expansion and lower irreversible expansion can be restored by increasing the cycle time. This merits future investigation.

A logical synthetic strategy capable of altering the levels of crosslinking within polypyrroles has been developed. By altering the levels of crosslinking within PPy(DBS) we have been able to see how this effects the actuation performance. In order to successfully implement our synthetic strategy (blocking approach) significant preliminary work had to be undertaken.

It was observed that the actuation of the homopolymers 3,4-DMPPy(DBS) and 3MPPy(DBS) in all cases resulted in failure of the films. In the case of 3,4-DMPPy(DBS) failure was almost immediate occurring in the first few cycles and more typically in the first cycle, via brittle fracture. For 3MPPy(DBS) failure also typically occurred after a small number of cycles, but there was a tendency for these films to actuate for more cycles prior to failure compared to 3,4-DMPPy(DBS). Experimentation with different polymerization potentials and use of porous gold electrodes did not succeed in producing films of these homopolymers that could be successfully actuated for more than a small number of cycles without failure.

Copolymerization of Py with 3MPy and 3,4DMPy to form 3MPPy-co-PPy(DBS) and 3,4-DMPPy-co-PPy(DBS) films proved more successful. Control over copolymer ratios was achieved by employing different volume ratios of each monomer in the polymerization electrolyte. It was found that actuation of copolymer films could be undertaken in the long term without failure provided the volume of 0.1 M blocked monomer used to prepare the polymerization solutions was below a critical level. For 3MPy and 3,4DMPy this was 1 ml and 0.7 ml respectively. The actuation of copolymers prepared with volumes greater than these levels, underwent actuations for tens of cycles, but during this time they were subject to deformation and ultimately failed via fracture and delamination. In addition, it was necessary to use a porous gold working electrode

to prevent delamination of copolymer films. Copolymers actuated on normal (non-porous) gold working electrodes, even when prepared using volumes of blocked-monomer below the aforementioned critical levels, tended to delaminate prior to reaching a stable state.

Using this blocking strategy, it has been shown that increasing the levels of blocked monomer within the copolymer films for both 3,4-DMPPy-co-PPy(DBS) and 3MPPy-co-PPy(DBS) series, results in an increase in irreversible expansion compared to PPy(DBS) (see Fig 3.11). For all copolymer films the amount of irreversible expansion was higher than for PPy(DBS). It was interesting to note that some of the 3MPy-co-PPy copolymers, which contain blocking groups in just one of the beta-positions of the pyrrole ring, display a higher irreversible expansion than some of the 3,4-DMPPy-co-PPy(DBS) copolymers, which contain monomer having both beta-positions blocked. A possible explanation for this is that 3,4-DMPy would be expected to block both crosslinking and branching equally, whereas this is not necessarily the case for 3MPy which still has one beta-position available for substitution. It is therefore possible that a low level of crosslinking in combination with relatively high levels of branching can result in a greater increase in irreversible expansion than an equal decrease in both crosslinking and branching i.e. low levels of crosslinking combined with relatively high levels of branching might produce some of the greatest increase in irreversible expansion. It would appear that the ratio of crosslinking to branching is important here.

It has also been shown that there is an increase in the reversible expansion with increased levels of blocked monomer within the 3,4-DMPPy-co-PPy(DBS) series of copolymers. This is in keeping with the initial hypothesis that a decrease in crosslinking would result in an increase in reversible expansion due to the ability of the polymer chains to move more freely. However, for the 3MPPy-co-PPy series an increase in reversible expansion was not observed. In fact there appeared to be a slight decrease across the series with increased blocking on a single beta position. It might be that in the range investigated for this copolymer series the expected increase in reversible expansion accompanying the decrease in crosslinking is off-set by other factors such as the level of branching or the levels of polarons/bipolarons present in the network. For example, a branched polymer network containing low levels of crosslinking might be expected to undergo relatively large irreversible expansion, but its network would not be expected to be as capable of being “re-packed” as densely on oxidation, as a network with the same levels of crosslinking but lower levels of branching. A network containing both low levels of crosslinking and branching could fold and align its chains so as to be packed more densely in a way that a branched network could not, producing larger reversible expansions.

The maximum actuation rate was shown to increase and the time to 80 % maximum expansion decrease with increasing blocked monomer content for the 3,4-DMPPy-co-PPy(DBS) copolymer series. The 3MPPy-co-PPy(DBS) series also showed a decrease

in the time to 80 % maximum expansion, but the actuation rate for this series copolymer showed little change across the series with increasing blocked monomer content. In addition the error bars were very large in figure 3.12. There would appear to be a real increase in actuation speed for the 3,4-DMPPy-co-PPy(DBS) copolymer series with increasing blocked monomer content.

Through the use of a blocking approach it has been shown that the level of crosslinking strongly correlates with amount of irreversible expansion observed during actuation. In addition it would appear that relatively high levels of branching along with low levels of crosslinking produce a greater increase in irreversible expansion than low crosslinking levels alone. This result has been used to indirectly monitor the levels of crosslinking in PPy(DBS) formed at different polymerization potentials. In addition, instrumented indentation was used "in parallel" as a secondary method of monitoring levels of crosslinking in order to support our findings.

In addition, it would appear that decreased levels of crosslinking not only lead to increased levels of irreversible expansion but also to increased levels of reversible expansion and increased actuation rates, based on the data obtained for the 3,4-DMPPy-co-PPy(DBS) series. The 3MPPy-co-PPy(DBS) series also showed an increase in irreversible expansion with a decrease in crosslinking. However, the increase in reversible expansion and actuation rate with decreasing crosslinking seen for the 3,4-DMPPy-co-PPy(DBS) copolymer series was not observed. The difference in reversible expansion seen across the 3MPPy-co-PPy series has been attributed to the relative changes occurring in both the crosslinking and branching across. Thus the ratio of crosslinking to branching appears to be an important factor. The variation in the replicate data for the maximum expansion rate meant that any changes occurring within the 3MPPy-co-PPy series with decreasing crosslinking are being hidden.

The affect of polymerization potential on the structure and actuation performance of PPy(DBS) has been investigated. It has been suggested that an increase in polymerization potential will produce an increase in crosslinking[30]. By employing higher polymerization potentials more energy would be available to potentially cause more substitution in the pyrrole ring during electropolymerization, leading to increased branching and crosslinking. A similar conclusion has been made that increasing the temperature during electropolymerization will lead to increased substitution of the pyrrole ring and hence increased branching and crosslinking[31,32].

Using a major result of the copolymer work, the levels of crosslinking and branching were monitored using irreversible expansion. Instrumented indentation was also used as a secondary method for monitoring crosslinking based on the correlation that is known to exist with the mechanical properties of the film[57].

A suitable range for polymerization potential was found to be 0.5 V to 0.90 V. At lower potentials than 0.5 V polymerization was very slow and above 0.90 V the growth too

rapid for the accurate control of film thicknesses (Fig. 4.2). In addition it is known that electropolymerization at too high an electrical potential leads to degradation of the polymer (overoxidation). Through the use of FTIR microscopy no signs of overoxidation were noted within this range (Fig 4.3 and Fig. 4.5).

The charge consumed during polymerization of the PPy(DBS) films was in general observed to decrease with increasing polymerization potential. This might be explained by a decrease in density of the films accompanying an increase in the number of defects.

Based on the hypothesis that increased polymerization potentials lead to increased crosslinking, it was expected to see a decrease in both the reversible and irreversible expansion with increasing polymerization potential and crosslinking. This was observed (Fig. 4.7 and Fig. 4.9). However, there was an unexpected decrease in irreversible expansion in the range 0.5 V to 0.55 V. It is believed here that this can be explained by an increase in both branching and crosslinking that is taking place in the films in this range. This is in agreement with the earlier copolymer work, which concluded that increase in branching can lead to increased irreversible expansion. This is supported by density measurements which show a relatively large decrease in density on going from 0.5 V films to 0.55 V films (Fig. 4.24) and is consistent with an increase in branching leading to a lower packed network structure (Fig. 4.23).

The fastest actuating PPy(DBS) films were found to be those synthesized at 0.60 V. At higher potentials (0.60 V to 0.90 V) the films actuated more slowly. Again, this is consistent with the copolymer work and supportive of the view that increased crosslinking leads to decreased rates of actuation. The increase in actuation speed between 0.50 V and 0.60 V, might be attributed to the increase in branching leading to a lower density, more open and porous structure. This would facilitate ion movement into and out of the polymer by the increase in the number of "ion channels" available. It may also be that the crosslinking that is present within the films produced at lower polymerization potentials (0.50 V and 0.55 V) are shorter in length (shorter "spacer" lengths). Shorter spacer lengths might be expected at lower polymerization potentials due to the lower growth (kinetic) rates (Fig 4.2). More densely packed PPy networks crosslinked by shorter chains would be more likely to obstruct movement of ions through the polymer network. The presence of shorter crosslinks at low polymerization potential, 0.50 V, might also contribute to the lower level of irreversible expansion observed for 0.50 V compared to 0.55 V films.

Instrumented indentation has revealed that there is an increase in the stiffness (increase in the elastic modulus, E) and resistance to plastic deformation (decrease in H/E^2) with increasing polymerization potential (Fig. 4.16 and Fig. 4.22). Again, this is consistent with an increase in the level of crosslinking with increasing polymerization potential. The micro-hardness was found to be minimum for films polymerized at 0.7 V. In the region 0.5 V to 0.7 V the micro-hardness decreased from a maximum value at 0.5 V and

increased again in the range 0.70 V to 0.90 V (Fig 4.19). Hardness values are known to reflect changes in density, and the shape of the micro-hardness curve is similar to figure 4.24 which indicate polymer density changes for the prepared films. The decrease in micro-hardness observed between 0.50 V and 0.70 V has been attributed to a decrease in density of the films and possibly also to an increase in porosity accompanying increased branching. The increase in the micro-hardness in the range 0.70 V to 0.90 V has been attributed to a "re-densification" of the polymer network as a result of increased crosslinking (Fig 4.26 (a)).

A very interesting development has been the recent work undertaken by Schröder *et al* on the nanoindentation of crosslinked gold nanoparticle filled polymer films[89,90]. This work has shown that the increase in crosslinking and density accompanying the use of shorted linker lengths (shorter crosslinks) results in an increase in the elastic modulus and hardness of the films. These observations are consistent with findings presented in this thesis. In particular his results supports the idea that the increase in irreversible expansion observed for PPy(DBS) films on going from 0.5 V to 0.55 V are due to an decrease in density caused both by an increase in branching and an increase in crosslinking (spacer) length.

Both of the methods that have been used for monitoring crosslinking are supportive of each other and giving consistent results. They have allowed a model for the structural changes that we believe occur at different polymerization potentials to be proposed.

Based on a theoretical discussion of the changes that occur during branching and crosslinking a method is proposed (elemental analysis) which has the potential of providing a more direct and quantitative assessment of the levels of crosslinking in polypyrroles. In addition, this theoretical consideration of polymer network structure provides support to the notion that low levels of crosslinking produce more dense structures due to a better packing efficiency; whereas branched structures produce a less dense and more open/porous structure. It would be beneficial to develop this work further modelling networks in three dimensions using suitable software.

This work represents the first study of its kind aimed at understanding the impact that crosslinking and branching have upon the actuation performance of polypyrroles. As a result of this work the ability to synthesize polypyrroles with improved actuator properties such as greater strains and strain rates is closer.

1.2 Conclusions

The main outcomes of this work are as follows:

- An increase in crosslinking results in a decrease in both the reversible and irreversible expansion of polypyrrole films.
- An increase in branching leads to an increase in the irreversible expansion of polypyrrole films.
- Low levels of crosslinking and high branching produce the largest irreversible expansions and visa versa.
- An increase in branching results in a decrease in the density of polyrrole films.
- Instrumented indentation can be used to monitor structural changes, with an increase in crosslinking leading to an increase in the elastic modulus and a decrease in the parameter H/E^2.
- The micro-hardness values obtained from instrumented indentation can be used to reveal changes in film density, crosslinking and branching.
- For PPy(DBS) films an increase in polymerization potential results in an increase in branching and crosslinking, with the change in branching being dominant in the range 0.50 V to 0.55 V and the change in crosslinking being dominant in the range 0.55 V to 0.90 V.
- PPy(DBS) polymerized at 0.50 V produces films with a maximum strain.
- PPy(DBS) polymerized at 0.60 V produces films with a maximum strain rate.

Through undertaking this work we have:

1. Developed a new method for determining the electroactive performance of electropolymerized films, using it to show the affect of film thickness on actuation.
2. Noted that this method has the potential for studying ion movements during redox, via the Mirage Effect, which could not only aid further understanding of the actuation mechanism, but also be useful in the development of applications for controlled release of chemicals/drugs.
3. Devised and implemented a strategy for altering the levels of crosslinking and branching in polypyrroles based upon the use of blocking groups.
4. Shown the effect that structural changes such as crosslinking, branching and density have on the actuation performance of polypyrroles.
5. Developed a new approach for monitoring structural changes in polypyrrole based upon changes in the irreversible expansion.
6. Used instrumented indentation as a secondary method for monitoring crosslinking changes.

7. Developed a model for the structural changes that occur at different polymerization potentials for PPy(DBS).
8. Proposed that CHNS elemental analysis should be capable of the quantitatively determining crosslinking levels in polypyrrole, based on an in-depth discussion of network structure.

1.3 Further work

The work has raised further questions requiring answers. Further research that might be undertaken to both supplement and build upon the work presented in this thesis is as follows:

1. Investigate the use of elemental analysis for the quantitative determination of crosslinking in polypyrroles.
2. Obtain density and porosity data for PPy(DBS) films polymerized at different polymerization potentials (0.50 V to 0.90 V).
3. Use FTIR/ATR to obtain evidence that the irreversible expansion of PPy(DBS) films observed during actuation is the result of solvent (H_2O) swelling[132].
4. Synthesize polypyrroles using dimers, trimers and linear oligomers and assess their actuation performance[133].
5. Attempt to synthesize polypyrroles containing more linear chained polymer, at low temperatures[134], in aqueous electrolytes, using super-cooled aqueous electrolytes and natural antifreeze molecules.
6. Explore strategies for increasing the rate of actuation of polypyrroles.

References

[1] Jager, E. W. H., Inganäs, O., Lundström, I. (2001). Perpendicular actuation with individually controlled polymer microactuators. Advanced Materials, 13 (1), p. 76-79

[2] Jager, E. W. H., Smela, E., Inganäs, O. (2000). Microfabricating Conjugated Polymer Actuators. Science, 290, p. 1540-1545.

[3] Jager, E. W. H., Inganäs, O., Lundström, I. (2000). Microrobots for Micrometer-Size Objects in Aqueous Media: Potential Tools for Single-Cell Manipulation. Science, 288, p. 2335-2338.

[4] Jager, E. W. H., Smela, S., Inganäs, O. (1999). On-chip microelectrodes for electrochemistry with moveable PPy bilayer actuators as working electrodes. Sensors and Actuators B, 56, p. 73-78.

[5] Smela, E. (2003). Conjugated Polymer Actuators for Biomedical Applications. Adv. Mater., 15 (16), p. 484-494.

[6] Svennersten, K., Berggren, M., Richter-Dahlfors, A., Jager, E. W. H. (2011). Mechanical stimulation of epithelial cells using polypyrrole microactuators. Lab on a Chip - Miniaturisation for Chemistry and Biology, 11 (19), p. 3287-3293.

[7] Jager, E. W. H., Immerstrand, C., Peterson, K. H., Magnusson, K.-E., Lundström, I., Inganäs, O. (2002). The cell clinic: Closable microvials for single cell studies. Biomedical Microdevices, 4 (3), p. 177-187.

[8] Wilson, S. A., Jourdain, R. P. J., Zhang, Q, Dorey, R. A., Bowen C. R, Willander, M., Wahab, Q. U., Persson, K. (2007). New materials for micro-scale actuators and sensors – an engineering review. Mat. Sci. and Eng. R: Reports, 56 (1-6), 1-129.

[9] Calvert, P., Liu, Z. (1999). Electrically stimulated bilayer hydrogels as muscles. Proceedings of SPIE, 3669, p. 236-241.

[10] Solari, M. (1994). Evaluation of the mechanical-properties of a hydrogel fiber in the development of a polymeric actuator. J. Intel. Mat. Syst. and Struct., 5 (3), p. 295-304.,

[11] Bel'nikevich, N. G., Budtova, T. V., Vesnebolotskaya, S. A., Elyashevich, G. K. (2008). Effect of degree of cross-linking of sodium acrylate hydrogels on their selling in variously acidic solutions. Russ. J. App. Chem., 81 (10), p. 1818-1820.

[12] Yasunaga, H., Ando, I. (1993). Dynamic Behaviour of Water in Hydro-swollen Crosslinked Polymer Gel as Studied by PGSE 1H NMR and Pulse 1H NMR. Polymer Gels and Networks, 1, p. 83-92.

[13] Yasunaga, H., Ando, I. (1993). Effect of Cross-linking on the Molecular Motion of Water in Polymer Gel as Studied by Pulse 1H NMR and PGSE 1H NMR. Polymer Gels and Networks, 1 (4), p. 267-274.

[14] Yasunaga, H., Ando, I. (1993). A 13C PST/MAS NMR study of the structure and molecular motion of crosslinked polymer in the gel phase. J. Molecular Structure, 301, p. 129-136.

[15] Yanbin, W., Sony, J., Aluru, N. R. (2009). Effect of cross-linking on the diffusion of water, ions, and small molecules in hydrogels. J. Phys. Chem. B, 113, p. 3512-3520.

[16] Krongauz, V. V. (2010). Diffusion in polymers dependence on cross-linking density: Eyring approach to mechanism. J. Thermal Analysis and Calorimetry, 102(2), p. 435-445.

[17] Lu, W., Fadeev, A. G., Qi, B. H., Smela, E., Mattes, B. R., Ding, J., Spinks, G. M., Mazurkiewicz, J., Zhou, D. Z., Wallace, G. G., MacFarlane, D. R., Forsyth, S. A., Forsyth, M. (2002). Use of ionic liquids for π-conjugated polymer electrochemical devices. Science, 297 (5583), p. 983-987.

[18] Wallace, G. G., Ding, J., Lu, L., Spinks, G. M., Zhou, D., Forsyth, S., Forsyth, M., McFarlane, D. (2002). Factors influencing performance of electrochemical actuators based on inherently conducting polymers (ICPs). SPIE, Smart Structures and Devices, EAPAD, 4695, p. 8-16.

[19] Immerstrand, K., Holmgran-Peterson, K. E., Magnusson, Jager, E., Krogh, M., Skoglund, M., Selbing, A., Inganäs, O. (2002). Electroactive organic materials. MRS Bull, 27 (6), p. 441-445.

[20] Palagi, S., Mazzolai, B., Beccai, L. (2012). Modeling of a Propulsion Mechanism for Swimming Microrobots Inspired by Ciliate Metachronal Waves. Fourth IEEE RAS/EMBS International Conference on Biomedical Robotics and Biomechatronics, June 24-27, 2012, Roma, Italy.

[21] Scott, J.C., Bredas, J. L., Yakushi, K., Pfluger, P., Street, G. B. (1984). The evidence for bipolarons in pyrrole polymers. Synthetic Metals, 9, p. 165-172.

[22] Brédas, J. L., Belijonne, D., Coropceanu, V., Cornil, J. (2004). Charge-Transfer and Energy-Transfer Processes in π-Conjugated Oligomers and Polymers: A Molecular Picture. Chem. Rev., 104, p. 4971-5003.

[23] Coropceanu, V., Cornil, J., da Silva Filho, D. A., Olivier, Y., Silbey, R., Brédas, J. L. (2007). Charge Transport in Organic Semiconductor. Chem. Rev., 107, p. 926-252.

[24] Brédas, J. L., Street, G. B., Thémans, B., André, J. M. (1985). Organic polymers based on aromatic rings (polyparaphenylene, polypyrrole, polythiophene): Evolution of

the electronic properties as a function of the torsional angle between adjacent rings. J. Chem. Phys, 83 (3), p. 1323-1329.

[25] Komura, T., Goisihara, S., Yamaguti, T., Takahasi, K. (1985). Electron and ion transport in polypyrrole/polystyrenesulfonate composite films. J. Electroanal. Chem., 456 (1-2), p. 121-129.

[26] Wallace, G. G., Teasdale, P. R., Spinks, G. M., Kane-Maguire, L. A. P. (2008). Conductive Electroactive Polymers: Intelligent Polymer Systems, 3rd ed. CRC Press, Florida, USA. p. 71.

[27] Skotheim, T. A. (2008). Handbook of Conducting Polymers, 2nd ed. Marcel Dekker, New York, USA.

[28] Pringle, J. M., Efthimiadis, J., Howlett, P. C., MacFarlane, D. R. Chaplin, A. B., Hall, S. B., Officer, D. L., Wallace, G. G., Forsyth, M. (2004). Electrochemical synthesis of polypyrrole in ionic liquids. Polymer, 45, p. 1447-1453.

[29] Meerholtz, K., Heinze, J. (1993). Influence of Chain Length and Defects on the Electrical Conductivity of Conducting polymers. Synth. Met., 55-57, p. 5040-5045.

[30] Pyo, M., Bohn C. C., Smela E., Reynolds J. R., Brennan A. B. (2003). Direct Strain Measurement of Polypyrrole Actuators Controlled by the Polymer/Gold Interface. Chem. Mater., 15, p. 916-922.

[31] Yurtsever, M., Yurtsever, E. (1999). Structural studies of polypyrroles: I. An ab-initio evaluation of bonding through α and β carbons. Synth. Met., 98 (3), p. 221-227.

[32] Yurtsever, E., Esenturk, O., Pamuk, H. O., Yurtsever, M. (1999). Structural studies of polypyrroles: II. a Monte Carlo growth approach to the branch formation. Synth. Met., 98 (3), p. 229-236.

[33] Y. Dai and E. Blaisten-Barojas (2010). Monte Carlo study of oligopyrroles in condensed phases. J. Chem. Phys., 133(3), art. no. 034905.

[34] Kanazawa, k., Diaz, A. F., Gill, W. D., Grant, P. M., Street, G. B., Gardini, G. P., Kwak, J. F. (1980). Polypyrrole: An electrochemically synthesized conducting organic polymer. Synth. Met., 1 (3), p. 329-336.

[35] Street, G. B., Lindsey, S. E., Nazzal, A. I., Wynne, K. J. (1985). The Structure and Mechanical Properties of Polypyrrole. Mol. Cryst. Liq. Cryst., 118, p. 137-148.

[36] Geiss, R. H., Street, G. B., Volksen, W., Economy, J. (1983). Polymer Structure Determination Using Electron Diffraction Techniques. IBM J. Res. Dev., 27 (4), p. 321-329.

[37] Wernet, W., Monkenbusch, M., Wegner, G. (1985). On Structure and Properties of Polypyrrole Alkylsulphonates. Mol. Cryst. Liq. Cryst., 118, p. 193-197.

[38] Mitchell, G. R., Davis, F. J., Kiani, M. S. (1990). Influence of synthesis on the structure of electrochemically prepared electrically conducting polymers. Br. Polym. J., 23 (1-2), p. 157-164.

[39] Pruneanu, S., Graupner, W., Oniciu, L., Brie, M., Turcu, R. (1996). Electrochemical and X-ray diffraction studies on polypyrrole films. Mater. Chem. Phys., 46 (1), p. 55-60.

[40] Mitchell, G. R., Geri, A. (1987). Molecular organisation of electrochemically prepared conducting polypyrrole films. J. Phys. D: Appl. Phys., 20 (11), art. no. 2, p. 1346-1353.

[41] Pruneanu, S., Resel, R., Leising, G., Brie, M., Graupner, W., Oniciu, L. (1997). Structural investigations on polypyrrole and poly(vinyl chloride)-polypyrrole composite films. Mater. Chem. Phys., 48 (3), p. 240-245.

[42] Yamaura, M., Hagiwara, T., Iwata, K. (1988). Enhancement of electrical conductivity of polypyrrole film by stretching: Counter ion effect. Synth. Met., 26 (3), p. 209-224.

[43] Davidson, R. G., Hammond, L. C., Turner, T. G., Wilson, A. R. (1996). An electron and X-ray diffraction study of conducting polypyrrole/dodecyl sulphate. Synth. Met., 81 (1), p. 1-4.

[44] Yoon, C. O., Sung, H. K., Kim, J. H., Barsoukov, E., Kim, J. H., Lee, H. (1999). The effect of low-temperature conditions on the electrochemical polymerization of polypyrrole films with high density, high electrical conductivity and high stability. Synth. Met., 99 (3), p. 201-212.

[45] Li, J., Wang, E., Green, M., West, P. E. (1995). In situ AFM study of the surface morphology of polypyrrole film. Synth. Met., 74 (2), p. 127-131.

[46] Barisci, J. N., Stella, R., Spinks, G. M.; Wallace, G. G. (2000). Characterization of the topography and surface potential of electrodeposited conducting polymer films using atomic force and electric force microscopies. Electrochim Acta, 46 (4), p. 519-531.

[47] Gandi, M., Spinks, G. M., Burford, R. P., Wallace, G. G. (1995). Film substructure and mechanical properties of electrochemically prepared polypyrrole. Polymer, 36(25), p. 4761-4765.

[48] Bay, L., Jacobsen, T., Skaarup, S., West, K. (2001). Mechanism of Actuation in Conducting Polymers: Osmotic Expansion. J. Phys. Chem. B, 105, p. 8492-8497.

[49] Jafeen, M. J. M., Careem, M. A., Skaarup, S. (2010). Speed and Strain of Polypyrrole actuators: dependence on cation hydration number. Ionics, 16, p. 1-6.

[50] Franks, F. (Ed). (1988). Water Science Reviews 3: Vol. 3: Water Dynamics, Cambridge University Press, Cambridge, p. 91.

[51] Smela, E., Gadegaard, N. (2001). Volume Change in Polypyrrole Studied by Atomic Force Microscopy. J. Phys. Chem. B, 105, p. 9395-9405.

[52] Yagüe, J. L., Agulló, N., Borrós, S. (2008). Plasma Polymerization of Polypyrrole-like Films on Nanostructured Surfaces. Plasma Process. Polym., 5, p. 433-443.

[53] Bouldin, R., Ravichandran, S., Kokil, A., Garhwal, R., Nagarajan, S.,Kumar, J., Bruno, F.F., Nagarajan, R. (2011). Synthesis of polypyrrole with fewer structural defects using enzyme catalysis. Synth. Met., 161 (15-16), p. 1611-1617.

[54] Sadki, S., Schottland, P., Brodie, N., Sabouraud, G. (2000). The mechanism of pyrrole electropolymerization. Chem. Soc. Rev., 29, p. 283-293.

[55] Funt, B. L., Diaz, A. F. (1991). Organic Electrochemistry: an Introduction and a Guide, Marcel Dekker, New York, p. 1337.

[56] Genies, E. M., Bidan, G., Diaz A. F. (1983). Spectroelectrochemical study of polypyrrole films. J. Electroanal. Chem., 149 (1-2), p. 101-113.

[57] Wallace, G. G., Spinks, G. M., Kane-Maguire L. A. P., Teasdale, P. R. (2008). Conductive Electroactive Polymers – Intelligent Polymer Systems, 3rd ed. CRC Press, Florida, p. 70-71.

[58] Cho, S. H., Song, K. T., Lee, J. Y. (2007). Handbook of Conducting Polymers: Theory, Synthesis, Properties and Characterization, Eds. Skotheim, T., Reynolds, J. R., 3rd ed, CRC Press, Florida, p. 8-1.

[59] Turcu, R., Graupner, W., Filip, C., Bot, A., Brie, M., Grecu, R. (1999). Studies of the intermolecular interactions in polypyrrole and conjugated composites based on polypyrrole. Adv. Mater. Opt. Electron, 9 (4), p. 157-165.

[60] Ribó, J.M., Dicko, A., Vallès, M.A., Claret, J., Dallemer, P., Ferrer-Anglada, N., Bonnett, R., Bloor, D. (1993). On the structure of polypyrrole: Polypyrroles with dipyrrin-1(10H)-one end groups. Polymer, 34 (5), p. 1047-1053.

[61] Khonakdar, H. A., Jafari, S. H., Taheri, M., Wagenknecht, U., Jehnichen, D., Häussler, L. (2006). Thermal and Wide Angle X-ray Analysis of Chemically and Radiation-Crosslinked Low and High Density Polyethylenes. J. Polym. Sci., 100, p. 3264-3271.

[62] Gatiyatullina, G. V., Battalov, E. M., Prochukhan Y. A., Muslukhov, R. R. (2003). Degree of Cross-linking of Epoxy-Acrylate Polymers Prepared by Photopolymerization. Rus. J. Appl. Chem., 76 (3), p. 448-451.

[63] Beake, B. D., Leggett, G. J., Alexander, M. R. (2002). Characterization of the mechanical properties of plasma-polymerized coatings by nanoindentation and nanotribology. J. Mater. Sci., 37, p. 4919-4927.

[64] Bielinski, D., Lipinski, P., Slusarski, L., Grams, J., Paryjczak, T., Jagielski, J., Turos, A., Madi, N. K. (2004). Surface layer modification of ion bombarded HDPE. Surface Science, 564, p. 179-186.

[65] Beake, B. D. (2006). Modelling indentation creep of polymers: a phenomenological approach. J. Phys. D: Appl. Phys., 39, p. 4478-4485.

[66] Pfluger, P., Street, G. B. (1984). Chemical, electronic, and structural properties of conducting heterocyclic polymers: A view by XPS. J. Chem. Phys., 80(1), p. 544-553.

[67] Joo, J., Lee J. K., Baeck, J. S., Kim, K. H., Oh, E. J., Epstein, J. (2001). Electrical, magnetic, and structural properties of chemically and electrochemically synthesized polypyrroles. Synth. Met., 117, p. 45-51.

[68] Fahlman, M., Head of Division of Surface Physics and Chemistry, Linkoping University, Sweden (2010). Personal communication.

[69] Estrany, F., Oliver, R., Cabot, P. –L., Brillas, E. (2006). Effect of monomer molecular flow on electrode surface on the structure of poly(α-tetrathiophene) obtained by anodic polymerization. European Polymer Journal, 42, p. 563-572.

[70] Lei, J., Liang, W., Martin, C. R. (1992). Infrared investigations of pristine, doped and partially doped polypyrrole. Synth. Met., 48, p. 301-312.

[71] Menon, V. P., Lei, J., Martin, C. R. (1996). Investigation of Molecular and Supermolecular Structure in Template-synthesized Polypyrrole Tubules and Fibrils. Chem. Mater., 8, p. 2382-2390.

[72] Tian, B., Zerbi, G. (1990). Lattice dynamics and vibrational spectra of polypyrrole. J. Chem. Phys., 92 (6), p. 3886-3890.

[73] Tian, B., Zerbi, G. (1990). Lattice dynamics and vibrational spectra of pristine and doped polypyrrole: Effective conjugation coordinate. J. Chem. Phys., 92 (6), p. 3892-3898.

[74] Devreux, F., Bidan, G., Syed, A. A., Tsintavis, C. (1985). Solid state 13C NMR in conducting polymers. J. Phys (Paris), 46 (9), p. 1595-1601.

[75] Wehrle, B., Limbach, H. H., Mortensen, J., Heinze (1990). Solid-state 15N CPMAS NMR study of the structure of polypyrrole. J. Synth. Met., 38 (3), p. 293-298.

[76] Kikuchi, M., Kurosu, H., Ando, I. (1992). Structural characterization of polypyrrole in the solid state by high resolution 15N NMR spectroscopy combined with quantum chemistry. J. Mol. Struct., 269, p. 183-195.

[77] Hellgren, A. –C., Wallin, M., Weissenborn, P. K., McDonald, P. J., Glover, P. M., Keddie, J. L. (2001). New techniques for determining the extent of crosslinking in coatings. Progress in Organic Coatings, 43, p. 85-98.

[78] Hermann, V., Böhner, T., Blümich, B. (2004). Application of NMR in the tire industry. KGK Kautschuk, Gummi, Kunststoffe, 57, p. 22-27.

[79] Guthausen, G., Todt, H., Burk, W., Kamlowski, A., Schmalbein, D. (2003) Quality Control with NMR: Selected Examples and Applications in Polymer Industry. KGK Kautschuk, Gummi, Kunststoffe, 56, p. 578-581.

[80] Mathew, R., Mattes, B. R., Espe, M. P. (2002). A solid state NMR characterization of cross-linked polyaniline powder. Synth. Met., 131, p. 141-147.

[81] Adriaensens, P., Pollaris, A., Kelchtermans, M., Gelan, J. (2003). Determination of the local Cross-linking Density in Polyisobutylene-Based Elastomers by NMR Imaging. Macromol., 36, p. 706-711.

[82] Barth, P., Hafner, S., Denner, P. (1996). Material Property NMR Imaging of Cross-linked Polymers Based on Longitudinal Relaxation in the Rotating Frame. Macromol., 29, p. 1655-1659.

[83] Bieliński, D. M., Lipiński, P., Urbaniak, M., Jagielski, J. (2006). Influence of ion bombardment on tribological properties of UHMWPE. Tribology Letters, 23 (2), p. 139-143.

[84] Turos, A., Jagielski, J., Piątkowska, A., Bieliński, D. M, Ślusarski, L., Madi, N. K. (2003). Ion beam modification of surface properties of polyethylene. Vacuum, 70, p. 201-206.

[85] Fischer-Cripps, A. C. (2011). Nanoindentation, 3rd Ed. Springer, New York. P21-36.

[86] Oliver, W. C., Pharr, G. M. (1992). Improved technique for determining hardness and elastic modulus using load and displacement sensing indentation experiments. J. Mater. Res. 7 (6), p. 564-1580.

[87] Oliver, W. C., Pharr, G. M. (2004). Measurement of hardness and elastic modulus by instrumented indentation: Advances in understanding and refinements in methodology. J. Mater. Res., 19 (1), p. 3-20.

[88] Fischer-Cripps, A. C. (2009). The Ibis Handbook of Nanoindentation. Fischer-Cripps Laboratories Pty Ltd, Forestville, Australia. p. 41.

[89] Schlicke, H., Schröder, J. H., Trebbin, M., Petrov, A., Ijeh, M., Weller, H., Vossmeyer, T. (2011). Freestanding films of crosslinked gold nanoparticles prepared via layer-by-layer spin-coating. Nanotechnology, 22 (30), art. no. 305303.

[90] Jan H. Schröder (2012). Doctoral thesis: Herstellung und Charakterisierung von Schichtsystemen aus Gold Nanopartikeln, Universität Hamburg, Hamburg.

[91] Carraher, C. E. (2003). Seymour/Carraher Polymer Chemistry, CRC Press, Florida, USA. p. 44–45.

[92] Beake, B. Goodes, S., Jones, S., Parkinson, R., Pickford, N., Roberts, L., Smith, J., (2002). NanoTest User Manual, Version 2. Micromaterials Ltd., Wrexham, UK. p. 44.

[93] Murthy, N. S., Shacklette, L. W., Baughman, R. H. (1987). Effect of charge transfer on chain dimension in trans-polyacetylene. J. Chem Phys. 87 (4), p. 2346-2348.

[94] Winokur, N. S., Moon, Y. B., Heeger, A. J., Barker, J., Bott, D. C. (1988). The relationship between charge transfer and structure in alkali doped polyacetylene. Solid Stat. Commun., 68 (12), p. 1055-59.

[95] Kertesz, M., Vonderviszt, F., Pekker, S. (1982). Change of geometry of polyacetylene upon charge transfer. Chem. Phys. Lett., 90 (6), p. 430-433.

[96] Baughmann, R. H., Murthy N. S., Eckhardt, H., Kertesz, M. (1992). Charge oscillations and structure for alkali-metal-doped polyacetylene. Phys. Rev. B, 46 (39), p. 10515-10517.

[97] Heinze, J., Meerholz, K., Bilger, R. (1989). Electronic Properties of Conjugated Polymers III (Eds: Kuzmany, H., Mehring, M., Roth, S.), Vol 91. Springer-Verlag, Berlin. p. 146.

[98] Winokur, M. J., Walmsley, P., Moulton, J., Smith, P., Heeger, A. J. (1991). Structural evolution in iodine-doped poly(3-alkylthiophenes). Macromolecules, 24 (13), p. 3812-3815.

[99] Yoshino, K., Morita, S., Nakao, K. (1991). Characteristics of conducting polymer gels and their doping effect. Synth. Met., 41 (3), p. 1039-1044.

[100] Pei, Q., Inganäs, O. (1993). Electroelastomers: Conjugated poly(3-octylthiophene) gels with controlled crosslinking. Synth. Met., 57 (1), p. 3724-3729.

[101] Anquetil, P. A., Yu, H. –h, Madden, J. D., Madden, P. G., Swager, T. M., Hunter, I. W. (2002). Thiophene-based conducting polymer molecular actuators. Proceedings of SPIE - The International Society for Optical Engineering 4695, p. 424-434.

[102] Lahav, M., Durkan, C., Gabai, R., Katz, E., Willner, I., Welland, M. E. (2001) Redox activation of a polyaniline-coated cantilever: An electro-driven microdevice. Angew. Chem. Int. Ed., 40 (21), p. 4095-4097.

[103] Pei, Q., Inganäs, O. (1993). Electrochemical applications of the bending beam method; a novel way to study ion transport in electroactive polymers. Solid State Ionics, 60 (1-3), p. 161-166.

[104] Gandi, M. R., Murray, P., Spinks, G. M., Wallace, G. G. (1995). Mechanism of electromechanical actuation in polypyrrole. Synth. Met., 73 (3), p247-256.

[105] Otero, T. F., Grande H., Rodriquez, J., (1996). Reversible electrochemical reactions in conducting polymers: A molecular approach to artificial muscles. J. Phys. Org. Chem., 9 (6), p. 381-386.

[106] Chiarelli, P., Della Santa, A., De Rossi, D., Mazzoldi, A. (1995). Actuation Properties of Electrochemically Driven Polypyrrole Free-Standing Films. J. Intell. Mater. Syst. Struct., 6 (1), p. 32-37.

[107] Della Santa, A., De Rossi, D., Mazzoldi, A. (1997). Performances and Work Capacity of a Polypyrrole Conducting Polymer Linear Actuators. Synth. Met., 90 (2), p93-100.

[108] Pei, Q., Inganäs, O. (1993). Electrochemical Applications of the Bending Beam Method. 2. Electroshrinking and Slow Relaxation in Polypyrrole. J. Phys. Chem., 97 (22), p. 6034-6041.

[109] Smela, E., Kallenbach, M., Holdenried, J. (1999). Electrochemically Driven Polypyrrole Bilayers for Moving and Positioning Bulk Micromachined Silicon Plates. J. Electromech. Syst., 8(4), p. 374-383.

[110] Li, Y. (1997). On the Large Overpotential of the First Reduction of Polypyrrole Perchlorate Films in Organic Solutions. Electrochim. Acta., 42(2), p. 203-210.

[111] Otero, T. F. (1997). Artificial Muscles, Electrodissolution and Redox Processes in Conducting Polymers, in Vol. 4. Conductive Polymers; Transport Photophysics and Applications; Nalwa, H. S. (Ed), John Wiley & Sons, New York. p. 517.

[112] Slama, M., Tanguy, J. (1989). Electrogravimetrical Study of Polypyrrole. Synth. Met., 28 (1-2), p. 171-176.

[113] Suárez, M. F., Compton, R. G. (1999). In Situ Atomic Force Microscopy Study of Polypyrrole Synthesis and the Volume Changes Induced by Oxidation and Reduction of the Polymer. J. Electroanal. Chem., 462 (2), p. 211-221.

[114] Imisides, M. D., Wallace, G. G. (1988). Deposition and electrochemical stripping of mercury ions on polypyrrole based modified electrodes. J. Electroana. Chem., 246 (1), p. 181-191.

[115] Smela, E. (1999). Microfabrication of PPy microactuators and other conjugated polymer devices. J. Micromech. & Microeng., 9 (1), p. 1-18.

[116] Wang, X., Smela, E. (2009). Color and volume change in PPy(DBS). J. Phys. Chem. C, 113 (1), p. 359-368.

[117] Barbero, C., Miras, M. C., Kötz, R., Haas, O. (1993). Probe beam deflection: a useful tool for the study of ion transport in polymers. Solid State Ionics, 60, p. 167-172.

[118] Melling, D, Wilson, S., Berggren, M., Jager, E.W.H. (2011). Altering the structure of polypyrrole and the influence on electrodynamic performance. Proceedings of SPIE - The International Society for Optical Engineering, Vol. 7976, art. no. 79760Z.

[119] Barbero, C., Miras, M. C., Calvo, E. J., Kötz, R., Haas, O. (2002). A Probe Beam Deflection Study of Ion Exchange at Poly(vinylferrocene) films in Aqueous and Non-aqueous electrolytes. Langmuir, 18, p. 2756-2764.

[120] Higgins, M., University of Wollongong, Australia (2012). Personal communication.

[121] Gupta, R. C., Pradhan, A., Gupta, S. (2010). Refraction-Based Alternative Explanation for: Bending of Light Near a Star, Gravitational Red/Blue Shift and Black-Hole. Cornell University Library Archive, USA: arXiv:1004.1467v1, p. 1-9.

[122] Bray, B. L., Mathies, P. H., Naef, R., Solas, D. R., Tidwell, T. T., Artis, D. R., Muchowski, J. M. (1990). N-(Triisopropysilyl)pyrrole. A Progenitor “Par Excellence” of 3-substituted Pyrroles. J. Org. Chem., 55 (26), p. 6317-6328.

[123] Ichimura, K., Ichikawa, S., Imamura, K. (1976). The Synthesis of 3, 4-Dimethyl-1H-pyrrole. Bull. Chem. Soc. Japan, 49 (4), p. 1157-1158.

[124] Lin-Vien, D., Colthup, N. B., Fateley, W. G., Grasselli, J. G. (1991). The handbook on Infrared and Raman Characteristic Frequencies of Organic Molecules. Academic Press, San Diego, USA. p. 301-303.

[125] Sykes, P. (1970). A Guidebook to Mechanism in Organic Chemistry, 6th ed. Longman, Harlow, UK. p. 21-22 and p82-83.

[126] Liu, Y., Gan, Q., Baig, S., Smela, E. (2007). Improving PPy Adhesion by Surface Roughning. J. Phys. Chem. C., 111, p. 11329-11338.

[127] Rodriguez, I., Scharifker, B. R., Mostany, J. (2000). In situ FTIR study of redox and overoxidation processes in polypyrrole films. J. Electroana. Chem., 491 (1-2) p. 117-125.

[128] Kostic, R., Rakovic, D., Stepanyan, S. A., Davidova, I. E., Gribov, L. A., (1995). Vibrational spectroscopy of polypyrrole, theoretical study. J. Chem. Phys., 102 (8), p. 3104-3109.

[129] Audebert, P., Miomandre, F., Di Magno, S. G., Smirnov, V. V., Hapiot, P., (2000). Polymerization of 3,4-difluoropyrrole: Electrochemical and physicochemical behavior of poly(difluoropyrrole). Chem. Mater., 12 (7), p. 2025-2030.

[130] Naoi, K., Lien, M; Smyrl, W. H., (1991). Quartz crystal microbalance study. Ionic motion across conducting polymers. J. Electrochem. Soc., 138 (2), p. 440-445.

[131] Briscoe, B. J., Fiori, L., Pellillo, E. (1998). Nano-indentation of polymeric surfaces. J. Phys. D: Appl. Phys. 31(19), p. 2395-2405.

[132] Hartauer, K. J., Matheson, L. E., Guillory, J. K., (1988). Quantitative Determination of Absorbed Water in Co(polyether) Polyurethane Membranes Using FTIR/ATR. Applied Spectroscopy, 42 (4), p. 699-701.

[133] Groenendaal, L. The Chemistry of Oligopyrroles: Design, synthesis and characterization of well-defined and functional α–α linked oligomers. PhD thesis, Eindhoven University of Technology, ISBN 90-386-0268-5, Available on-line at: http://alexandria.tue.nl/extra3/proefschrift/PRF13A/9603963.pdf.

[134] Yoon, C. O., Sung, H. K., Kim, J. H., Barsoukov, E., Kim, J. H., Lee, H. (1999). "The effect of low-temperature conditions on the electrochemical polymerization of polypyrrole films with high density, high electrical conductivity and high stability". Synth. Met., 99, p. 201-212.

Appendix 1

Laser Scanning Micrometer (LSM) Control Unit and GPES Software settings:

LSM settings:

Press “C” (Yellow)

Press “Set” once

Press numbers to enter value

Press “E” (enter) to go to next row

Press “set” twice to exit

Press “Cont” to continuously send data to GPES

0 SEG 2

1 MR ARM 512

2 LL 0

2 LH 0

3 REF (sample dependant)

3 SCL 1

4 OFS 0

5 DAT O.C 0

6 SMP N1

GPES settings:

Multiplier = 4

Offset = same as “3 REF”

Appendix 2

Cyclic voltammetry can be used to demonstrate the presence of diffusion limited processes.

The CV results of films are governed by the kinetics of diffusion in series with charge exchange. There is an envelope of conditions in which diffusion becomes significant and this would mean that only a part of the thickness of the film is active in terms of exchange.

CV measurement performed at different scan rates would enable the sensitivity of a particular film/material to limitation by diffusion. Such measurements would show the existence of a plateau in the dependence of the CV results on rates towards the low rate. If the rates and time scales of the experiment are within the plateau then the film responds with its full thickness and diffusion does not play a role and visa versa.

That diffusion is the important part in the volume change of PPy and is generally the rate limiting step is well known and an established fact in the field of electroactive polymers[116]. In light of this previous work undertaken for PPy(DBS) we have taken diffusion to be the rate limiting step in the work conducted in Section C, 1.2 of this thesis.